

**COMPUTATION AND CHARACTERIZATION OF POWDER
MIXED ELECTRIC DISCHARGE MACHINING ON NICKEL
BASED ALLOY (INCONEL) AND TITANIUM GRADE 2**

Thesis submitted by
SOVAN BHOWMICK

**Doctor of Philosophy
(Engineering)**

**DEPARTMENT OF MECHANICAL ENGINEERING
FACULTY OF ENGINEERING & TECHNOLOGY
JADAVPUR UNIVERSITY
2025**

JADAVPUR UNIVERSITY
KOLKATA-700032, INDIA

INDEX NO. 252/18/E

REGISTRATION NUMBER: 1021811017

1. Title of Thesis:

COMPUTATION AND CHARACTERIZATION OF POWDER MIXED
ELECTRIC DISCHARGE MACHINING ON NICKEL BASED ALLOY
(INCONEL) AND TITANIUM GRADE 2

2. Name, Designation & Institution of the Supervisor(s):

Prof. (Dr.) Gautam Majumdar

Professor, Mechanical Engineering Department,
Jadavpur University,
Kolkata-700032

Dr. Nisantika Biswas

Assistant Professor, Department of Mechanical Engineering,
Academy of Technology,
Hoogly-712121

Dr. Subhasish Sarkar

Assistant Engineer,
Public Health Engineering,
Government of West Bengal

3. List of Publications:

Journal Publications:

- [1] Bhowmick, S., Barai, B., Naik, D., Sarkar, S., Biswas, N., Maity, S. K. and Majumdar, G., 2023. Parametric Study and Optimization of Inconel 625 Processing by ANN and Desirability Function Approach During Graphite Mixed EDM. *Jordan Journal of Mechanical and Industrial Engineering*, Vol. 17, No. 4, pp. 625-643.
DOI: <https://doi.org/10.59038/jjmie/170417>
- [2] Bhowmick, S., Mondal, R., Sarkar, S., Biswas, N., De, J. and Majumdar, G., 2023. Parametric optimization and prediction of MRR and surface roughness of titanium mixed EDM for Inconel 718 using RSM and fuzzy logic. *CIRP Journal of Manufacturing Science and Technology*, Vol. 40, pp. 10-28.
DOI: <https://doi.org/10.1016/j.cirpj.2022.11.002>

Publication from Conference:

- [1] Bhowmick, S., Sarkar, S., Biswas, N. and Majumdar, G., 2022. A comparative study relating machining properties and surface characteristics of Inconel 625 during powder mixed electric discharge machining. *Materials Today: Proceedings*.
DOI: <https://doi.org/10.1016/j.matpr.2022.12.147>
- [2] Bhowmick, S., Paul, A., Biswas, N., De, J., Sarkar, S. and Majumdar, G., 2022. Synthesis and Characterization of Titanium and Graphite Powder Mixed Electric Discharge Machining on Inconel 718. In *Advanced Production and Industrial Engineering*, IOS Press, pp. 58-63.
DOI: 10.3233/ATDE220722
- [3] Bhowmick, S., Majumdar, G. and Bandyopadhyay, A., 2021. A Brief Review of Experimental Investigations and Analytical Development of Powder Mixed Electric Discharge Machining (PMEDM). *Advances in Science and Technology*, Vol. 106, pp. 31-38.
DOI: <https://doi.org/10.4028/www.scientific.net/AST.106.31>

4. List of Patents: NIL

5. Presentation in National/International Conferences:

- [1] Bhowmick, S., Majumdar, G. and Bandyopadhyay, A. A brief review of Experimental Investigations and Analytical development of powder mixed electric discharge machining (PMEDM). 1st International Conference on Advances in Material Science and Mechanical Engineering on 7th to 9th February 2020 at NBKR Institute of Technology.
- [2] Bhowmick, S., Pal, A., Biswas, N., De, J., Sarkar, S. and Majumdar, G. Synthesis and Characterization of Titanium and Graphite Powder Mixed Electric Discharge Machining on Inconel 718. 7th International Conference on Advanced Production and Industrial Engineering on 11th to 12th June 2022 at NIT Delhi.
- [3] Bhowmick S, Sarkar S, Biswas N, Majumdar G. A Comparative Study Relating Machining Properties and Surface Characteristics of Inconel 625 during Powder Mixed Electric Discharge Machining. 1st International Conference on Advancement in Manufacturing Engineering on 12th to 13th November 2022 at NIT Delhi.

6. List of Book Chapters: NIL

JADAVPUR UNIVERSITY

FACULTY OF ENGINEERING & TECHNOLOGY

Statement of Originality

I Sovan Bhowmick registered on 03rd May 2018 do hereby declare that this thesis entitled **Computation and Characterization of Powder Mixed Electric Discharge Machining on Nickel Based Alloy (Inconel) and Titanium Grade 2** contains literature survey and original research work done by the undersigned candidate as part of Doctoral studies.

All information in this thesis have been obtained and presented in accordance with existing academic rules and ethical conduct. I declare that, as required by these rules and conduct, I have fully cited and referred all materials and results that are not original to this work.

I also declare that I have checked this thesis as per the “Policy on Anti Plagiarism, Jadavpur University, 2019”, and the level of similarity as checked by iThenticate software is **5%**.

Sovan Bhowmick

Signature of Candidate:

Date: *22/04/2025*

Certified by Supervisor(s):
(Signature with date, seal)

1. _____

Prof. (Dr.) Gautam Majumdar
Ex-Professor of Mechanical Engineering
Jadavpur University/Kol-32

2. _____

Nisantika Biswas

DR. NISANTIKA BISWAS
Assistant Professor
Department of Mechanical Engineering
Academy of Technology
Hoogly- 712121

3. _____

Subhasish Sarkar

Dr. SUBHASISH SARKAR
Assistant Engineer-I
Electrical Division, PHE
Govt. of West Bengal

JADAVPUR UNIVERSITY

FACULTY OF ENGINEERING & TECHNOLOGY

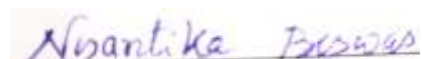
CERTIFICATE FROM THE SUPERVISOR/S

This is to certify that the thesis entitled **Computation and Characterization of Powder Mixed Electric Discharge Machining on Nickel Based Alloy (Inconel) and Titanium Grade 2** submitted by Sri. Sovan Bhowmick, who got his name registered on 03.05.2018 for the award of Ph.D. (Engineering) degree of Jadavpur University is absolutely based upon his own work under the supervision of Prof. (Dr.) Gautam Majumdar, Dr. Nisantika Biswas and Dr. Subhasish Sarkar and that neither his thesis nor any part of the thesis has been submitted for any degree/ diploma or any other academic award anywhere before.

 22/04/2025

Prof. (Dr.) Gautam Majumdar
Ex-Professor of Mechanical Engineering
Jadavpur University/Kol-32

.....
1. Signature of the Supervisor with
Date and Office Seal

 22/04/2025

DR. NISANTIKA BISWAS
Assistant Professor
Department of Mechanical Engineering
Academy of Technology
Hoogly- 712121

.....
2. Signature of the Supervisor with
Date and Office Seal

 22/04/2025

Dr. SUBHASISH SARKAR
Assistant Engineer-I
Electrical Division, PHE
Govt. of West Bengal

.....
3. Signature of the Supervisor with
Date and Office Seal

ACKNOWLEDGEMENT

The present work has been carried out under the supervision of **Prof. (Dr.) Gautam Majumdar** of Mechanical Engineering, Jadavpur University, Kolkata, India. I shall remain forever grateful to my supervisor for his guidance and valuable suggestions during the experimental and computational work. I am very thankful to Gautam Majumdar, sir; without his inspiration, it would have been impossible to do Ph.D. work. I offer my sincere thanks to my guide, **Dr. Subhasish Sarkar**, Co-Supervisor of my PhD work, whose technical, mental and all kinds of inspiring support helped me to accomplish this work. Again, I sincerely thank my Co-Supervisor, **Dr. Nisantika Biswas**, for helping me in all technical and other support. My sincere thanks to **Prof. Buddhadeb Oraon** and **Prof. Rajat Subhra Sen** for constantly motivating me in this work.

I am heartily thankful to the late **Prof. Ashish Bandyopadhyay**, who guided me at the beginning of my PhD journey by giving me the idea of the work and helped me a lot to formulate the problem for my research work. I would not be successful without the blessings of Sir.

The experimental work has been carried out at the Advanced Manufacturing Technology Lab, Department of Mechanical Engineering, Heritage Institute of Technology. I am thankful to **Prof. Sukanta Sarkar**, HOD, Department of Mechanical Engineering, Heritage Institute of Technology. The responses of this work have been measured from the Metrology and Measurements Lab and the Surface Engineering Lab, Department of Mechanical Engineering, Jadavpur University. I am therefore thankful to all the laboratory assistants of those labs.

The characterizations have been conducted in academic institutions like the Centre of Excellence, NIT Durgapur for using the SEM, EDAX and XRD analysis. I am really thankful to **Mr. Sambhu Sarkar**, Lab Assistant, Centre of Excellence, NIT Durgapur. Some of the characterizations have been performed at the SN Bose Innovation Centre, University of Kalyani, CRNN, Calcutta University and Department of Physics, IISER Kolkata. I am really grateful to **Ms. Debismita Naik** for her support to perform AFM work in IISER Kolkata. I offer my sincere thanks to **Mr. Dipayan Sen** of University of Kalyani and **Mr. Pratush Saha** of CRNN.

I am thankful to my friends and colleagues **Mr. Sudipta Roy, Dr. Pritam Ghosh, Dr. Arup Jyoti Bhowal, Dr. Sumanta Banerjee** and **Dr. Manik Barman** for their encouragement and help for the completion of this work. Special thanks to **Mr. Sudipta Roy** for motivating me throughout my PhD journey.

I would like to thank my junior friends **Rupam Mandal, Binod Barai, Vikash Kumar, Chandrasekhar Routela** and my senior **Mr. Biplab Baran Mandal** and others who helped me a lot in the research work throughout this period. I am thankful to **Mr. Rupam Mandal**, whose endless support in my PhD research work made this successful. Without his contribution, it is almost impracticable to complete the work

I am also grateful to **Mr. Anupam Biswas, Mr. Rajib Khan, Mr. Monoj Chatterjee, Mrs. Moumita Koley, Mr. Suprotim Chakroborty, Mr. Subham Jana** and other TAs of the Department of Mechanical Engineering, Heritage Institute of Technology, for their endless support in constructing the setup of PMEDM.

I am also thankful to Indian Railways and other transport organizations for providing me with economical and quality service by which I have reached the destination to do all my necessary work.

Now, I would like to thank my father, **Mr. Bimal Bhowmick**, my mother, **Mrs. Bisnupriya Bhowmick**, my brother, **Mr. Sourav Bhowmick**, my father-in-law, **Mr. R. C. Malakar**, my mother-in-law **Mrs. Sampa Malakar** and my sister in law, **Ms. Rikta Malakar**, for their support in this journey.

Finally, I would like to thank my wife, **Mrs. Riya Malakar**, for her continuous support in pursuing this research.


SOVAN BHOWMICK

Date: 22/04/2025

Place: Kolkata

INDEX

Sl. No.	Description	Page No.
	List of Publications	i
	Statement of Originality	iii
	Certificate from supervisors	iv
	Acknowledgement	v
	Index	vii
	List of Figures	xi
	List of Tables	xvi
	Abstract	xviii
Chapter 1	Introduction	1
1.1	Introduction	2
1.2	Description of Electric Discharge Machining	3
1.3	Set up and material removal mechanism for material removal for the powder mixed electric discharge mechanism	4
1.4	Types of EDM	6
1.5	Advantages and Disadvantages of PMEDM	7
1.6	Application of EDM	7
Chapter 2	Literature Review and Objective of the Present Work	9
2	Literature survey	10
2.1	Effect of Process Parameters	10
2.2	Application of Mathematical Model	12
2.3	Surface Characterization of the machined sample	14
2.4	Formulation of the Objectives	16
Chapter 3	Materials, Experimental Methods and Computation Techniques	18
3	Introduction	19
3.1	Experimental setup	19
3.3	Selection of workpiece and powder material	20
3.3.1	Selection of powder and workpiece material for titanium mixed EDM	20
3.3.2	Selection of work material for graphite mixed EDM	22
3.4	Selection of Tool Material	24
3.5	Selection of input parameters and responses for titanium mixed EDM	25
3.6	Selection of input parameters and responses for graphite mixed EDM	26
3.7	Measurement of responses in titanium mixed EDM	27
3.8	Measurement of responses in graphite mixed EDM	28
3.9	Methodology of experiments	29
3.10	Analysis of variance (ANOVA)	30
3.11	Fuzzy logic used in Inconel 718 machining	30
3.12	Mathematical model using artificial neural network used in Inconel 625 machining	31

3.13	Desirability function based multi objective optimization	33
3.14	Surface characterization using field effect scanning electron microscopy (FESEM)	34
3.15	Elemental analysis by energy dispersive X-ray analysis (EDX)	35
3.16	X-ray diffraction (XRD) characteristics of EDM sample	35
3.17	Atomic force microscopy (AFM) analysis for measuring surface roughness	36
	Research plan of studying titanium and graphite added electric discharge machining	38
Chapter 4	Effect of titanium mixed EDM on MRR with Surface Roughness of Inconel 718 and Titanium Grade 2	39
4.1	Introduction	40
4.2	Effect of titanium mixed EDM on Inconel 718	40
4.2.1	Effect of input parameters on MRR	42
4.2.2	Effect of input parameters on SR	43
4.2.3	ANOVA of MRR and Surface roughness	44
4.2.4	Multi variable regression analysis of MRR and Surface roughness	47
4.2.5	Normal Probability Plot of MRR and Surface roughness	47
4.3.6	3D Surface Plot for MRR and Surface roughness	49
4.3	Effect of titanium mixed EDM on Titanium Grade 2	52
4.3.1	Effect of input parameters on MRR	55
4.3.2	Effect of input parameters on SR	56
4.3.3	ANOVA of MRR and Surface roughness	57
4.3.4	Multi variable regression analysis of MRR and Surface roughness	59
4.3.5	Normal Probability Plot of MRR and Surface roughness	60
4.3.6	3D Surface Plot for MRR and Surface roughness	61
4.4	Comparison between MRR and surface roughness of Inconel 718 and Titanium grade 2 machining	65
Chapter 5	Effect of graphite mixed EDM on MRR, Tool wear rate and Surface Roughness of Inconel 625 and Titanium Grade 2	67
5.1	Introduction	68
5.2	Effect of graphite mixed EDM on Inconel 625	68
5.2.1	Effect of input parameters on MRR	70
5.2.2	Effect of input parameters on TWR	71
5.2.3	Effect of input parameters on SR	72
5.2.4	ANOVA of MRR, TWR and Surface Roughness	73
5.2.5	Multi variable regression analysis of MRR and Surface roughness	77
5.2.6	Normal Probability Plot of MRR, TWR and Surface roughness	78
5.2.7	3D Surface Plot for MRR, TWR and Surface roughness	78
5.3	Effect of graphite mixed EDM on Titanium Grade 2	82
5.3.1	Effect of input parameters on MRR	82
5.3.2	Effect of input parameters on TWR	85
5.3.3	Effect of input parameters on SR	87
5.3.4	ANOVA of MRR, TWR and Surface Roughness	88
5.3.5	Multi variable regression analysis of MRR and Surface roughness	91
5.3.6	Normal Probability Plot of MRR, TWR and Surface roughness	93
5.3.7	3D Surface Plot for MRR, TWR and Surface roughness	94
5.4	Comparison between MRR, TWR and surface roughness between Inconel 625 and Titanium grade 2 machining	97

Chapter 6	Mathematical Modelling with Fuzzy logic, Artificial Neural Network and Multi Response Optimization	100
6.1	Introduction	101
6.2	Mamdani based fuzzy logic for modelling of Inconel 718 processing using titanium mixed EDM	101
6.2.1	Formulation of fuzzy model	101
6.2.2	Error and accuracy of the fuzzy model	104
6.3	Desirability function based optimization for Inconel 718 processing using titanium mixed EDM	105
6.3.1	Result of optimization	106
6.3.2	Confirmatory test result	106
6.4	Desirability function based optimization for Titanium Grade 2 processing using titanium mixed EDM	107
6.4.1	Result of optimization	107
6.4.2	Confirmatory test result	107
6.5	Back propagation type Neural Network for Inconel 625 processing using titanium mixed EDM	110
6.6	Desirability function based optimization for Inconel 625 processing using graphite mixed EDM	115
6.6.1	Result of optimization	115
6.6.2	Confirmatory test result	116
6.7	Desirability function based optimization for Titanium Grade 2 processing using graphite mixed EDM	117
6.7.1	Result of optimization	117
6.7.2	Confirmatory test result	118
Chapter 7	Surface characterization of titanium and graphite mixed EDM samples	121
7.1	Introduction	122
7.2	Characterization of Inconel 718 and Titanium grade 2 surface machined with titanium mixed EDM	122
7.2.1	Study of surface morphology of Inconel 718 using scanning electron microscopy	122
7.2.2	Elemental analysis of Inconel 718 using EDX	125
7.2.3	Study of surface morphology of Titanium grade 2 using scanning electron microscopy	126
7.2.4	Elemental analysis of Titanium grade 2 using EDX	129
7.3	Characterization of Inconel 625 and Titanium grade 2 surface machined with graphite mixed EDM	129
7.3.1	AFM study of Inconel 625 surface	131
7.3.2	Study of surface morphology of Inconel 625 using scanning electron microscopy	132
7.3.3	Analysis of the XRD pattern of the Inconel 625 surface	133
7.3.4	AFM study of Titanium Grade 2 surface	136
7.3.5	Study of surface morphology of Titanium Grade 2 using scanning electron microscopy	136
7.3.6	Analysis of XRD pattern of the Titanium Grade 2 surface	139
Chapter 8	Conclusion and Future Scope of Work	141
	References	146

List of Figures

Figure No.	Description	Page No.
Fig. 1.1.	Schematic diagram of a typical setup of electric discharge machine	3
Fig. 1.2.	Powder mixed in dielectric fluid	4
Fig. 1.3.	Particle bridging during discharge	5
Fig. 1.4.	Ionisation of particles during electric discharge	5
Fig. 1.5.	Schematic diagram to differentiate die sinking EDM and Wire EDM	6
Fig. 3.1.	Schematic view of the experimental setup of PMEDM	19
Fig. 3.2.	Photographic view of experimental setup of powder mixed EDM	20
Fig. 3.3.	Photographic view of Inconel 718 machined by titanium mixed EDM	22
Fig. 3.4.	Construction of (a) RSM-CCD and (b) RSM-BBD design	26
Fig. 3.5.	The photographic view of Talysurf instrument.	27
Fig. 3.6.	The photographic view of weighing machine of accuracy 0.0001 g.	28
Fig. 3.7.	Three layer based neural network for predicting the responses	31
Fig. 3.8.	The photographic view of (a) FESEM with EDX and (b) SEM with EDX setup	34
Fig. 3.9.	The photographic view of XRD setup	36
Fig. 3.10	Photographic view of AFM setup.	36
Fig. 3.11.	Research planning of titanium and graphite mixed EDM	37
Fig. 4.1.	Main effects plot for MRR of Inconel 718 machined by titanium mixed EDM	43
Fig. 4.2.	Main effects plot for Surface Roughness of Inconel 718 machined by titanium mixed EDM	44
Fig. 4.3.	Normal probability plot of residuals for MRR of Inconel 718	48
Fig. 4.4.	Normal probability plot of residuals for Surface Roughness of Inconel 718	48
Fig. 4.5.	Surface plots of MRR with the interaction of powder concentration and pulse current during the machining of Inconel 718	49
Fig. 4.6.	Surface plots of MRR with the interaction of powder concentration and gap voltage during the machining of Inconel 718	50
Fig. 4.7.	Surface plots of MRR with the interaction of pulse current and gap voltage during the machining of Inconel 718	50
Fig. 4.8.	Surface plots of surface roughness with the interaction of powder concentration and pulse current during the machining of Inconel 718	51
Fig. 4.9.	Surface plots of surface roughness with the interaction of powder concentration and gap voltage during the machining of Inconel 718	51

Fig. 4.10.	Surface plots of MRR with the interaction of powder concentration and gap voltage during the machining of Inconel 718	52
Fig. 4.11.	Main effects plot for MRR of Titanium Grade 2 machined by titanium mixed EDM	55
Fig. 4.12.	Main effects plot for Surface Roughness of Titanium Grade 2 machined by titanium mixed EDM	56
Fig. 4.13.	Normal probability plot of residuals for MRR of Titanium Grade 2	60
Fig. 4.14.	Normal probability plot of residuals for Surface Roughness of Titanium Grade 2	61
Fig. 4.15.	Surface plots of MRR with the interaction of powder concentration and pulse current during the machining of Titanium Grade 2	62
Fig. 4.16.	Surface plots of MRR with the interaction of powder concentration and gap voltage during the machining of Titanium Grade 2	62
Fig. 4.17.	Surface plots of MRR with the interaction of pulse current and gap voltage during the machining of Titanium Grade 2	63
Fig. 4.18.	Surface plots of surface roughness with the interaction of powder concentration and pulse current during the machining of Titanium Grade 2	63
Fig. 4.19.	Surface plots of surface roughness with the interaction of powder concentration and gap voltage during the machining of Titanium Grade 2	64
Fig. 4.20.	Surface plots of MRR with the interaction of powder concentration and gap voltage during the machining of Titanium Grade 2	64
Fig. 4.21.	Comparison between MRR of Inconel 718 and Titanium grade 2 against (a) powder concentration (b) current and (c) gap voltage	65
Fig. 4.22.	Comparison between MRR of Inconel 718 and Titanium grade 2 against (a) powder concentration (b) current and (c) gap voltage	66
Fig. 5.1.	Main effects plot for MRR of Inconel 625 machined by graphite mixed EDM	70
Fig. 5.2.	Main effects plot for TWR of Inconel 625 machined by graphite mixed EDM	71
Fig. 5.3.	Main effects plot for Surface Roughness of Inconel 625 machined by graphite mixed EDM	73
Fig. 5.4.	Normal probability plot of residuals for MRR of Inconel 625	78
Fig. 5.5.	Normal probability plot of residuals for TWR of Inconel 625	79
Fig. 5.6.	Normal probability plot of residuals for SR of Inconel 625	79
Fig. 5.7.	Surface plots of MRR with the interaction of (a) powder concentration and pulse current (b) Powder concentration and mesh size and (c) Current and powder mesh size during the machining of Inconel 625	80
Fig. 5.8.	Surface plots of TWR with the interaction of (a) powder concentration and pulse current (b) Powder concentration and	81

Fig. 5.9.	mesh size and (c) Current and powder mesh size during the machining of Inconel 625 Surface plots of SR with the interaction of (a) powder concentration and pulse current (b) Powder concentration and mesh size and (c) Current and powder mesh size during the machining of Inconel 625	82
Fig. 5.10.	Main effects plot for MRR of Inconel 625 machined by graphite mixed EDM	85
Fig. 5.11.	Main effects plot for TWR of Inconel 625 machined by graphite mixed EDM	86
Fig. 5.12.	Main effects plot for Surface Roughness of Inconel 625 machined by graphite mixed EDM	87
Fig. 5.13.	Normal probability plot of residuals for MRR of Titanium grade 2	92
Fig. 5.14.	Normal probability plot of residuals for TWR of Titanium grade 2	93
Fig. 5.15.	Normal probability plot of residuals for SR of Titanium grade 2	93
Fig. 5.16.	Surface plots of MRR with the interaction of (a) powder concentration and current (b) Powder concentration and mesh size and (c) Current and powder mesh size during the machining of Titanium Grade 2	94
Fig. 5.17.	Surface plots of TWR with the interaction of (a) powder concentration and current (b) Powder concentration and mesh size and (c) Current and powder mesh size during the machining of Titanium Grade 2	95
Fig. 5.18.	Surface plots of SR with the interaction of (a) powder concentration and current (b) Powder concentration and mesh size and (c) Current and powder mesh size during the machining of Titanium Grade 2	96
Fig. 5.19.	Comparison between MRR of Inconel 625 and Titanium grade 2 against (a) current (b) powder concentration	97
Fig. 5.20.	Comparison between TWR of Inconel 625 and Titanium grade 2 against (a) current (b) powder concentration	97
Fig. 5.21.	Comparison between surface roughness of Inconel 625 and Titanium grade 2 against (a) current (b) powder concentration	98
Fig. 6.1.	Fuzzy inference system for PMEDM.	101
Fig. 6.2.	Membership function for input parameters (a) powder concentration (b) Pulse current (c) gap voltage and (d) pulse on time (e) pulse off time	103
Fig. 6.3.	Fuzzy membership function for responses (a) MRR and (b) surface roughness	103
Fig. 6.4.	Comparison of fuzzy predicted results with the experimental result for (a) MRR and (b) surface roughness	104
Fig. 6.5.	Rule viewer for the fuzzy predicted value of response at optimized condition	105
Fig. 6.6.	Desirability function approach of optimizing the Inconel 718 machined by titanium based EDM	106
Fig. 6.7.	Bar diagram for comparison between the optimized result and confirmatory test result for Inconel 718 machined by titanium mixed EDM	108

Fig. 6.8.	Desirability function approach of optimizing Titanium grade 2 machined by titanium mixed EDM	109
Fig. 6.9.	Bar diagram for comparison between the RSM model and confirmatory test result of Titanium grade 2 machined by titanium mixed EDM	110
Fig. 6.10.	Comparison of ANN result and actual result for tested data of (a) MRR, (b) TWR and (c) SR	113
Fig. 6.11.	R- Values of the ANN model	114
Fig. 6.12.	Epoch vs MSE plot during the training of the network	114
Fig. 6.13.	Result of multi objective optimization by desirability function approach of Inconel 625 machined by graphite mixed EDM	116
Fig. 6.14.	Bar diagram for comparison between the optimized result and confirmatory test result of Inconel 625 machined by graphite mixed EDM	118
Fig. 6.15.	Result of multi objective optimization by desirability function approach of Titanium grade 2 machined by graphite mixed EDM	119
Fig. 6.16.	Bar diagram for comparison between the optimized and confirmatory test results of Titanium grade 2 machined by graphite mixed EDM	120
Fig. 7.1.	SEM micrography of Inconel 718 surface machined by titanium mixed EDM with powder concentration 2 g/l at the magnification of (a) 500× (b) 2000×	123
Fig. 7.2.	SEM micrography of Inconel 718 surface machined by titanium mixed EDM with powder concentration 5 g/l at the magnification of (a) 500× (b) 2000×	123
Fig. 7.3.	SEM micrography of Inconel 718 surface machined by titanium mixed EDM with powder concentration 8 g/l at the magnification of (a) 500× (b) 2000×	124
Fig. 7.4.	SEM micrography of optimized Inconel 718 surface machined by titanium mixed EDM at the magnification of (a) 500× (b) 2000×	124
Fig. 7.5.	EDX analysis of Inconel 718 surface machined by titanium mixed EDM with powder concentration 8 g/l.	125
Fig. 7.6.	SEM micrography of Titanium Grade 2 surface machined by titanium mixed EDM with powder concentration 2 g/l at the magnification of (a) 500× (b) 2000×	126
Fig. 7.7.	SEM micrography of Titanium Grade 2 surface machined by titanium mixed EDM with powder concentration 5 g/l at the magnification of (a) 500× (b) 2000×	127
Fig. 7.8.	SEM micrography of Titanium Grade 2 surface machined by titanium mixed EDM with powder concentration 8 g/l at the magnification of (a) 500× (b) 2000×	127
Fig. 7.9.	EDX analysis of Titanium Grade 2 surface machined by titanium mixed EDM with powder concentration 8 g/l	128
Fig. 7.10.	AFM analysis of Inconel 625 sample machined by graphite mixed EDM at currents of (a) 4 A (b) 8 A and (c) 12 A	129
Fig. 7.11.	SEM micrography of Inconel 625 surface machined by graphite mixed EDM with powder concentration 2 g/l at the magnification of (a) 500× (b) 5000×	130

Fig. 7.12.	SEM micrography of Inconel 625 surface machined by graphite mixed EDM with powder concentration 5 g/l at the magnification of (a) 500× (b) 5000×	131
Fig. 7.13.	SEM micrography of Inconel 625 surface machined by graphite mixed EDM with powder concentration 8 g/l at the magnification of (a) 500× (b) 5000×	132
Fig. 7.14.	XRD patterns of Inconel 625 surface machined by graphite mixed EDM at the currents of 4 A, 8 A, 12 A with (a) complete view of all the planes (b) enlarged view of (111) plane	132
Fig. 7.15.	AFM analysis of Titanium Grade 2 sample machined by graphite mixed EDM at currents of (a) 4 A (b) 8 A and (c) 12 A	134
Fig. 7.16.	SEM micrography of Titanium Grade 2 surface machined by graphite mixed EDM with powder concentration 2 g/l at the magnification of (a) 500× (b) 7500×	135
Fig. 7.17.	SEM micrography of Titanium Grade 2 surface machined by graphite mixed EDM with powder concentration 5 g/l at the magnification of (a) 500× (b) 7500×	138
Fig. 7.18.	SEM micrography of Titanium Grade 2 surface machined by graphite mixed EDM with powder concentration 8 g/l at the magnification of (a) 500× (b) 7500×	138
Fig. 7.19.	XRD patterns of Titanium Grade 2 surface machined by graphite mixed EDM at the current of 4 A, 8 A, 12 A	139

List of Tables

Table No.	Description	Page No.
Table 1.1	Applications of EDM	8
Table 3.1	Composition of Inconel 718	21
Table 3.2	Mechanical, Thermal and Electrical Properties of Inconel 718	21
Table 3.3	Mechanical, electrical and thermal properties of titanium powder	22
Table 3.4	Composition of Titanium Grade 2	23
Table 3.5	Properties of Titanium Grade 2	23
Table 3.6	Alloying element percentage of Inconel 625	23
Table 3.7	Properties of Inconel 625	24
Table 3.8	Properties of graphite powder	24
Table 3.9	Mechanical, electrical and thermal properties of copper	25
Table 3.10	Input parameters and their levels for titanium mixed EDM	25
Table 3.11	Input parameters with their levels for graphite mixed EDM	26
Table 4.1	Experimental result for MRR and surface roughness of Inconel 718 machined by titanium mixed EDM	40
Table 4.2	ANOVA result for MRR of Inconel 718 machined by titanium mixed EDM	45
Table 4.3	ANOVA result for Surface Roughness of Inconel 718 machined by titanium mixed EDM	46
Table 4.4	Experimental result for MRR and surface roughness of Titanium Grade 2 machined by titanium mixed EDM	53
Table 4.5	ANOVA result for MRR of Titanium Grade 2 machined by titanium mixed EDM	57
Table 4.6	ANOVA result for Surface Roughness of Titanium Grade 2 machined by titanium mixed EDM	58
Table 5.1	Experimental result for MRR, TWR and surface roughness of Inconel 625 machined by graphite mixed EDM	68
Table 5.2	ANOVA result for MRR of Inconel 625 machined by graphite mixed EDM	74
Table 5.3	ANOVA result for TWR of Inconel 625 machined by graphite mixed EDM	75
Table 5.4	ANOVA result for SR of Inconel 625 machined by graphite mixed EDM	76
Table 5.5	Experimental result for MRR, TWR and surface roughness of Titanium Grade 2 machined by graphite mixed EDM	83
Table 5.6	ANOVA result for MRR of Titanium Grade 2 machined by graphite mixed EDM	88
Table 5.7	ANOVA result for TWR of Titanium Grade 2 machined by graphite mixed EDM	89
Table 5.8	ANOVA result for SR of Titanium Grade 2 machined by graphite mixed EDM	90
Table 6.1	Parameter values of fuzzy membership functions of input parameters.	102
Table 6.2	Parameter values of fuzzy membership functions of responses	102
Table 6.3	Desirability function based optimization of Inconel 718 machined by titanium mixed EDM.	107

Table 6.4	Comparison between optimized result and confirmatory test result of Inconel 718 machined by titanium mixed EDM.	108
Table 6.5	Multi-objective optimization using the desirability function of Titanium grade 2 machine by titanium mixed EDM	109
Table 6.6	Comparison between optimized result and confirmatory test result of Titanium grade 2 machined by titanium mixed EDM.	110
Table 6.7	Predicted result of MRR, TWR and SR using ANN	111
Table 6.8	Result of multi objective optimization using desirability function of Inconel 625 machined by graphite mixed EDM	117
Table 6.9	Comparison between optimized result and confirmatory test result of Inconel 625 machined by graphite mixed EDM	117
Table 6.10	Result of multi objective optimization using desirability function of Titanium grade 2 machined by graphite mixed EDM	119
Table 6.11	Comparison between optimized result and confirmatory test result of Titanium grade 2 machined by graphite mixed EDM	120

Abstract

Powder mixed electric discharge machining (PMEDM) is an advanced version of the ordinary electric discharge machining (EDM) process. Ordinary EDM is a non-conventional machining process in which material is removed by melting, vapourization and flushing of dielectric fluid. The application of high energy electric discharge transfers a large amount of heat to the workpiece material under the die-electric fluid medium to melt and vaporise the material from the surface. This is an efficient machining process in which hard material can be easily machined with different peripheral shapes of the machining surface. However, the major disadvantages of the process are a very low material removal rate (MRR) and worse surface quality compared to other machining process.

In powder mixed EDM, electrically conductive micro powder materials have been added to the dielectric fluid and a homogeneous mixture of fluid is applied before machining. During machining, the powder particles get electrically induced and start discharging along with the main spark. This process is called local discharge which removes materials additionally from every point of the surface. The removal of excess material from the workpiece helps to improve the MRR. Along with that the application of the powder particles provides uniform distribution of thermal energy in the form of a local spark which improves the surface quality by reducing the roughness. The tool wear is also prevented slightly by increasing the powder particles. Nevertheless, it can be well said that the quality of the machining enhances with the application of conductive micro particles.

The EDM is classified into two types. One is die sinking EDM which is used to produce high precision dies, moulds, fixtures, tools, etc. It is also used to produce an arbitrary-shaped hole on the surface of difficult-to-machine materials. This machining is also used to manufacture surgical instruments, components of aeroplanes, defence equipment and many more. Normally, the powder particles are applied to die sinking EDM for the manufacturing of a high precision moulding process. Along with that, PMEDM is now being used for coating on hard materials and super alloys. The other type of EDM is wire EDM which has extensive use of cutting gears, cams and other components. It is also used to cut a large plate of difficult to machined material precisely and without making a large amount of waste.

In the present study, titanium and graphite micro powders have been selected as powder material and their effect have been investigated on Inconel 718, Inconel 625 and Titanium grade 2. Along with that a comparative study has been made between Inconel 718 with Titanium grade 2 and Inconel 625 with Titanium grade 2. The objectives of the present research work are given below.

- The effects of responses have been investigated and analyzed for machining of titanium mixed EDM and graphite mixed EDM.
- The ANOVA and regression analysis have been performed to find the significant parameters and the relation of responses with process parameters respectively for both the powders.
- Mamdani based fuzzy logic and back propagation neural network have been developed and checked their acceptance has been checked for titanium mixed EDM and graphite mixed EDM respectively.
- Desirability approach based multi objective optimization has been performed to find the optimal setting of process parameters and validated with a confirmatory test result.
- Surface morphology has been studied where the distribution of recast layers and measurement of the width of the surface have been represented.
- Elemental analysis of titanium mixed EDM by EDX analysis and AFM study of surface roughness and XRD analysis to study the change of phase for graphite mixed EDM have been done in this experimental study.

Chapter 1 illustrates the introduction of the powder mixed EDM, types of EDM, mechanism of material removal and application of EDM.

In Chapter 2, a detailed discussion of the previous researches has been done regarding the processes, statistical methods, optimization techniques, mechanical and metallurgical characterization and elemental analysis. From the detailed literature review, it has been observed that the effects of titanium and graphite powder on two significant material i.e. Inconel and Titanium have not been analyzed earlier. Therefore, the objective of the present study based on this research gap.

Chapter 3 discusses about the materials with their compositions and properties, experimental setup, detail methodology, design of experiments, mathematical modelling, optimization techniques and characterization.

Chapter 4 represents the variation of MRR and surface roughness which have been investigated on Inconel 718 and Titanium grade 2 after the machining of titanium mixed EDM. The main effects

plots, ANOVA and Regression equations have been discussed for both the results of Inconel 718 and Titanium grade 2.

In Chapter 5, the study of the effects of MRR, tool wear rate and surface roughness has been represented for Inconel 625 and Titanium grade 2.

Chapter 6 illustrates the analysis of mamdini based fuzzy logic formulated on the experimental data of Inconel 718 and backpropagation type neural network formulated on the experimental data of Inconel 625. Along with that, Desirability approach based optimization techniques have been applied to all the results and compared with the confirmatory test results.

Chapter 7 compares the surface morphological characteristics of three samples from each of the experiments. Along with that, elemental analysis for titanium mixed EDM and AFM and XRD analysis for graphite mixed EDM have been discussed.

Chapter 8 concludes the research work and discusses the future scope of the present work.

Date: 22/04/2025

Sovan Bhowmick

Sovan Bhowmick

Chapter 1

Introduction

1.1. Introduction

In recent days, unconventional machining processes are playing an important role in machine shops for processing the difficult to machine materials like ferrous alloys, non-ferrous super alloys, ceramics, carbides, titanium and many more. The increasing demands for processing of material with high accuracy and precision, complex geometry and optimized production rate boost to advance the machining processes. Electric discharge machining (EDM) is such an unconventional, contactless machining process in which the material is taken out by thermal erosion occurred when a series of high energy spark impinges successively on the surface [1]. The material is melted and vapourized at large temperature generated by the spark [2]. EDM is commonly used to make dies and cut the material plate and blocks into desired shape. In the electric discharge machining, materials having extreme hardness and uneconomical machinability like tool steel, stainless steel and high carbon steel in conventional machining processes are normally machined.

One of the advancements has been made by applying micro particles in dielectric fluid called powder mixed dielectric machining. The common EDM associates with an electrode having a servo control device, power supply, work fixture and a dielectric tank full of dielectric fluid. In PMEDM, small particles of micro or nano range have been added with dielectric fluid and stirred thoroughly to make a homogeneous mixture. During the machining processes, the particles present in the spark gap i.e. the gap between the electrode and workpiece also discharge the local spark along with the main spark. The additional spark increases the material removal rate, the surface uniformity and decreases the tool wear rate. There are large number of input parameters which influence the machining characteristics in powder added electric discharge machining. The application of powder mixed electric discharge machining is still limited. Very few die manufacturing industries in their limited capacity use this process. However, continuous modifications have been incorporating in this process through sound research and development to introduce the setup in large scale in industrial application.

For rapid and sustainable development of a society, one of the important ingredients is to develop and process the new materials. In earlier days, the most useful materials were ferrous alloys like mild steel, high carbon steel, stainless steel etc. and wood. With the need of the present time, materials have been evolved and the importance of the materials having superior strength, hardness and toughness with less weight and corrosion rate are increasing sharply. Inconel and Titanium are the two materials which have the above properties and they are used

largely in industrial sector. Inconel is nickel based super alloy having high strength, hardness and red hardness and low corrosion rate. Titanium is a metal having all the similar properties except the low density and high hardness compared to Inconel. Inconel is commonly used in aerospace, nuclear reactors, marine engineering etc. and titanium is used in medical science, defence, automobile sector and many other areas.

1.2. Description of electric discharge machining

In this process, powerful electric sparks are generated which provide thermal erosion at elevated temperature of the work surface. Fig. 1.1 represents the setup of electric discharge machine. In this process, an electrically conductive tool of a particular shape is kept near the workpiece under dielectric fluid medium. Both the tool and workpiece are energized by DC pulsating electric energy at standard voltage and high current. After putting electrical potential in tool and workpiece and if their potential difference overcomes the work function of tool material, the tool starts discharging electrons towards the workpiece. The electrons at a half to three fourth speed of light collide with air particles and make a thin plasma channel. Through that plasma channel, a larger number of electrons pass through and strike the workpiece.

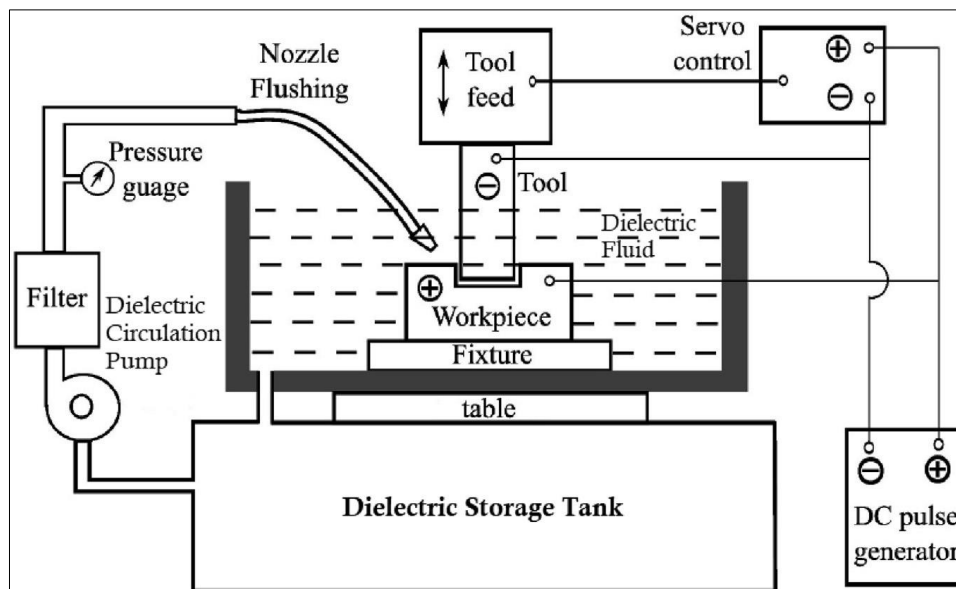


Fig. 1.1. Schematic diagram of a typical setup of electric discharge machine [1].

The application of high speed electrons collide over the workpiece and heat is transferred from the kinetic energy of the electrons. The ionised plasma column incidents over the surface, the temperature reaches to 9000°C to 19000°C . At such a high temperature the material melts and evaporated. The pulse is provided in a very short length of time. After that it is shut down and restarted after a certain amount of time. During the off period, the materials which gets melted

and vapourized become solid particles and are flushed away by the flow of flushing nozzle. In this way the material has been removed from the work surface.

1.3. Setup and material removal mechanism for powder mixed electric discharge mechanism

One of the developments of electric discharge machining has been performed by adding conductive microparticles in dielectric fluid and applying them in this process. When the electric field is applied the powder particles arrange themselves in a series of long chains between electrode and workpiece as shown in Fig. 1.2. The particles are also induced electrically which is sufficient to produce discharge and contribute to the plasma column. Fig. 1.3 represents the steps which have been governed during the sparking. At first, the particles are arranged in a bridge between electrode and workpiece. At this time the particles are also charged. According to Fig. 1.4 particles are ionized and accumulation of charges takes place in two different sides of it.

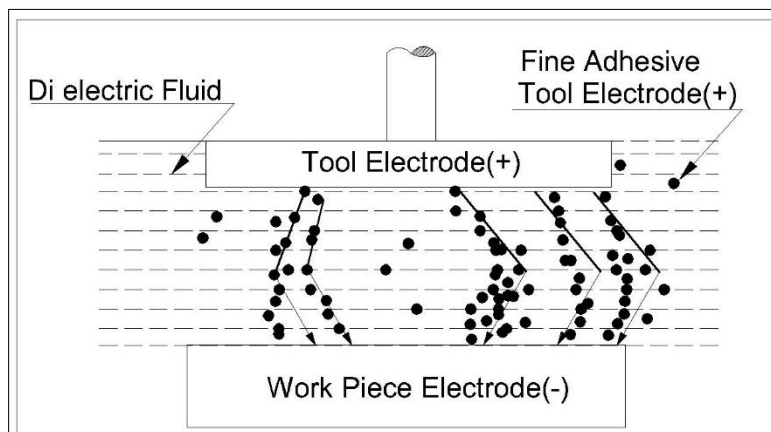


Fig. 1.2. Powder mixed in dielectric fluid.

When the energy of the pulsating current is at the peak level main spark started and the chain of particles breaks to make a gap between them. Due to this, an explosion takes place which contribute the local sparks toward workpiece surface. During this time, the particles disturbed and goes into zig-zag motion and pulse off time comes. When the pulse started again, the bridge formation takes place further and starts the nest cycle. In this way, the particles discharges electrons by the induction of main electrode and provide the local spark along with the main spark. The effect of this discharging provides a great impact in the machining characteristics. Due to the formation of bridge the spark gap of the machining increases. Normally increase of spark gap causes unstable arc, but in this case a stable arc is produced by the help of particle discharges. During conventional EDM, a very less amount of total energy emitting from the

electrode is used. But in PMEDM, the unused energy is converted into used energy by the powder particles. The basic advantage of this method is to utilize additional energy which helps to remove more material from the surface. In this way, material removal as well as production rate is amplified.

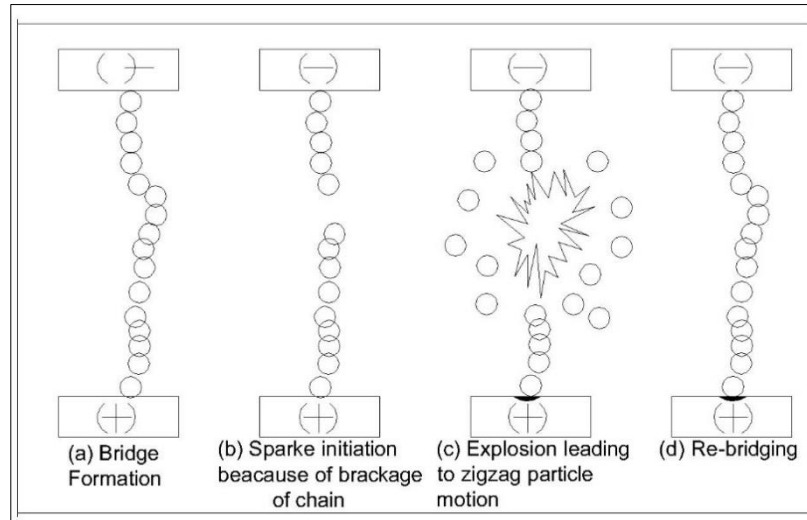


Fig. 1.3. Particle bridging during discharge.

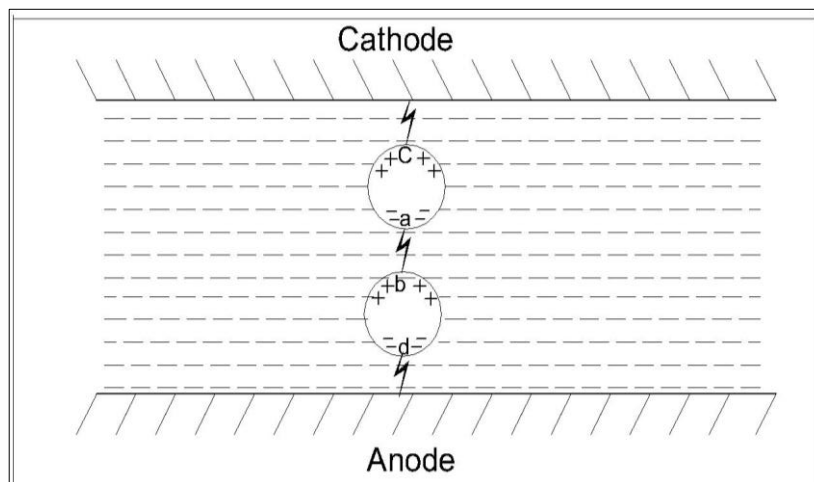


Fig. 1.4. Ionisation of particles during electric discharge.

Further, the use of local sparks and enhanced stable spark gap make increases the surface quality compared to the normal EDM. The basic disadvantage of this process is to separate the powder particles from the dielectric at the end of the machining and maintaining homogeneous mixture of the dielectric fluid solution during machining.

1.4. Types of EDM

There are two types of electric discharge machines. Such as die sinker type which is normally used for making holes and contours and wire cut machine for cutting the workpiece into particular shape.

In die sinker EDM, a solid metallic rod is used as electrode whose tip is manufactured according to the die to be manufactured. The electrode may be of an integral part of the design or the shape may be attached to the rod. The rod is further attached to the machine's electrical circuit with servo controlled device. The electrical circuit energizes the tool electrode and the servo control device provides the necessary feed motion to make the die impression on the workpiece. In this process, the whole impression is normally immersed in the dielectric fluid. The machining can be performed normally on the external surface but internal machining is also possible. The die sinker EDM is normally used heavily in the manufacturing of dies in factory for different works. Along with that, for making impression on the metallic surface this method is also used in automobile and aerospace industries. This work has been performed in die sinker EDM.

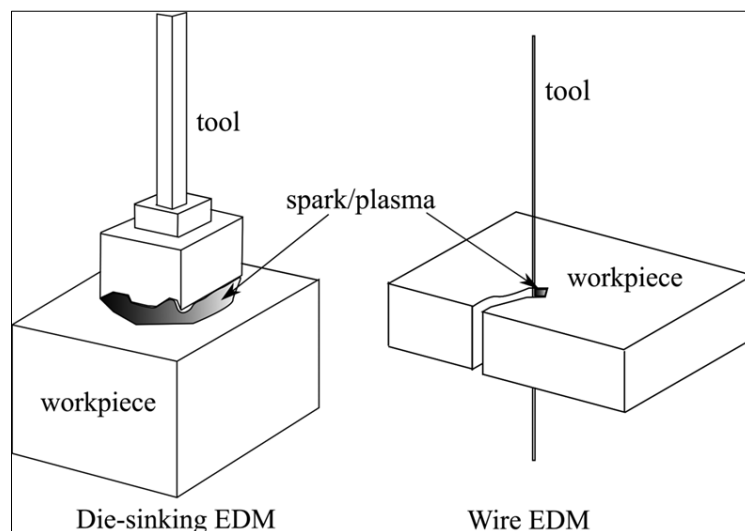


Fig. 1.5. Schematic diagram to differentiate die sinking EDM and Wire EDM.

Wire EDM uses a very fine wire as electrode. The electric discharge takes place between wire and the workpiece to make a kerf which helps to cut the workpiece into pieces. Very complex shape, precise cutting can be performed by this process. The precision of cutting is much better in this process compared to die sinking EDM. In this setup, the fine wire is attached between two junctions of the machine and attach through smooth wheel. When the wire is energized, the spark takes place at the vicinity of wire and work piece and starts discharging under the

dielectric. The cutting takes place perpendicular to the length of wire. Fig. 1.5 represents the difference between die sinking EDM and wire EDM.

1.5. Advantages and Disadvantages of PMEDM

The advantages and disadvantages of the PMEDM are discussed below.

1.5.1. Advantages of PMEDM

Powder mixed electric discharge machining is advantageous comparatively normal EDM in some aspects. The advantages of the process are discussed below.

- In this process, the rate of material removal is more compared to normal EDM.
- The surface roughness is less compared to normal EDM. The quality of surface is improved.
- The erosion of tool is comparatively less.
- In this process, stable but enlarged spark gap can be generated which helps to maintain dimensional accuracy with proper finish.
- The width and length of the sub surface cracks reduce with the addition of proper amount of micro powders in dielectric.

1.5.1. Disadvantages of PMEDM

The disadvantages of the powder mixed electric discharge machining are discussed below.

- The powder cost of the process enhances the overall cost of the process. Some of the powder is very much costly like Ti nano particles, chromium particles etc.
- The separation of the powder particles is difficult. In most of the cases separate arrangement is provided which incorporates more cost and time.
- The chance of intruding powder particles on the machined surface is high which can change different characteristics of the workpiece material. The amount of impurity may enhance.
- The back side of the machined surface may pitted with the powder discharge from the back side.
- Only electrically conductive powder material can be used for machining and the work material has to be also electrically conductive.

1.6. Applications of EDM

The application of die-sinker electric discharge machine is primarily to manufacture high precision moulds and dies. The moulds used for injection moulding process are generated by EDM on hard materials of ferrous alloy and non-ferrous superalloys. It is also used to make fixtures, tools gauges of hard materials like tool and die steel, H11 and EN31 alloys.

Table 1.1.

Applications of EDM

Sl no.	Types of EDM	Applications
1	Die-Sinking EDM	(a) making of dies and moulds (b) making of moulds for plastic injection moulding (c) Complex shaped hole generation on hard materials (d) Surgical instruments in medical sector (e) Fixtures, tools, gauges etc. on H11, EN31, tool steel etc. (f) Aerospace and defence sector
2	Wire EDM	(a) Cutting a complex shaped blank from a plate (b) Making gears, cams and other equipment.
3	Powder mixed EDM	(a) Little application on high precision die manufacturing industry (b) research laboratory for enhancing the MRR and surface quality (c) Surface coating on superalloys and hard materials

Die-sinking EDM is one of the suitable processes by which a hole of any shape can be generated easily on hard alloys. EDM is also used in the aerospace sector, the medical instruments manufacturing sector, the defence equipment manufacturing sector and many more. Wire EDM is used to generate many products like gears, cams, typical contour cutting for making a blank etc. Powder mixed EDM has been incorporated in both the die sinking and wire EDM but is limited in number. In several research, the powder mixed EDM has been used to enhance its two major responses that is MRR and surface quality. It is also used to develop surface coating on super alloys and hard materials. Table 1.1 shows the category wise application of EDM.

Chapter 2

Literature Survey and Objective of the Research Work

2. Literature survey

2.1. Effects on different process parameters

Several developments have been employed to overcome the difficulties in which hybridization of the EDM process using rotary tool electrode, ultrasonic vibration-assisted electrode and cryogenic treatment on machined surfaces and mixing of electrically conductive micro and nanopowders with dielectric fluid [4-6] is found highly effective regarding the effectiveness of machining. Out of these methods, addition of powder particles in dielectric fluid is one of them.

In this process, conductive particles situated in the electrode gap are electrically induced by the voltage applied and a series of local sparks are generated from them. The addition of spark into the gap improves the different machining parameters like MRR (material removal rate), TWR (tool wear rate) and surface roughness. Research shows that application of powder in dielectric fluid affects the machining process significantly. In the study made by Talla et al., a parametric optimization was performed by the grey associated PCA technique to achieve large MRR and small surface roughness for aluminium /alumina metal matrix composites [7]. The analysis recommended that the optimized result can be found with an error of 4% from the actual data.

Unune et al. performed a dual approach with ANN and NSGA-II optimization were employed to model and optimize the parameters of SiC mixed electric discharge grinding [8]. NSGA-II optimization provided a closer result with the experimental values for getting maximum MRR and minimum surface roughness. Tripathy and Tripathy applied TOPSIS and GRA oprtimization which were used for optimizing the process during the machining of H-11 die steel [9]. The research concludes that influence of five process parameters has been seen on material removal, tool wear and roughness of the surface, the optimized result of the process parameters found very much close to the confirmatory test result.

Bhattacharya et al. did a study on EN 31 steel, H11 tool steel and HCHCr die steel which were machined by varying seven input variables [10]. They are current, pulse off, pulse on, electrode, dielectric fluid and work material itself. It has been see that MRR of H11 is smaller than EN31 but higher than H11 tool steel. Kansal et al. added pure silicon powder for performing the experiments on AISI D2 steel [11]. In the result, the optimized condition for machining rate was obtained during the setting of peak current at 10 A, powder concentration at 4 g/l, pulse on time at 100 μ s, pulse off time at 15 μ s and gain at 1 mm/s. Jahan et al. mixed graphite nanopowders during the machining of WC-Co alloy and concluded that the least

surface roughness and maximum MRR were obtained at a powder concentration ranging between 0.2-0.6 g/l [12]. Alam et al. performed a comparative study on the effect between the effects of graphite and titanium oxide powder during the PMEDM of titanium grade 5 (Ti-6Al-4V) material [13]. The result of the comparison showed that titanium oxide has been found 3.42, 2.88 and 1.73 times more efficient than graphite powder for the removal of material, wear of the tool and roughness.

Prakash et al. did an experimental study on β -titanium alloy by using silicon mixed EDM [14]. The result confirmed that the addition of 4 g/l silicon powder decreases a significant amount of surface crack density and a low surface porosity was found at the 8 g/l concentration and current of 15 A. Ou and Wang performed an experimental research where hydroxyapatite powder is added to titanium and titanium alloy to study different machining parameters [15]. It was found in research that an addition of HA powder of 5 g/l concentration significantly increases the MRR to 28.6×10^{-4} g/min and reduces the surface roughness to 2.1 μm .

Sahu et al. did an experiment where SiC powder was applied to Inconel 718 processing [16]. The analysis indicated that the concentration of 6 g/l SiC powder provides substantially high MRR with reduced surface roughness and wear of the tool. In a research, Sagar et al. performed PMEDM experiments with rotary tool of Cu and W for Inconel 718 [17]. It has been seen that the addition of 0.5 g/l to 1.5 g/l of aluminium oxide powder influences material removal, the redeposited layer and surface quality and wear of the tool. In other research, Khadar et al. showed the effect of boron carbide powder on Inconel alloy [18]. The analysis indicates that along with powder concentration, current and pulse on time influence the surface roughness and recast layer significantly.

Ahmed et al. performed an experimental investigation on high performance electrical discharge machining by applying nano aluminium powder on dielectric fluid [19]. In this research, the addition of powder increases MRR but not reduces the roughness lower than 8.62 μm for high performance EDM. Majumdar et al. [20] studied the characteristics of graphene nano powder on Inconel 625 during the PMEDM. Three process parameters such as current, powder concentration and pulse on time were selected and studied their characteristics on MRR. The result indicates that the maximum MRR was found at a graphene concentration of 0.4 weight %. Talla et al. [21] analyzed the PMEDM study on Inconel 625 with three different powders viz. graphite, silicon and aluminium. MRR, surface roughness, microhardness and overcut have been studied in this research. In the result, the best MRR was found during the graphite mixed

EDM whereas the best surface quality, microhardness and least overcut were found during silicon mixed EDM. Zhao et al. did the experiment where 40 g/l aluminium powder was added and performed rough machining on steel [22]. The result shows a 30% increase of machining efficiency by adding the powder. In the study of Marashi et al., the effect of Gr, Al, Ti, W, TiC, SiC and Cu powder on steel and found that only Cu has no effect on the machinability characteristics [23]. The addition of other powders with any dielectric fluid enhances the material erosion and reduces the roughness value of the steel sample. Han et al. performed electrochemical discharge machining by applying 0.5 g/l graphite powder on electrolyte solution [24]. The effect on borosilicate glass has been analyzed and found that the surface roughness decreases from 4.86 μm to 1.44 μm compared to conventional processes.

2.2. Application of mathematical model

In recent times, different mathematical and predictive models using the concept of machine learning have become popular and they are being used in the field of manufacturing for mathematical analysis. The RSM desirability function has been used in a study made by Dwivedi and Shau to minimize the corrosion rate of Aluminium based composite with the optimal setting of input parameters [25]. The result shows that the accuracy of the RSM desirability function is more than 90% to optimize the corrosion rate. Rahimi and Fazlollahtabar [26] applied two optimization methods for optimizing the closed loop green supply chain network and compared the two optimization techniques. It was found that the genetic algorithm is more efficient than particle swarm optimization technique with respect to relative percentage deviation and solution time. Like another area of research, these models can also be used to study and analyze the EDM models.

Artificial Neural Network (ANN) has been formulated to analyze the SKD 11 tool steel machining by EDM [27]. In this study, the network was used to forecast the roughness value and found mean square error and R value as 0.31355 and 0.999 respectively. In another research, fuzzy predictive models were employed to predict the responses. ANFIS based fuzzy logic were developed in an experimental result performed by Sharma et al. [28] during the EDM of Inconel 718. The ANFIS based fuzzy logic predicted the MRR, surface roughness and TWR with the accuracy of 95.55%, 97.82% and 90.35% respectively.

In the research made by Jarin et al. the effect of 0.5 g/l to 2 g/l graphite powder on the EDM of gold coated silicon [29] has been done. The research shows that the MRR and spark space has been enhances 33% and 159% respectively. Jatti and Bagane made a thermo electric model in ANSYS 15.0 for PMEDM of Be Cu alloy and compared with the experimental result [30]. It

has been found that a 7.8% error has been realized between actual and the predicted values of MRR. Kim and Chu applied graphite mixed EDM on STS 303 steel and found that the machining time and tool wear length were decreased by 30.9% and 28.3% respectively [31]. Tiwary et al. performed PCA to find the optimized parameters during PMEDM of titanium alloy [32]. The optimized value of the responses has a closeness of above 95% with the actual result.

Rajkumar et al. have applied Mamdani-based fuzzy logic on the result of PMEDM of AA2014/Si₃N₄/Mg/Cenosphere Hybrid Composites [33]. In a result, it has been found that the fuzzy predicted result is much closer to the experimental result with a mean error of around 5%. Singh and Sharma applied grey relation analysis to find the optimized value of micro hardness and roughness during machining of tungsten carbide [34]. The result shows that there exists a 0.49% error between optimized value and confirmatory test value.

Rathi and Mane used Taguchi analysis with the S/N ratio larger is better for the PMEDM result of Inconel 718 [35]. In the result, it has been observed that maximum MRR has been obtained at 18 A current, 85% duty cycle, 5 μ s pulse time and graphite powder. Singh and Bharti applied TLBO to optimize the drilling ratio (DR) and TWR during the PMEDM of titanium alloy [36]. The deviation between confirmatory test and TLBO predicted result is lower than 5%. Chakraborty et al. also performed TLBO algorithm to optimize the corner inaccuracy and surface roughness during the machining of titanium alloy and found the optimized result as roughness with 1.199 μ m and corner inaccuracy at 12982.67 μ m² [37].

Dinesh et al. utilized ANN model on RSM result of die steel processing using PMEDM [38]. The desirability value of the applied ANN model is found to be 0.908 which is higher than RSM model with 0.87 desirability value. Kumar et al. performed Taguchi-based ANN model on PMEDM result of titanium alloy and found a high closeness of predicted result with actual one [39]. Mohanty et al. used particle swarm optimization method to optimize MRR, surface roughness and TWR during PMEDM of AlSiCp material and found the deviation from the confirmatory test result less than 5% for all responses [40]. Padhee et al. utilized non dominating sorting genetic algorithm and fuzzy logic to optimize and predict surface roughness and machining efficiency of silicon mixed EDM [41]. As a result, both the models are found adequate to use in industrial application. Ramesh and Jenarathanan used combination of fuzzy logic and GRA for the prediction and optimization of MRR, electrode wear and roughness for PMEDM and found 6% deviation from the experimental result [42].

Faisal and Kumar compared two unique optimization techniques on EDM results of EN 31 steel [43]. The comparative analysis depicts that the BBO technique is more efficient than the PSO technique. The TOPSIS process has been performed on Taguchi result during titanium based EDM [44]. The results found that the optimized MRR, surface roughness and hardness values are 38.79 mm³/min, 2.71 µm with 771 HV, respectively. In an experimental study, Elumalai et al. compared support vector regression and random forest algorithms applied on the surface roughness data of micro electric discharge milling of Inconel 718 [45]. It can be observed that both model predicts surface roughness value with high accuracy. Another study was made where three machine learning processes like linear regression, random forest regression and AdaBoost regression were applied on EDM operations and found AdaBoost was the most suitable one for modelling the problem [46]. Also, Kaigude et al. applied linear regression, random forest and decision tree on EDM application found that random forest provides the best solution among all [47].

2.3. Surface characterization of the machined surface

Apart from parametric optimization, surface characterizations and surface micro defects have been investigated in several studies. In this process, a series of sparks provide thermal load on the surface. Again, rapid and uneven cooling of the surface during the spark cutoff causes extreme contraction and generates micro cracks, voids and holes. The relation of the surface area of electrode with surface roughness, crater depth and white layer thickness was found in a study made by Pecas and Henriques [48]. It was evident that the addition of the powder reduced the redeposited layer and crater depth significantly.

In the study made by Liew et al., the application of carbon nanofibers in dielectric resulted in a significant reduction in the formation of crater length and micropore on the work surface [49]. The machined surface generated by wire EDM was analyzed and found that a significant reduction of micro holes and globules can be observed when a proposed control of parameters had been set [50]. Furutani et al. added Ti powder with EDM oil dielectric fluid and applied for enhancing the surface quality of workpiece sample by rotating the electrode of different shapes [51].

It has been found from the cross sectional SEM image and XRD analysis that the gear shaped electrode deposited maximum powders and the thickest layer of Ti and TiC has been observed. Mohal and Kumar performed powder mixed EDM using multiwalled carbon nanotubes on metal matrix composites [52]. The SEM result shows that the diameter of the crater and pores

is reduced by the application of carbon nanotubes. Kolli and Kumar [53] performed an investigation where graphite powder was added with EDM oil and applied on titanium alloy for EDM. The result shows that the discharge current and powder concentration mostly affect the MRR and tool wear rate whereas the surface roughness and the recast layer thickness (RLT) are affected by current and surfactant concentration.

Bai et al. analyzed surface morphology of the near-dry PMEDM during different workpiece and tool combinations [54]. The characterization result shows that MRR has a correlation with thermal conductivity and residual heat generation of workpiece and the melting point temperature of the electrode. Wong et al. studied the near mirror finish phenomenon on steel during the EDM by addition of graphite, silicon and aluminium powder [55]. The characterization result shows that the application of powder particles fills the craters of the normal EDM surface and produces a near mirror finish surface. Xie et al. performed TiC coating by titanium electrode and graphite mixed EDM and analyzed the tribological properties of the surface [56]. The result depicts that the application of graphite powder reduces the non-uniformity in the coating thickness and the surface microcracks.

Singh et al. found a 42.85 % reduction of recast layer thickness from cross-sectional SEM analysis during the PMEDM of AA6061/10% SiC composite [57]. Malhotra et al. performed gas-assisted powder mixed EDM on hybrid metal matrix composites [58]. The SEM micrography indicates that the application of gas helps to take away the extracted materials during machining and provides a thinner recast layer on the surface. A comparison have been done between the machining characteristics of conventional EDM and PMEDM [59]. The analysis indicates the PMEDM surface is much smoother than the conventional surface. Prabhu and Vinayagam performed atomic force microscopy analysis on the PMEDM surface of Inconel 825 [60]. The effects of carbon nanotubes on surface roughness have been clearly visible and found a better surface roughness compared to other surface machined by different powders. Guu and Hou performed the AFM and EDS analysis of EDM surface on Fe-Mn-Al alloy [61]. The results indicate the lower surface roughness and the included elements on the machined surface. Beri et al. made a correlation between surface microhardness and XRD peak of Inconel surface duly machined by EDM [62]. The XRD analysis indicates the improvement of surface micro hardness has happened due to the presence of $\text{Fe}_2\text{W}_3\text{C}_6$ phase on the surface.

Yih-Fong et al. did an elemental analysis on PMEDM sample where it was found a very small amount of particles such as 1% to 3% by weight had been placed from the tool to the work

material during the time of melting and solidification of the material [63]. It was also concluded that careful control of parameters could resist the material infiltration towards the work surface. In a review study done by Viega et al. [64], it has been shown that the influence of the mechanical properties of titanium greatly affected the machinability of the titanium alloy. The feed has a great effect on the force component during the study of different titanium materials [65]. The changes in plastic layer during normal and hybrid turning have been shown in a microstructural view of a study [66]. Since the properties of titanium have great influence on machining, the titanium powder has been selected for this study. Sahu and Mandal did an elemental analysis on the Nimonic 263 sample made by graphite and alumina powder mixed EDM [67]. In the EDAX result, it has been found that the inclusion of copper material is maximum in the case of alumina mixed EDM and least in conventional EDM.

After carefully reviewing the literature several research gaps have been found. Firstly, the effect of powder mesh size and its interaction with other parameters have been studied in very few studies. The formulation of fuzzy logic has not been applied in any studies for five five-parameter based study. Therefore, in this research, the effect of mesh size and its interaction, application of fuzzy logic and ANN, comparison of the effect of two powders and crack width analysis by characterization have been extensively applied and their results have been explained.

2.4. Formulation of the objectives

The objective of the present studies, after thoroughly reviewing the literature has been formulated and stated as below

- In this study, experiments have been conducted by applying two types of micro powder added to the dielectric. They are titanium and graphite.
- Firstly, the effect of current, pulse on time, pulse off time, gap voltage and powder concentrations was seen on MRR and roughness value of the surface at the machining of Titanium Grade 2 with Inconel 718 material using titanium mixed EDM.
- The result have also been analyzed by ANOVA to find significant parameters.
- 3D surface plots have been generated to find the interactions of current, powder concentrations and gap voltages.
- Mamdani-based fuzzy logic have been implemented with the data and compared its result with actual data.

- Multi-objective optimization using desirability functions have been performed to find the minimum surface roughness and maximum material removal rate.
- SEM and EDX investigations have been carried out to analyze the changes in microcrack width and elemental inclusion after machining.
- Secondly, current, pulse on time, powder concentrations, duty cycle, and powder mesh size are the parameters which were selected for the analysis of MRR, roughness of surface and rate of tool wear during the machining of Inconel 625 and Titanium Grade 2 using graphite mixed EDM.
- The results have been analyzed by ANOVA to find significant parameters, lack of fit and model significance.
- 3D surface plots have been generated to find the interactions of current, powder concentrations and Powder mesh size for individual parameters.
- Back propagation type neural network has been implemented using the data and compared its predicted result with the actual result.
- Multi-objective optimization using desirability functions has been performed to get the minimum surface roughness, minimum tool wear rate and maximum MRR.
- SEM investigations have been carried out to analyze the changes recast layers and width of the microcracks.
- XRD analysis has been performed to investigate the retention and changes in phases after machining by PMEDM.

Chapter 3

*Materials, Experimental Methods and
Computation Techniques*

3.1. Introduction

The present research has been carried out by performing four experimental works. Firstly, titanium micro particles were mixed in different concentrations into EDM oil and two experimental works were performed by machining Inconel 718 and Titanium Grade 2 material. The experimental design for performing the experiments was a central composite design (CCD) enabling response surface methodology. Further, graphite micro particles of different concentrations and mesh sizes were added in the same dielectric fluid and two experiments have been performed by machining of Titanium grade 2 with Inconel 625 materials. Here, the experimental design has been planned by Box-Behnken based response surface methodology (RSM-BBD).

3.2. Experimental setup

The experiments were conducted in die-sinking EDM of model no ENC 20 of 400×250 manufactured by Reliable Enterprises, Maharashtra, India. The setup has been shown schematically in Fig. 3.1.

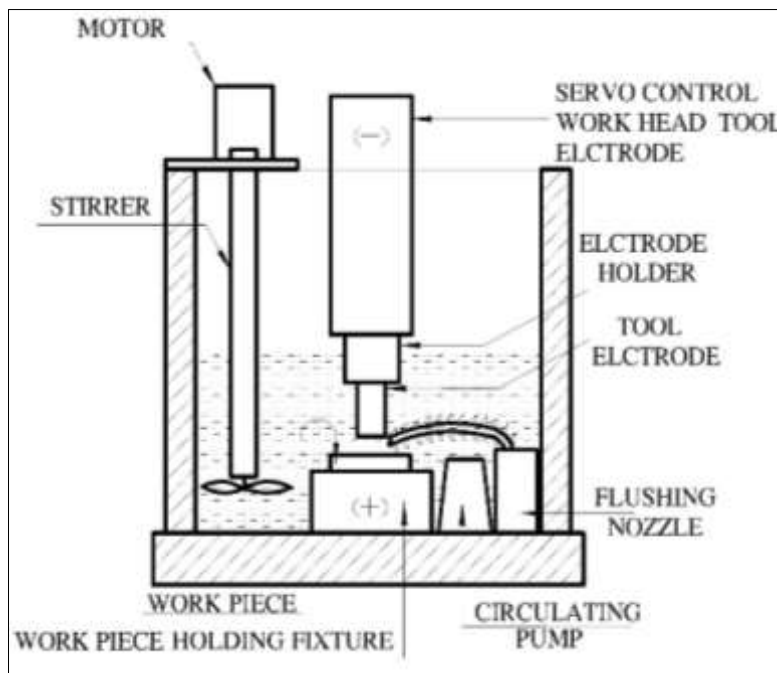


Fig. 3.1. Schematic view for the setup of PMEDM.

A container has been further assembled where the mixing of particles takes place. The dimension of the tank is $440 \text{ mm} \times 280 \text{ mm} \times 280 \text{ mm}$ as shown in Fig. 3.2. In this process, the acrylic sheet of thickness 10 mm has been used.

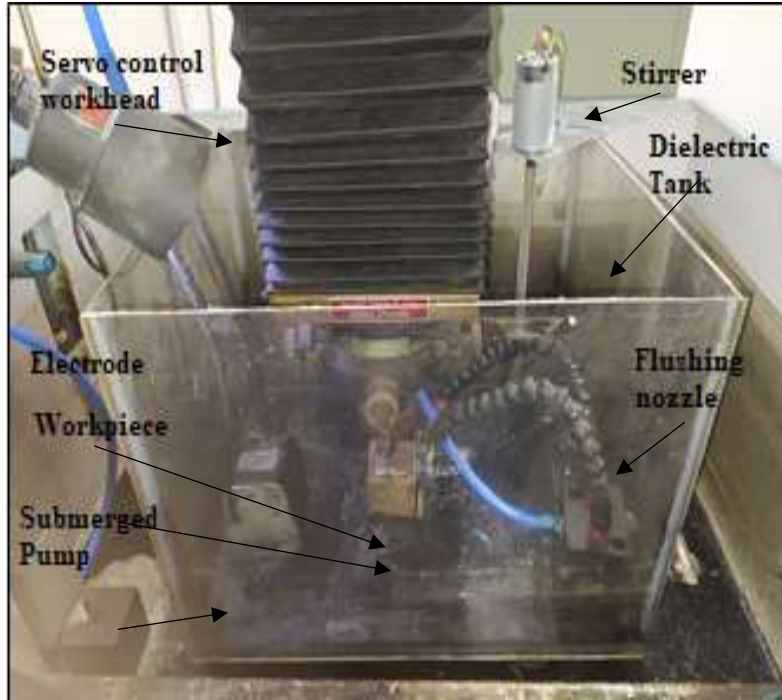


Fig. 3.2. Photographic view of experimental setup of powder mixed EDM.

Inside the tank, a submerged pump of flow rate 10 litres per minute was situated with two nozzles. The nozzle circulates the mixed dielectric to flush away the extracted material from the spark gap. The dielectric used for machining was taken as the carol EDM oil having a specific gravity of 0.82, kinematic viscosity of 2 centistokes at 15 °C and flushing point 110 °C. Before conducting the experiment, the EDM oil was stored at a volume of 12 litres in the container using a measuring cylinder. A stirrer mechanism with a rated speed of 750 rpm is attached to stir the dielectric fluid with powder.

3.3. Selection of workpiece and powder material

The work material for performing the experiments has been selected for two major categories. Firstly, Inconel 718 and Titanium Grade 2 have been selected for titanium mixed EDM and Inconel 625 and Titanium Grade 2 have been selected for graphite mixed EDM.

3.3.1. Selection of powder and workpiece material during titanium mixed EDM

In this experiment, Inconel 718 has been chosen as material for sample. The weight percentage of every alloying element of Inconel 718 was measured, which is listed in Table 3.1. In Table 3.2, the properties of the material have been listed. The workpiece samples of size 30 mm × 30 mm were prepared from a plate with a 3 mm thickness. In each sample, two experiments were conducted in a diagonal position with an average radial distance of 3 mm. Before

experimenting, samples were cleaned using distilled water and a polishing was performed by sand paper of grade 1100. At the start of each experiment, the working surface of the electrode was ground with an emery paper (grade 1100) to remove the deposition taken place during the machining. Fig. 3.3 represents the pictorial view of the Inconel 718 sample machined by EDM.

Table 3.1.

Inconel 718 composition

Components	Ni	Fe	Cr	Ti	Mo	Nb	Al
%	50.5	20.4	19.2	1.1	2.8	4.1	1.9

Table 3.2.

Mechanical, Thermal and Electrical properties of Inconel 718

Material properties	Values
Density (kg/m ³)	8192
Tensile strength (MPa)	1240
Hardness (Rockwell)	42
Melting point (°C)	1370-1430
Thermal Conductivity (W/mK)	6.5
Resistance (ohm-cm)	0.000125
Specific heat (J/g °C)	0.435

Titanium powder of grain size 25 µm was added to the EDM oil 15 minutes into the experiment with specified concentrations and stirred continuously till the end of the experiment to ensure the uniformity of the mixture during the machining. Table 3.3 represents the mechanical characteristics of titanium powder. After completion of the set of experiments performed under a particular concentration, the EDM oil along with the powder was pumped out and filtered by a filter paper to get the powderless dielectric. The filtered dielectric was used in the next set of experiments.



Fig. 3.3. Photographic view of Inconel 718 machined by titanium mixed EDM.

Table 3.3.

Mechanical, electrical and thermal properties of titanium powder

Powder properties	Values
Average grain size (μm)	25
Density (kg/m^3)	4540
Melting point ($^{\circ}\text{C}$)	1668
Thermal Conductivity (W/mK)	21.9
Electrical resistivity (ohm-cm)	0.000042

Further, Titanium Grade 2 material has been processed and utilized in a similar manner. But here a single sample has been used for individual experiments. Table 3.4 lists the major constituents of Titanium Grade 2, whereas Table 3.5 lists the mechanical, electrical and thermal properties of it.

3.3.2. Selection of work material for graphite mixed EDM

Inconel 625 has been selected for workpiece material in this study. It is a nickel based superalloy that contains around 60% nickel 20% chromium. The chemical composition of the alloy was analyzed by Positive Material Identification testing machine (Makers: Thermo Fisher, Model: XL 2 800, Sr. No: 76526) and listed in Table 3.6. The properties of the material are shown in Table 3.7. The preparation of Inconel 625 of thickness 1.27 mm was made by cutting into square pieces using wire cut EDM at a dimension of 15×15 mm. Before machining,

the samples were cleaned with an acid solution followed by water. Further they were polished by emery paper (grade 1100) for 10 minutes to remove the dust particles and oil film.

Table 3.4.

Composition of Titanium Grade 2

Element	Ti	Fe	O	C	N	H
%	98.9	0.30	0.25	0.08	0.03	0.015

Table 3.5.

Properties of Titanium Grade 2

Material properties	Values
Density (kg/m ³)	4510
Tensile strength (MPa)	485
Hardness (Rockwell)	80
Melting point (°C)	1665 ⁰ C
Thermal Conductivity (W/mK)	21.97
Resistance (ohm-cm)	0.000535
Specific heat (J/g °C)	0.523

Table 3.6.

Alloying element percentage of Inconel 625

Element	Ni	Fe	Cr	Ti	Mo	Nb
%	62.1	4.79	21.30	0.1	8.11	3.68

In this experiment also, Titanium Grade 2 material have been selected with Box- Behnken design. Total 46 samples have been cut from a plate and used for the experiments. The samples are polished by emery paper of grade 1100.

Graphite micro powder was added with Carol EDM oil dielectric fluid before conducting the experiment and stirred thoroughly before initiating the discharge. Three size of powder particles were used here viz. 15 µm, 25 µm and 35 µm. The properties of graphite micro powders are listed in Table 3.8. The mass of the graphite micro powders of each mesh size was measured and then it is mixed in EDM oil.

Table 3.7.

Properties of Inconel 625

Material properties	Values
Density (kg/m ³)	8440
Tensile strength (MPa)	992.9
Hardness (Brinell)	210
Melting point (°C)	1320
Thermal Conductivity (W/mK)	9.86
Resistance (ohm-cm)	0.000126
Specific heat (J/g °C)	0.402

Table 3.8.

Properties of graphite powder

Powder properties	Values
Average grain size (µm)	15, 25, 35
Density (kg/m ³)	1300
Melting point (°C)	4550
Thermal Conductivity (W/mK)	0.25
Electrical resistivity (ohm-cm)	0.0005

3.4. Selection of Tool Material

A cylindrical copper rod with 99.5% purity was selected for the tool material. The tool is prepared by a CNC machine by making the diameter 12 mm and the length 90 mm. The tool wear rate has been measured in graphite mixed electric discharge machining by the difference in weights before and after the work processing. In Table 3.9, the properties of copper have been listed.

Table 3.9.

Mechanical, electrical and thermal properties copper

Properties	Values
Density (kg/m ³)	8830

Melting point (°C)	1085
Thermal Conductivity (W/mK)	398
Electrical resistivity (ohm-cm)	0.0000172
Specific heat (J/g °C)	0.385

3.5. Selection of input parameters and responses for titanium mixed EDM

The input parameters have been selected as powder concentration, gap voltage, pulse current, gap pulse on time and pulse off time. For each parameter, the level value has been considered as three. Table 3.10 provides the input parameters and their level values. Material removal rate (MRR) and surface roughness are the responses for analyzing their effects.

Table 3.10.

Input parameters with levels for titanium mixed electric discharge machining

Input Parameter	Unit	Low	Medium	High
Powder concentration (C_p)	g/l	2	5	8
Pulse current (I_p)	A	6	9	12
Spark voltage (V_g)	V	30	45	60
Pulse on time (T_{on})	μs	150	200	250
Pulse off time (T_{off})	μs	20	40	60

Before conducting the main experiments, several pilot experiments were conducted, from which it was observed that the parameters were most influential between the low and high level values shown in Table 3.10. The design for the experiment has been planned using the central composite design method. Fig. 3.4 (a) represents the construction of the RSM-CCD design. In this experiment, a total 52 number of experimental runs were performed.

3.6. Selection of input parameters and responses for graphite mixed EDM

The machining characteristics are largely affected by several electrical and powder related input parameters. In this particular experiment, five input parameters were selected with three levels out of which, three were electrical and two were parameters of powder. Current (I), pulse on time (P_{on}), duty cycle (D), powder concentration (C_p) and mesh size (m) have been selected

as powder parameters. Based on the machining capacity and availability of powders, the minimum, intermediate and maximum levels of each input parameter were chosen.

Table 3.11.

Input parameters with their levels for graphite mixed EDM

Input Parameter	Unit	Low	Medium	High
Current (I)	A	4	8	12
Pulse on time (P_{on})	μs	35	55	75
Duty Cycle (D)		0.5	0.7	0.9
Powder concentration (C_p)	g/l	2	5	8
Mesh Size (m)	μm	15	25	35

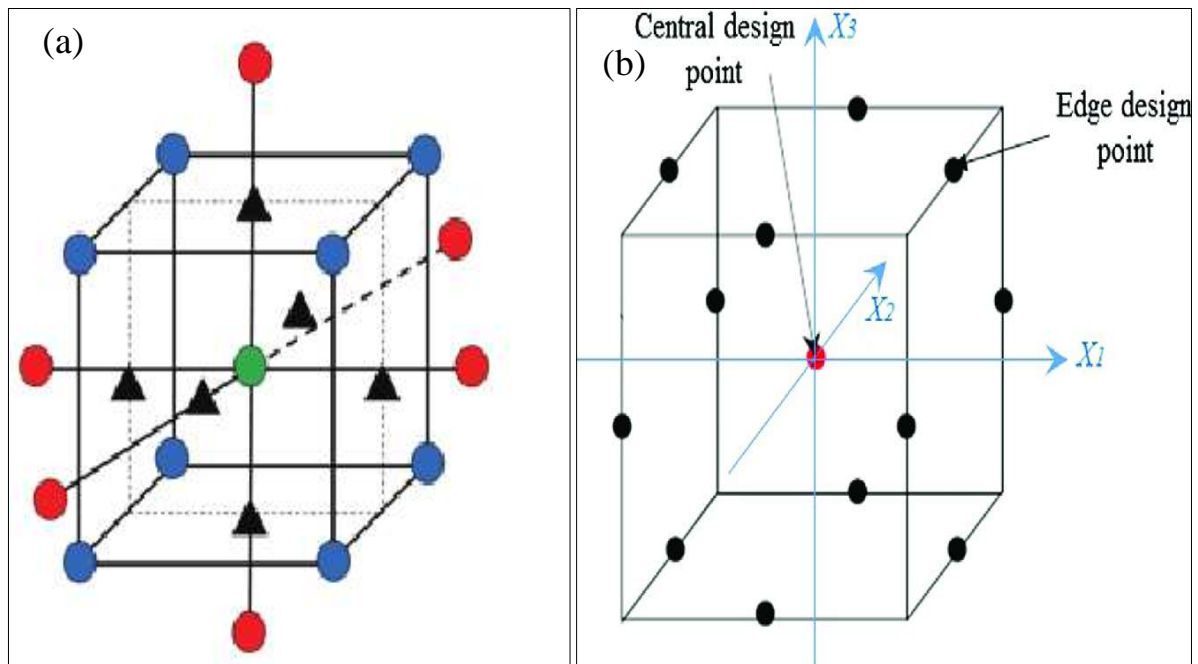


Fig. 3.4. Construction of (a) RSM-CCD and (b) RSM-BBD design.

The values of the levels of each parameters have been represented in Table 3.11. The planning of the experimental work have been performed by Box- Behnken design. The BBD design provides a high order quadratic model with small number of experimental run compared to other design of the RSM model. Fig. 3.4 (b) represents the construction of RSM-BBD design. Along with that, the variance of the model is uniform in design space. For 5 factors BBD design, total 40 edge points and 6 center points have been considered and the L46 array of design has been developed. The experimental table have been made by MINITAB software.

3.7. Measurement of responses in titanium mixed EDM

As discussed earlier, MRR and surface roughness were measured as responses, as these two major parameters determine the production rate and machining quality of EDM. The rate of mass decaying during the machining is called MRR and measured as per Eq. (3.1). A weighing machine model no. 8068 series was used to measure the sample weight before and after the experiment.

$$MRR = \frac{(W_i - W_f) \times 1000}{\rho \times t} \quad (3.1)$$



Fig. 3.5. The photographic view of Talysurf instrument.

Here, W_i is the weight of the sample measured before machining in (g), W_f is the weight measured in (g) after finishing of the machining, ρ is the density measured in (g/cc) and machining time is represented by t (min). MRR is calculated in mm^3/min . The density of Inconel 718 was taken as 8.17 g/cc and the density of Titanium Grade 2 has been taken as 4.51 g/cc.

Surface roughness was measured by a stylus type precision profilometer (model name: Talyor Hobson, Surtronic 3+) on the R_a scale. In each sample, three measurements were taken in three arbitrary positions of the machined surface. The average of three data has been selected as the surface roughness value. Fig. 3.5 shows the image of Talysurf instrument.

3.8. Measurement of responses in graphite mixed EDM

After the experiment, the responses which are measured are surface roughness, material removal rate and tool wear rate. MRR represents the productivity of the process which is determined by measuring the volume of material removed per unit time. TWR represents the consumption of the electrode which is measured as the volume of tool decay per unit time. In this study, the MRR calculation has already been represented and TWR were measured according to Eq. 3.2 and expressed in terms of mm³/min. The accuracy of the weighing machine measured for TWR is 0.0001 g. Fig. 3.6 shows the pictorial view of the weighing machine.



Fig. 3.6. The photographic view of weighing machine of accuracy 0.0001 g.

The surface roughness is the vertical unevenness of the machined surface measured from a mean line. SR relates the quality of machining and the texture of the newly developed surface. The center line average (CLA) or R_a surface roughness was measured in this study by a stylus-type precision profilometer (model name: Taylor Hobson, Surtronic 3+).

$$TWR = \frac{(\text{Difference of mass of the tool before and after machining} \times 1000)}{(\text{machinig time} \times \text{density of tool material})} \quad (3.2)$$

In this study, the density of Inconel 625 was taken as 8.44 g/cm³ and the density of the copper was taken as 8.83 g/cm³. The density of Titanium grade 2 has been taken as 4.51 g/cc. The machining time for each sample was kept constant at 15 minutes.

3.9. Methodology of the experiments

Response surface methodology is used mainly to optimize different manufacturing, production and chemical processes. The approach of RSM is initiated with developing an experimental design considering input parameters and their levels. It is the mathematical process by which an approximate relationship is generated between input parameters and response. The complex studies, associating the effect of several controlling parameters and their interactions are generally modelled by a second order polynomial equation Eq. (3.3) of response surface methodology [68].

$$Y = \beta_0 + \sum_{i=1}^5 \beta_i x_i + \sum_{i=1}^5 \beta_{ii} x_{ii}^2 + \sum_{i=1}^5 \sum_{j=1, (j \neq i)}^4 \beta_{ij} x_i x_j + \varepsilon \quad (3.3)$$

Here, Y is the response, β_0 is the fitted value of the centre point response, β_i , β_{ii} , β_{ij} are the coefficients of the regression as linear, quadratic and interaction terms, x_i and x_j are input parameters coded by normal values and ε represents the error associated with the model.

The adequacy of the model can be determined by calculating the value of the coefficient of determination (R^2), adjusted R^2 and predicted R^2 . The definition of R^2 provides the variance of the response explained by the input parameters divided by the total variation. An R^2 value closer to 1 indicates the goodness of fit of the regression equation with the experimental values. Along with R^2 , the adjusted R^2 and predicted R^2 have been evaluated to find out the closeness of fit with the different number of variables and the degree of overfitting of the model respectively.

3.10. Analysis of variance (ANOVA)

ANOVA is one of the important mathematical tool which indicates parameters which are significant in this process. F-value and P-value are used for finding out the significant factors in ANOVA. Using p values the significant parameters can be chosen. With less than 0.05 p-value, the process parameter is considered significant. F-value is determined as the summation of factor's square divided by the error variance. Therefore, a larger F value will provide a significant factor with respect to others.

3.11. Fuzzy logic used in Inconel 718 machining

The fuzzy logic was used to analyze uncertainty for a particular event using a mathematical tool [69]. Usually, complex problems like nonlinear relations between input and output variables are analyzed by the fuzzy prediction model. Unlike binary logic, where the membership value of an object is 0 or 1, fuzzy logic assigns several intermediate truth values between 0 and 1 for the fuzzy variables. The structure of fuzzy logic consists of five components which are fuzzification of input variables into fuzzy variables, construction of membership function, implementation of fuzzy rules, fuzzy prediction using rule viewer and defuzzification of the fuzzy variable into a crisp variable.

Fuzzy variables are converted from normal value, which is called fuzzification at first. These variables belong to the fuzzy set level and fuzzy inference for analysis and prediction. The membership functions are then constructed to describe the fuzziness of the fuzzy variable set. Here, the construction of the fuzzy membership function can be assigned based on human intuition or some other algorithmic operation. Further, the IF and THEN-based fuzzy rules are essentially implemented based on the normal value of fuzzy variables. In this system, IF is used as a condition part argument and THEN is used as a conclusion part argument. Further, according to fuzzy rules provided, the fuzzy inference system provides output values. The working principle of fuzzy inference system is to combine the measured fuzzified input variable with relevant fuzzy rules and then predict the fuzzy output. Out of several fuzzy inference systems, here the simplest one i.e. Mamdani max-min inference system is used. Finally, the defuzzification process is used to convert the fuzzy output variables into crisp variables with the predicted values. The defuzzification process can be employed with the centre of area method, where the output variable can be calculated by Eq. (3.4).

$$Y = \frac{\sum_{i=1}^n y_i \mu_{Ai}(y)}{\sum_{i=1}^n \mu_{Ai}(y)} \quad (3.4)$$

Here, the output variable is Y and $\mu_{Ai}(y)$ represents membership function at y_i .

3.12. Mathematical model using artificial neural network used in Inconel 625 machining

Artificial neural network (ANN) is a part of deep learning process used to predict an output after a rigorous training of similar type data. Like main unit of the nervous system, this network also consists of several neurons connecting to other set of neurons with a mathematical

relationship. ANN is basically a statistical and mathematical model where the responses are predicted after several training of the model with an experimental data set.

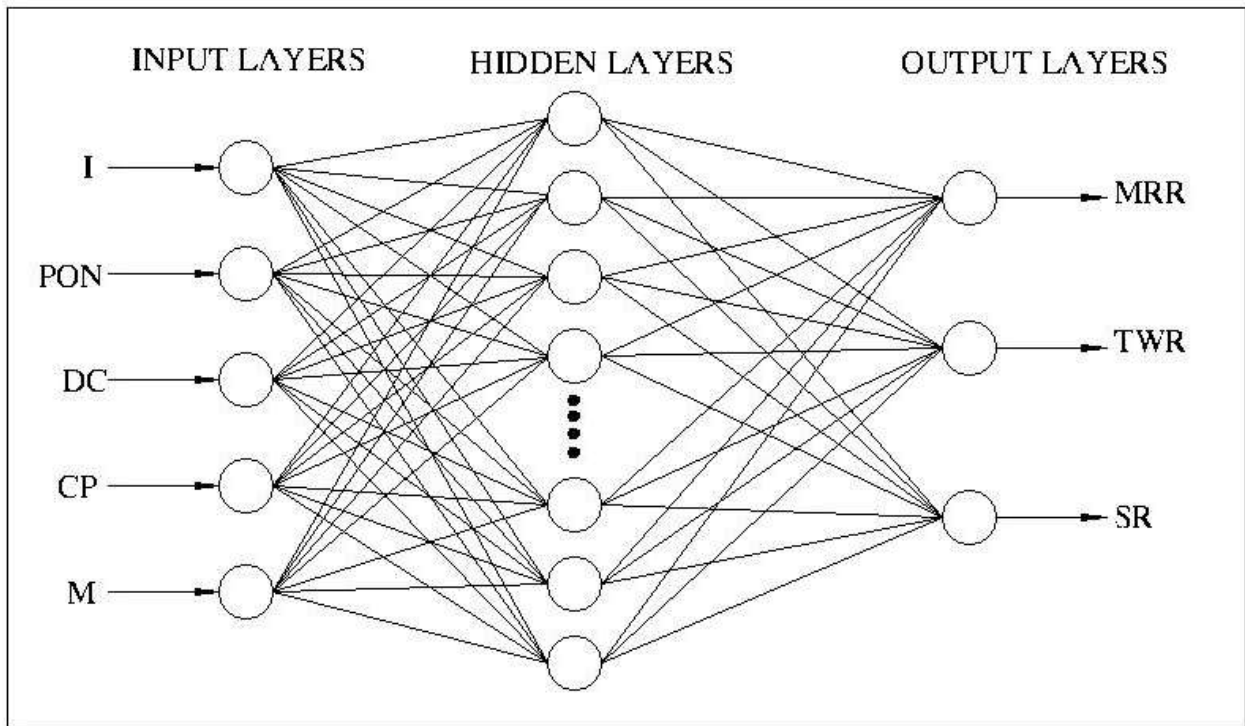


Fig. 3.7. Three layer based neural network for predicting the responses.

In this method, a set of data points for each input parameter is assigned to the neurons of the input layers. Now the values (also called signal) are transferred to the next layer by multiplying the weight factor allotted by the model itself. Each neuron of the hidden layer receives the input as a sum of the weighted signal coming from every neuron of the input layer. Further, the signal received by the neuron of hidden layer is activated by an activating function and transferred to the next layer (output layer in this case) again by multiplying a weight factor. Finally, the neuron of the output layer generates the predicted response by converting the received signal into output training function. It is quite obvious the output signals will not match the actual values of responses. Hence, the mean square error (MSE) is calculated between the actual and the predicted. If the error is found to be large, the feedback will be received by the network and it changes the weight factor in each synapse and repeats the training process further. This complete cycle consisted of training of the network, MSE measurement, feedback generation and backpropagation is called an epoch. The network is performing its computation till it reaches the specified number of epochs or a value of MSE, whichever is achieved earlier [70]. Six types of activation functions are normally used in neural networks. However, the selection

of activation function solely depends on the nature of problem, non-linear complex relationship between input and output and the number of data points.

The scheme of the ANN model is shown in Fig. 3.7. In this model, the circles represent the neurons and they are connected by the straight lines called synapses. The synapses are assigned a weight factor. One neurons receive a signal from another neuron by multiplying the signal weight factor. The network consists of at least three layers viz. one input layer, one output layer and one hidden layer. However, multiple hidden layers may be used based on the requirements of the model.

For the requirement of the present study, a three-layer neural network has been constructed where the input layer and output layer consist of 5 and 3 neurons, respectively. Since a very large and a too small number of neurons reduce the accuracy of prediction, the hidden layer has been constructed with 20 neurons. This number has been considered after making several trials.

$$\%Relative\ error = \frac{(actual\ data - predicted\ data) \times 100}{actual\ data} \quad (3.5)$$

$$Mean\ error = \frac{\sum \% relative\ error}{number\ of\ data\ point} \quad (3.6)$$

The mean error and percentage relative error between actual and predicted data are the measures of accuracy. During the network modeling, 2/3rd of the total experimental data were selected as training data and 1/3rd data were further tested by it. Testing is performed with the remaining data after completion of training, and the predicted result is compared with the actual data. The relative error was calculated by Eq. 3.5 and the mean error is calculated by Eq. 3.6.

3.13. Desirability function based multi objective optimization

Multi-objective optimization using the desirability function approach was carried out with the obtained result. In this method, at first, a desirability function $d_i(y_i(x))$ is created with the response function $y_i(x)$. $y_i(x)$ is the regression equation constructed using the response surface equation for that particular response. As per the proposal made by Derringer and Suich in 1980, each desirability function is constructed with the upper, lower and importantly one target value.

It is done based on the multiple desired goals of responses imposed in the model. RSM is one of the simple mathematical approaches which does not require any complicated equations. In this study, the desirability function approach is used by conjugating three objectives such that the optimization provides maximum MRR, minimum TWR and minimum SR. Initially, a desirability function $d_i(y_i)$ is derived from the regression equation y_i for each response. Eq. 3.7 and Eq. 3.8 depicts two methods to calculate the desirability function when the optimization is performed between the minimum and maximum value of the regression equation. In Eq. 3.7, $d_i(y_i)$ is used for maximization. However, to minimize the variable, Eq. 3.8 is used. In both equations, U_i and L_i indicate the top and bottom values for the equation. Further, if a response is to optimize at a target value, the U_i for maximization and L_i for minimization will be replaced by the target value (T_i). In this way, the desirability functions generated from the individual responses are then simply multiplied to obtain the composite desirability function (D) as shown in Eq. 3.9. Further, D is maximized and the optimal result is obtained [71].

$$d_i(y_i) = \frac{y_i - L_i}{U_i - L_i} \quad (3.7)$$

$$d_i(y_i) = \frac{y_i - U_i}{L_i - U_i} \quad (3.8)$$

$$D = \left(\prod_{i=1}^n d(y_i) \right)^{1/n} \quad (3.9)$$

Presently, y_i is the regression equation of the i^{th} response, and $d(y_i)$ is the desirability function of it. The overall desirability is denoted by D and a number of responses is n .

3.14. Surface characterization using field effect scanning electrode microscopy (FESEM)

In the present study, surface morphological studies have been performed by field effect scanning electrode microscope (FESEM) [model: Sigma Smart Sem version 5.09, maker's name: Carl Zeiss Microscopy Ltd.] and scanning electrode microscope (SEM) [model: EVO version 18, maker's name: Carl Zeiss Microscopy Ltd.].



Fig. 3.8. The photographic view of (a) FESEM with EDX and (b) SEM with EDX setup.

Fig. 3.8 (a) and Fig. 3.8 (b) represent the photographic view of FESEM and SEM respectively. Normal SEM is used to study the recast layer distribution, crack lines, micro holes and material deposition on recast layer at the magnification of $500\times$. The FESEM is used to analyze the micro crack width, its distribution and deposition near micro cracks. The width of the micro cracks at different positions have been measured directly by the machine itself. In each experiments, three samples machined under lower, medium and higher concentration of powder particles have been analyzed and compared the recast layer distribution and width of the micro cracks. Before analyzing the machined surface, each samples have been cleaned

properly. The cleaning was done by plenty of water with a brush initially and dipped thereafter into acetone solution for 15 minutes. Again, the samples are cleaned by water and wrapped with cotton to ensure no foreign particles, oil film, dust and other impurities are present on the samples.

3.15. Elemental analysis by energy dispersive X-ray analysis (EDX)

Along with surface morphology, energy dispersive X-Ray analysis denoted by EDX provides the elements of the workpiece material, the inclusion of powder, electrode materials and their amount. The EDX setup is attached to the SEM instrument. In Fig. 3.8 (a) and (b), it can be observed that a separate EDX attachment has been placed at the left side of the instrument. The EDX analysis has been performed only for titanium mixed EDM samples. In this case, only one sample from each experiment machined by the medium concentration of titanium powder has been analyzed. The spectral analysis of elements and their atomic weight percentage has been represented in the result.

3.16. X-ray diffraction (XRD) characteristics of the EDM sample

In a study with graphite mixed EDM machining process of Inconel 625 and Titanium grade 2, the X-ray diffraction analysis (XRD) has been performed for three samples machined under three different concentrations of graphite particles. The XRD analysis provides the different phases associated with the chemical compound of the workpiece. In Fig. 3.9, the photographic view of the XRD instrument [Model: PANalytical XPert Pro Basic X-ray Powder Diffraction] has been shown. During this measurement, the sample is mounted on its holding device and kept inside the measuring chamber in a definite place. The chamber is made vacuum to eliminate any diffraction with air. Further, the X-ray gun provides a monochromatic X-ray on the sample and the diffracted rays from the sample have been collected and analyzed by a rotating receiver. The precision of the rotating receiver is 0.02 degrees. The receiver rotates between two angles specified in the system as 2θ diffraction angle.



Fig. 3.9. The photographic view of XRD setup.

3.17. Atomic force microscopy (AFM) analysis for measuring surface roughness

Atomic force microscopy (AFM) instrument [Makers name: NT-MTD] has been utilized to measure the surface roughness in 3D plane system at nano scale.

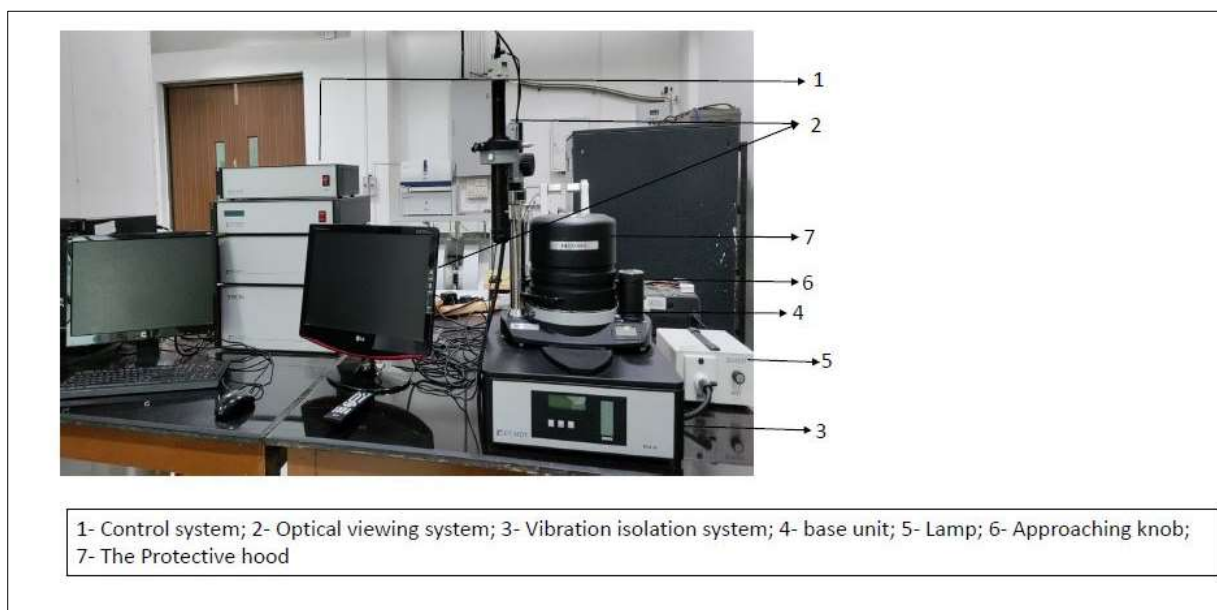


Fig. 3.10. Photographic view of AFM setup.

In the study of Inconel 625 and Titanium grade 2 machining by graphite mixed EDM, the nano level surface roughness have been measured for three surfaces measured under three different levels of current. In this measurement, a very tiny stylus having point diameter 6 to 10 nm is making a contact with the work piece surface and travel over a particular area on it. The vertical projections present in the surface deflects the stylus and the vibration is transferred by the cantilever beam on which the stylus is attached. The sophisticated sensor attached with the beam measure the vibration and provide the surface roughness value at the projections on 3D plane [72]. Fig. 3.10 represents the photographic view of the AFM setup.

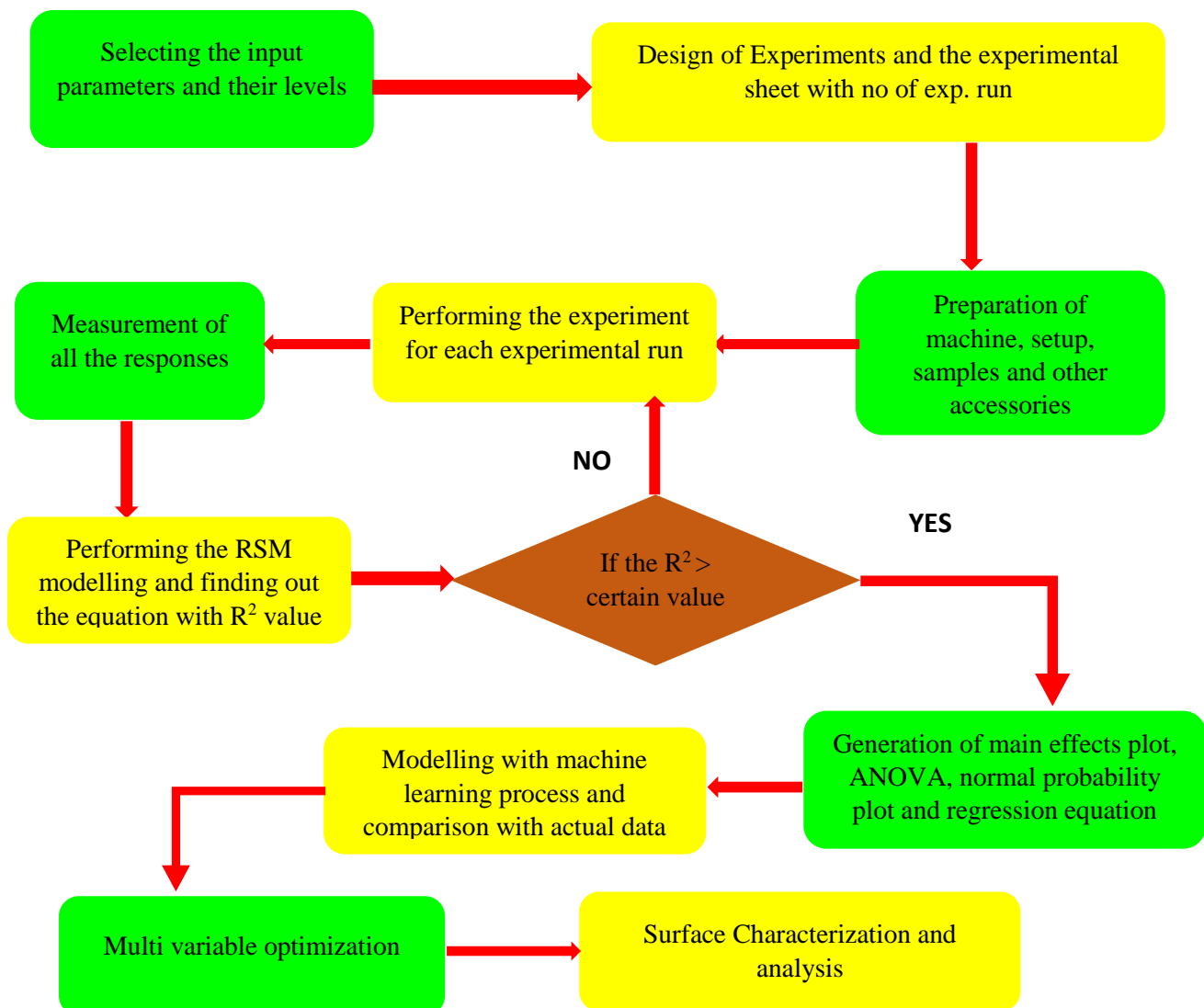


Fig. 3.11. Research planning of titanium and graphite mixed EDM.

3.18. Research plan of studying titanium and graphite added electric discharge machining

In this study, the research plan for studying the powder mixed EDM process has been represented in the flow chart shown in Fig. 3.11. The research has been started with performing the experiment, analyzing the result and characterizing of surface. In the experimental work, the design of the experiment with process parameters and their levels, the experiment and the enlistment of responses have been performed. In the computation part, modelling with RSM, applying a machine learning process and multi variable optimization have been performed. Finally, the surface characterization with SEM analysis, EDX analysis, XRD analysis and AFM study has been done and presented.

Chapter 4

*Effect of titanium mixed EDM on MRR with
Surface Roughness of Inconel 718 and
Titanium Grade 2*

4.1. Introduction

In this section, the effects of the input parameters on MRR and surface roughness are analyzed and discussed for titanium mixed EDM. Inconel 718 and Titanium grade 2 have been selected as the workpiece materials. Titanium powder was added to dielectric fluid and pure copper rod is selected as electrode material.

4.2. Effect of titanium mixed EDM on Inconel 718

The experimental result, consisting of MRR and surface roughness for Inconel 718 is represented in Table 4.1. From the result, it can be found that the highest and lowest values of MRR are 23.914 mm³/min and 5.128 mm³/min respectively. However, the surface roughness has the highest and lowest values as 5.57 µm and 2.89 µm respectively.

Table 4.1.

Experimental result for MRR with surface roughness during the machining of Inconel 718 by titanium mixed EDM

Run no.	Powder Concentration (g/l)	Pulse Current (A)	Pulse on Time (µs)	Gap voltage (V)	Pulse off Time (µs)	MRR (mm ³ /min)	Surface Roughness (R _a) (µm)
1	2	12	150	60	20	16.336	5.25
2	5	9	200	60	40	13.867	4.17
3	2	6	250	30	20	8.640	3.83
4	2	12	250	60	20	18.888	5.36
5	5	9	200	45	40	12.434	4.31
6	5	6	200	45	40	10.826	3.75
7	2	12	250	30	60	19.465	5.57
8	2	12	150	60	60	16.629	5.15
9	8	12	150	60	20	20.609	4.19
10	8	6	250	30	20	12.029	3.58
11	5	9	200	45	40	11.193	4.25
12	2	6	150	30	60	8.262	3.68
13	5	9	250	45	40	17.694	4.67
14	5	9	200	45	40	13.481	4.28

15	2	6	150	60	20	6.489	3.46
16	8	12	250	60	60	20.269	5.27
17	5	9	200	45	40	13.055	4.38
18	5	12	200	45	40	15.812	5.34
19	8	12	250	30	20	23.914	5.29
20	8	12	250	60	20	21.690	4.97
21	8	6	250	30	60	10.553	3.63
22	2	12	150	30	60	16.092	5.24
23	5	9	200	45	20	13.872	4.29
24	2	12	250	30	20	18.116	5.46
25	5	9	200	45	40	13.016	4.35
26	2	6	250	60	20	8.169	3.65
27	5	9	200	45	40	13.092	4.34
28	8	9	200	45	40	15.812	4.43
29	2	6	250	60	60	8.163	3.58
30	5	9	150	45	40	13.385	4.39
31	8	12	250	30	60	22.095	5.25
32	8	6	150	60	20	10.263	3.12
33	2	12	250	60	60	17.768	5.26
34	8	6	150	30	20	10.140	3.09
35	5	9	200	45	60	13.628	4.42
36	8	6	150	60	60	9.518	2.89
37	2	12	150	30	20	18.385	5.04
38	8	6	250	60	20	13.265	3.29
39	5	9	200	45	40	14.094	4.34
40	2	6	150	30	20	8.262	3.39
41	5	9	200	30	40	15.303	4.54
42	8	12	150	60	60	17.754	4.79
43	5	9	200	45	40	13.139	4.42
44	2	9	200	45	40	11.193	4.48
45	8	6	250	60	60	12.367	3.18
46	8	12	150	30	20	22.420	4.79

47	5	9	200	45	40	13.407	4.40
48	8	6	150	30	60	10.495	3.24
49	2	6	250	30	60	9.573	3.55
50	2	6	150	60	60	5.128	3.64
51	8	12	150	30	60	21.236	4.89
52	5	9	200	45	40	13.367	4.38

4.2.1. Effect of input parameters on MRR

In Fig. 4.1, the main effect plots for MRR have been represented to analyze the variation of MRR with the input parameters for the machining sample of Inconel 718. It is observed that an increase in powder concentration in the dielectric fluid increases the MRR. However, increase in concentration brings more powder particles to the spark gap which discharges more number of local sparks on the surface and enhances the removal of material. Secondly, an increase in pulse current significantly increases MRR because a high pulse current draws more electric energy which increases the temperature of the spark. The high temperature spark accelerates the melting rate and enhances the removal process. It is visible in Fig. 2 (a) that with a higher gap voltage, MRR decreases from 30 V and stopped at 45 V. Further, it slightly increases to 60 V. Increase of gap voltage increases the energy of the spark but distributes the spark at a larger surface area. An increase in the surface area decreases the energy density which reduces the rate of melting and thus reduces the removal of material. However, if the gap voltage increases further, the spark energy increases to such an extent and the melting takes place at a faster rate again. The spark time enhances with the increase of pulse on time during a fixed cycle time of spark on and spark off. The higher spark time for a fixed cycle removes more material and increases the MRR. However, MRR decreases and increases slightly when pulse off time increases. Also, the gap time between two successive energy pulses increases. So with high time gap, the energy input over the workpiece surface decreases which causes a decrease of MRR primarily. Later further increase of pulse off time increases the spark intensity during the cycle time and increases the electrical energy intensity. This causes slight increase of MRR.

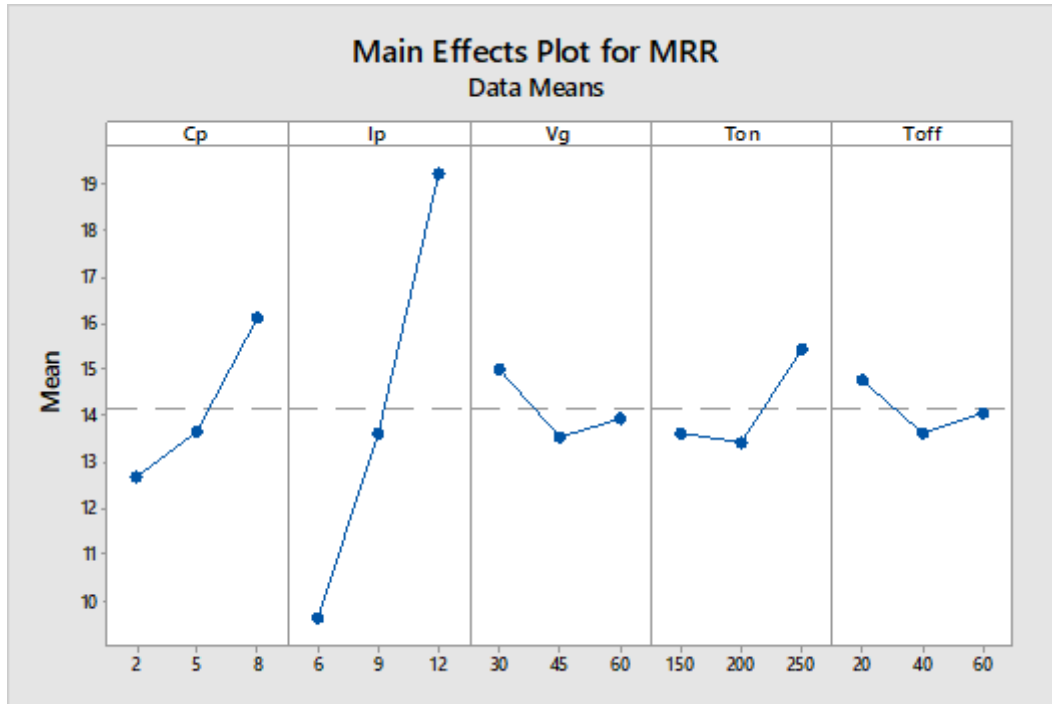


Fig. 4.1. Main effects plot for MRR of Inconel 718 machined by titanium mixed EDM.

4.2.2. Effect of input parameters on surface roughness

Fig. 4.2 shows that surface roughness increases with the increase of pulse current and pulse on time and decreases with the increase of powder concentration and gap voltage. High energy spark caused by a high current penetrates the surface at a larger depth. As a result, the depth of the crater increases during the material removal. When the powder concentration is increased, it allows more local discharges throughout the area of machining and causes a uniform spark distribution on the surface which creates a small depth of craters. Also, if the concentration of powder enhances, the spark gap also enhances. As a result, the removed materials are removed easily by the dielectric fluid circulation. Now, deposition of the recast layer on the surface is prevented and surface roughness decreases. An increase of gap voltage distributes the spark at a large surface area which produces more number of densely spaced craters. This eventually increases the surface unevenness. However since the depth of the crater is very small the overall surface roughness increases slightly. After 45 V, the increase of voltage increases the spark energy at a large surface area which reduces the crater depth. Hence the surface roughness further decreases. When the pulse on time increases, the sparking time per cycle also increases and reduces the flushing time. However the pulse on time increases as the removed material further deposited at high rate. Further, the surface roughness increases at first with decreases

later with increase of pulse of because more time gap between two successive pulse enhances the crater depth of the surface.

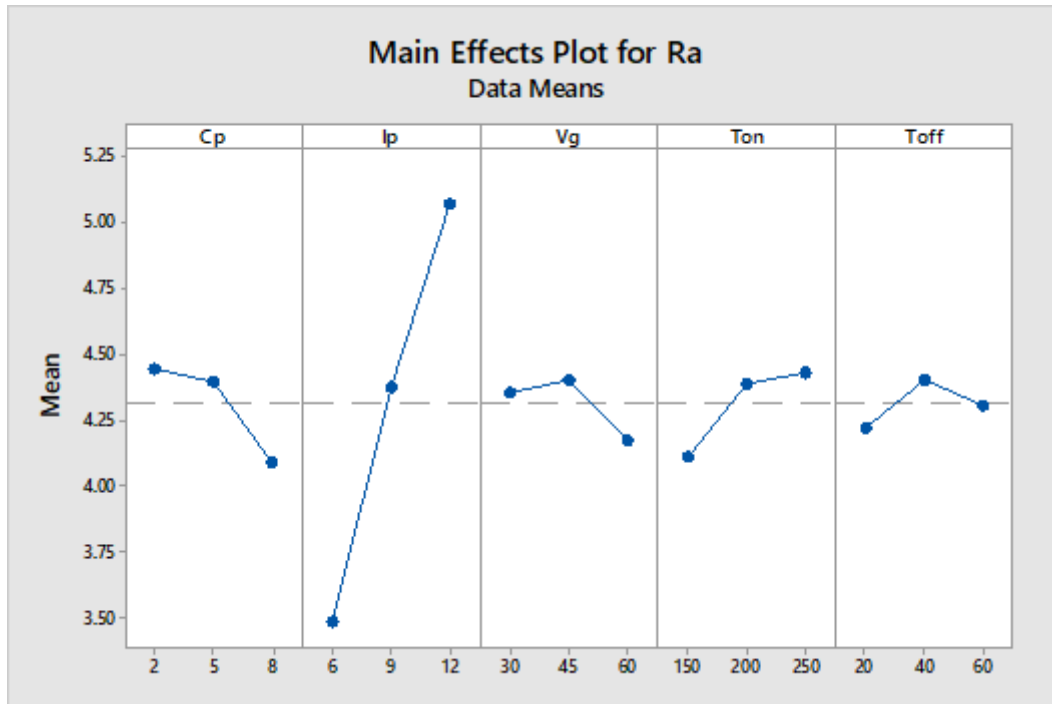


Fig. 4.2. Main effects plot of surface roughness during the processing of Inconel 718 by titanium mixed EDM.

4.2.3. ANOVA of MRR and surface roughness

ANOVA provides the significant terms along with their square terms and interactions for the machining sample of Inconel 718. In Table 4.2 and Table 4.3, the ANOVA of MRR and surface roughness have been depicted. It can be seen from the ANOVA result of MRR that the P-value of the powder concentration, pulse current, gap voltage, pulse on time and the square of pulse on time is less than 0.05 which ascertain these parameters can significantly affect material removal rate at a 95% confidence level.

The ANOVA result of surface roughness depicts that the significant parameters are powder concentration and pulse current. The comparative less significant are gap voltage, pulse on time, the interaction of power concentration with gap voltage and interaction of powder concentration with pulse on time. The F-value for pulse current is 1419.31 which indicates that the pulse current has the maximum significance on the surface roughness. Having P- values less than 0.05, of the model of MRR and surface roughness for the present study are found significant.

Table 4.2.

ANOVA result for MRR of Inconel 718 machined by titanium mixed EDM

Source	Degree of freedom	Adjusted SS	Adjusted MS	F-value	P-value
Model	20	975.30	975.30	37.06	0.000*
C_p	1	101.94	101.94	77.46	0.000*
I_p	1	804.00	804.00	610.98	0.000*
V_g	1	9.33	9.33	7.09	0.012*
T_{on}	1	28.73	28.73	21.83	0.000*
T_{off}	1	4.59	4.59	3.49	0.071
C_p^2	1	0.44	0.44	0.34	0.567
I_p^2	1	0.91	0.91	0.69	0.413
V_g^2	1	1.08	1.08	0.82	0.372
T_{on}^2	1	6.46	6.46	4.91	0.034*
T_{off}^2	1	0.08	0.08	0.06	0.812
$I_p \times C_p$	1	0.17	0.17	0.63	0.718
$C_p \times V_g$	1	0.13	0.13	0.13	0.751
$T_{on} \times C_p$	1	0.01	0.01	0.10	0.933
$C_p \times T_{off}$	1	1.92	1.92	0.01	0.236
$I_p \times V_g$	1	1.61	1.61	1.46	0.277
$T_{on} \times I_p$	1	0.07	0.07	1.23	0.824
$I_p \times T_{off}$	1	1.07	1.07	0.05	0.374
$V_g \times T_{on}$	1	2.40	2.40	0.81	0.187
$V_g \times T_{off}$	1	0.49	0.49	1.82	0.544
$T_{off} \times T_{on}$	1	0.35	0.35	0.38	0.611
Error	31	40.79	1.32	0.26	
Total	51	1016.09			

Table 4.3.

ANOVA result for Surface Roughness of Inconel 718 machined by titanium mixed EDM

Source	Degree of freedom	Adjusted SS	Adjusted MS	F-value	P-value
Model	20	26.634	1.33	78.79	0.000*
C_p	1	0.956	0.956	56.53	0.000*
I_p	1	23.990	23.990	1419.31	0.000*
V_g	1	0.237	0.237	14.03	0.001*
T_{on}	1	0.780	0.780	46.15	0.000*
T_{off}	1	0.041	0.041	2.42	0.130
C_p^2	1	0.001	0.001	0.05	0.820
I_p^2	1	0.012	0.012	0.74	0.397
V_g^2	1	0.035	0.035	2.07	0.160
T_{on}^2	1	0.008	0.008	0.46	0.503
T_{off}^2	1	0.035	0.035	2.07	0.160
$C_p \times I_p$	1	0.001	0.001	0.03	0.861
$V_g \times C_p$	1	0.085	0.085	5.03	0.032*
$T_{on} \times C_p$	1	0.131	0.131	7.77	0.009*
$T_{off} \times C_p$	1	0.011	0.011	0.64	0.429
$I_p \times V_g$	1	0.001	0.001	0.02	0.882
$T_{on} \times I_p$	1	0.054	0.054	3.17	0.085
$T_{off} \times I_p$	1	0.037	0.037	2.20	0.148
$T_{on} \times V_g$	1	0.017	0.017	0.99	0.329
$V_g \times T_{off}$	1	0.001	0.001	0.02	0.882
$T_{on} \times T_{off}$	1	0.055	0.055	3.27	0.080
Error	31	0.524	0.017		
Total	51	27.158			

4.2.4. Multi variable regression result of MRR and surface roughness

The process parameters and responses are related by regression method can be evaluated by a regression equation for the machining sample of Inconel 718.

The regression equation for MRR is available in (Eq. 4.1). The coefficient of determination value denoted by R^2 is 0.9599. It represents that the variation between the model-generated data and the actual data can be clarified by 95.99% with the quadratic equation. R^2 value closer to 1 indicates how the actual points are closer around the regression line. The value of R^2 (adjusted) and R^2 (predicted) are 0.9340 and 0.8692 respectively.

Eq. 4.2 represents the surface roughness (R_a) regression. The R^2 of the surface roughness is 0.9807. The result tells the quadratic model has been fitted suitably and the experimental data points are situated closer to the regression curve. The R^2 (adjusted) and R^2 (predicted) values are 0.9683 and 0.9329 respectively.

$$\begin{aligned}
 MRR = & 18.7 + 1.048 Cp + 3.20 Ip - 0.318 Vg - 0.258 Ton + 0.062 Toff \\
 & - 0.0469 Cp^2 - 0.0673 Ip^2 + 0.00294 Vg^2 + 0.000646 Ton^2 \\
 & - 0.00044 Toff^2 + 0.0082 CpIp + 0.00144 CpVg + 0.00011 CpTon \\
 & - 0.00408 CpToff - 0.00499 IpVg - 0.00030 IpTon \\
 & - 0.00305 IpToff + 0.000365 VgTon - 0.000414 VgToff \\
 & + 0.000104 TonToff \quad (4.1)
 \end{aligned}$$

$$\begin{aligned}
 Ra = & 1.92 - 0.077 Cp + 0.066 Ip + 0.0550 Vg - 0.0075 Ton + 0.0277 Toff \\
 & - 0.00211 Cp^2 + 0.00789 Ip^2 - 0.000529 Vg^2 + 0.000022 Ton^2 \\
 & - 0.000298 Toff^2 - 0.00045 CpIp - 0.001146 CpVg \\
 & + 0.000427 CpTon + 0.000307 CpToff - 0.000076 IpVg \\
 & + 0.000273 IpTon + 0.000568 IpToff - 0.000030 VgTon \\
 & - 0.000011 VgToff - 0.000042 TonToff \quad (4.2)
 \end{aligned}$$

4.2.5. Normal Probability Plot of MRR and Surface roughness

Fig. 4.3 represents normal probability plot generated from the MRR equation for the machining sample of Inconel 718.

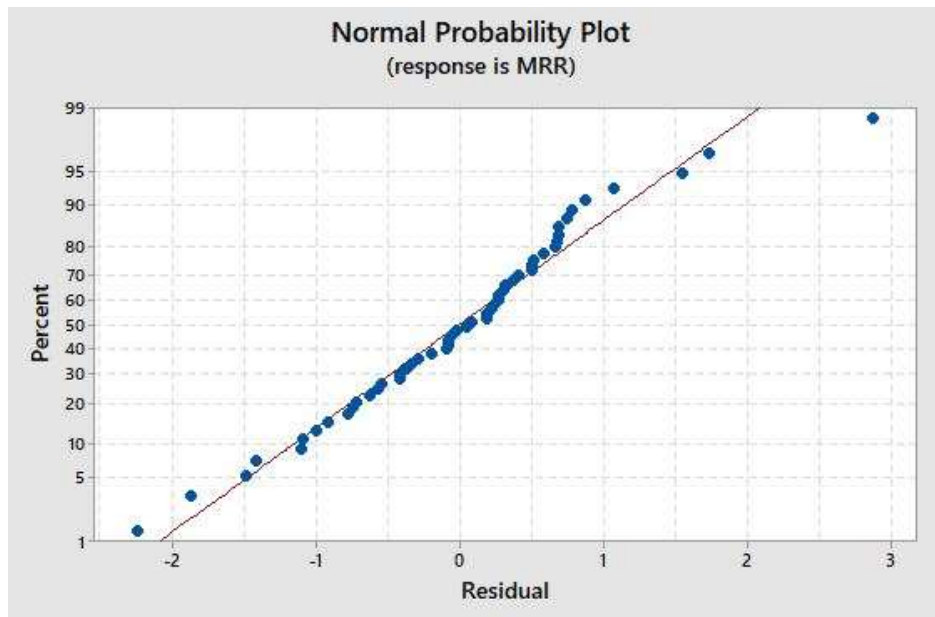


Fig. 4.3. Normal probability plot for MRR of Inconel 718.

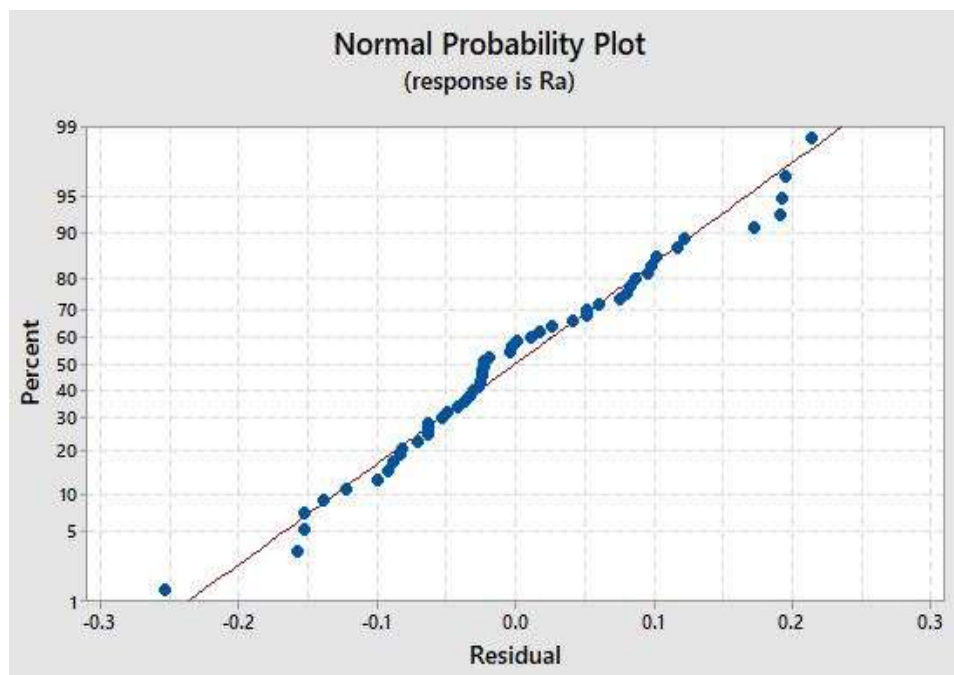


Fig. 4.4. Normal probability plot for surface roughness of Inconel 718.

The plot shows that the deviation of the residual from the straight line is less. Major points are situated closer to the line which indicates normal distribution of residuals. The normally distributed result proves that a good fitness of the model with the data has been achieved.

The plot of residual of surface roughness has been shown in Fig. 4.4. Most of the residual points are situated closer to the line and it tells that there exists a normal distribution of residuals.

4.2.6. 3D Surface Plot for MRR and Surface roughness

Here, surface plots have been generated using Design Expert 12 software where the interaction of two input parameters on responses has been shown keeping the other input parameters fixed at the central value.

Surface plots for MRR

In Fig. 4.5, Fig. 4.6 with Fig. 4.7, the blue zone in the plot represents the lowest value and the yellow indicate the highest value of the responses for the machining sample of Inconel 718. The surface plot as depicts in Fig. 4.5 indicates that a maximum MRR can be attained at a pulse current of 12A and a powder concentration with 8 g/l. The interaction of high electrical energy produced by pulse current and more local spark generated by powder particles produce maximum MRR.

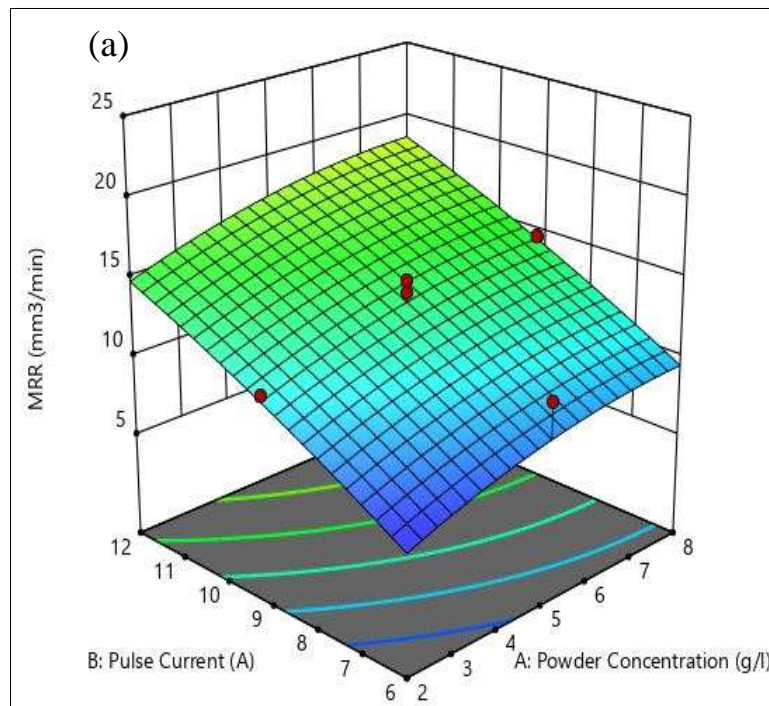


Fig. 4.5. Surface plots of MRR with the association of powder concentration with pulse current during the machining of Inconel 718.

In Fig. 4.6, it is found that the highest MRR can be achieved at powder concentration of 8 g/l with gap voltage is 30 V. The combined effect of more local spark generated by high powder concentration with concentrated narrow spark region caused by low gap voltage produces the maximum MRR. In Fig. 4.7, the highest MRR can be got at a gap voltage of 60V and pulse current of 12A.

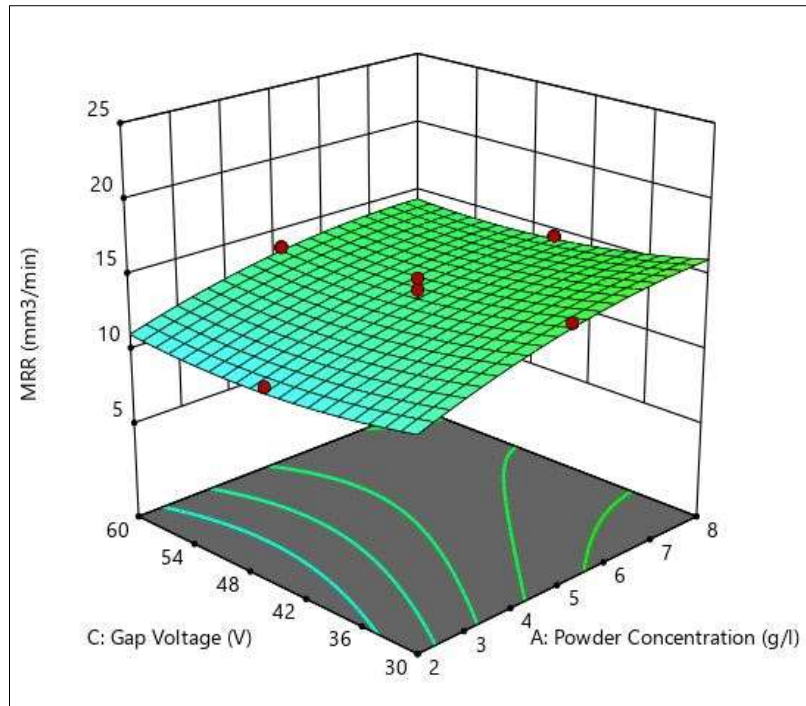


Fig. 4.6. Surface plots of MRR with the association of powder concentration with gap voltage Inconel 718 machining.

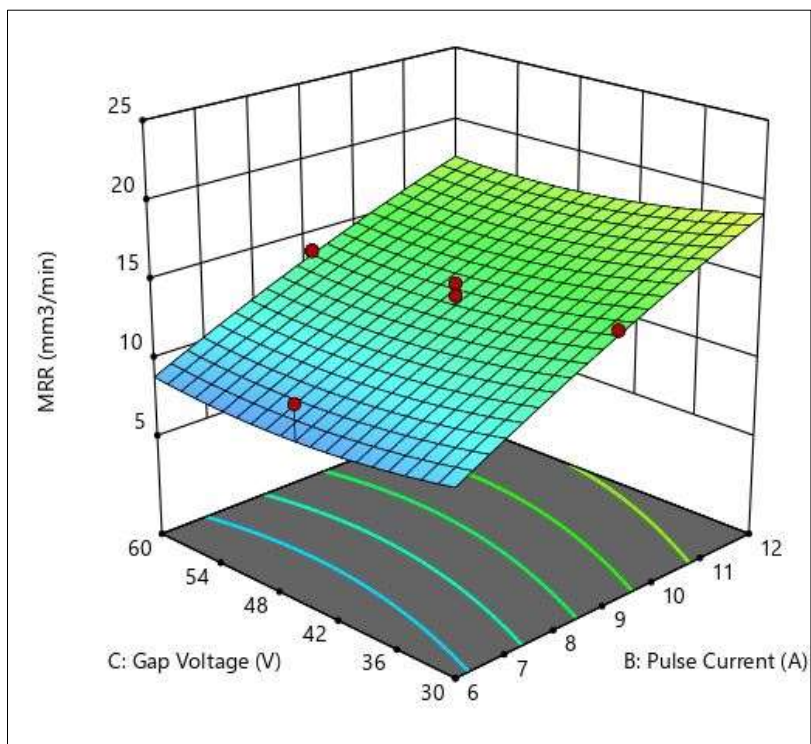


Fig. 4.7. Surface plots of MRR at the association of pulse current with gap voltage during the machining of Inconel 718.

High pulse current and gap voltage produce extremely high spark energy and the combined effect produces maximum MRR.

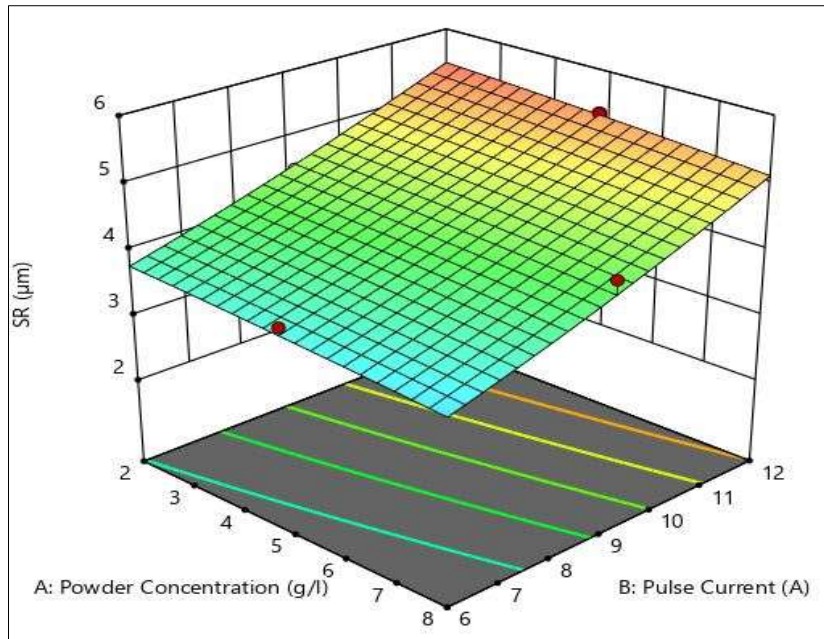


Fig. 4.8. Surface plots of surface roughness with the association of powder concentration with pulse current at Inconel 718 processing.

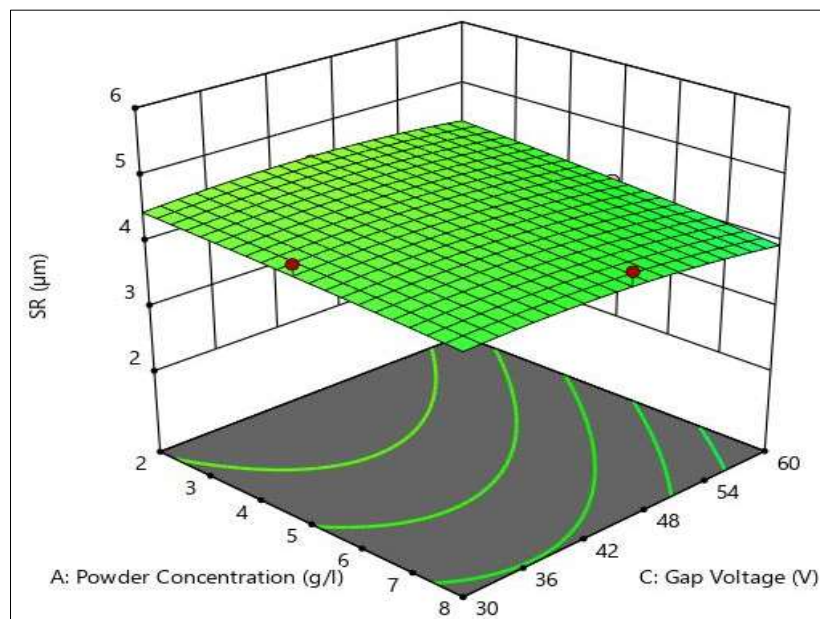


Fig. 4.9. Surface plots of surface roughness with the association of powder concentration with gap voltage at Inconel 718 processing.

Surface plots for surface roughness

In Fig. 4.8, 4.9 and 4.10 the blue region in the plot indicates the minimum value and the red region indicates the maximum value of the surface roughness for the machining sample of

Inconel 718. In Fig. 4.8, the roughness value is lowest at a low pulse current of 6 A with a high concentration of 8 g/l. This combined effect of less discharge energy caused by current and uniform spark distribution caused by powder concentration generates the least surface roughness. In Fig. 4.9, the least surface roughness has been found at a maximum of 60 V gap voltage with a maximum powder concentration of 8 g/l. The conjugate effect of uniform spark distribution and less deposition of recast layer caused by pulse on time constitutes the lowest value of roughness. The gap voltage and pulse current interaction is shown in Fig. 4.10 where lowest roughness is achieved at the pulse current of 6 A and voltage of 30 V.

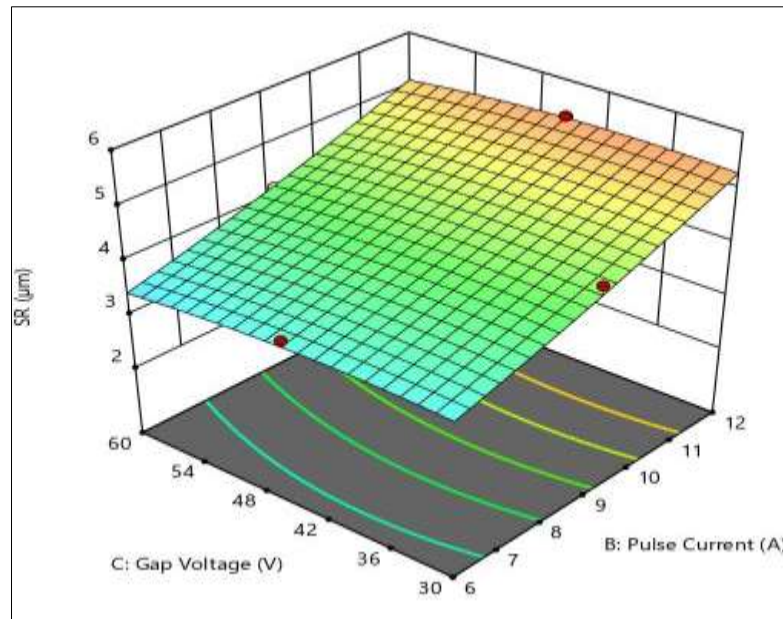


Fig. 4.10. Surface plots of MRR with the association of powder concentration with gap voltage at Inconel 718 processing.

4.3. Effect of titanium mixed EDM on Titanium Grade 2

The experimental result consists of MRR and surface roughness of Titanium grade 2 has been represented in Table 4.4. The powder and the electrode have been selected as titanium and copper. From the result, it has been found that the highest and lowest values of MRR are 1.552 mm³/min and 0.355 mm³/min respectively whereas the highest and lowest values of surface roughness are 15.026 μm and 5.889 μm.

Table 4.4.

Experimental of Titanium Grade 2 machined by titanium mixed EDM

Run no.	Powder Concentration (g/l)	Pulse Current (A)	Pulse on Time (μs)	Gap voltage (V)	Pulse off Time (μs)	MRR (mm³/min)	Surface Roughness (Ra) (μm)
1	2	12	150	60	20	0.843	12.648
2	5	9	200	60	40	0.976	8.421
3	2	6	250	30	20	0.931	11.664
4	2	12	250	60	20	0.887	9.147
5	5	9	200	45	40	1.552	6.995
6	5	6	200	45	40	1.109	9.983
7	2	12	250	30	60	0.931	6.190
8	2	12	150	60	60	0.843	15.026
9	8	12	150	60	20	0.887	9.147
10	8	6	250	30	20	0.887	9.147
11	5	9	200	45	40	0.798	8.622
12	2	6	150	30	60	0.887	9.147
13	5	9	250	45	40	1.153	9.578
14	5	9	200	45	40	0.931	13.954
15	2	6	150	60	20	1.109	8.414
16	8	12	250	60	60	0.976	13.414
17	5	9	200	45	40	0.887	9.147
18	5	12	200	45	40	0.621	7.527
19	8	12	250	30	20	0.355	8.218
20	8	12	250	60	20	0.621	7.266
21	8	6	250	30	60	0.887	9.147
22	2	12	150	30	60	1.064	6.218
23	5	9	200	45	20	1.020	8.014
24	2	12	250	30	20	0.887	9.133
25	5	9	200	45	40	0.931	8.547
26	2	6	250	60	20	0.798	8.426
27	5	9	200	45	40	0.976	6.889
28	8	9	200	45	40	0.887	9.147

29	2	6	250	60	60	1.153	9.374
30	5	9	150	45	40	0.931	8.450
31	8	12	250	30	60	0.887	9.147
32	8	6	150	60	20	0.843	12.209
33	2	12	250	60	60	0.931	7.968
34	8	6	150	30	20	0.754	7.204
35	5	9	200	45	60	0.931	5.889
36	8	6	150	60	60	0.887	9.147
37	2	12	150	30	20	0.887	7.743
38	8	6	250	60	20	1.242	6.465
39	5	9	200	45	40	0.887	9.706
40	2	6	150	30	20	0.931	12.988
41	5	9	200	30	40	1.064	8.832
42	8	12	150	60	60	1.330	9.118
43	5	9	200	45	40	0.887	9.147
44	2	9	200	45	40	0.843	9.051
45	8	6	250	60	60	1.020	8.041
46	8	12	150	30	20	1.109	7.687
47	5	9	200	45	40	0.532	8.253
48	8	6	150	30	60	1.020	9.683
49	2	6	250	30	60	0.576	7.494
50	2	6	150	60	60	1.020	9.543
51	8	12	150	30	60	0.887	14.068
52	5	9	200	45	40	1.064	9.449

4.3.1. Effect of input parameters on MRR

In Fig. 4.11, the main effects plots for MRR have been represented to analyze the MRR changes with the input parameters for the machining of Titanium grade 2. In the Fig. 4.11, it is visible that MRR enhances with the addition of titanium concentration and current. However, this decreases with gap voltage. As per pulse on time with pulse off time is concerned, variation of MRR is very small and mainly decreasing with the increase of these two parameters. An

increase in titanium concentration brings higher concentrations of particles which discharges more number of local sparks on the surface and enhances the removal of material.

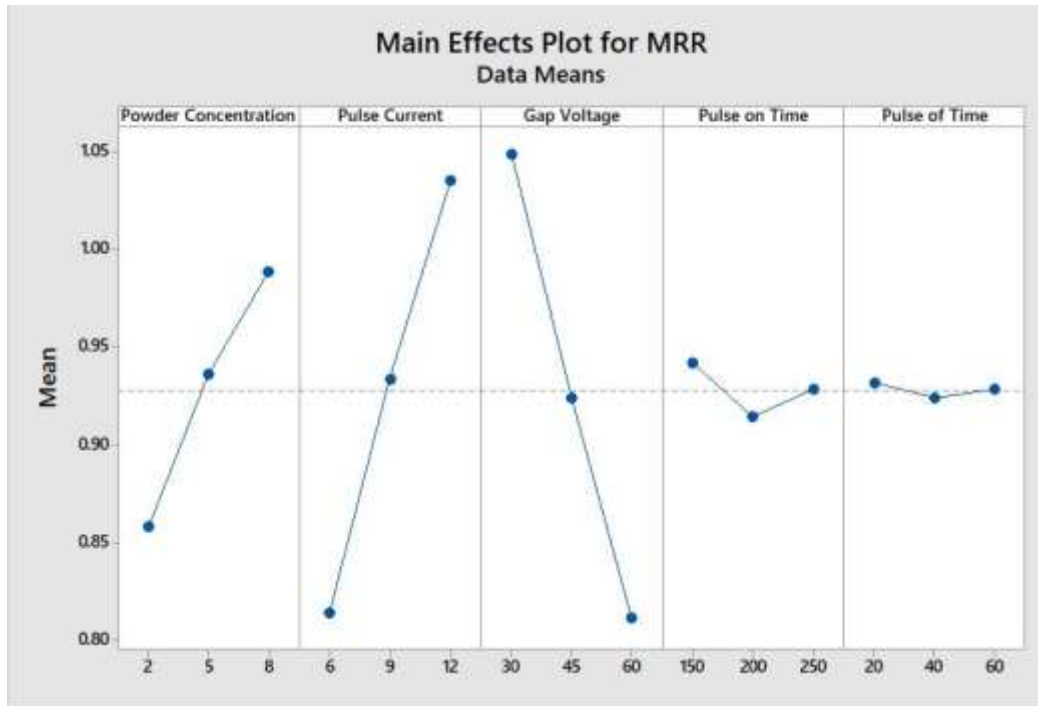


Fig. 4.11. Main effects plot of MRR of Titanium Grade 2 machined by titanium mixed EDM

On the other hand, an increase in pulse current significantly increases MRR because a high pulse current draws more electric energy which increases the temperature of the spark. The high temperature spark accelerates the melting rate and enhances the removal process. The enhancement of voltage with the same current deflects the electron flow outward from the center which reduces the intensity of the energy on the surfaces and the removal of material decreases. When the pulse on time increases, it provides more amount of energy for larger time but the particles are dissociated at that time and make random collision among themselves. The reduction of local spark contribution reduces the MRR primarily but further with the energy provided by the main spark, MRR enhances slightly.

4.3.2. Effect of input parameters on surface roughness

It can be observed in Fig. 4.12 that surface roughness increases with the growing of pulse current, gap voltage with pulse time and reduces with the growing of concentration and pulse off. High energy spark caused by a high current penetrates the surface at a larger depth to remove the material.

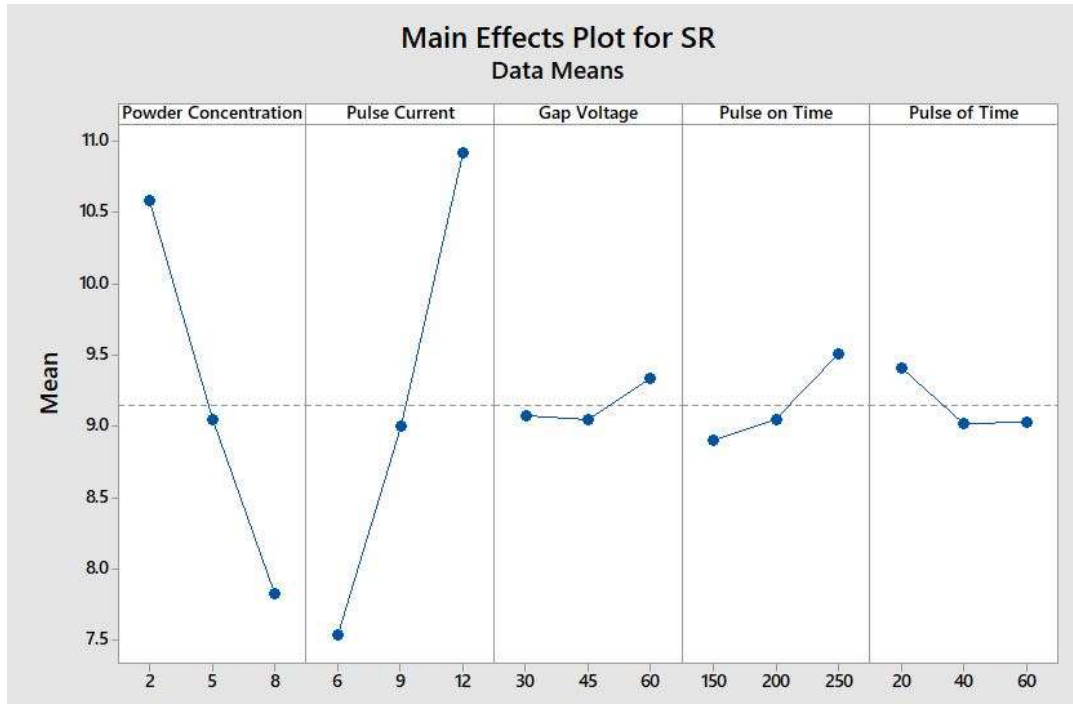


Fig. 4.12. Main effects plot of surface roughness of Titanium Grade 2 machined by titanium mixed EDM.

When the powder concentration is increased, it allows more local discharges throughout the area of machining and causes a uniform spark distribution on the surface which creates a small depth of craters. Also, the gap of electrodes enhances with the increase of concentration. As a result, the removed materials are washed out easily by the flow and the recast layer on the surface is prevented and surface roughness decreases. An increase of gap voltage distributes the spark at a large surface area which produces more number of craters over the surface. Within a fixed area of surface, number of craters increases with by the distribution of the spark. This reflects an enhancement of roughness with voltage. When the pulse time increases, sparking time per cycle also increases and reduces the flushing time. As a result, the roughness enhances with growing of pulse time.

4.3.3. ANOVA of MRR and surface roughness

The significance of input parameters on each response was evaluated by ANOVA along with their square terms and interactions for the machining of Titanium Grade 2. The ANOVA result for MRR and surface roughness have been presented in Table 4.5 and Table 4.6 respectively. It can be observed from the ANOVA result of MRR that the P-value of the powder

concentration, pulse current, gap voltage and the square of pulse on time which ascertain these parameters can significantly affect material removal rate at a 95% confidence level. There are some interaction terms which are significant for MRR. They are interactions of powder concentration with pulse current and pulse off time, pulse current with pulse off time, pulse on time, gap voltage and pulse off time and pulse on time with pulse of time. The gap voltage has major significance on MRR with the maximum F value of 114.54.

Table 4.5.

ANOVA result for MRR of Titanium Grade 2 machined by titanium mixed EDM

Source	DF	MRR			
		Adjusted SS	Adjusted MS	F-value	P-value
Model	20	1.729	0.086	20.69	0.000*
C_p	1	0.144	0.144	34.52	0.000*
I_p	1	0.418	0.418	100.04	0.000*
V_g	1	0.478	0.478	114.54	0.000*
T_{on}	1	0.001	0.001	0.34	0.564
T_{off}	1	0.006	0.006	0.02	0.902
C_p^2	1	0.019	0.019	4.60	0.040
I_p^2	1	0.010	0.010	2.59	0.117
V_g^2	1	0.001	0.001	0.31	0.583
T_{on}^2	1	0.030	0.030	7.34	0.011*
T_{off}^2	1	0.001	0.001	0.31	0.583
$I_p \times C_p$	1	0.166	0.166	39.71	0.000*
$C_p \times V_g$	1	0.012	0.012	2.88	0.100
$T_{on} \times C_p$	1	0.015	0.015	3.76	0.062
$T_{off} \times C_p$	1	0.108	0.108	25.89	0.000*
$I_p \times V_g$	1	0.088	0.088	21.22	0.000*
$T_{on} \times I_p$	1	0.048	0.048	11.55	0.002*
$I_p \times T_{off}$	1	0.153	0.153	36.81	0.000*
$T_{on} \times V_g$	1	0.006	0.006	1.47	0.235
$T_{off} \times V_g$	1	0.024	0.024	5.88	0.021*

$T_{\text{off}} \times T_{\text{on}}$	1	0.012	0.012	2.90	0.099
Error	31	0.129	0.004	3.46	
Total	51	1.859			

The ANOVA result of surface roughness depicts that the significant parameters are powder concentration, pulse current, pulse on time and the interaction of power concentration with pulse current, pulse current with pulse off time, interaction of pulse current with pulse off time.

Table 4.6.

ANOVA result for Surface Roughness of Titanium Grade 2 machined by titanium mixed EDM

Source	DF	Surface Roughness (R_a)			
		Adjusted SS	Adjusted MS	F-value	P-value
Model	20	199.63	9.981	20.66	0.000*
C_p	1	64.573	64.573	133.67	0.000*
I_p	1	96.884	96.884	200.56	0.000*
V_g	1	0.561	0.561	1.16	0.290
T_{on}	1	3.183	3.183	6.59	0.015*
T_{off}	1	1.228	1.228	2.54	0.121
C_p^2	1	0.024	0.024	0.05	0.824
I_p^2	1	0.228	0.228	0.47	0.498
V_g^2	1	0.014	0.014	0.03	0.865
T_{on}^2	1	0.007	0.007	0.01	0.905
T_{off}^2	1	0.044	0.044	0.09	0.766
$C_p \times I_p$	1	20.871	20.871	43.20	0.000*
$C_p \times V_g$	1	0.268	0.268	0.55	0.462
$C_p \times T_{\text{on}}$	1	0.788	0.788	1.63	0.211
$T_{\text{off}} \times C_p$	1	0.780	0.780	1.61	0.213
$I_p \times V_g$	1	1.036	1.036	2.14	0.153
$I_p \times T_{\text{on}}$	1	4.004	4.004	8.29	0.007*
$I_p \times T_{\text{off}}$	1	2.486	2.486	5.15	0.030*

$V_g \times T_{on}$	1	1.983	1.983	4.10	0.051
$V_g \times T_{off}$	1	0.033	0.033	0.07	0.794
$T_{off} \times T_{on}$	1	0.276	0.276	0.57	0.456
Error	31	14.975	0.483	0.293	
Total	51	214.606			

However, the F-value for pulse current is 200.56 which indicates that the pulse current has the maximum significance on the surface roughness. The P-value of the model for both MRR and surface roughness is less than 0.05. It indicates that the ANOVA model associated with MRR and surface roughness for the present study are found significant.

However, the other parameters and their interactions were considered insignificant as the p values of those terms are greater than 0.05.

4.3.4. Multi variable regression result of MRR and Surface roughness

The input parameters during the machining of Titanium grade 2 has been related to the responses by regression equation. Eq. 4.3 shows the regression equation of MRR. The R^2 value is 0.9303. It represents that the variation between the model-generated data and the actual data can be clarified by 93.03% with the quadratic equation. R^2 value closer to 1 indicates how the actual points are closer around the regression line. The R^2 (adjusted) and R^2 (predicted) are 0.8853 and 0.7600 respectively.

Eq. 4.4 indicates the regression relationship of surface roughness. The R^2 for surface roughness is 0.9302 that indicates relationship has been fitted suitably and the experimental data points are situated closer to the regression curve. The R^2 (adjusted) and R^2 (predicted) are 0.8852 and 0.7433 respectively.

$$\begin{aligned}
MRR = & 2.684 + 0.058 Cp + 0.082 Ip - 0.025 Vg - 0.015 Ton - 0.012 Toff \\
& - 0.0098 Cp^2 - 0.0074 Ip^2 + 0.0001 Vg^2 + 0.0004 Ton^2 \\
& + 0.0005 Toff^2 + 0.00800 CpIp - 0.00043 CpVg - 0.00015 Cp Ton \\
& + 0.00097 CpToff + 0.00117 IpVg - 0.00026 IpTon \\
& + 0.00116 IpToff + 0.00002 VgTon - 0.00009 VgToff \\
& - 0.00002 TonToff \quad (4.3)
\end{aligned}$$

$$\begin{aligned}
Ra = & 8.29 + 0.261 Cp + 0.299 Ip - 0.006 Vg - 0.031 Ton - 0.005 Toff \\
& - 0.0110 Cp^2 + 0.0337 Ip^2 - 0.0003 Vg^2 - 0.0002 Ton^2 \\
& + 0.0003 Toff^2 - 0.08970 CpIp + 0.00203 CpVg + 0.00105 CpTon \\
& - 0.00260 CpToff - 0.00400 IpVg + 0.00236 IpTon \\
& - 0.00465 IpToff + 0.00033 VgTon + 0.00012 VgToff \\
& + 0.00009 TonToff \quad (4.2)
\end{aligned}$$

4.3.5. Normal Probability Plot of MRR and surface roughness

In the Fig. 4.13, normal probability plot for the MRR equation has been shown. The plot shows that the deviation of the residual from the straight line is less. Major points are situated near to the line which indicates the residuals are normally placed. The normally distributed result proves that a good fitness of the model with the data has been achieved.

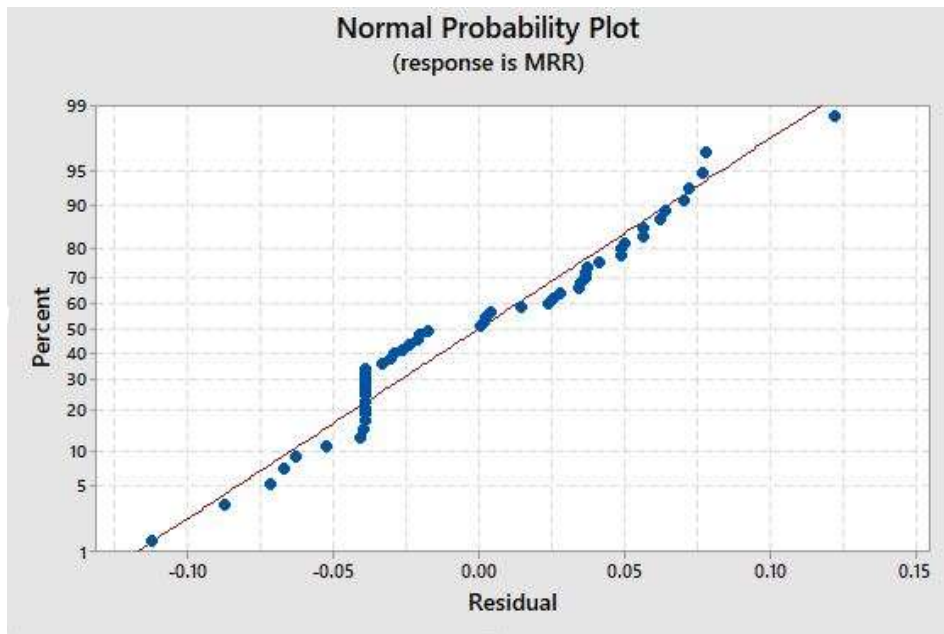


Fig. 4.13. Normal probability plot of MRR of Titanium Grade 2.

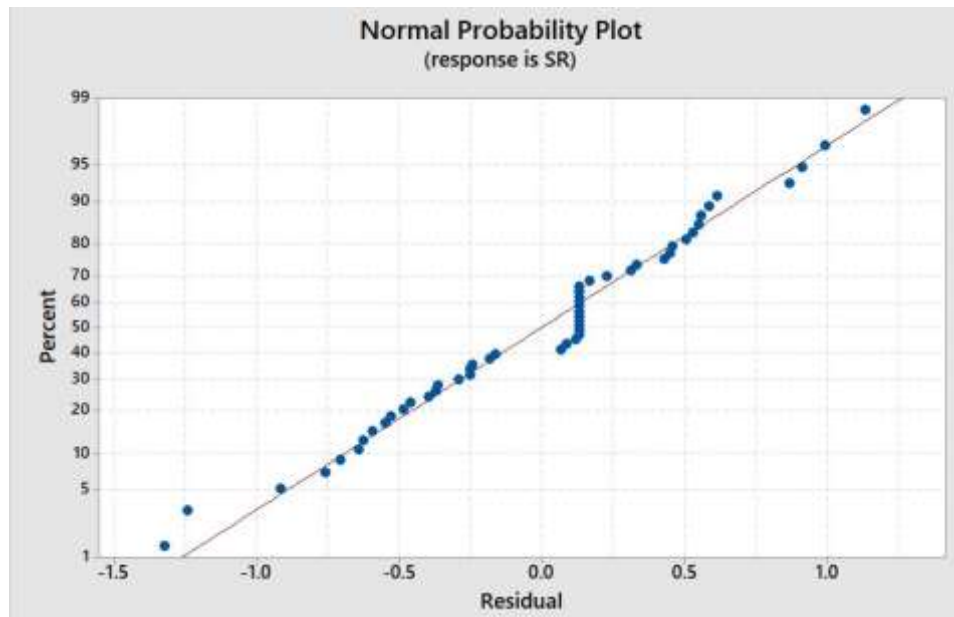


Fig. 4.14. Normal probability plot of Surface Roughness of Titanium Grade 2.

In Fig. 4.14, the normal probability plot for surface roughness have been represented. Most of the residual points are situated near to line which indicates the residuals are normally placed.

4.3.6. 3D Surface Plot for MRR and surface roughness

This study represents the surface plots generated using Design Expert 12 software where the interaction of two input parameters on responses has been shown by keeping the other input parameters fixed at the central value.

Surface plots for MRR

In the Fig. 4.15, Fig. 4.16 and Fig. 4.17, the blue zone in the plot represents the lowest and the yellow zone represents the highest value for the responses.

The 3D plot represented in Fig. 4.15 indicates that a maximum MRR can be attained at a pulse current of 12A and a concentration of 8 g/l. The interaction of high electrical energy produced by pulse current and more local spark generated by powder particles produce maximum MRR. In Fig. 4.16, it is found that the highest MRR can be achieved when concentration is 8 g/l with voltage is 30 V. The combined effect of more local spark generated by high powder concentration with concentrated narrow spark region caused by low gap voltage produces the maximum MRR.

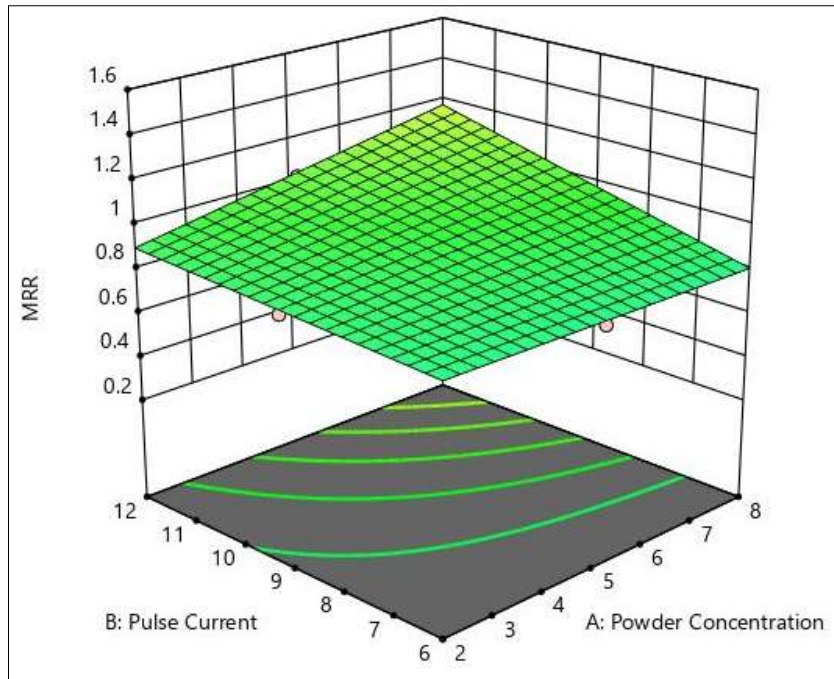


Fig. 4.15. Surface plots of MRR with the association of powder concentration with pulse current during Titanium Grade 2 machining.

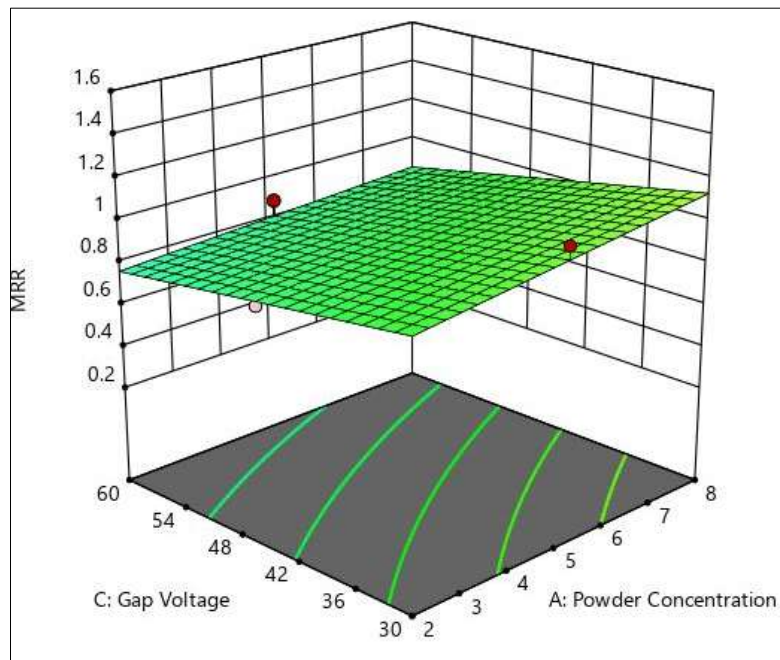


Fig. 4.16. Surface plots of MRR with the association of powder concentration with gap voltage during Titanium Grade 2 machining.

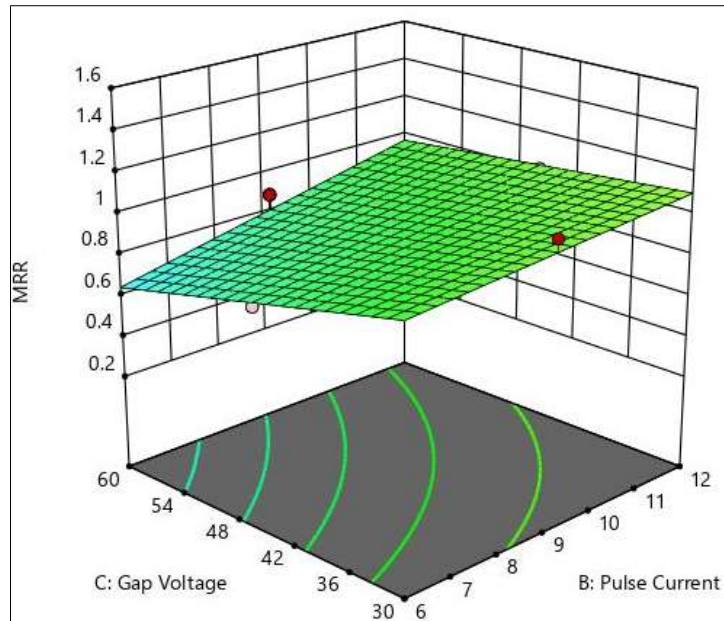


Fig. 4.17. Surface plots of MRR with the association of pulse current with gap voltage during the machining of Titanium Grade 2

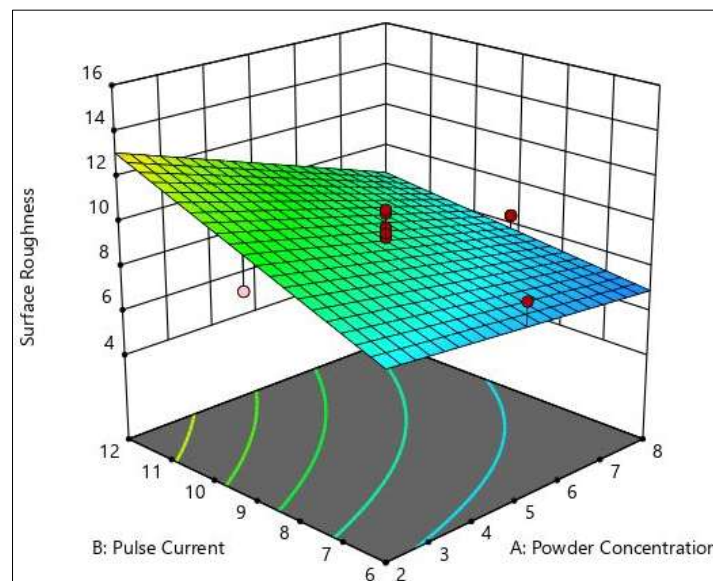


Fig. 4.18. Surface plots of surface roughness with the association of powder concentration with pulse current Titanium Grade 2 machining.

Surface plots for surface roughness

In Fig. 4.18, 4.19 and 4.20 the blue region in the plot indicates the minimum value and the red region indicates the maximum value of the surface roughness. In Fig. 4.18, it can be seen that the roughness is minimum at a low value of 6 A current and a high concentration of 8 g/l. Hence, the combined effect of less discharge energy caused by current and uniform spark distribution caused by powder concentration generates the least surface roughness. In Fig. 4.19,

the least surface roughness has been found at a maximum voltage of 30 V and a maximum concentration of 8 g/l.

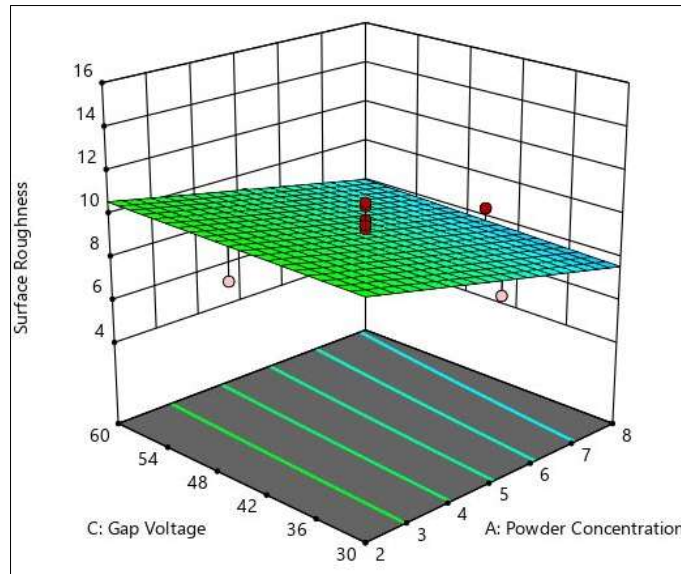


Fig. 4.19. Surface plots of surface roughness with the association of concentration with gap voltage during Titanium Grade 2 machining.

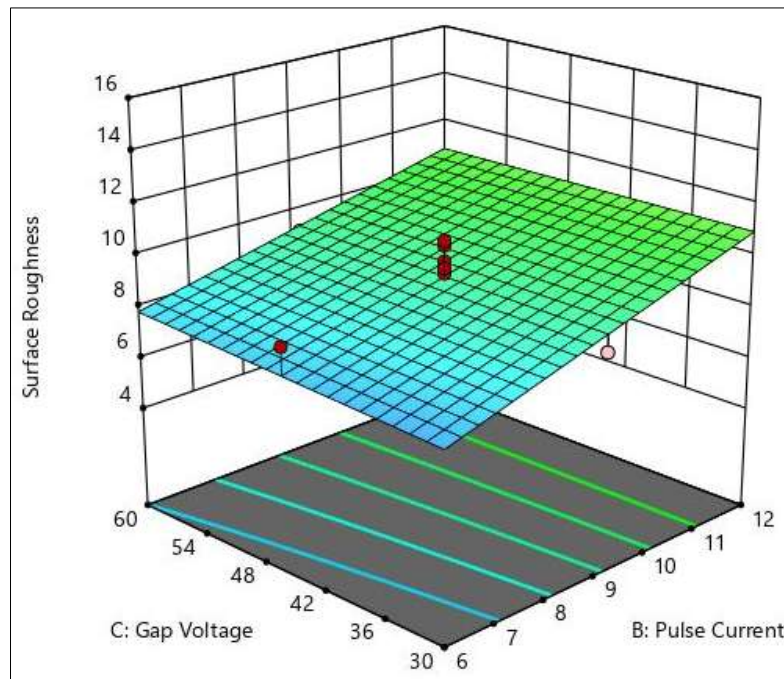


Fig. 4.20. Surface plots of MRR with the association of powder concentration and gap voltage during the machining of Titanium Grade 2

The stable and uniform spark distribution caused by low gap voltage and high powder concentration are responsible for generating the least surface roughness. The conjugate effect of uniform and stable spark distribution makes less deposition of recast layer and constitutes

the lowest value of roughness. Interaction of voltage and pulse current have been represented in Fig. 4.20 in which lowest surface roughness has been achieved at the current of 6 A and voltage of 30 V. The low intensity energy caused by low current and stable spark caused by low voltage reduces the surface roughness in their interactions.

4.4. Comparison between surface roughness and MRR of Titanium grade 2 and Inconel 718 machining

In this section, a comparative study have been between the responses of Inconel 718 and Titanium grade 2 machined during powder mixed EDM of titanium particles. Since the input process parameters, their level values, design of experiment and measurement of responses of both the materials are unaltered, the comparison can easily be performed. The common significant input parameters from ANOVA for both the responses are powder concentration and pulse current. Hence the comparative study of MRR and surface roughness were being performed against these two input parameters. Fig 4.21 and Fig 4.22 represent the comparison of MRR and surface roughness against powder concentration and pulse current respectively. The plots are drawn based on the data points taken from main effects plot where three data points have been chosen for lower, intermediate and upper value of the process parameters.

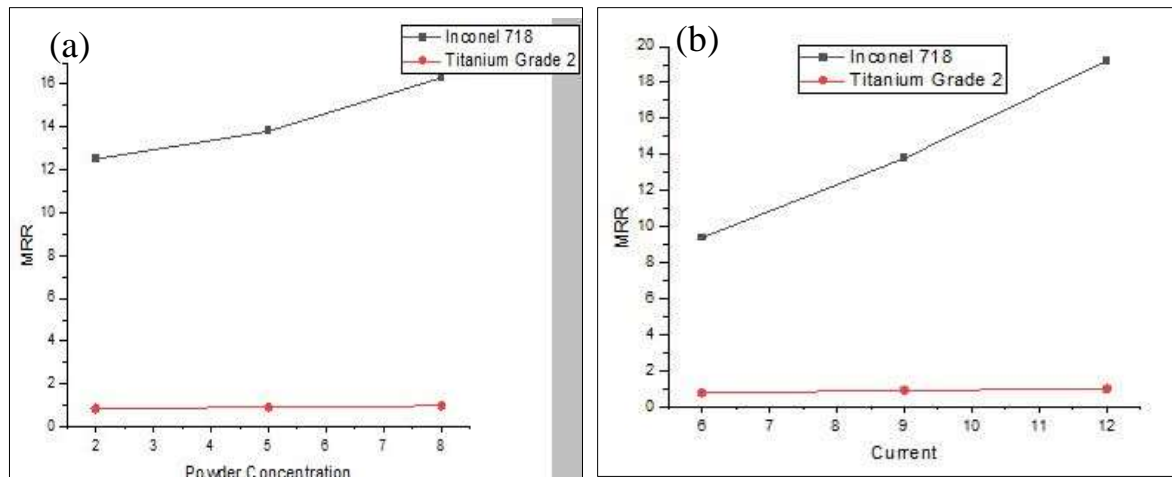


Fig. 4.21. Comparison between MRR of Inconel 718 and Titanium grade 2 against (a) powder concentration (b) current.

From Fig. 4.21 (a) – (b), this can be seen that enhancement of MRR found continuously with the increase of powder concentration and pulse current respectively. However, the MRR values and rate of increment of Inconel 718 machining are much higher than the Titanium grade 2 machining. These have happened because the hardness and melting point of Inconel 718 is much lower than Titanium grade 2. When the discharges takes place at same rate, Inconel 718

having a low hardness and melting point melts and eroded at faster rate than Titanium grade 2. Hence the MRR value of Inconel 718 is more. Along with that with the increase of powder concentration and pulse current, more amount of discharges takes place which essentially increases the MRR value but due to high melting point, Titanium grade 2 resists the rate of melting and erosion. Due to which the rate of increment of MRR is found to be less in case of titanium grade 2 compared to Inconel 718 during the increase of powder concentration and pulse current.

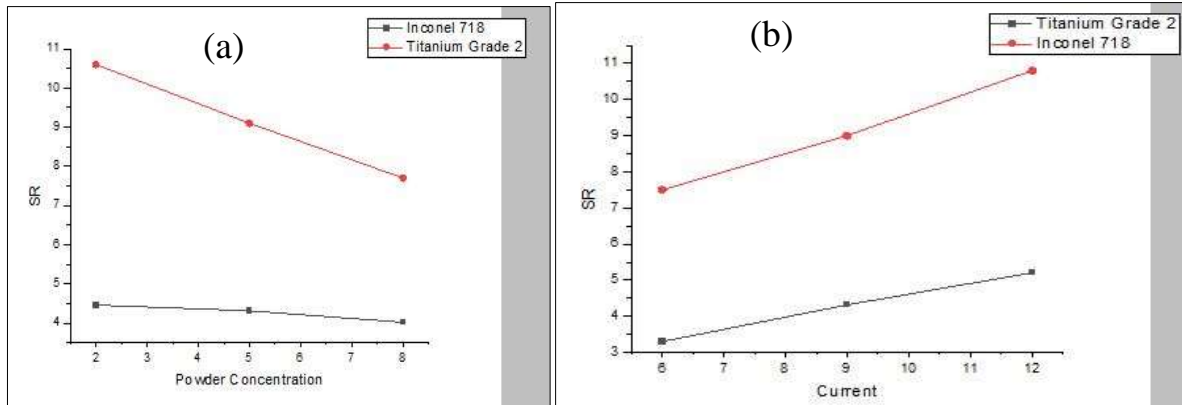


Fig. 4.22. Comparison between surface roughness of Inconel 718 and Titanium grade 2 against (a) powder concentration (b) current and (c) gap voltage.

In Fig. 4.22 (a)-(b), the variations of surface roughness have been compared against powder concentration and pulse current respectively. It has been found that roughness of both the materials decrease with the increase of powder concentration and increase with increase of current. However in both the cases the surface roughness is higher in Titanium sample compared to Inconel 718. Due to the application of high current the more energy transferred to the surface. The excessive energy causes enhanced thermal distortion to the surface which increases the depth of the crater. Along with that, titanium having high hardness and brittleness experiences more distortion than Inconel 718. The depth and randomness of surface irregularities increases in Titanium and causes high surface roughness. However, the uniformity of spark caused by enhance powder concentration reduces the surface roughness in both the materials but the reduction rate is higher in case of Titanium because with high uniformity of spark, the hard and titanium surface experiences less distortion of surface.

Chapter 5

Effect of graphite mixed EDM on MRR, Tool wear rate and Surface Roughness of Inconel 625 and Titanium Grade 2

5.1. Introduction

Material removal rate, tool wear rate and surface roughness are the responses to characterize Inconel 625 and Titanium grade 2. Graphite micro powder has been added to the EDM oil dielectric fluid and machining has been performed with that.

5.2. Effect of graphite mixed EDM on Inconel 625

The result of the present experiment has been presented in Table 5.1 by listing the measured values of all three responses.

Table 5.1.

Experimental result of MRR, TWR and SR for Inconel 625 machined by graphite mixed EDM

Run no.	Current	Duty Cycle	Pulse on Time	Powder Concentration	Powder mesh size	MRR	TWR	SR
	(A)		(μ s)	(g/l)	(μ m)	(mm ³ /min)	(mm ³ /min)	(μ m)
1	8	0.7	55	5	25	16.659	0.0797	9.08
2	8	0.5	75	5	25	18.780	0.0810	9.99
3	12	0.7	55	5	35	29.068	0.1627	8.50
4	8	0.9	55	5	35	20.468	0.0882	8.34
5	8	0.7	55	2	35	16.736	0.0574	10.32
6	8	0.7	55	5	25	18.602	0.0763	8.86
7	8	0.7	35	8	25	16.563	0.0680	7.41
8	4	0.7	55	8	25	3.989	0.0190	4.67
9	12	0.7	35	5	25	28.919	0.1493	12.33
10	12	0.7	55	8	25	29.452	0.1419	9.11
11	8	0.9	75	5	25	15.450	0.0921	9.08
12	8	0.7	55	2	15	19.879	0.0863	8.69
13	12	0.7	75	5	25	27.923	0.1654	10.39
14	8	0.9	55	2	25	16.983	0.0762	8.69
15	8	0.7	55	8	15	23.324	0.0664	9.58
16	8	0.9	55	5	15	21.771	0.0782	8.46

17	12	0.7	55	5	15	30.772	0.1656	11.56
18	8	0.5	35	5	25	12.994	0.0861	8.74
19	4	0.9	55	5	25	4.404	0.0157	4.20
20	8	0.7	35	5	15	14.739	0.0881	9.53
21	8	0.5	55	8	25	20.468	0.0728	8.29
22	8	0.7	55	5	25	18.697	0.0991	6.72
23	12	0.5	55	5	25	23.697	0.1738	11.62
24	8	0.7	75	5	15	27.921	0.0685	9.55
25	4	0.7	55	5	35	4.333	0.0249	3.12
26	4	0.5	55	5	25	4.542	0.0132	4.10
27	8	0.7	55	5	25	20.024	0.0823	7.58
28	8	0.9	35	5	25	13.586	0.0813	9.57
29	8	0.9	55	8	25	23.726	0.0775	7.13
30	8	0.5	55	5	15	19.431	0.0650	10.79
31	12	0.7	55	2	25	20.472	0.2039	10.93
32	8	0.5	55	5	35	16.055	0.0998	6.74
33	8	0.7	75	2	25	17.546	0.0789	9.86
34	8	0.5	55	2	25	12.576	0.0737	10.98
35	8	0.7	55	8	35	20.438	0.0642	7.81
36	8	0.7	75	8	25	20.201	0.0781	7.43
37	8	0.7	35	2	25	15.521	0.0991	8.28
38	4	0.7	55	2	25	6.536	0.0884	6.12
39	8	0.7	55	5	25	16.543	0.0944	10.14
40	4	0.7	35	5	25	2.204	0.0159	4.60
41	8	0.7	55	5	25	19.589	0.0775	8.66
42	4	0.7	75	5	25	7.701	0.0261	4.53
43	4	0.7	55	5	15	4.147	0.0129	3.92
44	12	0.9	55	5	25	27.429	0.1886	10.76
45	8	0.7	75	5	35	8.672	0.0713	10.14
46	8	0.7	35	5	35	27.429	0.0827	7.90

Table 5.1 represents the highest MRR, TWR and SR as 30.772 mm³/min, 0.2039 mm³/min and 12.33 μm respectively whereas the lowest values are 2.204 mm³/min, 0.0129 mm³/min and 3.12 μm respectively.

5.2.1. Effect of input parameters on MRR

In the Fig. 5.1, the variations of MRR are shown against their mean values with respect to the input parameters. It can be observed that the MRR varies notably with current, powder concentration and mesh size. Also, in the Fig. 5.1, the variation of MRR is found to be maximum in the case of a change in current from lower to a higher level. From Table 5.1, the average of MRR values for lower, intermediate and higher levels can be calculated as 4.732 mm³/min, 18.379 mm³/min and 27.217 mm³/min respectively. The principal reason for the increase in MRR is the enhancement of energy transfer rate on the surface. Material is melted and vaporized at a higher rate due to the high energy transfer. Now, high energy transfer occurs mainly due to an increase of the current which directly provides more energy to the discharges.

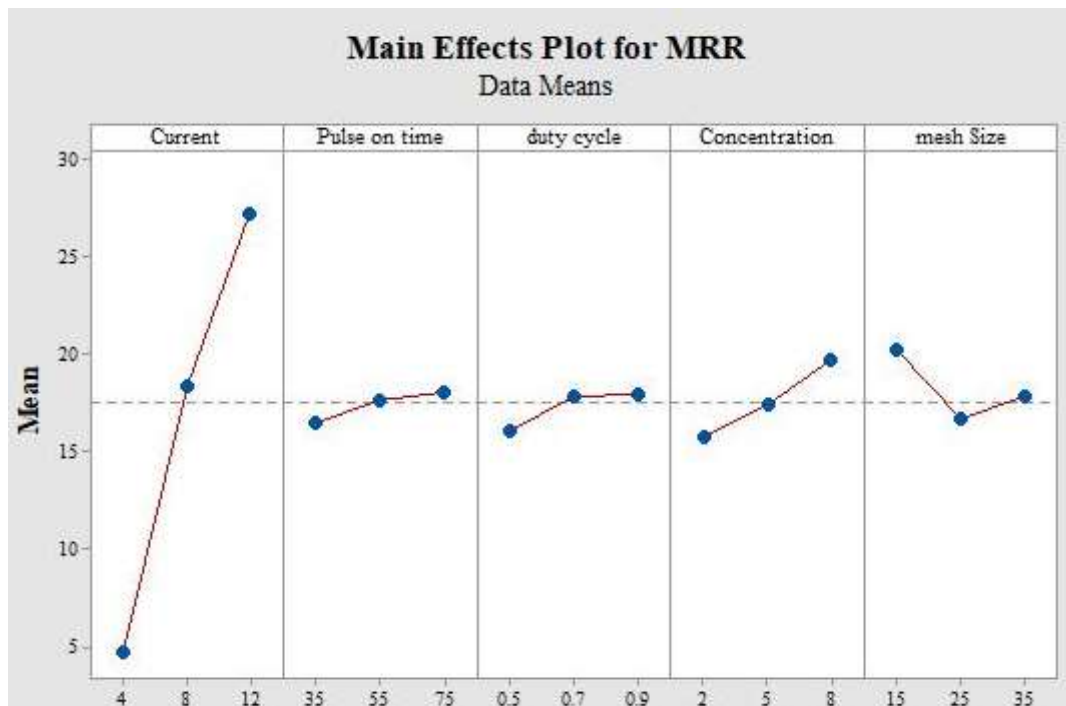


Fig. 5.1. The main effects plot of MRR for Inconel 625 machined by graphite mixed EDM.

The concentrated graphite particles thus emits more local discharges and utilize the spark energy uniformly over the machining surface. Along with this, increase of graphite concentration increases the electrical conductivity of the solution. Graphite microparticles are arranged in a chain from electrode to workpiece surface at different locations which provides a varying conductivity over the machining region and creates additional discharges from each

chain. With the increase of graphite particles the number of chains and thus conductivity increase which leads to the enhancement of discharges. As a result, the removal of material increases compared to the removal rate at lower powder concentrations.

Fig. 5.1 represents that MRR decreases when mesh size increases from 15 μm to 25 μm and increases slightly till 35 μm . The rate of mixing with dielectric for small particles is better than for large particles. Therefore, the small particles can effectively take part in local discharging compared to large particles and remove materials from the surfaces. However, a little large particle can induce and discharge high-energy spark as it has a high surface area. Therefore, the MRR increases slightly when the mesh size changes from 25 μm to 35 μm .

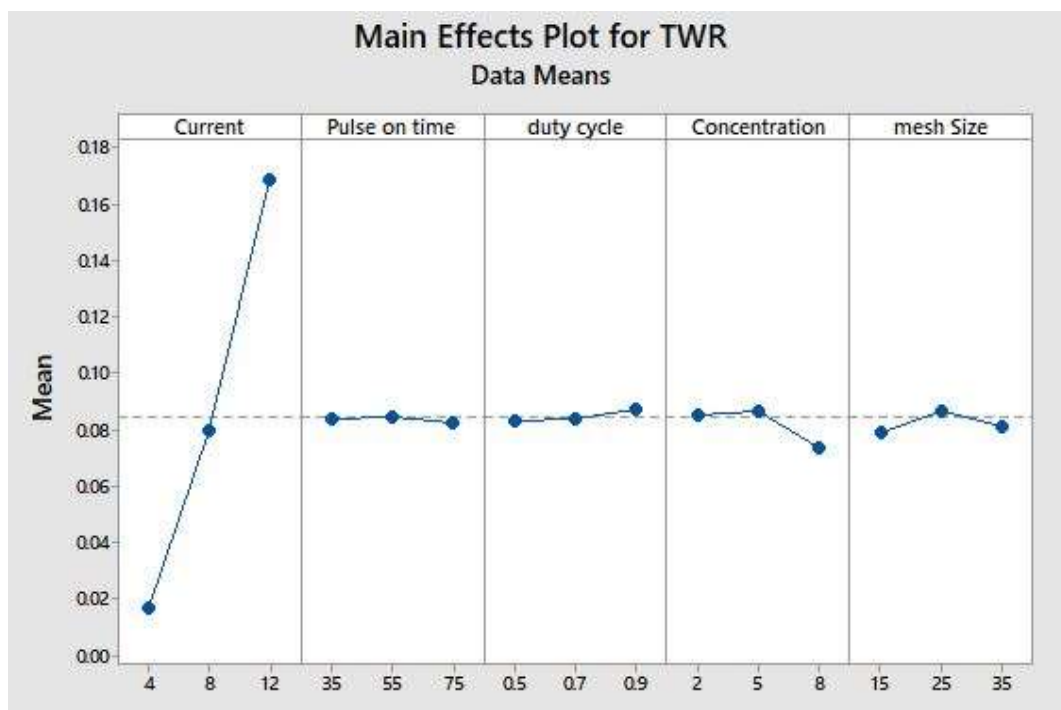


Fig. 5.2. The main effects plot of TWR for Inconel 625 machined by graphite mixed EDM.

5.2.2. Effect of input parameters on TWR

In EDM, the tool erodes because of the melting and vapourization of the tiny material from the tool electrode due to the rise of temperature beyond the melting point at certain portions of the surface. The transfer of thermal energy is the main reason behind the increase of temperature of the surface. When the electrode is discharging and electrons are flowing through the plasma channels, the positive ions are moving opposite direction towards electrode surface and transfer heat energy on it. The addition of graphite particles disrupts the movement of positive ions for their random motion. The movement of particles and their discharges deflect the route of positive ions towards the surface and slowdowns the tool wear. Fig. 5.2 shows TWR increases

significantly due to current enhancement. Whereas the tool wear rate is constant when graphite concentration is enhanced from 2 g/l to 5 g/l and decreased from 5 g/l to 8 g/l. This phenomenon can be explained by the disruption of positive ions are very low during the change of graphite proportion between 2 g/l and 5 g/l, and it is very high at 5 g/l and 8 g/l because more graphite particles enhance the disruption in a better way. The temperature of the tool surface increases and the rate of tool wear increases. However, these conjugate actions of these two phenomena make the TWR constant in the first section and lower down at the second section. The changes of tool wear for the other three parameters are found to be less significant in this study. Like MRR, the variation of TWR is maximum in case of change in current from lower to higher level shown in the Fig. 5.2. From Table 5.1, the average of TWR values for lower, intermediate and higher level can be calculated as 0.0170 mm³/min, 0.0800 mm³/min and 0.1690 mm³/min respectively.

5.2.3. Effect of input parameters on surface roughness

The new surface has been generated by melting the material from the workpiece. When the surface melts, it leaves a small concave-shaped crater on the surface. Moreover, the melted material further deposits on the freshly generated surface as a redeposited layer with non-uniform distribution. These are the reasons for getting high surface roughness. In the Fig. 5.3, the changes in SR have been shown with respect to the increase of input parameters. The major influences have been investigated for current, powder concentration and powder mesh size. SR remarkably enhances when more current flows through the circuit but reduces with graphite concentration and graphite mesh size. The increase in current removes the material at a faster rate which increases the crater depth by removing more material from a particular area. This contributes to enhancing the peak to valley distance of a particular point. Whereas the high graphite concentration distributes sparks uniformly over surface. This increases the number of spark in different region of the cutting surface. Due to which, more number of craters are generated in unit areas due to the removal of material. The craters get overlapped as their density in the unit area increase which leads to a reduction in their depth and inside unevenness. The reduction in crater depth and unevenness therefore reflected on the surface roughness to reduce. However, large mesh size reduces the energy density of the particles at the discharged region. Due to these, the surface craters get shallower with respect to the discharge of small meshed graphite particles. This leads to a lower roughness value seen on the sample after the machining. The pulse on time and duty cycle are less effective on the roughness value.

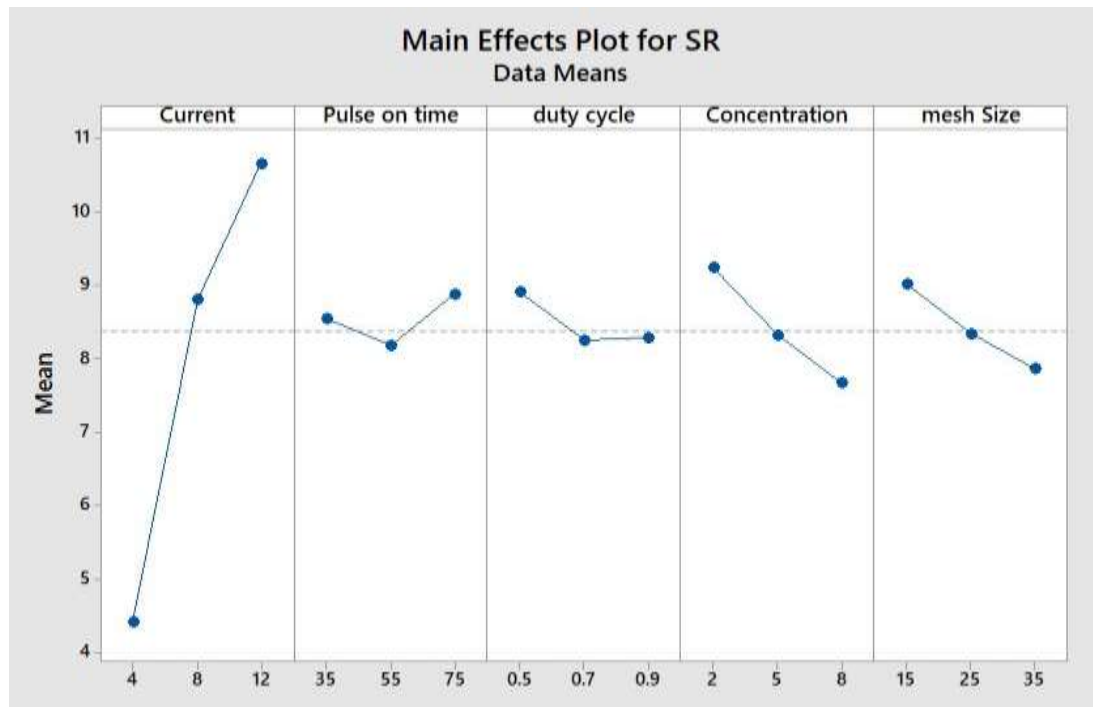


Fig. 5.3. The main effects plot for surface roughness of Inconel 625 machined by graphite mixed EDM.

Normally roughness enhances with increase of pulse on time as higher pulse time increases the crater depth. The increase of duty cycle promotes the sufficient flushing time for removed material which prevents the deposition of removed material for which SR decreases. Refer to Fig. 5.3, The variation of SR is found maximum in case of change in current from lower to higher level shown like MRR and TWR. From Table 5.1, the average of SR values for lower, intermediate and higher level can be calculated as 4.407 μm , 8.811 μm and 10.650 μm respectively.

5.2.4. ANOVA of MRR, TWR and surface roughness

In the ANOVA, adjusted sum of square, mean square, F value and P value of each parameter and their interaction terms are calculated. Along with that, contribution of those parameters on the response has been calculated as the ratio of adjusted sum of square of that parameter to total adjusted sum of square.

Table 5.2 represents the ANOVA result calculated for MRR. In the analysis, the p values for current, powder concentration, mesh size, square term of the current and mesh size and interaction term of current with pulse on time and pulse on time with mesh size are found less than 0.05. Hence, the contribution of these terms are significant to change the responses. The contribution of current, powder concentration and mesh size are 75.55%, 2.38% and 0.82%

respectively. In this study, pulse time is an insignificant parameter but interacting with current and mesh size, it changes the responses significantly as the latter two terms are highly significant.

Table 5.2.

ANOVA result for MRR of Inconel 625 machined by graphite mixed EDM

Source	DF	Adj SS	Adj MS	F Value	p Value
Model	20	2555.29	127.76	26.36	0.000*
I	1	2022.21	2022.21	417.20	0.000*
P _{on}	1	9.36	9.36	1.93	0.177
DC	1	14.58	14.58	3.01	0.095
C _p	1	63.65	63.65	13.13	0.001*
M	1	22.05	22.05	4.55	0.043*
I ²	1	50.05	50.05	10.33	0.004*
P _{on} ²	1	4.05	4.05	0.84	0.369
DC ²	1	8.68	8.68	1.79	0.193
C _p ²	1	0.00	0.00	0.00	0.993
M ²	1	26.37	26.37	5.44	0.028*
I × P _{on}	1	10.54	10.54	2.17	0.153
I × DC	1	3.74	3.74	0.77	0.388
I × C _p	1	33.22	33.22	6.85	0.015*
I × M	1	0.89	0.89	0.18	0.671
P _{on} × DC	1	3.85	3.85	0.79	0.382
P _{on} × C _p	1	0.65	0.65	0.13	0.717
P _{on} × M	1	255.02	255.02	52.61	0.000*
DC × C _p	1	0.33	0.33	0.07	0.796
DC × M	1	1.07	1.07	0.22	0.642
C _p × M	1	0.02	0.02	0.00	0.954
Lack of Fitness	20	110.53	5.53	2.60	0.147
Error	5	10.65	2.13		
Total	45	2676.46			

Table 5.3.

ANOVA result for TWR of Inconel 625 machined by graphite mixed EDM

Source	DF	Adj SS	Adj MS	F Value	p Value
Model	20	0.097519	0.004876	40.22	0.000*
I	1	0.092952	0.092952	761.23	0.000*
P _{on}	1	0.000005	0.000005	0.04	0.838
DC	1	0.000066	0.000066	0.54	0.469
C _p	1	0.000576	0.000576	4.75	0.039*
M	1	0.000026	0.000026	0.21	0.650
I ²	1	0.001120	0.001120	9.24	0.005*
P _{on} ²	1	0.000023	0.000023	0.19	0.667
DC ²	1	0.000384	0.000384	0.07	0.793
C _p ²	1	0.000384	0.000384	3.16	0.087
M ²	1	0.000290	0.000290	2.39	0.135
I × P _{on}	1	0.000009	0.000009	0.07	0.791
I × DC	1	0.000038	0.000038	0.31	0.581
I × C _p	1	0.001318	0.001318	10.87	0.003*
I × M	1	0.000056	0.000056	0.46	0.505
P _{on} × DC	1	0.000063	0.000063	0.52	0.477
P _{on} × C _p	1	0.000230	0.000230	1.89	0.181
P _{on} × M	1	0.000017	0.000017	0.14	0.713
DC × C _p	1	0.000001	0.000001	0.01	0.921
DC × M	1	0.000154	0.000154	1.27	0.271
C _p × M	1	0.000178	0.000178	1.47	0.237
Lack of Fitness	20	0.002576	0.000129	1.42	0.374
Error	5	0.000454	0.000091		
Total	45	0.100549			

Table 5.3 represents the ANOVA of tool wear rate. In this analysis, the significant terms are found current, concentration of graphite, square of the current and interaction of current and powder concentration.

Table 5.4.

ANOVA result for surface roughness of Inconel 625 machined by graphite mixed EDM

Sl no.	DOF	Adj SS	Adj MS	F Value	p Value
Model	20	203.839	10.192	10.20	0.000
I	1	155.875	155.875	155.94	0.000*
P _{on}	1	0.426	0.426	0.43	0.520
DC	1	1.575	1.575	1.58	0.221
C _p	1	9.672	9.672	9.68	0.005*
M	1	5.303	5.303	5.30	0.030*
I ²	1	11.913	11.913	11.92	0.002*
P _{on} ²	1	1.426	1.426	1.43	0.244
DC ²	1	0.545	0.545	0.55	0.467
C _p ²	1	0.041	0.041	0.04	0.842
M ²	1	0.013	0.013	0.01	0.909
I × P _{on}	1	0.874	0.874	0.87	0.359
I × DC	1	0.230	0.230	0.23	0.635
I × C _p	1	0.034	0.034	0.03	0.855
I × M	1	1.277	1.277	1.28	0.269
P _{on} × DC	1	0.757	0.757	0.76	0.392
P _{on} × C _p	1	0.608	0.608	0.61	0.443
P _{on} × M	1	1.232	1.232	1.23	0.277
DC × C _p	1	0.319	0.319	0.32	0.577
DC × M	1	3.861	3.861	3.86	0.061
C _p × M	1	2.890	2.890	2.89	0.101
Lack of Fitness	20	17.795	0.890	0.62	0.799
Error	5	7.196	1.439		
Total	45	228.829			

In case of roughness value, ANOVA analysis has been shown in Table 5.4. The significant terms are found current, powder concentration and mesh size and the square of current. The contribution of the significant terms are 68.11%, 4.22% and 2.31% respectively. From the

ANOVA of three responses, it is clear that current and powder concentration as are the most influential parameters responsible to vary all the three responses. From the analysis, lack of fit are found insignificant which tells that the RSM formulation is significant. The other terms are insignificant with p values greater than 0.05.

5.2.5. Multi variable regression analysis of MRR and surface roughness

Experimental data are used to construct a second order equation using multivariable least square regression including all the interaction terms. Eq. 5.1, Eq. 5.2 and Eq. 5.3 represent the expression for MRR, TWR and SR respectively.

$$\begin{aligned} MRR = & -80.3 + 4.57 I + 1.524 P_{on} + 39.4 DC - 1.35 C_p + 1.112 M - 0.1497 I^2 - \\ & 0.0017 P_{on}^2 - 24.9 DC^2 + 0.0008 C_p^2 + 0.01738 M^2 - 0.0203 I \times P_{on} + 1.21 I \times DC + \\ & 0.2401 I \times C_p - 0.0118 I \times M - 0.245 P_{on} \times DC + 0.0067 P_{on} \times C_p - 0.03992 P_{on} \times \\ & M - 0.48 DC \times C_p + 0.259 DC \times M + 0.0021 C_p \times M \end{aligned} \quad (5.1)$$

$$\begin{aligned} TWR = & -0.061 + 0.01384 I - 0.00131 P_{on} - 0.037 DC + 0.0043 C_p + 0.00425 M + \\ & 0.000708 I^2 - 0.000004 P_{on}^2 + 0.0247 DC^2 - 0.000737 C_p^2 - 0.000058 M^2 + \\ & 0.000018 I \times P_{on} + 0.00384 I \times DC - 0.001513 I \times C_p - 0.000093 I \times M + \\ & 0.00099 P_{on} \times DC + 0.000126 P_{on} \times C_p + 0.000010 P_{on} \times M + 0.00092 DC \times C_p - \\ & 0.00310 DC \times M + 0.000222 C_p \times \\ & M \end{aligned} \quad (5.2)$$

$$\begin{aligned} SR = & 4.7 + 2.872 I - 0.017 P_{on} - 16.6 DC + 0.463 C_p - 0.319 M - 0.073 I^2 + \\ & 0.001010 P_{on}^2 + 6.25 DC^2 + 0.0076 C_p^2 + 0.00039 M^2 - 0.00584 I \times P_{on} - 0.3 I \times DC - \\ & 0.0077 I \times C_p - 0.0141 I \times M - 0.109 P_{on} \times DC - 0.00650 P_{on} \times C_p + 0.00277 P_{on} \times \\ & M + 0.471 DC \times C_p + 0.491 DC \times M - 0.0283 C_p \times M \end{aligned} \quad (5.3)$$

However, the normal, adjusted and predicted R^2 for MRR are 0.9547, 0.9185 and 0.8291 respectively. It indicates the closeness of fit with the model is quite satisfactory and the over fitting with each independent parameters are significantly less. Hence the model can be accepted. The same values for TWR are 0.9699, 0.9457 and 0.8910 respectively. Also, the normal, adjusted and predicted R^2 for SR are 0.8908, 0.8034 and 0.6437 respectively. Hence, adequacy of the RSM model of SR is found very well and the overfitting of the data is within the range.

5.2.6. Normal Probability Plot of MRR, TWR and surface roughness

The normal probability plots the distribution of the residuals along the normal probability line. Fig. 5.4, 5.5 and 5.6 represent the residual points of MRR, TWR and SR which are situated close to the probability line. Hence, it can be stated that the residuals are distributed normally and confirms that the fitness of the quadratic models are adequate.

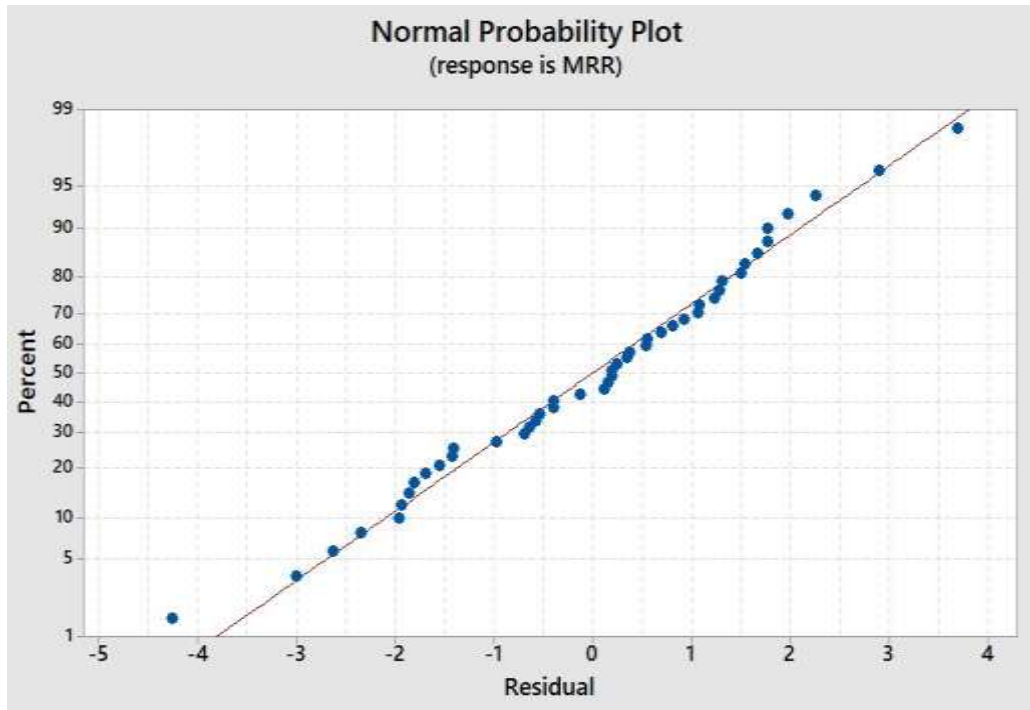


Fig. 5.4. Normal probability plot for MRR of Inconel 625.

5.2.7. 3D Surface Plot for MRR, TWR and surface roughness

Here, 3D response surfaces can be generated for each of the three responses considering the interaction of two input parameters. The surfaces are generated using DESIGN EXPERT 12 software. Fig. 5.7 (a)-(c) shows the interaction plots of MRR. It indicates that the maximum MRR can be achieved at 12 A current with a graphite concentration of 8 g/l; 15 μm mesh size with 8 g/l concentration and 15 μm mesh size with 12 A current. Since MRR is increasing with high energy transfer into the system which can be promoted by an increase of current, graphite concentration and a decrease of graphite particle size, the maximum value can be achieved at the maximum current, graphite concentration and minimum particle size.

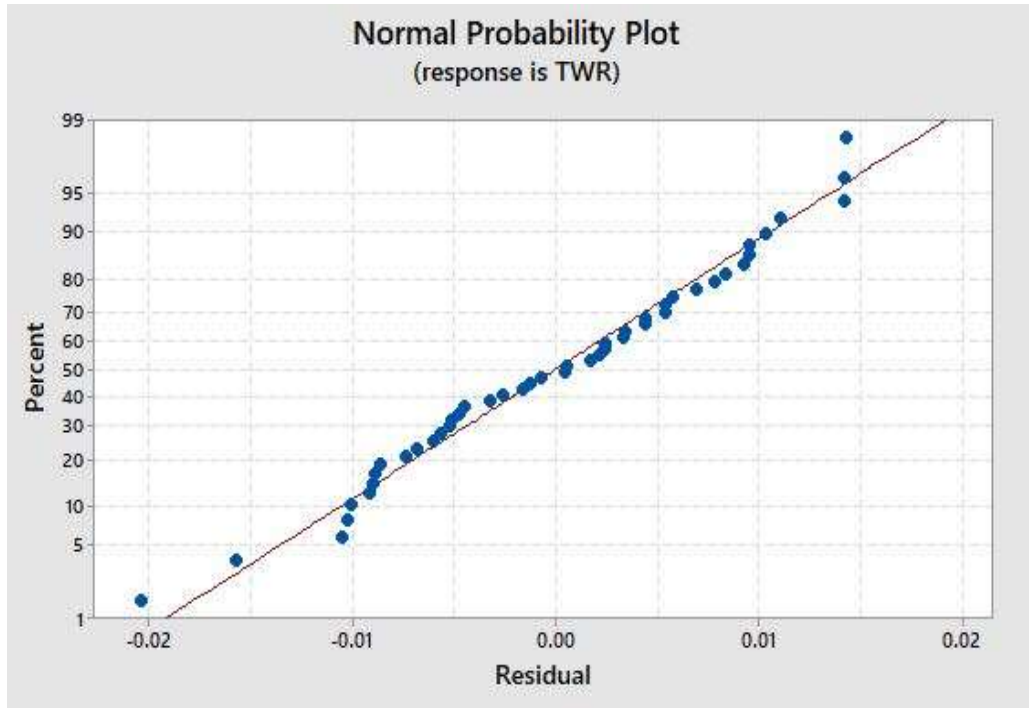


Fig. 5.5. Normal probability plot for TWR of Inconel 625.

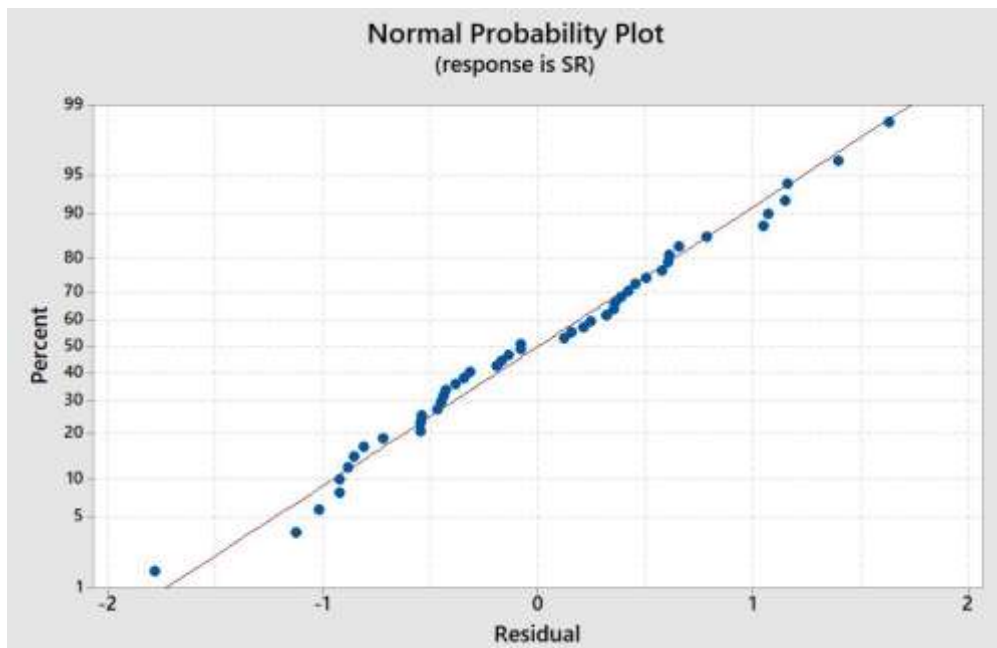


Fig. 5.6. Normal probability plot of residuals for SR of Inconel 625.

In Fig. 5.8 (a)-(c), the surface plot of TWR is represented which conveys the minimum TWR can be achieved at the current of 4 A with the powder concentration of 8 g/l, mesh size 15 μm with powder concentration 8 g/l and mesh size 15 μm with current 4 A

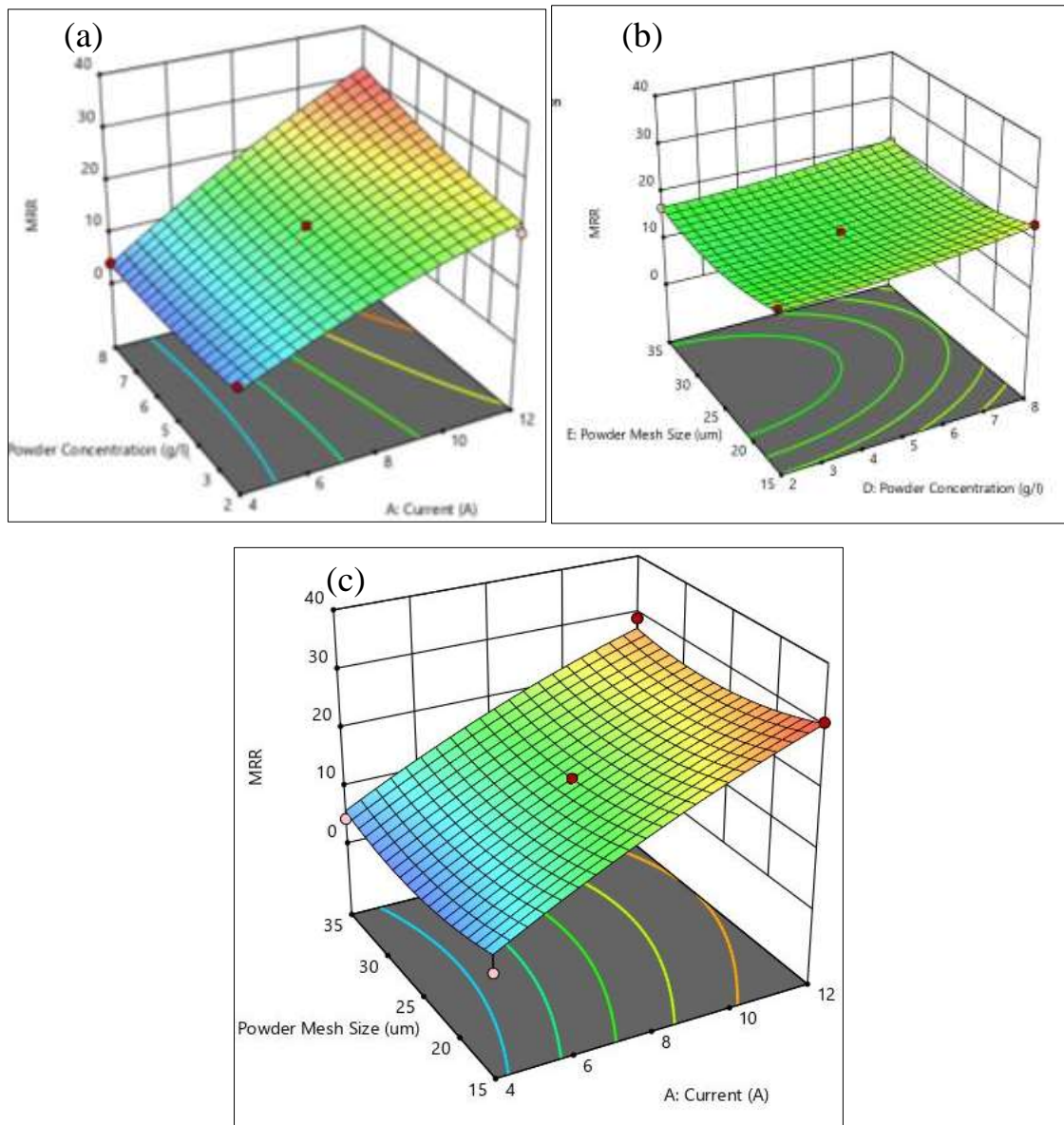


Fig. 5.7. 3D plots of MRR with the association of (a) graphite concentration and pulse current (b) graphite concentration and mesh size and (c) Current and powder mesh size during the machining of Inconel 625.

It is already proved that at low current, high graphite concentration and low mesh size of graphite, the flow of positive ions toward electrode decelerates and disrupts. As a consequence, the minimum TWR is achieved at the above said values. In Fig. 5.9 (a)-(c), the nature of the surface plot is slightly different than other two responses. A convex type surface plot is achieved where roughness become lowest at a current of 4 A with graphite concentration of 8 g/l; mesh size of 35 μm with graphite concentration 8 g/l and mesh size 15 μm with current 4 A. At the low current discharge, the depth of the crater becomes small because of the little

amount of removal. Also at high powder concentration, more local discharges take place which produce uniform and shallow craters in the discharge region.

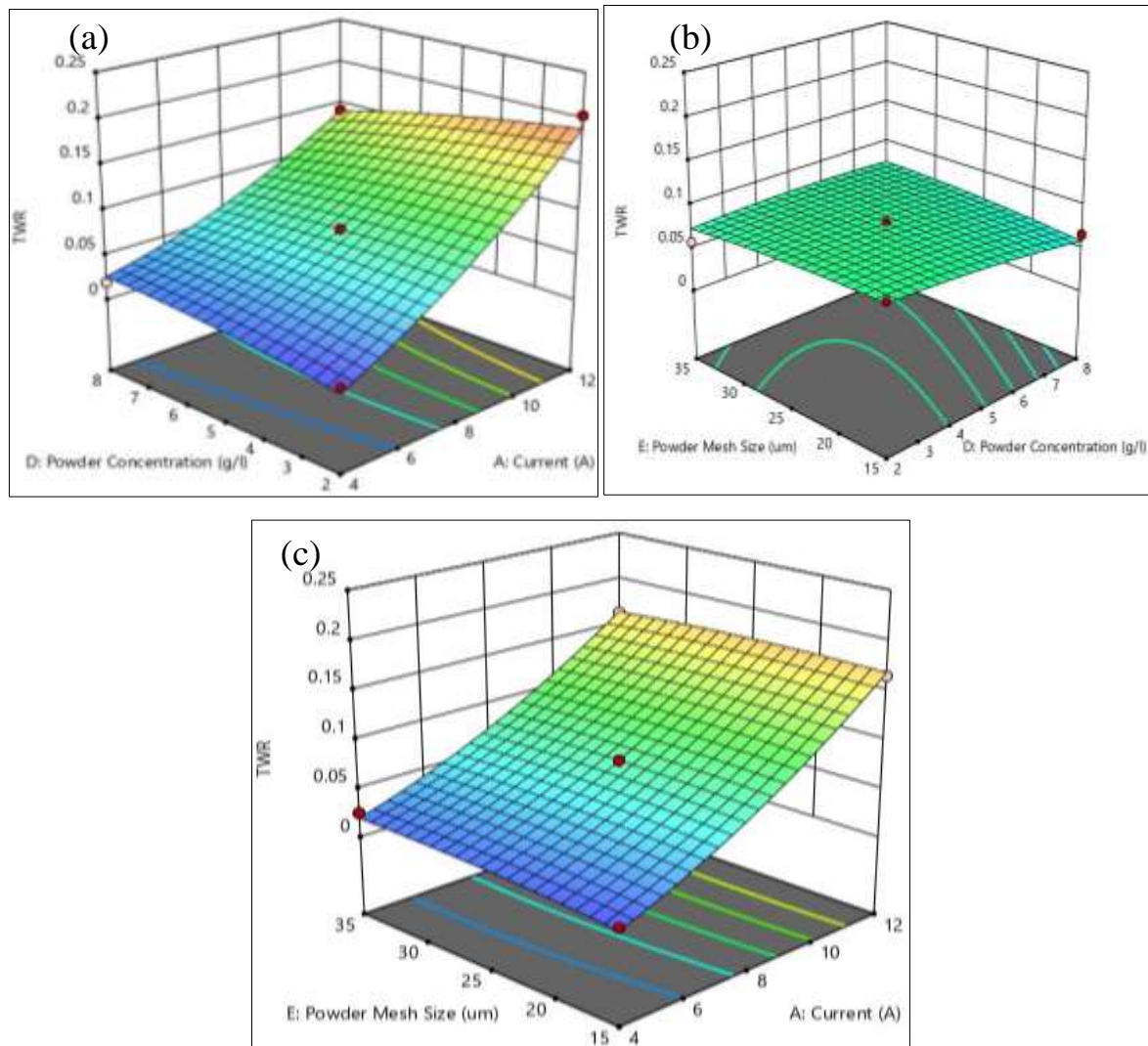


Fig. 5.8. 3D plots of TWR with the association of (a) graphite concentration and pulse current (b) graphite concentration and mesh size and (c) Current and powder mesh size during the machining of Inconel 625.

Along with that large surface area provides shallow crater on the surface which reduces the surface roughness.

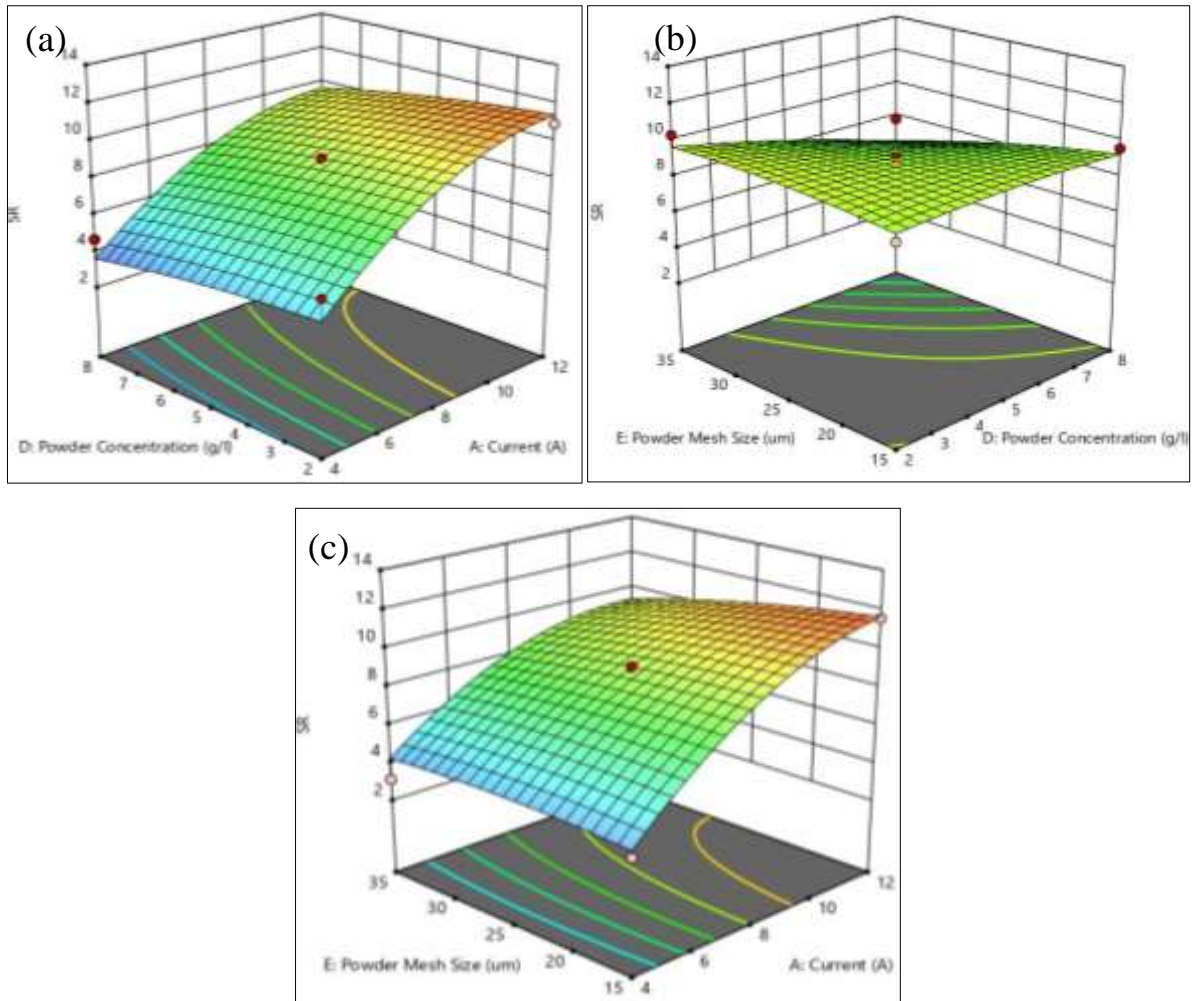


Fig. 5.9. 3D plots of SR with the association of (a) graphite concentration and pulse current (b) graphite concentration and mesh size and (c) current and powder mesh size during the machining of Inconel 625.

5.3. Effect of graphite mixed EDM on Titanium Grade 2

The result of the present experiment has been represented in Table 5.5 by enlisting the measured values of all the three responses. Table 5.5 tells that the highest values of MRR, TWR and SR are 1.718 mm³/min, 0.202 mm³/min and 15.592 μm respectively whereas the minimum values are 0.480 mm³/min, 0.013 mm³/min and 4.081 μm respectively.

5.3.1. Effect of input parameters on MRR

In industrial application, MRR needs to be maximized to enhance the production. Fig. 5.10 provides variations of MRR are shown against their mean values with respect to the input parameters.

Table 5.5.

Experimental result for MRR, TWR and SR of Titanium Grade 2 machined by graphite mixed EDM

Run no.	Current	Duty Cycle	Pulse on Time	Powder Concentration	Powder mesh size	MRR	TWR	SR
	(A)		(μ s)	(g/l)	(μ m)	(mm ³ /min)	(mm ³ /min)	(μ m)
1	8	0.7	55	5	25	0.976	0.0612	6.846
2	8	0.5	75	5	25	1.508	0.1699	5.567
3	12	0.7	55	5	35	1.153	0.0589	5.293
4	8	0.9	55	5	35	1.015	0.0917	9.423
5	8	0.7	55	2	35	0.976	0.1382	6.643
6	8	0.7	55	5	25	0.859	0.0297	10.316
7	8	0.7	35	8	25	1.264	0.1663	8.220
8	4	0.7	55	8	25	1.197	0.0702	7.319
9	12	0.7	35	5	25	0.843	0.0747	10.232
10	12	0.7	55	8	25	1.457	0.0929	4.578
11	8	0.9	75	5	25	0.931	0.0272	5.356
12	8	0.7	55	2	15	0.517	0.0132	5.398
13	12	0.7	75	5	25	1.321	0.1321	10.232
14	8	0.9	55	2	25	1.552	0.0906	11.426
15	8	0.7	55	8	15	1.232	0.0906	9.322
16	8	0.9	55	5	15	0.637	0.0156	7.909
17	12	0.7	55	5	15	0.984	0.0883	9.323
18	8	0.5	35	5	25	0.621	0.0521	7.224
19	4	0.9	55	5	25	0.765	0.1019	7.764
20	8	0.7	35	5	15	1.386	0.1048	7.634
21	8	0.5	55	8	25	0.843	0.0589	7.247
22	8	0.7	55	5	25	0.843	0.0861	8.096
23	12	0.5	55	5	25	1.109	0.0612	6.777
24	8	0.7	75	5	15	1.342	0.0589	7.950
25	4	0.7	55	5	35	0.976	0.0770	9.141

26	4	0.5	55	5	25	1.248	0.1048	9.115
27	8	0.7	55	5	25	0.843	0.0770	4.081
28	8	0.9	35	5	25	1.107	0.0861	8.096
29	8	0.9	55	8	25	0.931	0.0181	8.800
30	8	0.5	55	5	15	0.931	0.0544	9.236
31	12	0.7	55	2	25	0.554	0.0434	7.369
32	8	0.5	55	5	35	1.242	0.0834	7.789
33	8	0.7	75	2	25	0.693	0.0283	8.233
34	8	0.5	55	2	25	1.304	0.1472	10.371
35	8	0.7	55	8	35	0.931	0.0861	6.892
36	8	0.7	75	8	25	0.976	0.1744	15.592
37	8	0.7	35	2	25	0.931	0.0883	6.456
38	4	0.7	55	2	25	1.242	0.0906	9.067
39	8	0.7	55	5	25	0.480	0.0434	4.487
40	4	0.7	35	5	25	1.109	0.1042	10.067
41	8	0.7	55	5	25	0.976	0.0974	8.342
42	4	0.7	75	5	25	1.109	0.0906	10.080
43	4	0.7	55	5	15	1.153	0.0838	10.325
44	12	0.9	55	5	25	1.330	0.2016	13.281
45	8	0.7	75	5	35	1.064	0.0657	5.934
46	8	0.7	35	5	35	1.718	0.1217	13.801

Current, pulse time and graphite concentration affects maximally on MRR. Here, the principal reason of enhancing MRR is transferring more energy on the surface. Material is melted and vaporized at a higher rate due to the high energy transfer. Now, high energy transfer occurs mainly due to increase of the current which directly provides more energy to the discharges. More graphite are added with the increase of concentration. The concentrated graphite particles thus emits more local discharges and utilize the spark energy uniformly over the machining surface. The conductivity of the solution has also been enhanced. Graphite powders are arranged in a chain from electrode to workpiece surface at different locations which provides a varying conductivity over the machining region and creates additional discharges from each chain. With the increase of graphite particles the number of chains and thus conductivity

increase which lead to the enhancement of discharges. As a result, the removal of material increases compared to the removal rate at lower powder concentration.

It has also been found that the MRR decreases with pulse on time because with high pulse on time the graphite particles provide more number of sparks for a larger time which hampers the effective flushing from the spark gap and the material is redeposited on the surface. Hence, the MRR decreases.

MRR affected at less quantity by mesh size and duty cycle. With increase of particle size, more charge can be accumulated on the particle surface which leads to high heat transfer on the surface and MRR decreases. Increase of duty cycle reduces the pulse gap time and induces more power which leads to increase MRR but further increase of duty cycle hampers the flushing of material and decreases the MRR.

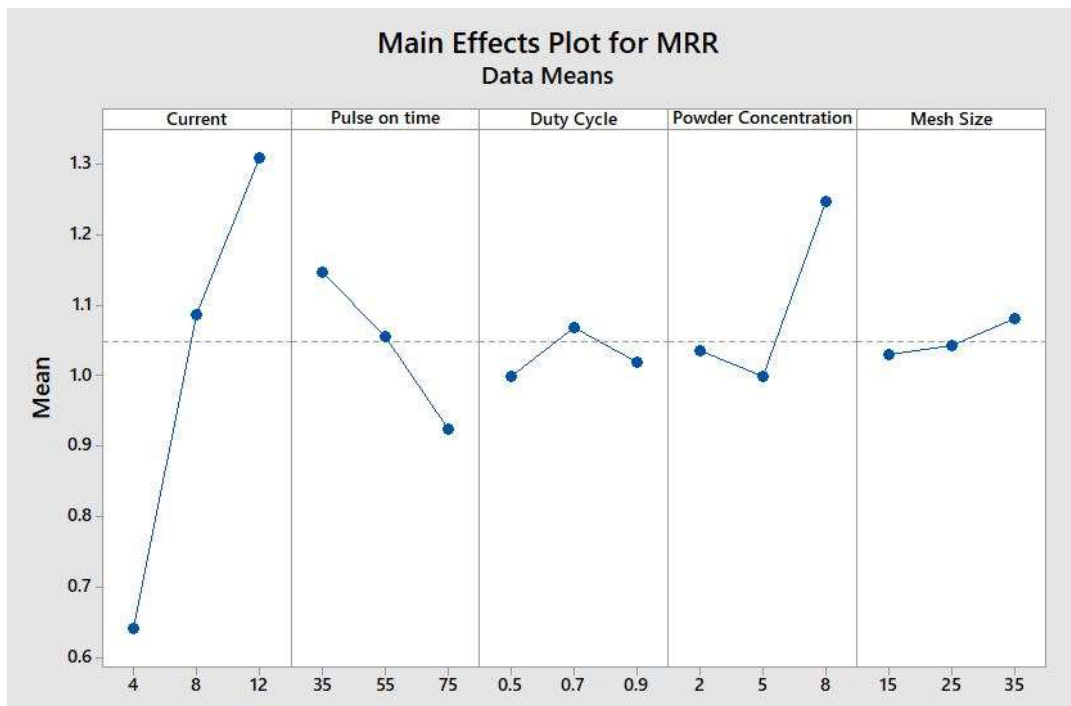


Fig. 5.10. Main effects plot for MRR of Inconel 625 machined by graphite mixed EDM.

5.3.2. Effect of input parameters on TWR

During machining of a surface the material from tool also gets eroded which is called tool wear. In EDM, the tool wear occurs because small particles are melted from tool electrode due to the rise of temperature beyond the melting point at certain portions of the surface. The transfer of thermal energy is the main reason behind the increase of temperature of the surface. When the electrode is discharging and electrons are flowing through the plasma channels, the positive ions are moving opposite direction towards electrode surface and transfer heat energy on it.

But the addition of graphite disrupts the movement of positive ions with random motions during their discharges. The movement of particles and their discharges deflect the route of positive ions and slowdowns tool erosion.

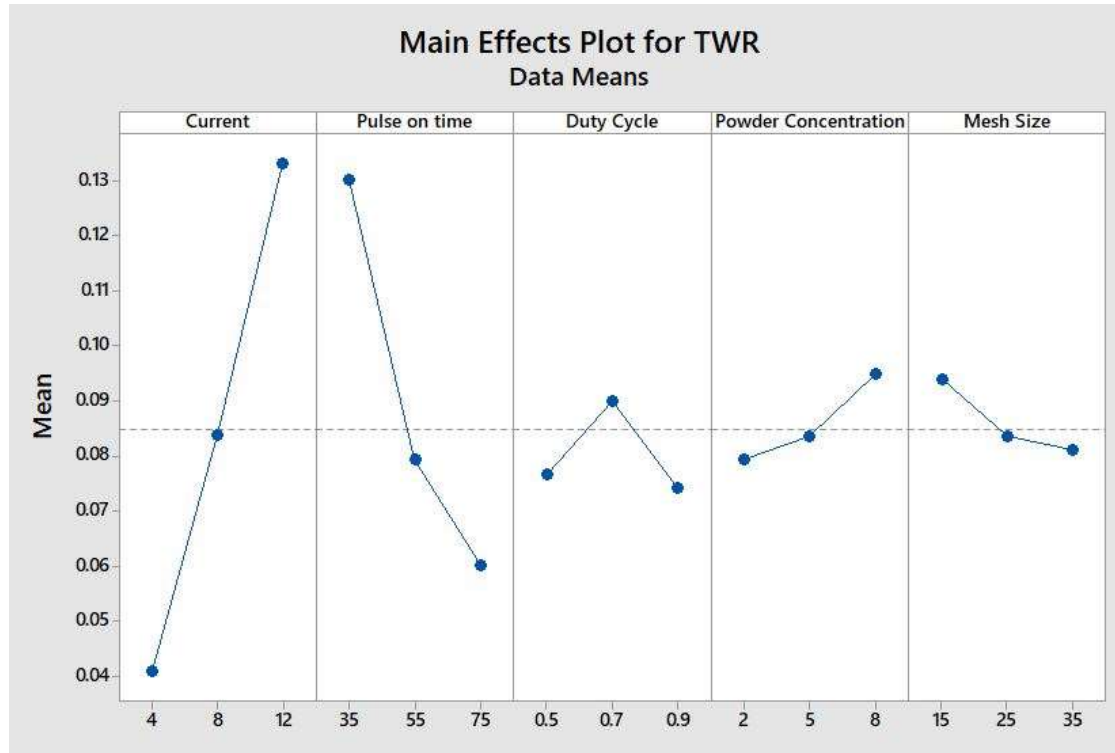


Fig. 5.11. Main effects plot for TWR of Inconel 625 machined by graphite mixed EDM.

Fig. 5.11 depicts TWR enhances significantly when more current flows and more graphite powder is added. Whereas the TWR decreases with pulse time and mesh size. With the increase of current and powder concentration, more thermal energy introduces on the system. Along with workpiece material tool material also get decayed at higher rate by increase of these two parameters. However, discharge time of graphite powder becomes also higher with increase of pulse time which disturbs the flushing time. Due to which TWR is also reduced. By enhancing the powder size, maximum energy has been transferred through the surface area of the powder particles. Hence the tool wear become less. With the increase of duty cycle, TWR increases first and decrease thereafter. This has happened as duty cycle provides long time of energy transfer which increases the TWR as well as hampers the flushing of tool material which reduces the TWR at further increase of it

5.3.3. Effect of input parameters on surface roughness

When the materials melts and removes from the surface, it leaves a small concave shaped crater on the surface. Moreover, the melted material further deposits on the freshly generated surface in the form of re-solidified molten material layers and the distribution of this layer is not uniform. These are two major reasons of getting high surface roughness. In the Fig. 5.12, the changes in SR has been shown with respect to the increase of input parameters. The major influences have been investigated for current, powder concentration and powder mesh size. SR remarkably enhances with high flow of current but decreases with addition of more graphite and large mesh size.

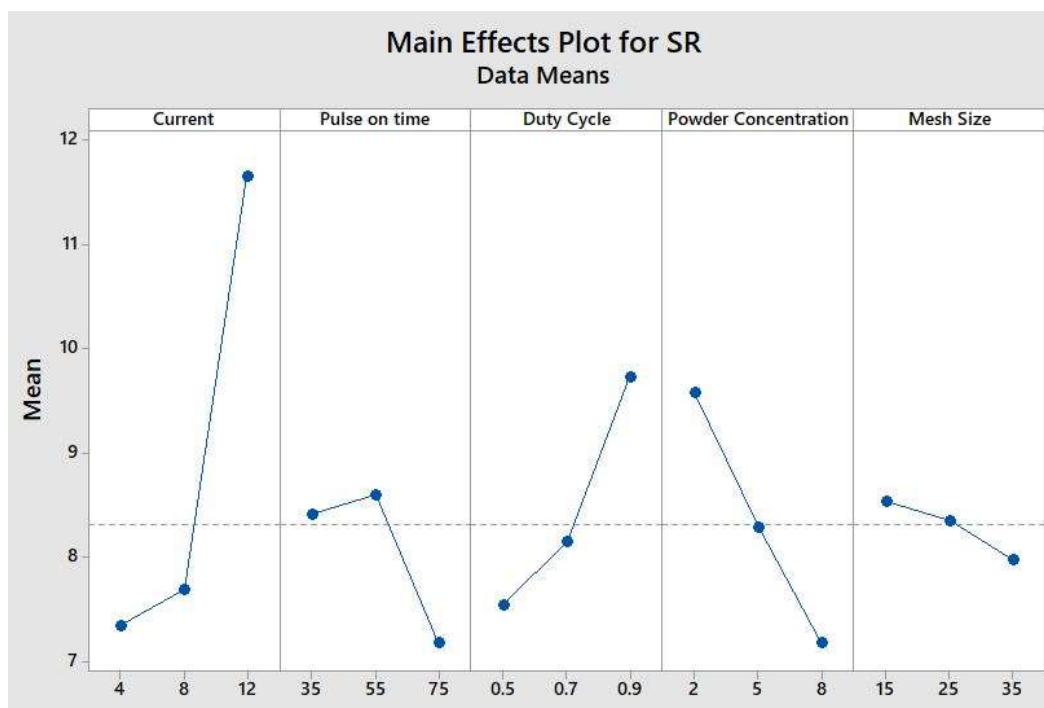


Fig. 5.12. The main effects plot of Surface Roughness for Inconel 625 machined by graphite mixed EDM.

The increase of current removes the material at a faster rate which increases the crater depth by removing more material from a particular area. This contributes to enhance the peak to valley distance of a particular point. However, reach concentration of particles distributes spark uniformly over the surface. This increases the number of spark at the different region of the cutting surface. Due to which, more number of craters are generated in unit areas due to removal of material.

The craters get overlapped as their density in the unit area increase which leads to reduce their depth and inside unevenness. The reduction in crate depth and unevenness therefore reflected

on the surface roughness to reduce. However, a large mesh size reduces the energy density of the particles at the discharged region. This leads to a low roughness value visible on the sample after the machining. Normally, surface roughness increases with increase in pulse time. The duty cycle brings a longer time of energy input which amplifies the roughness value.

5.3.4. ANOVA of MRR, TWR and surface roughness

Table 5.6 represents the ANOVA result calculated for MRR. In the analysis, the p values for current, pulse on time, powder concentration, square term of the current and powder concentration and interaction term of current with pulse on time and pulse on time with powder concentration are found to be less than 0.05.

Hence, the contribution of these terms to varying these responses is significant during the machining. Table 5.6 represents the ANOVA of tool wear rate. In this analysis, the significant terms are found to be current, pulse time and its square, interaction of pulse on time and powder concentration. This is quite significant that during the machining of Titanium grade 2, TWR has not been affected by powder concentration or powder mesh size.

The ANOVA for SR has been shown in Table 5.7. The significant terms are found current, powder concentration, pulse on time, duty cycle and the square of current and duty cycle. The significant interaction terms are current and powder concentration and powder concentration and mesh size. However, the experimental analysis with the quadratic polynomial is found accepted as the lack of fitness value is insignificant in the analysis of all the responses. The other terms having >0.05 value of p are insignificant for all the three responses.

Table 5.6.

ANOVA result for MRR of Titanium Grade 2 machined by graphite mixed EDM

Source	Degree of freedom	Adjusted SS	Adjusted MS	F Value	p Value
Model	20	2.974	0.148	7.56	0.000*
I	1	1.781	1.781	90.52	0.000*
P _{on}	1	0.199	0.199	10.10	0.004*
DC	1	0.001	0.001	0.07	0.790
C _p	1	0.178	0.178	9.04	0.006*
M	1	0.010	0.010	0.51	0.481
I ²	1	0.104	0.104	5.29	0.030*

P_{on}^2	1	0.007	0.007	0.37	0.549
DC^2	1	0.035	0.035	1.80	0.192
C_p^2	1	0.109	0.109	5.56	0.026*
M^2	1	0.002	0.002	0.00	0.972
$I \times P_{on}$	1	0.001	0.001	0.06	0.813
$I \times DC$	1	0.032	0.032	1.66	0.210
$I \times C_p$	1	0.180	0.180	9.16	0.006*
$I \times M$	1	0.037	0.037	1.90	0.180
$P_{on} \times DC$	1	0.024	0.024	1.23	0.278
$P_{on} \times C_p$	1	0.096	0.096	4.90	0.036*
$P_{on} \times M$	1	0.010	0.010	0.51	0.482
$DC \times C_p$	1	0.003	0.003	0.02	0.899
$DC \times M$	1	0.024	0.024	1.23	0.278
$C_p \times M$	1	0.059	0.059	3.04	0.094
Lack of Fitness	20	0.3673	0.0183	0.74	0.717
Error	5	0.1244	0.0248		
Total	45	3.466			

Table 5.7.

ANOVA result for TWR of Titanium Grade 2 machined by graphite mixed EDM

Source	Degree of freedom	Adjusted SS	Adjusted MS	F Value	p Value
Model	20	0.067512	0.003376	6.23	0.000*
I	1	0.033902	0.033902	62.55	0.000*
P_{on}	1	0.019576	0.019576	36.12	0.000*
DC	1	0.000024	0.000024	0.04	0.834
C_p	1	0.000963	0.000963	1.78	0.195
M	1	0.000647	0.000647	1.19	0.285
I^2	1	0.000405	0.000405	0.75	0.396
P_{on}^2	1	0.002708	0.002708	5.00	0.035*

DC ²	1	0.000656	0.000656	1.21	0.282
C _p ²	1	0.000429	0.000429	0.79	0.382
M ²	1	0.000490	0.000490	0.90	0.351
I × P _{on}	1	0.000112	0.000112	0.21	0.653
I × DC	1	0.001552	0.001552	2.86	0.103
I × C _p	1	0.000003	0.000003	0.01	0.944
I × M	1	0.001286	0.001286	2.37	0.136
P _{on} × DC	1	0.000032	0.000032	0.06	0.810
P _{on} × C _p	1	0.002483	0.002483	4.58	0.042*
P _{on} × M	1	0.000895	0.000895	1.65	0.210
DC × C _p	1	0.000298	0.000298	0.55	0.465
DC × M	1	0.000678	0.000678	1.25	0.274
C _p × M	1	0.000046	0.000046	0.09	0.773
Lack of Fitness	20	0.012762	0.000638	4.05	0.063
Error	5	0.000787	0.000157		
Total	45	0.081061			

Table 5.8.

ANOVA result for SR of Titanium Grade 2 machined by graphite mixed EDM

Sl no.	Degree of freedom	Adjusted SS	Adjusted MS	F Value	p Value
Model	20	220.223	11.011	8.14	0.000*
I	1	74.568	74.568	55.09	0.000*
P _{on}	1	6.137	6.137	4.53	0.043*
DC	1	19.018	19.018	14.05	0.001*
C _p	1	23.059	23.059	17.04	0.000*
M	1	1.254	1.254	0.93	0.345
I ²	1	36.838	36.838	27.22	0.000*
P _{on} ²	1	0.394	0.394	0.29	0.594
DC ²	1	7.060	7.060	5.22	0.031*
C _p ²	1	2.770	2.770	2.05	0.165

M^2	1	1.440	1.440	1.06	0.312
$I \times P_{on}$	1	0.557	0.557	0.41	0.572
$I \times DC$	1	5.464	5.464	4.04	0.055
$I \times C_p$	1	27.641	27.641	20.42	0.000*
$I \times M$	1	0.921	0.921	0.68	0.417
$P_{on} \times DC$	1	0.173	0.173	0.13	0.723
$P_{on} \times C_p$	1	0.385	0.385	0.28	0.598
$P_{on} \times M$	1	3.970	3.970	2.93	0.099
$DC \times C_p$	1	0.062	0.062	0.05	0.832
$DC \times M$	1	0.046	0.046	0.03	0.855
$C_p \times M$	1	11.834	11.834	8.74	0.007*
Lack of Fitness	20	28.941	1.4470	1.48	0.354
Error	5	4.896	0.9792		
Total	45	254.060			

5.3.5. Multi variable regression results for MRR and surface roughness

Second order equation using multivariable least square regression was constructed by the experimental data including all the interaction terms. Eq. 5.4, Eq. 5.5 and Eq. 5.6 represent the expression for MRR, TWR and SR respectively.

$$\begin{aligned}
 MRR = & -2.25 + 0.134 I + 0.037 P_{on} + 5.29 DC - 0.180 C_p + 0.005 M - 0.0068 I^2 - \\
 & 0.0007 P_{on}^2 - 1.59 DC^2 + 0.0124 - 0.0001 M^2 - 0.0002 I \times P_{on} - 0.1128 I \times DC + \\
 & 0.0177 I \times C_p + 0.0024 I \times M - 0.0194 P_{on} \times DC - 0.0026 P_{on} \times C_p - 0.0003 P_{on} \times \\
 & M - 0.015 DC \times C_p - 0.0389 DC \times M + 0.0041 C_p \times M
 \end{aligned} \quad (5.1)$$

$$\begin{aligned}
 TWR = & -0.166 + 0.0020 I - 0.0016 P_{on} + 0.374 DC + 0.0243 C_p + 0.00731 M + \\
 & 0.0004 I^2 + 0.000044 P_{on}^2 - 0.217 DC^2 + 0.0007 C_p^2 + 0.00007 M^2 - 0.00006 I \times P_{on} + \\
 & 0.0246 I \times DC + 0.000069 I \times C_p - 0.00045 I \times M - 0.00071 P_{on} \times DC - \\
 & 0.00042 P_{on} \times C_p - 0.000075 P_{on} \times M - 0.0144 DC \times C_p - 0.00651 DC \times M + \\
 & 0.000113 C_p \times M
 \end{aligned} \quad (5.2)$$

$$\begin{aligned}
SR = & 28.7 - 3.676 I + 0.179 P_{on} - 40.3 DC - 1.21 C_p + 0.271 M + 0.128 I^2 - \\
& 0.0005 P_{on}^2 + 22.49 DC^2 + 0.0626 C_p^2 + 0.0041 M^2 - 0.0047 I \times P_{on} + 1.461 I \times DC + \\
& 0.2191 I \times C_p + 0.0120 I \times M + 0.052 P_{on} \times DC - 0.0052 P_{on} \times C_p - 0.0049 P_{on} \times M + \\
& 0.207 DC \times C_p - 0.054 DC \times M - 0.057 C_p \times M
\end{aligned} \quad (5.3)$$

The normal, adjusted and predicted R^2 data for MRR are 0.8581, 0.7446 and 0.6243 respectively. It indicates the closeness of fit with the model is quite satisfactory and the over fitting with each independent parameters are significantly less. Hence the model can be accepted.

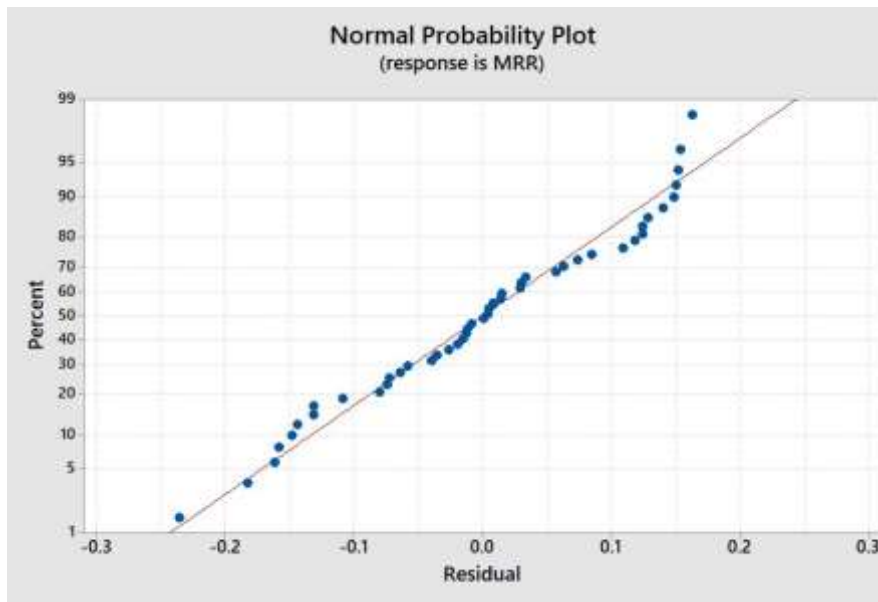


Fig. 5.13. Normal probability plot of MRR of Titanium grade 2.

The same values for TWR are 0.8329, 0.6991 and 0.6563 respectively and the TWR model is found satisfactory. Also, normal, adjusted and predicted R^2 for SR are 0.8668, 0.7603 and 0.7166 respectively. Therefore, it can be concluded that the adequacy of the RSM model of SR is found moderately acceptable and the overfitting of the data is within the range.

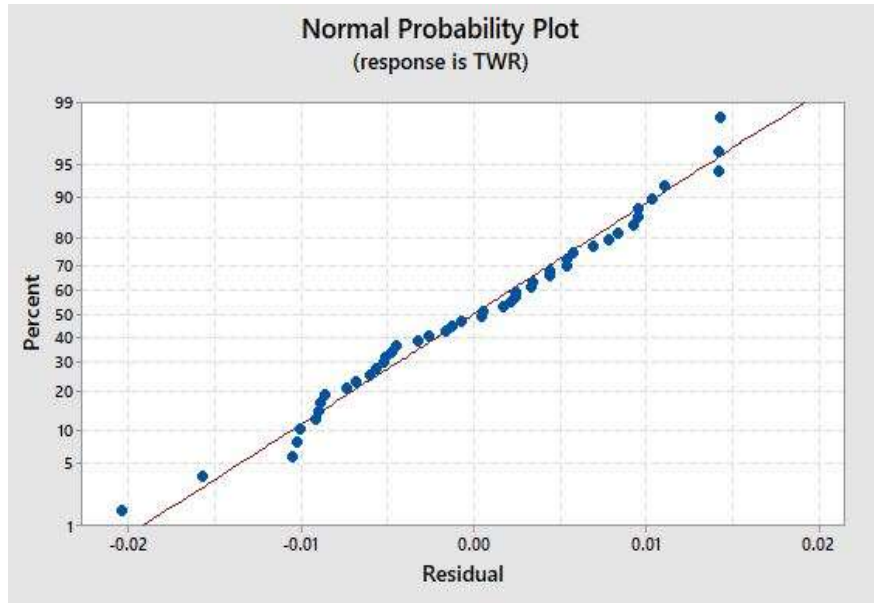


Fig. 5.14. Normal probability plot of TWR for Titanium grade 2.

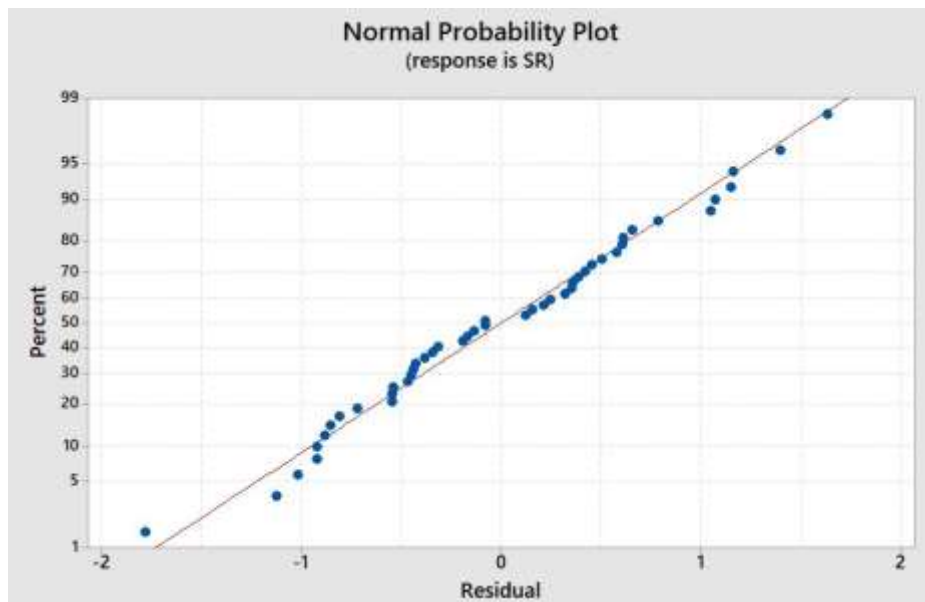


Fig. 5.15. Normal probability plot of SR for Titanium grade 2.

5.3.6. Normal Probability Plot of MRR, TWR and surface roughness

The normal probability plot measures the distribution of the residual points along the normal probability line. Fig. 5.13, 5.14 and 5.15 plots the residual points of MRR, TWR and SR which are situated close to the probability line. Hence, it can be stated that the residuals are distributed normally and confirms that the fitness of the quadratic models are adequate.

5.3.7. 3D Surface Plot for MRR, TWR and surface roughness

Here, 3D response surfaces have been generated for each of the three responses considering the interaction of two input parameters. DESIGN EXPERT 12 is used to make this graph. In the graph, the red represents the highest value and the lowest value of the responses has been represented by blue.

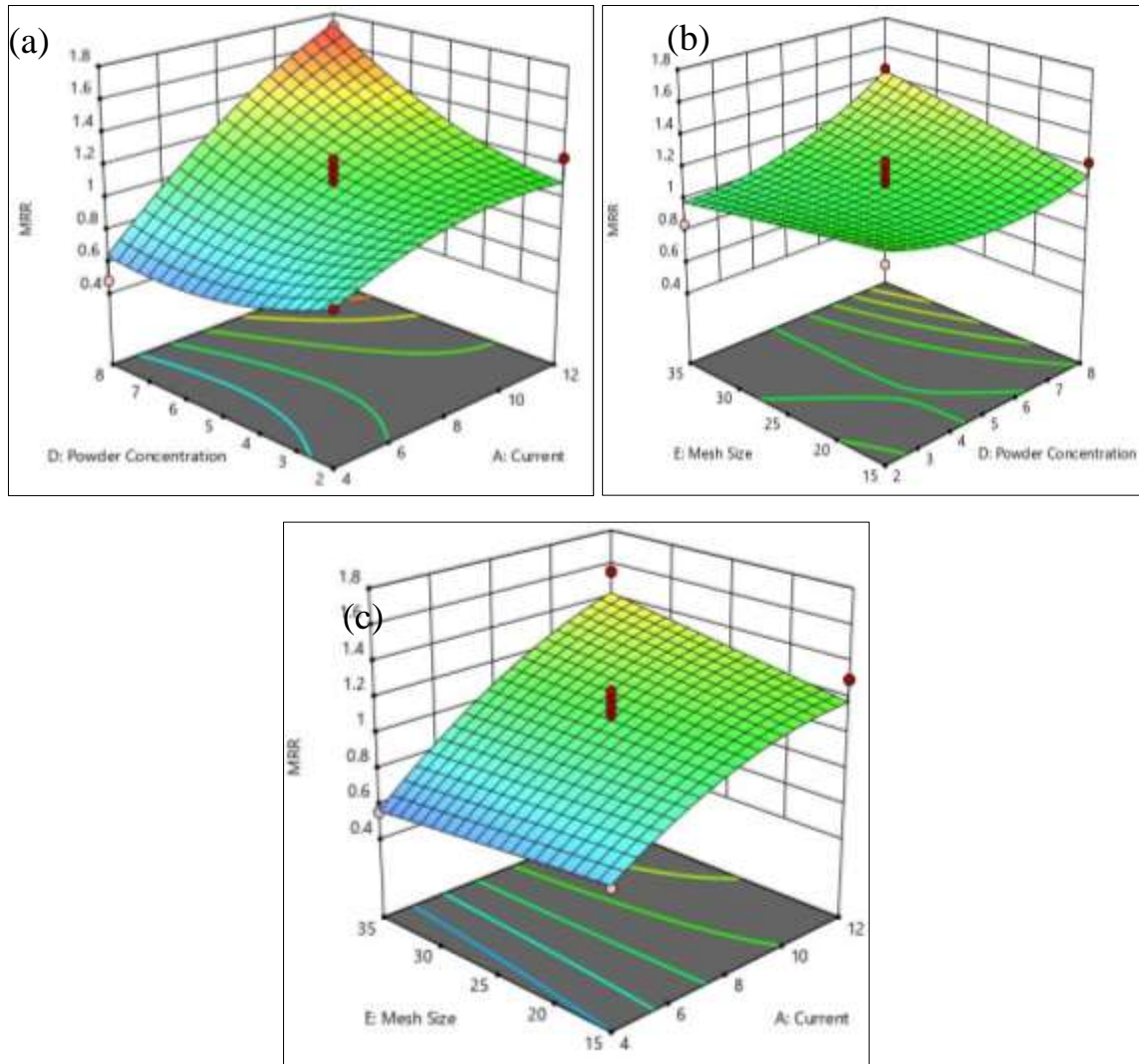


Fig. 5.16. 3D plots of MRR with the association of (a) graphite concentration and current (b) graphite concentration and mesh size and (c) Current and powder mesh size during the machining of Titanium Grade 2.

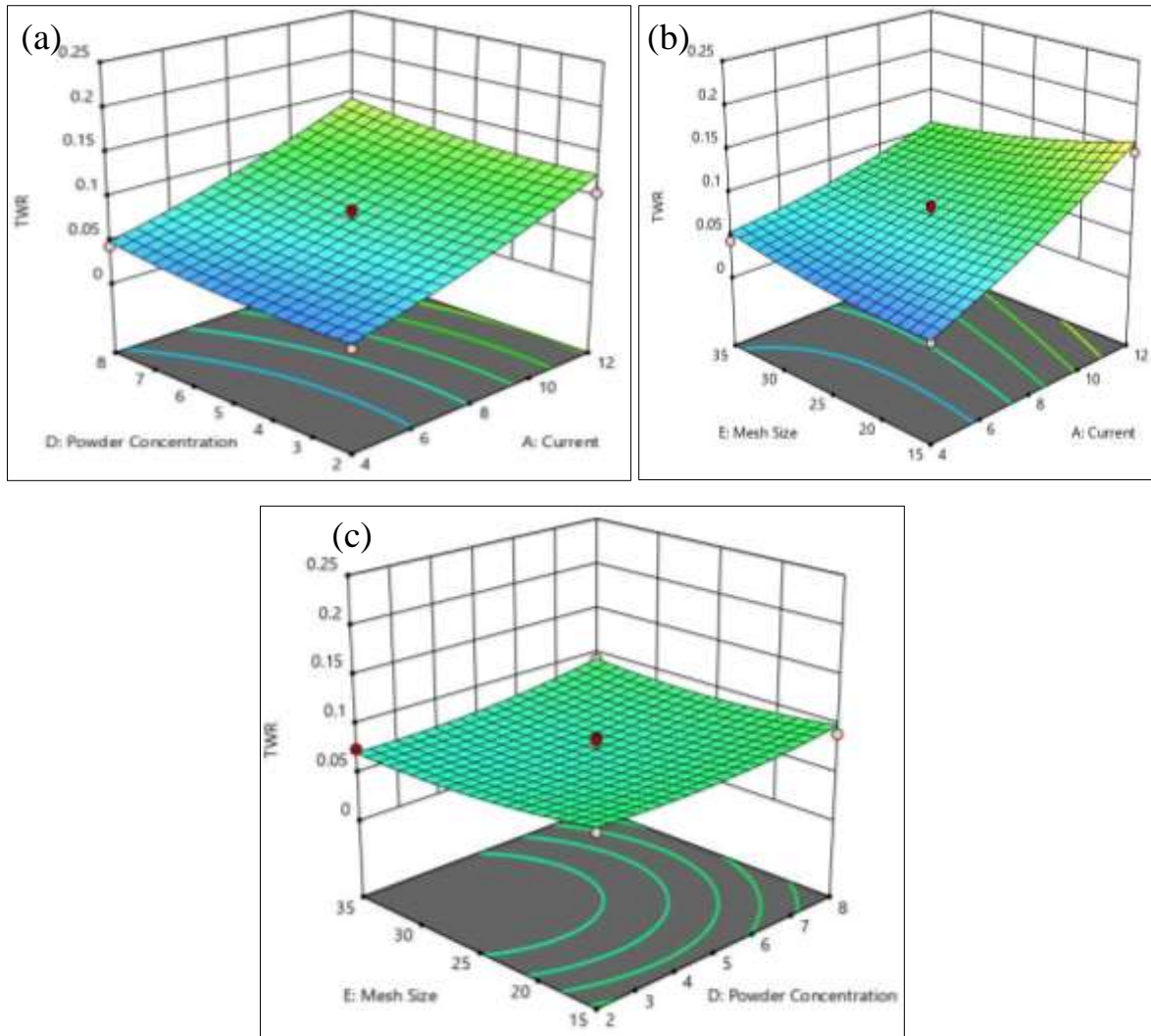


Fig. 5.17. 3D plots of TWR with the association of (a) graphite concentration and current (b) graphite concentration and mesh size and (c) current and powder mesh size during the machining of Titanium Grade 2.

Fig. 5.16 (a)-(c) shows the interaction plot of MRR. It indicates that the maximum MRR can be achieved when the interaction of current and powder concentration happened at 12 A and 8 g/l respectively. Again for the interaction of mesh size and graphite concentration values are found as 35 μm and 8 g/l respectively to achieve high material removal. Finally, the interaction of mesh size and current has the values of 35 μm and 12 A respectively to get the high MRR. In Fig. 5.17 (a)-(c), the surface plot of TWR is represented which conveys the minimum TWR can be achieved at the current of 4 A with 15 μm mesh size, graphite concentration of 8 g/l with 4 A current and 25 μm mesh size with of 4 g/l graphite concentration.

In Fig. 5.18 (a)-(c), the interaction plots of surface roughness have been represented. In this plots, the lowest surface roughness has been found at a current of 4 A with graphite

concentration of 8 g/l, mesh size 15 μm with current 4 A and mesh size 35 μm with graphite concentration 8 g/l. At the low current discharge, the depth of the crater becomes small as small material has been eroded. Also at high powder concentration, more local discharges take place which produce uniform and shallow craters in the discharge region. The combined effect of these two parameters at their aforesaid level values however produces the least surface roughness.

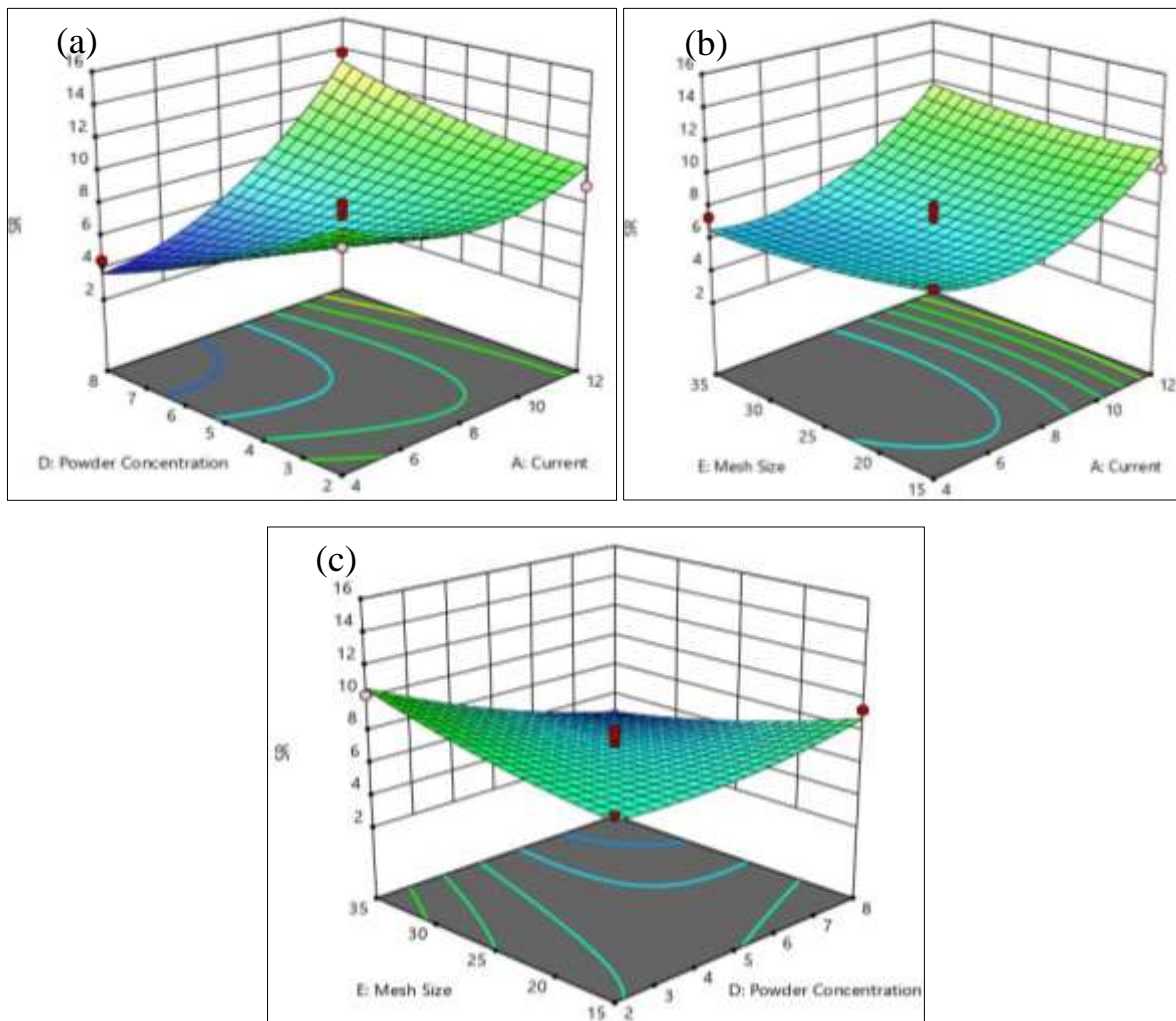


Fig. 5.18. 3D plots of SR with the association of (a) graphite concentration and current (b) graphite concentration and mesh size and (c) current and powder mesh size during the machining of Titanium Grade 2.

5.4. Comparison of MRR, TWR and surface roughness between Titanium grade 2 with Inconel 625 machining

In this section, a comparative study have been between the responses of Titanium and Inconel 625 and machined during powder mixed EDM of graphite particles. Here the comparison have been performed between MRR, TWR and surface roughness. From ANOVA, it has been found that the common significant input parameters are current and powder concentration. Hence the comparative study of MRR, TWR and SR have been done against these two input parameters.

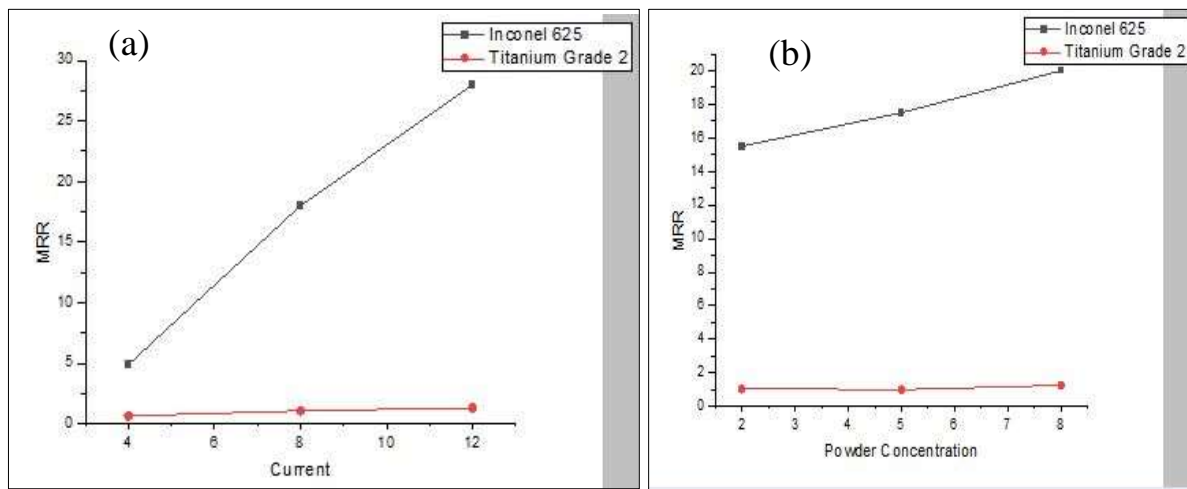


Fig. 5.19. Comparison between MRR of Inconel 625 with Titanium against (a) current (b) powder concentration.

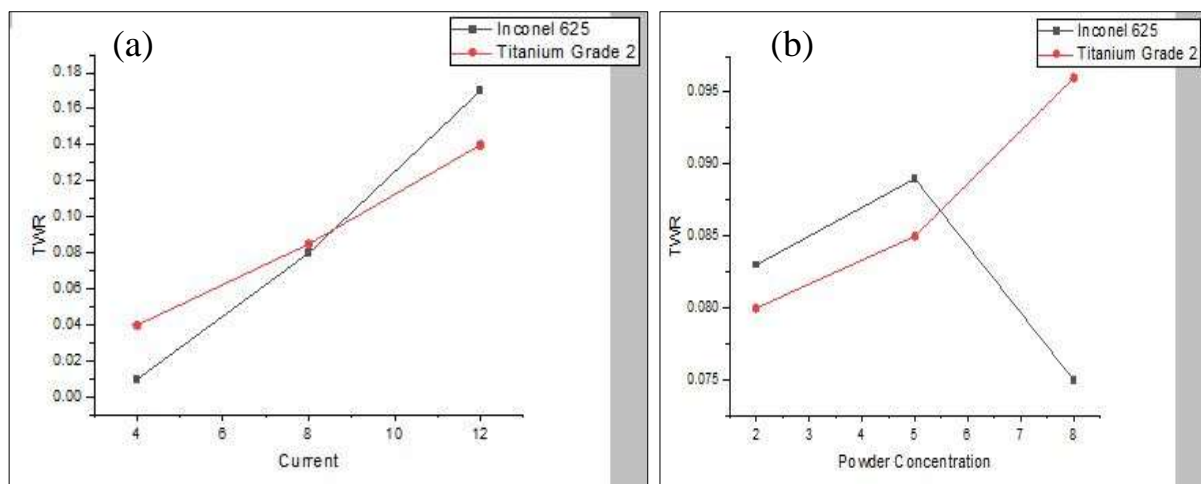


Fig. 5.20. Comparison between TWR of Inconel 625 with Titanium against (a) current (b) powder concentration.

Fig 5.19, Fig. 5.20 and Fig. 5.21 represent the comparison of MRR, TWR and surface roughness against powder concentration and pulse current respectively. The plots are drawn

based on the data points taken from main effects plot where three data points have been chosen for lower, intermediate and upper value of the process parameters.

In the Fig. 5.19 (a) - (b), it has been observed that that MRR value of Inconel 625 is much bigger than the MRR of Titanium grade 2 for both current and powder concentration respectively. Along with that the rate of increase with the increase of input parameters are also high. These two have happened due to the same reason that the hardness and multipoint of Titanium is much higher than high nickel Inconel 625. The rate of melting with same discharge is very low for Titanium grade 2. Therefore the MRR is higher in Inconel 625 compared to Titanium grade 2.

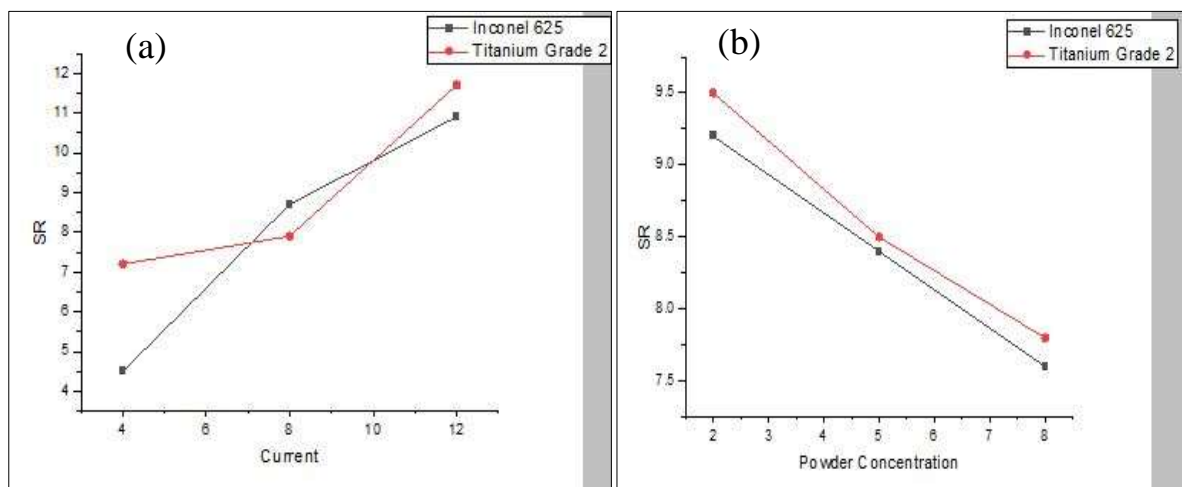


Fig. 5.21. Comparison between surface roughness of Inconel 625 and Titanium grade 2 against (a) current (b) powder concentration.

In the Fig. 5.20 (a) - (b), the tool wear rate (TWR) have been plotted against current and powder concentration for both the materials respectively. It has been observed that there is no significant difference more current flows. But when more graphite powder added, TWR had increased for Titanium grade 2 machining and showed an increasing decreasing pattern for Inconel 625. Due to the more discharges caused by increased powder concentration and low MRR, Titanium grade 2 has increased tool wear but the tool wear of Inconel 625 decreases later because of the rapid increase of MRR with powder concentration, removed material further deposited on tool itself and prevents wear.

In the Fig. 5.21 (a) - (b), the surface roughness have almost pattern and similar pattern and values for both the materials with respect to current and powder concentration respectively. The reason behind this pattern is the material melting and erosion structure is much brittle for

both the material. Titanium, being a hard material faces a brittle type deep and coarse crater over surface. Also high nickel hard Inconel 625 also faces similar type crater on the surface. Hence the surface roughness pattern for both the materials are same.

Chapter 6

*Mathematical Modelling with Fuzzy logic,
Artificial Neural Network and Multi Response
Optimization*

6.1. Introduction

In recent days, the demand for a prediction or mathematical model of an output using different machine learning methods is continuously increasing under the era of Industry 4.0. Along with that the optimized result for a particular setting of parameters using a multi-objective optimization model is also required to be presented. In this study, Fuzzy logic has been applied to make the predictive model of Inconel 718 and Titanium grade 2 processing using titanium mixed EDM. However, neural networks have also been applied, but on Inconel 625 and Titanium Grade 2 processing using graphite mixed EDM. Optimizing the result has been developed by the desirability function.

6.2. Mamdani based fuzzy logic for the machining of Inconel 718 using titanium mixed EDM

The experimental result was used to formulate the fuzzy model for predicting the MRR with the surface roughness. In MATLAB R2021a, a fuzzy toolbox was used to develop the fuzzy model with five input parameters and two responses represented in Fig. 6.1. Mamdani based inference system has been selected as it is the simplest and most efficient process to predict the response.

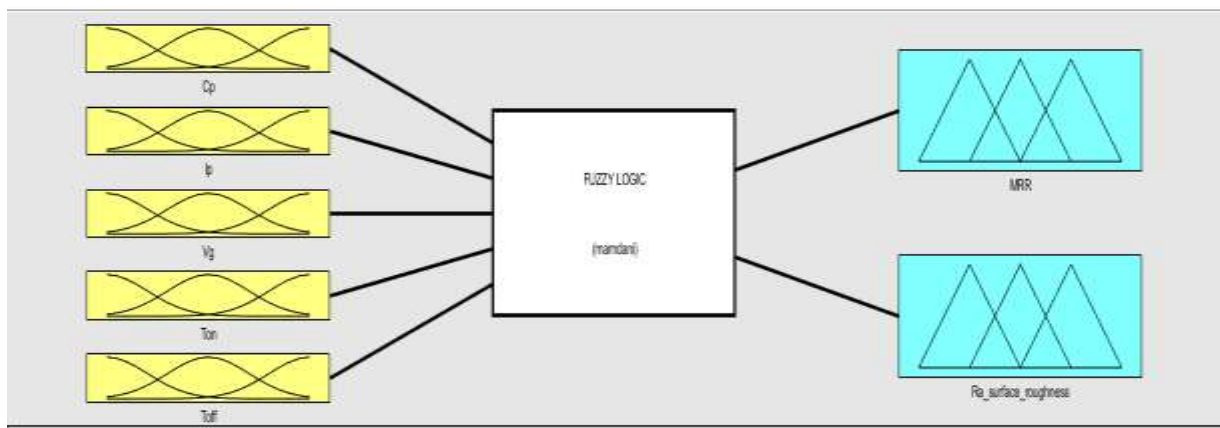


Fig. 6.1. Fuzzy inference system for PMEDM.

6.2.1 Formulation of fuzzy model

As discussed earlier, five steps fuzzy algorithm has been performed starting with fuzzification of the input variables. The input parameters are same as the input parameters chosen during the machining. Each input parameter was fuzzified into three fuzzy levels such as low (L), medium (M) and high (H). In the second step, the triangular membership functions were constructed

for all five input parameters, considering the level value of the parameter as the peak value of the membership function.

Table 6.1.

Parameter values of fuzzy membership functions of input parameters

Parameter	L	M	H
C_p	(1 2 5)	(2 5 8)	(5 8 10)
I_p	(3 6 9)	(6 9 12)	(9 12 15)
V_g	(15 20 40)	(20 40 60)	(40 60 65)
T_{on}	(100 150 200)	(150 200 250)	(200 250 300)
T_{off}	(15 20 40)	(20 40 60)	(40 60 65)

Table 6.2.

Parameter values of fuzzy membership functions of responses

Parameter	VL	L	M	H	VH
MRR	(0 5 9)	(5 9 13)	(9 13 17)	(13 17 21)	(17 21 25)
R_a		(1 2.5 3.5)	(2.5 3.5 4.5)	(3.5 4.5 5.6)	

Fig. 6.2 (a-e) represents all the membership functions with their linguistic values, whereas Table 6.2 represents the parameter values taken for each input parameter during the construction of fuzzy membership functions. MRR was fuzzified into five fuzzy levels, such as very less (VL), less (L), intermediate (M), high (H) and very high (VH). The surface roughness was fuzzified into three fuzzy levels such as less, intermediate and high. Table 8 represents parameters of the responses. The same triangular membership functions were used for MRR and surface roughness as shown in Fig. 6.3 and (b). In the third step, the construction of ‘IF’ and ‘THEN’ based fuzzy rules was implemented based on the logic implemented during the experimental work. The linguistic values of the input parameters and responses were assigned based on the result of the experimentation. Table 6.3 shows the IF and THEN-based fuzzy rules implemented for the modelling. The AND operator was used between any two input parameters. In the fourth step, the ‘Mamdani’ based fuzzy inference system works based on the developed fuzzy rules. In this process, a set of input is executed by a fuzzy inference system and it provides certain rules based on the fuzzy logic which are further used to generate the

output. In the fifth step, the fuzzy output was defuzzified by the centroid defuzzification method based on (Eq. 6) to generate the crisp value of responses.

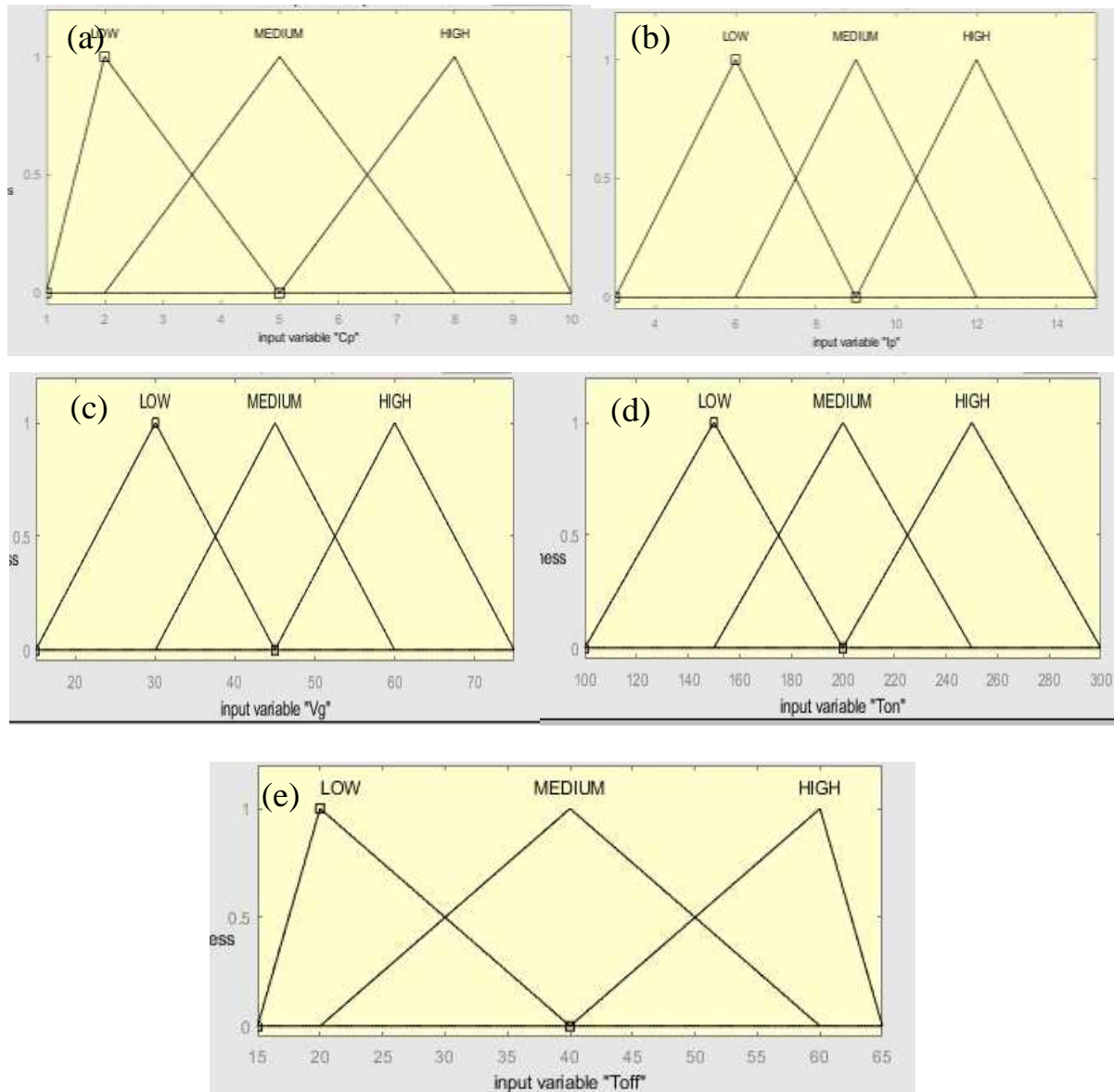


Fig. 6.2. Membership function for input parameters (a) powder concentration (b) Pulse current (c) gap voltage and (d) pulse on time (e) pulse off time.

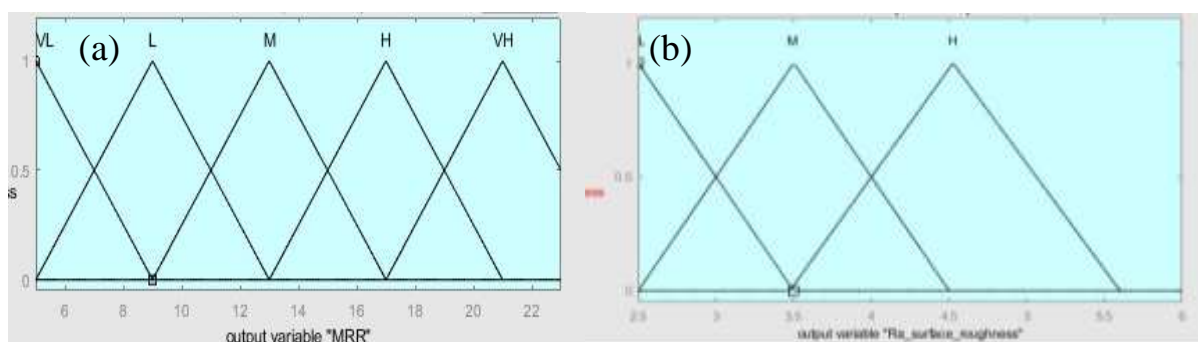


Fig. 6.3. Fuzzy membership function for responses (a) MRR and (b) surface roughness.

6.2.2 Error and accuracy of fuzzy model

The fuzzy rule base has been generated with all the 52 experimental results as the training data. The rules are constructed based on the level values and five classifications of the fuzzy system. For testing purposes, 13 combinations (25% of the total data) of input parameters have been selected arbitrarily from Table 5 and provided to rule base system. Further, the fuzzy predicted MRR with surface roughness were compared with the experimental result and represented in the Fig. 6.4 (a) and Fig. 6.4 (b) respectively. Here red rectangular points represent the predicted value obtained from the fuzzy model and the black circular points represent the actual or experimental value on the plot. To validate the model, the mean actual percentage error (MAPE) was calculated based on (Eq. 6.1). It is the mean error computed by subtracting predicted value from the actual value divided by actual value.

$$MAPE = \left(\frac{1}{N} \sum_{n=1}^N \frac{|actual\ value - predicted\ value|}{actual\ value} \right) \times 100 \quad (6.1)$$

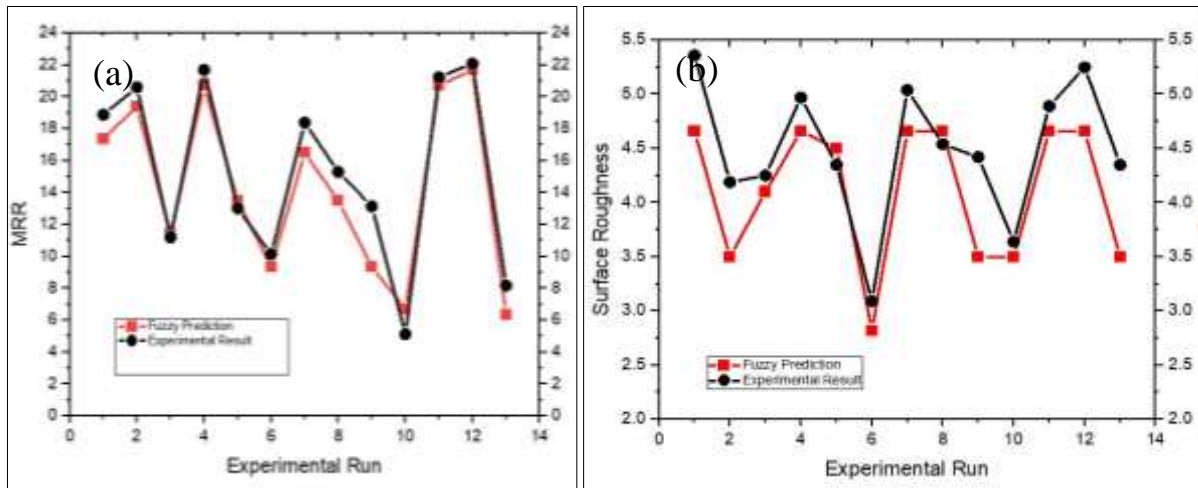


Fig. 6.4. Comparison of fuzzy predicted results with the experimental result for (a) MRR and (b) surface roughness.

Using the 13 experimental and predicted results, the MAPE of MRR and surface roughness are computed and found that the MAPE of MRR is 4.73% and the MAPE of surface roughness is 3.36%. These indicate the obtained fuzzy model can predict the MRR as 95.27% and surface roughness as 96.64% near to experimental results. However, the perfectness of the model for both the responses is above 95% it can be stated that the obtained fuzzy model is an efficient and effective model for predicting such responses having a non-linear relationship with input parameters.

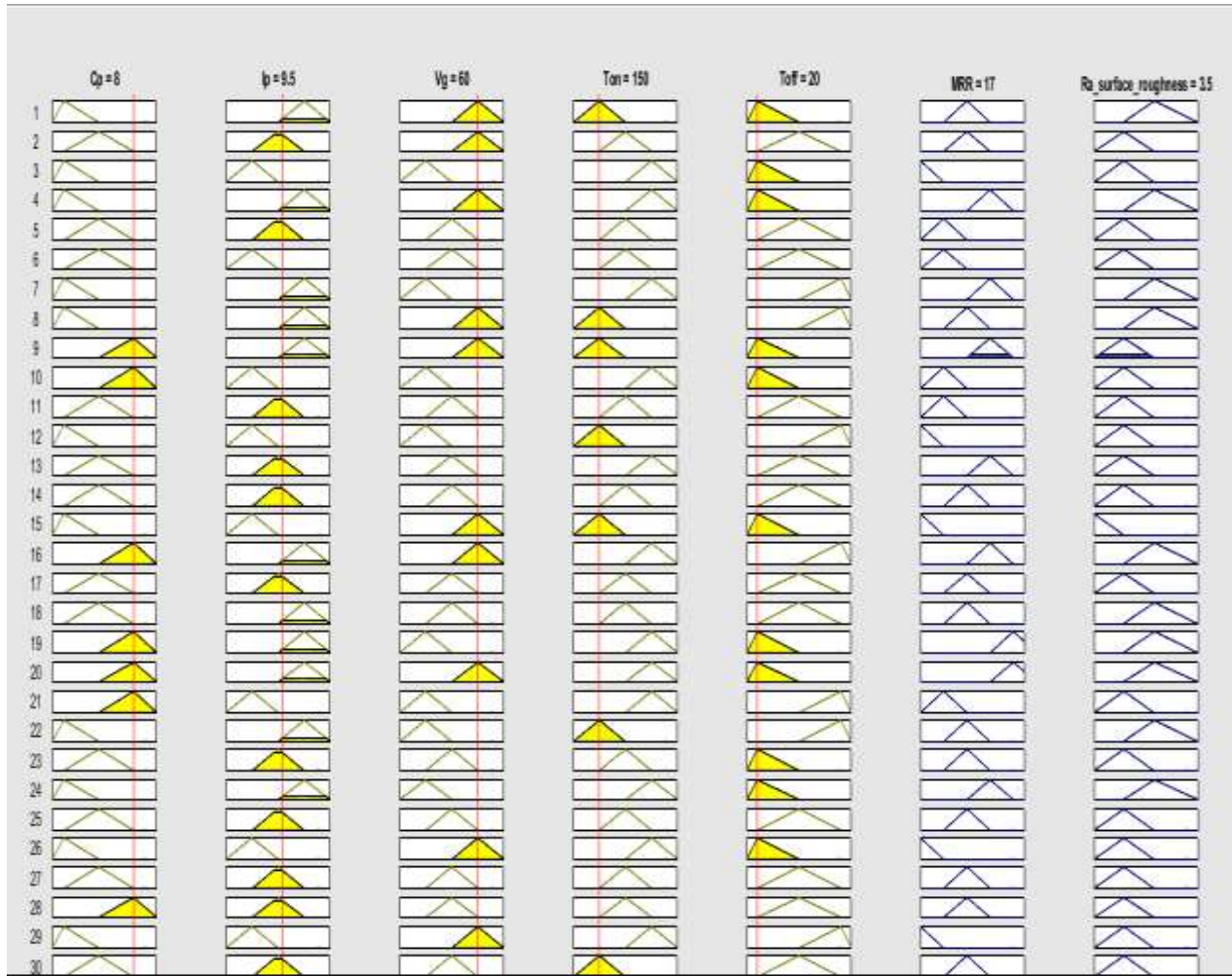


Fig. 6.5. Rule viewer for the fuzzy predicted value of response at optimized condition.

6.3. Desirability function based optimization for Inconel 718 processing using titanium mixed EDM

The optimization of processes parameters was further placed in a fuzzy rule viewer to predict the roughness value and MRR. Fig. 6.5 shows the input parameter setting and the corresponding response values through a fuzzy rule viewer developed during the fuzzy modelling. The fuzzy prediction of MRR and surface roughness were 17 mm³/min and 3.50 μm respectively. The deviation of the fuzzy predicted result concerning the optimized result is 2.27% for MRR and 5.66% for surface roughness. This indicates the fuzzy predicted result has a good agreement with the result obtained from RSM at the optimized value of input parameters.

6.3.1. Result of optimization

The result of optimization has been reported in Table 6.3. The optimization has been done with a composite desirability of 0.6514. Fig. 6.6 represents the desirability approach of optimizing MRR and Surface roughness. Here, input parameter values, at which optimization takes place are 8 g/l of powder concentration, 9.5 A of current, voltage as 60 V, pulse on time at 150 μ s with pulse off at 20 μ s. Finally, the optimized value of roughness and MRR are 3.71 μ m and 16.623 mm³/min respectively.

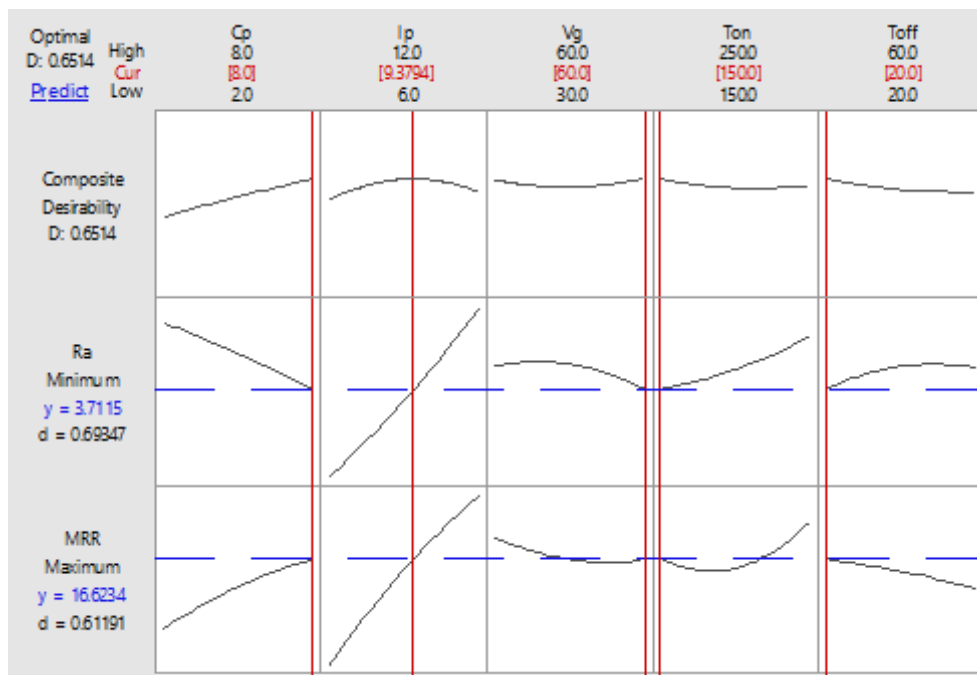


Fig. 6.6. Desirability function approach of optimizing the Inconel 718 machined by titanium based EDM.

6.3.2. Confirmatory test result

Furthermore, a confirmatory experiment was conducted considering the input parameters set at their optimal values. The roughness and MRR obtained from the confirmatory experiment were 3.64 μ m and 16.261 mm³/min, respectively as shown in Table 6.4. It is found that the deviation of roughness and MRR were 1.89% and 2.18% when the RSM result is compared with the confirmatory test result. In Fig. 6.7, the comparisons of the results obtained from RSM optimization and confirmatory experiment have been shown for roughness and MRR in the form of a bar diagram. The blue colour indicates the RSM result, and the green colour indicates the result of the confirmatory experiment. The bar diagrams indicate the RSM optimized result

and the confirmatory test result is very much closer to each other. Hence, the optimized result can be accepted and referred to the manufacturing industry for the machining of Inconel 718.

Table 6.3.

Desirability function based optimization of Inconel 718 machined by titanium mixed EDM

Optimal setting of input parameters	Optimized responses	
$C_p = 8 \text{ g/l}$ $I_p = 9.5 \text{ A}$ $V_g = 60 \text{ V}$ $T_{on} = 150 \text{ }\mu\text{s}$ $T_{off} = 20 \text{ }\mu\text{s}$	MRR (mm^3/min)	Surface Roughness (R_a) (μm)
	16.623	3.71

6.4. Desirability function based optimization for Titanium Grade 2 processing using titanium mixed EDM

6.4.1. Result of optimization

In this section, the result of optimization has been reported in Table 6.5. The optimization has been done with a composite desirability of 0.9040. Fig. 6.8 represents the desirability approach of optimizing MRR and Roughness. The values of process parameters at which the optimization takes place are 8 g/l of powder concentration, current at 11.4 A, gap voltage of 30 V, pulse time of 150 μs and pulse off with 60 μs . However, the optimized value of roughness and MRR are 7.17 μm and 1.493 mm^3/min respectively.

6.4.2. Confirmatory test result

Furthermore, a confirmatory experiment was conducted considering the input parameters set at their optimal values. The roughness and MRR obtained from the confirmatory experiment were 7.35 μm and 1.523 mm^3/min respectively as shown in Table 6.6. It is found that the deviation of MRR and surface roughness were 2.01% and 2.45% when the RSM result is compared with the confirmatory test result. In Fig. 6.9, the comparisons of the results obtained from RSM optimization and confirmatory experiment are shown for roughness and MRR in the form of a bar diagram. The blue portion indicates the RSM result, and the green portion indicates the result of the confirmatory experiment. The bar diagrams indicate the RSM

optimized result and the confirmatory test result are very much closer to each other. Hence, the optimized result can be accepted and referred to the manufacturing industry for the machining of Titanium grade 2.

Table 6.4.

Comparison between optimized result and confirmatory test result of Inconel 718 machined by titanium mixed EDM

Responses	RSM optimization	Confirmatory experiment result	% Deviation between optimized value and confirmatory test result
MRR	16.623	16.261	2.18
surface roughness	3.71	3.64	1.89

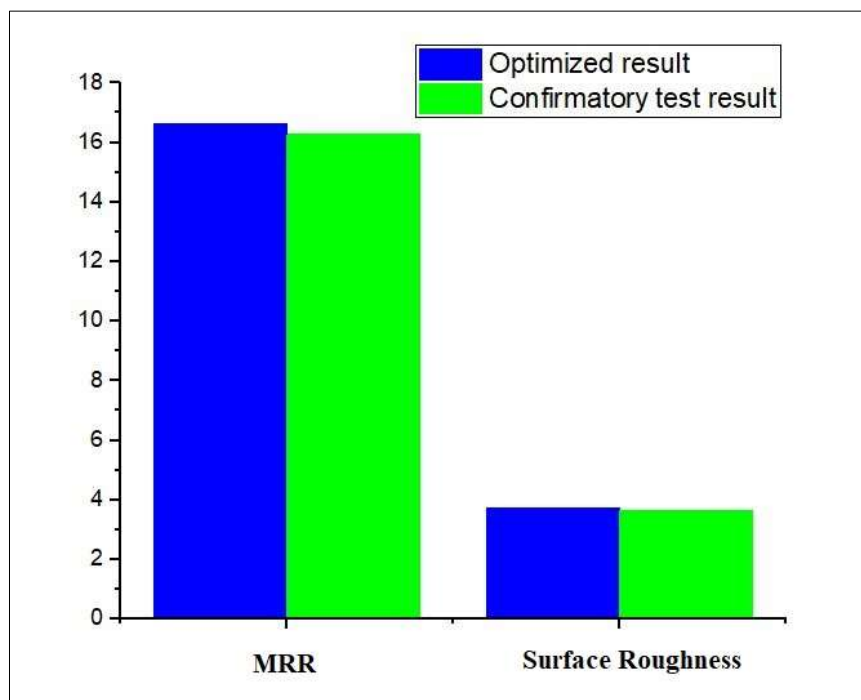


Fig. 6.7. Bar diagram for comparison between the optimized result and confirmatory test result for Inconel 718 machined by titanium mixed EDM.

Table 6.5.

Multi-objective optimization using the desirability function of Titanium grade 2 machined by titanium mixed EDM

Optimal setting of input parameters	Optimized responses	
$C_p = 8 \text{ g/l}$ $I_p = 11.4 \text{ A}$ $V_g = 30 \text{ V}$ $T_{on} = 150 \mu\text{s}$ $T_{off} = 60 \mu\text{s}$	MRR (mm^3/min)	Surface Roughness (R_a) (μm)
	1.493	7.17

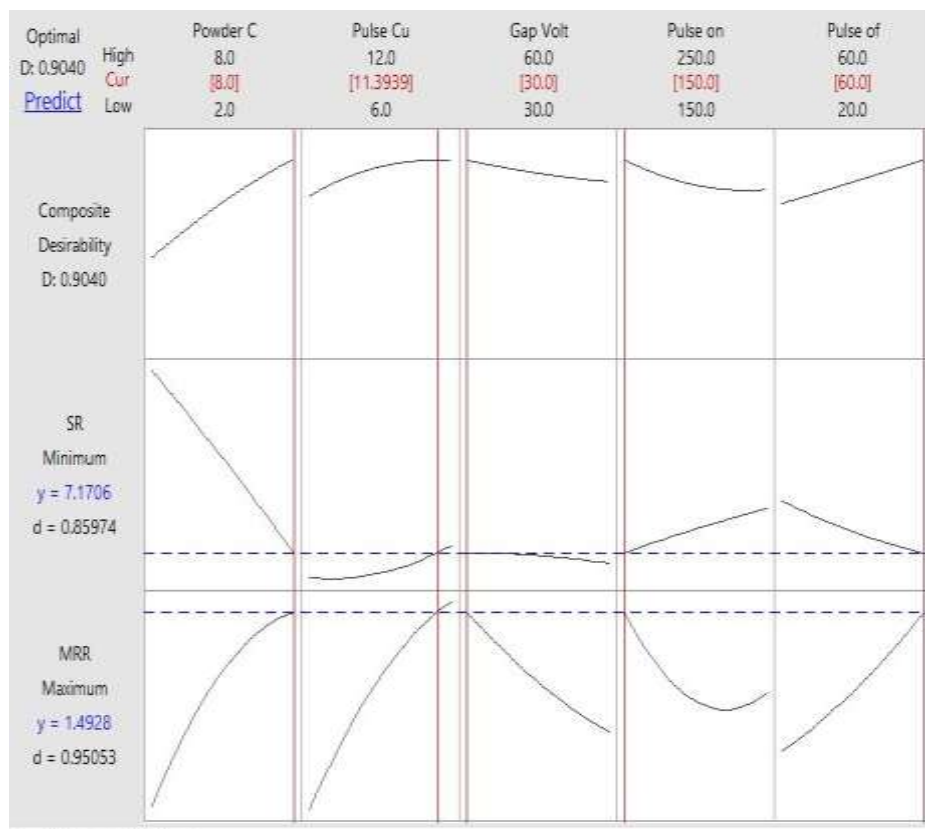


Fig. 6.8. Desirability function approach of optimizing Titanium grade 2 machined by titanium mixed EDM.

Table 6.6.

Comparison between optimized result and confirmatory test result of Titanium grade 2 machined by titanium mixed EDM

Responses	Optimized result	Confirmatory experiment result	% Deviation between optimized value and confirmatory test result
MRR	1.493	1.523	2.01
surface roughness	7.17	7.35	2.45

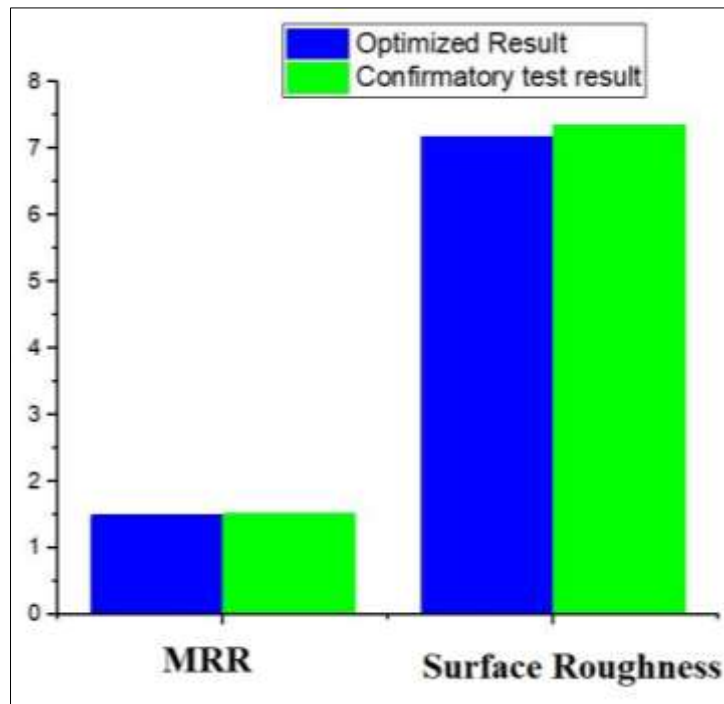


Fig. 6.9. Bar diagram for comparison between the RSM model and confirmatory test result of Titanium grade 2 machined by titanium mixed EDM.

6.5. Back propagation type Neural Network for Inconel 625 processing using graphite mixed EDM

In the present study, a 5-20-3 neural network has been developed using the neural network toolbox in MATLAB R2021a. It is a feed forward backpropagation type network where the training function, learning function and performance function are chosen as TRAINLM, LEARNMOM and MSE respectively. After several trials made by different combinations of network, a single hidden layer with 20 neurons has been selected for this analysis. In several studies, this can be clear that the effect of performance parameters on the responses during EDM is highly nonlinear. In ANN, the nonlinear interaction between hidden layers can be

efficiently performed by a nonlinear sigmoid function. During the training of the network, the stopping criterion was set as 1000 epochs or an error of 0 whichever reached earlier.

Table 6.7.

Predicted result of MRR, TWR and SR using ANN

Run No.	MRR				TWR			SR	
	Exp.	ANN pred.	%Error	Exp.	ANN pred.	%Error	Exp.	ANN pred.	%Error
Training data									
1	16.659	18.127	8.81	0.0797	0.0728	8.78	9.08	8.14	10.35
2	18.780	20.291	8.05	0.0810	0.0859	6.17	9.99	9.59	4.00
3	29.068	28.273	2.74	0.1627	0.1470	9.83	8.50	8.77	3.18
5	16.736	16.785	0.29	0.0574	0.0531	6.97	10.32	9.53	7.66
7	16.563	17.163	3.62	0.0680	0.0606	10.29	7.41	7.58	2.29
8	3.989	3.722	6.69	0.0190	0.0177	5.26	4.67	4.55	2.57
9	28.919	28.593	1.13	0.1493	0.1412	5.36	12.33	11.46	7.06
11	15.450	14.202	8.08	0.0921	0.0500	45.60	9.08	8.50	6.39
13	27.923	29.530	5.76	0.1654	0.1841	11.49	10.39	11.03	6.16
14	16.983	17.387	2.38	0.0762	0.0757	1.31	8.69	8.67	0.23
16	21.771	22.474	3.23	0.0782	0.0721	7.67	8.46	8.34	1.42
18	12.994	13.875	6.78	0.0861	0.0854	1.16	8.74	8.20	6.18
19	4.404	4.777	8.47	0.0157	0.0143	6.37	4.20	4.57	8.81
20	14.739	16.330	10.79	0.0881	0.0895	1.14	9.53	8.98	5.77
22	18.697	18.127	3.05	0.0991	0.0828	16.15	6.72	7.14	6.25
23	23.697	26.428	11.53	0.1738	0.1697	2.30	11.62	11.03	5.08
24	27.921	25.417	8.97	0.0685	0.0640	5.84	9.55	9.88	3.46
26	4.542	4.920	8.32	0.0132	0.0139	7.58	4.10	4.74	15.61
28	13.586	14.371	5.78	0.0813	0.0847	3.69	9.57	8.92	6.79
29	23.726	23.877	0.64	0.0775	0.0709	9.03	7.13	7.47	4.77
30	19.431	17.649	9.17	0.0650	0.0636	1.54	10.79	9.76	9.55
31	20.472	23.523	14.90	0.2039	0.2173	6.38	10.93	12.04	10.16
32	16.055	14.649	8.76	0.0998	0.0896	10.02	6.74	7.26	7.72
34	12.576	12.649	0.58	0.0737	0.0746	1.36	10.98	10.76	2.00

36	20.201	17.628	12.74	0.0781	0.0812	3.84	7.43	7.39	0.54
39	16.543	15.916	3.79	0.0944	0.0940	0.00	10.14	9.15	9.76
42	7.701	7.764	0.82	0.0261	0.0246	7.66	4.53	4.98	9.93
43	4.147	4.140	0.17	0.0129	0.0137	7.75	3.92	3.33	15.05
44	27.429	26.255	4.28	0.1886	0.1827	3.18	10.76	9.37	12.92
46	27.429	25.229	8.02	0.0827	0.0920	10.88	7.90	7.98	1.01
<i>Testing data</i>									
4	20.468	20.957	2.39	0.0882	0.0786	11.34	8.34	8.38	0.48
6	18.602	18.127	2.55	0.0763	0.0728	3.93	8.86	8.14	8.13
10	29.452	28.799	2.22	0.1419	0.1205	14.80	9.11	9.65	5.93
12	19.879	20.798	4.62	0.0863	0.0796	8.11	8.69	9.46	8.86
15	23.324	23.131	0.83	0.0664	0.0710	7.53	9.58	9.73	1.57
17	30.772	28.610	7.03	0.1656	0.1569	5.44	11.56	11.74	1.56
21	20.468	19.217	6.11	0.0728	0.0741	1.37	8.29	8.82	6.39
25	4.333	4.700	8.47	0.0249	0.0254	0.00	3.12	3.69	18.27
27	20.024	18.127	9.47	0.0823	0.0728	10.94	7.58	8.14	7.39
33	17.546	17.628	0.47	0.0789	0.0812	2.54	9.86	9.39	4.77
35	20.438	20.633	0.95	0.0642	0.0683	6.23	7.81	8.19	4.87
37	15.521	16.033	3.30	0.0991	0.0929	6.05	8.28	7.70	7.01
38	6.536	6.910	5.72	0.0884	0.0835	5.66	6.12	6.40	4.58
40	2.204	2.757	25.09	0.0159	0.0139	12.58	4.60	4.99	8.48
41	19.589	18.329	6.43	0.0775	0.0729	6.45	8.66	7.93	8.43
45	8.672	9.500	9.55	0.0713	0.0776	8.42	10.14	10.66	5.13

During the training of the network, arbitrarily 30 results were chosen for training of the network. The remaining 16 results were kept for testing the data. After completion of the training, the testing dataset was simulated with trained network and the predicted result was generated.

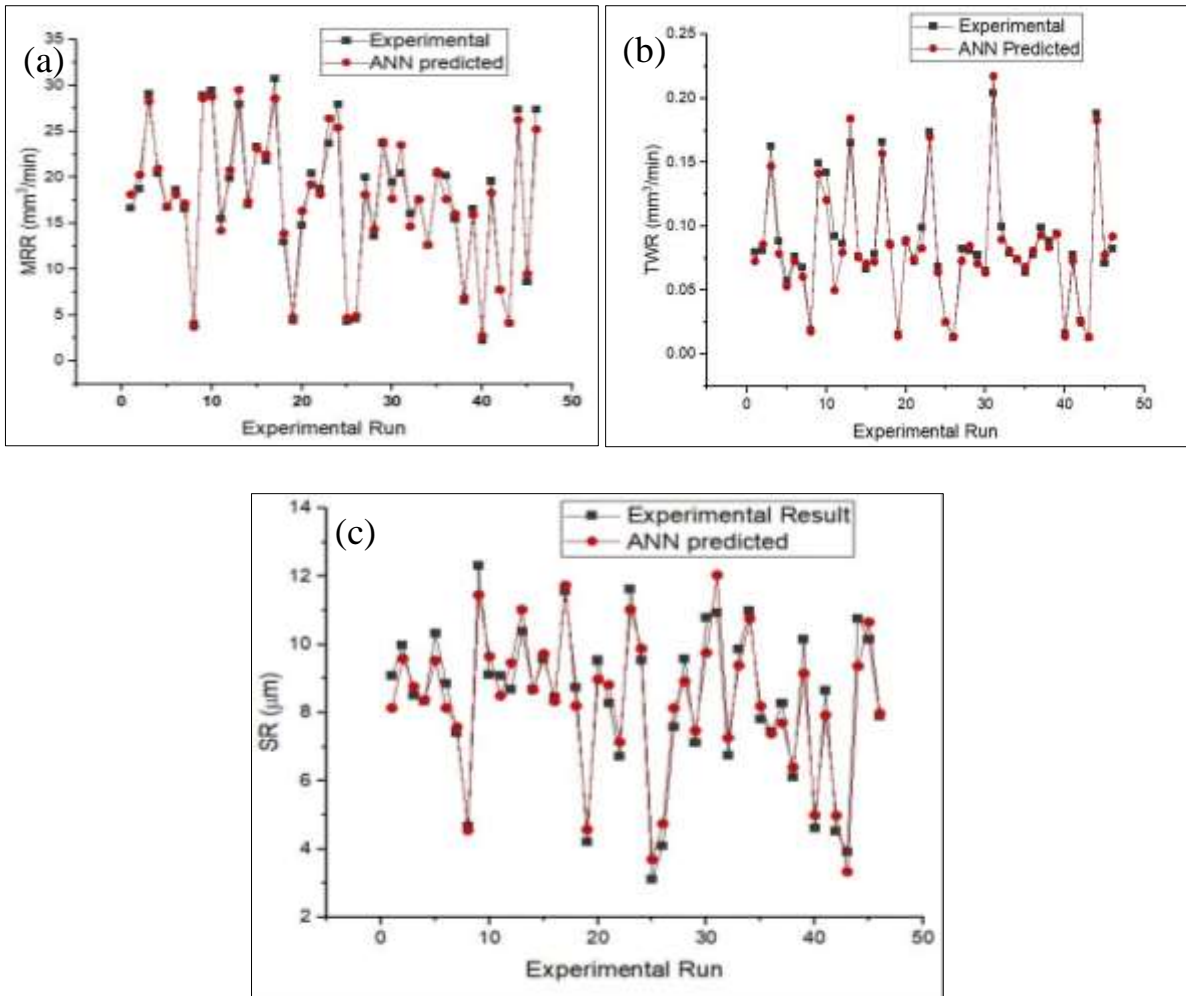


Fig. 6.10. Comparison of ANN result and actual result for tested data of (a) MRR, (b) TWR and (c) SR.

In Table 6.7, the prediction of the training and testing results have been provided. In the table, the experimental result and the predicted result are compared for all the three responses. A percentage relative error is calculated for every prediction. In the table, it can be observed that the percentage relative error has a wide range for different runs and different responses. The mean error for MRR, TWR and SR is 5.95%, 7.30% and 6.40% respectively. The mean error for all the responses are found less than 10% which indicates the ANN model can predict the responses 90% closer to the actual result.

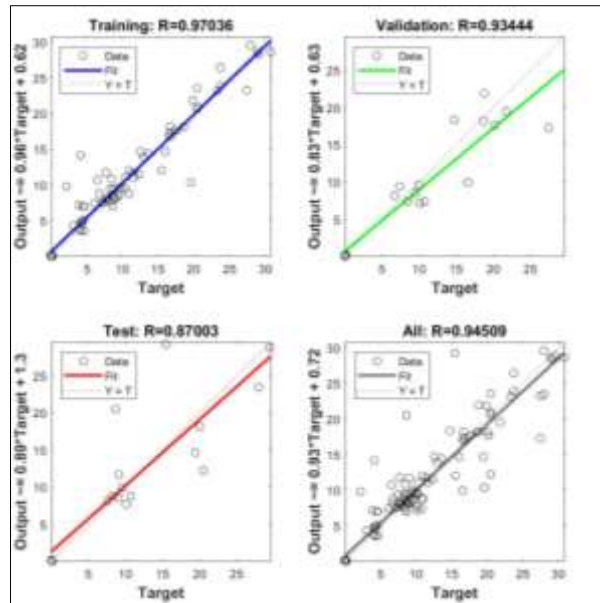


Fig. 6.11. R- Values of the ANN model.

In Fig. 6.10 (a)-(c), the predictions of the tested data are plotted against their experimental data for MRR, TWR and SR. In the graphical representation, red dots represent predicted data and black dots represent the actual data for all three responses. It can be observed that the prediction lines and the lines made with actual values are situated closely even coincide somewhere.

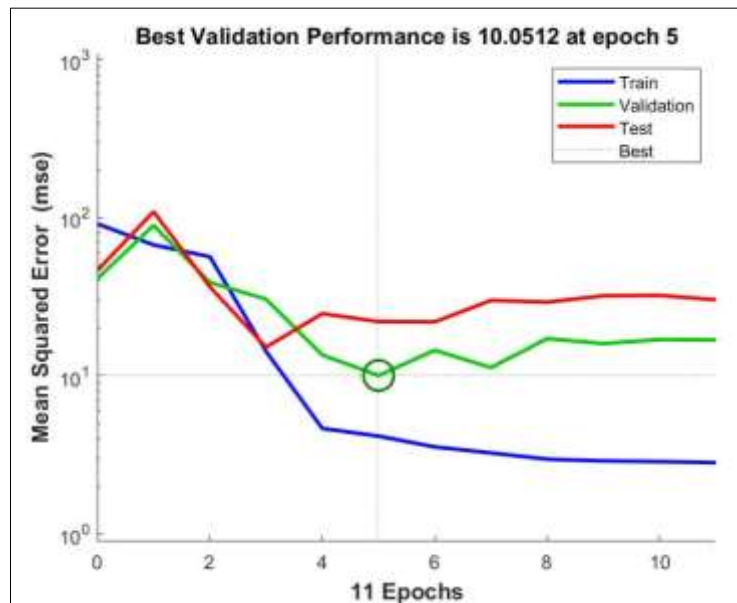


Fig. 6.12. Epoch vs MSE plot during the training of the network.

Fig. 6.11 shows the R-value (correlation coefficient) of training, validation, test and overall performance for the present neural network. Apart from test performance, the R-values of training and validation were found to be more than 0.9. The R-value of overall performance is

0.94509 which indicates the predicted values are distributed at close intervals with the target data. In Fig. 6.12, the mean square error is plotted against the value of epoch. It is observed that the training of the model has been completed with minimum error within 11 epochs. This indicates the training model takes less time of computation time during the training. In this study, two parameters related to the performance of neural network have been evaluated viz. mean error and R- value. In the manufacturing industry, a new ANN model is adopted for production, machining and other work only when the values of these two parameters are found closer to a standard one. In this study, the mean error and R values are found adequate to accept the model. With less than 10% mean error and R value as 0.94509, it can be well said that the model has a good correlation with experimental results and it can perform efficiently to predict the responses for the remaining combination of the input parameters in practice.

6.6. Desirability function based optimization for Inconel 625 processing using graphite mixed EDM

In the present study, desirability approach based optimization with multi variables was performed on RSM equations. The objective functions were selected as to maximize MRR, minimize SR and to get a target value of TWR at 0.08 mm³/min. The reason behind selecting a target level of TWR is to maximize MRR. In a practical approach, the TWR must be minimized but the priority of maximization of MRR is more than that. After several analyses with the different target values of TWR including the lowest value, the above said value which is approximately average of all the TWR has been found suitable for the optimization. The constraints were taken as upper and lower and upper value of each input parameter. At two sided confidence level of 95% the calculation was performed.

6.6.1. Result of optimization

Using MINITAB 17.0, the result of the optimization is achieved and enlisted in Table 6.8. Material removal rate, tool wear rate and surface roughness for the optimal setting of parameters are 26.136 mm³/min, 0.08 mm³/min and 5.82 µm respectively. The value of composite desirability is found 0.8398 as shown in Fig. 6.13. It indicates that the degree of optimization has achieved closer to 1 and supports for accepting the result. The value of input parameters at optimization is 8.6 A of current, 35 µs of pulse on time, 0.5 of duty cycle, 8 g/l of powder concentration and 35 µm of mesh size.

6.6.2. Confirmatory test result

The result of the optimization has been validated by conducting a validation experiment. In this experiment, input parameters were set with the feasible value corresponding to the optimal set of solutions achieved from the optimization. During the validation test, the result has been found as current as 8.5 A, pulse on time as 35 μ s, duty cycle as 0.5, powder concentration as 8 g/l and mesh size 35 μ m. The other input parameters and experimental environment were kept unaltered as done in the main experiment. The responses were measured in the same way as previously and are represented in Table 6.9. The values of MRR, TWR and SR are 25.864 mm^3/min , 0.0836 mm^3/min and 5.97 μm . Fig. 6.14 provides a comparative representation of the optimized result and the confirmatory test result. Therefore, a percentage relative error of the prediction is calculated against the actual result and found that the errors for MRR, TWR and SR are 1.03%, 4.50% and 2.51%. However, it is enough to accept the optimized result in the practical application having the same affecting parameters with the same level values.

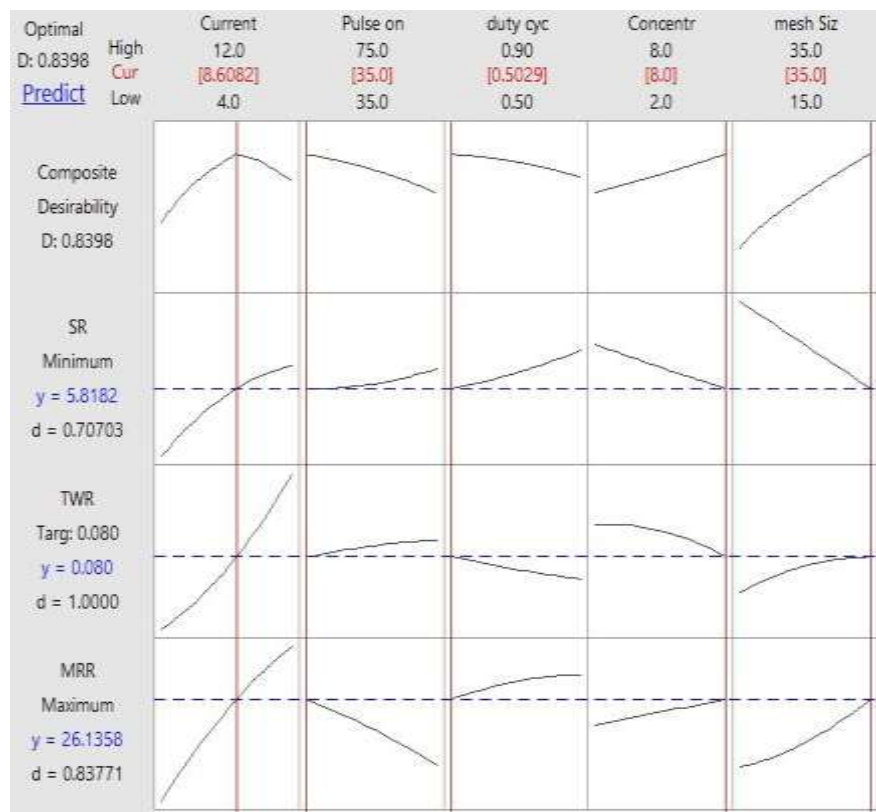


Fig. 6.13. Result of desirability function optimization of Inconel 625 machined by graphite mixed EDM.

Table 6.8.

Result of multi objective optimization using desirability function of Inconel 625 machined by graphite mixed EDM

Input parameters	Optimized result	MRR mm ³ /min	SR μm	TWR mm ³ /min
I (A)	8.6082	26.136	5.82	0.0800
P _{on} (μs)	35.0			
DC	0.5029			
C _p (g/l)	8.0			
M (μm)	35.0			

Table 6.9.

Comparison between optimized result and confirmatory test result of Inconel 625 machined by graphite mixed EDM

Responses	Optimized result	Confirmatory experiment result	% Deviation between optimized value and confirmatory test result
MRR	26.136	25.864	1.03
TWR	0.0800	0.0836	2.51
SR	5.81	5.97	4.50

6.7. Desirability function based optimization for Titanium Grade 2 processing using graphite mixed EDM

In the present study, desirability function has been utilized on RSM equations for the optimization. The objective functions were selected as to maximize MRR, minimize SR and minimize TWR. The constraints were taken as upper and lower and upper value of each input parameter. At two sided confidence level of 95% the calculation was performed.

6.7.1. Result of optimization

The optimization was performed in MINITAB 17. The result of the optimization has been enlisted in Table 6.10. The value of material removal rate, tool wear rate and surface roughness for optimal setting of parameters are 1.409 mm³/min, 0.0922 mm³/min and 4.54 μm respectively. The value of composite desirability is found 0.8658 as shown in Fig. 6.15. The

result of the optimization includes current at 7.8 A, 0.7 of duty cycle, 55 μ s pulse time, 8 g/l of powder concentration and of mesh size 35 μ m.

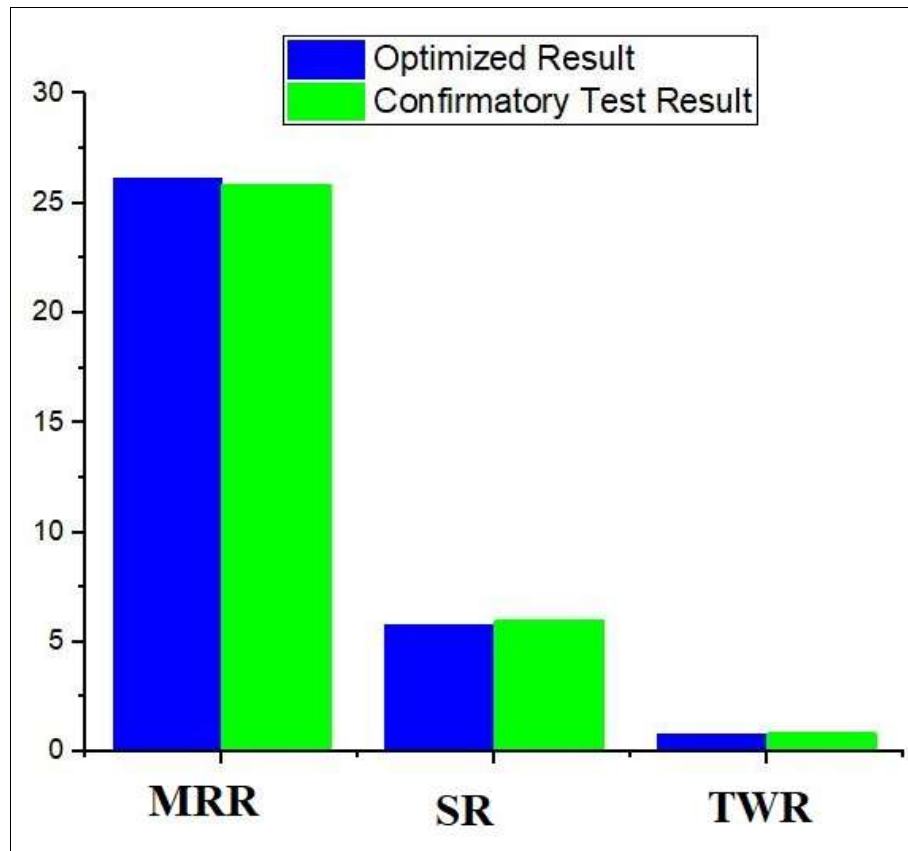


Fig. 6.14. Bar diagram for comparison between the optimized result and confirmatory test result of Inconel 625 machined by graphite mixed EDM.

6.7.2. Confirmatory test result

The result of the optimization has been validated by conducting a validation experiment. In this experiment, input parameters were set with the feasible value corresponding to the optimal set of solutions achieved from the optimization. In the validation test, current as 7.8 A, pulse time as 55 μ s, duty cycle as 0.7, concentration as 8 g/l and mesh size 35 μ m have been selected. The other input parameters and experimental environment were kept unaltered as done the main experiment. The responses were measured in the same way as measured previously and are represented in Table 6.11.

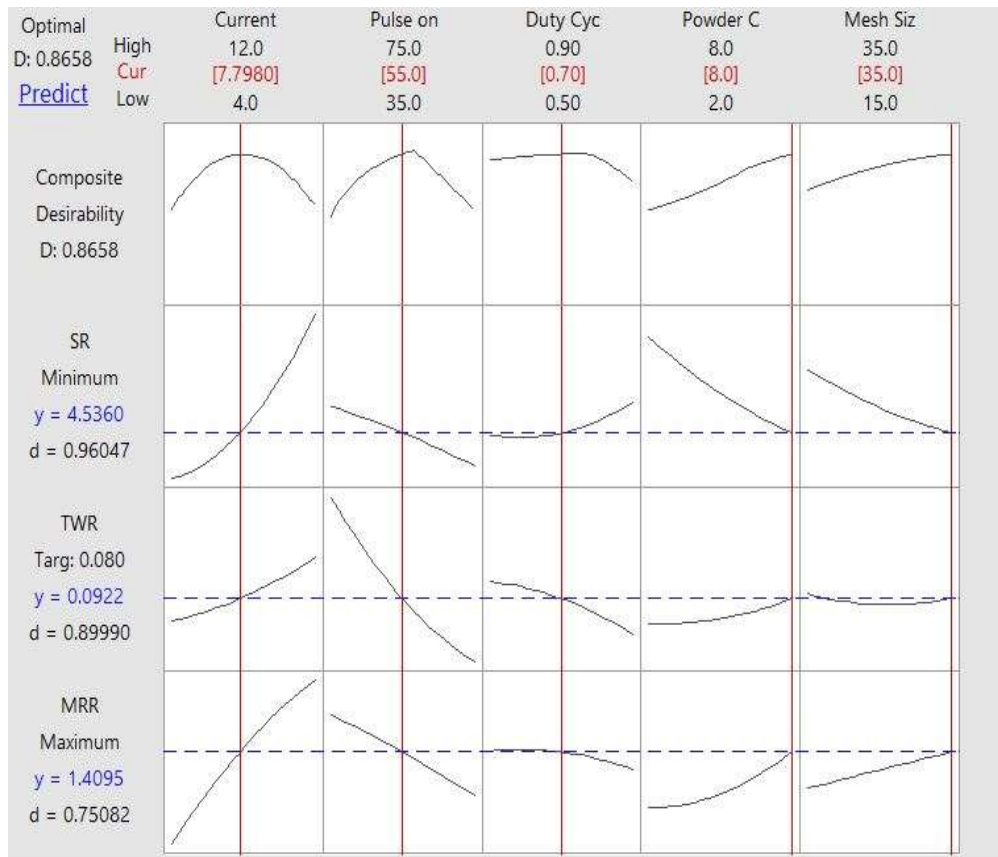


Fig. 6.15. Result of desirability function optimization of Titanium grade 2 machined by graphite mixed EDM.

Table 6.10.

Result of desirability function optimization of Titanium grade 2 machined by graphite mixed EDM

Input parameters	Optimized result	MRR mm ³ /min	SR μm	TWR mm ³ /min
I (A)	7.7980	1.409	4.54	0.0922
P _{on} (μs)	55			
DC	0.7			
C _p (g/l)	8			
M (μm)	35			

The values of MRR, TWR and SR are 1.398 mm³/min, 0.0891 mm³/min and 4.68 μm. Fig. 6.16 provides a comparative representation of optimized result and confirmatory test result. Therefore, a percentage relative error of the prediction is calculated against the actual result

and the errors for MRR, TWR and roughness are 0.81%, 3.47% and 3.08%. The deviation of the result from the optimized result is less than 5% which indicates the optimized data can be accepted and used in an industrial application.

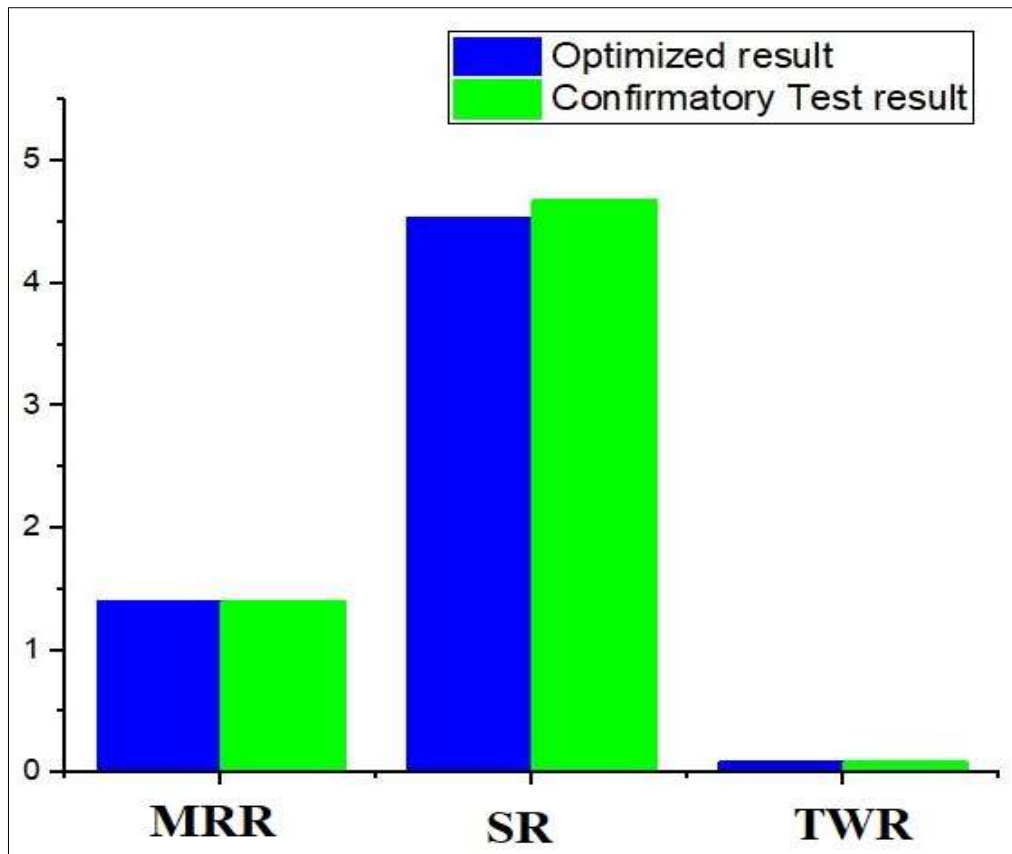


Fig. 6.16. Bar diagram for comparison between the optimized and confirmatory test results of Titanium grade 2 machined by graphite mixed EDM.

Table 6.11.

Comparison between optimized result and confirmatory test result of Titanium grade 2 machined by graphite mixed EDM

Responses	Optimized result	Confirmatory experiment result	% Deviation between optimized value and confirmatory test result
MRR	1.409	1.398	0.81
TWR	0.0922	0.0891	3.47
SR	4.54	4.68	3.08

Chapter 7

*Surface characterization of titanium and
graphite mixed EDM samples*

7.1. Introduction

Surface characterization of machined samples indicates the micro level to atomic level changes that happened during the machining. In the present work, scanning electron microscopy (SEM) images are analyzed for titanium mixed EDM to study the surface morphology and EDX (Energy dispersive X-ray analysis) have been performed for analysis of inclusion of foreign particles. Again, for graphite mixed EDM, atomic force microscopy (AFM), SEM and X-ray diffraction graphs have been presented to analyze the 3D surface profile, surface morphology and transformation of phase during the machining.

7.2. Characterization of Inconel 718 and Titanium grade 2 surface machined with titanium mixed EDM

In this study, the SEM and EDX analysis of Inconel 718 and Titanium Grade 2 surfaces are analyzed to study the morphology of the surface and the amount of copper inclusion during the machining.

7.2.1. Study of surface morphology of Inconel 718 using scanning electron microscopy

The surface morphology analysis has been investigated by scanning electrode microscope. Fig. 7.1 (a) and Fig. 7.1 (b) represent SEM micrography of the Inconel 718 surface machined when titanium concentration is 2 g/l at 500× and 2000× magnification respectively. Fig. 7.2 (a) and Fig. 7.2 (b) represent the SEM micrography of the Inconel 718 surface machined when titanium concentration is 5 g/l at 500× and 2000× magnification respectively. Finally, Fig. 7.3 (a) with Fig. 7.3 (b) represent SEM micrography of Inconel 718 surface machined when titanium concentration is 8 g/l at 500× and 2000× magnification respectively. In 500× magnification, the deposited recast layers and formation of microcracks on the machined surface are clearly visible. The molten material of Inconel 718 removed during the machining is normally flushed away by the circulation of fluid. However, molten material has been deposited and formed as the redeposited layer over the surface. Hence, the top surface of the redeposited layer experiences an abrupt change in temperature during the spark time and the spark off time which makes the surface extremely hard. In these figures, it is found that with the increase of powder concentration, the surface roughness get reduced and the recast layer depositions become less and fine which can be directly correlated with the surface roughness pattern. The formation of microcracks takes place on the hard recast layer. During the machining, a cyclic thermal load is generated on the surface due to the change in temperatures. As a result, thermal stress is

developed and cyclic thermal expansion and contraction are generated on the surface of the stressed zone. The formation of microcracks has taken place due to thermal cyclic thermal expansion and contraction.

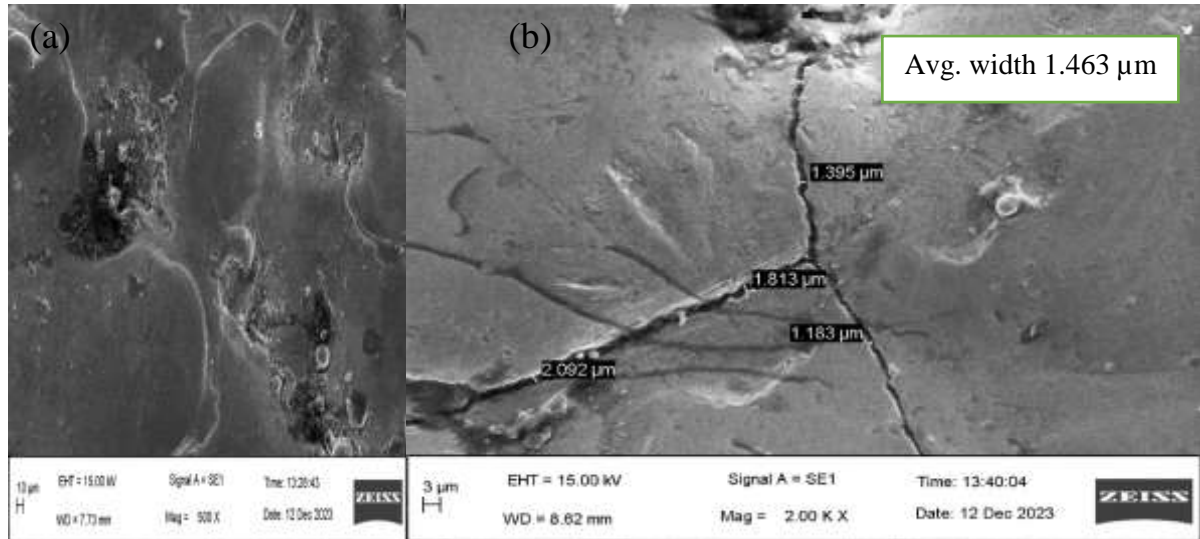


Fig. 7.1. SEM micrograph of Inconel 718 surface machined by titanium mixed EDM with powder concentration 2 g/l at the magnification of (a) 500× (b) 2000×.

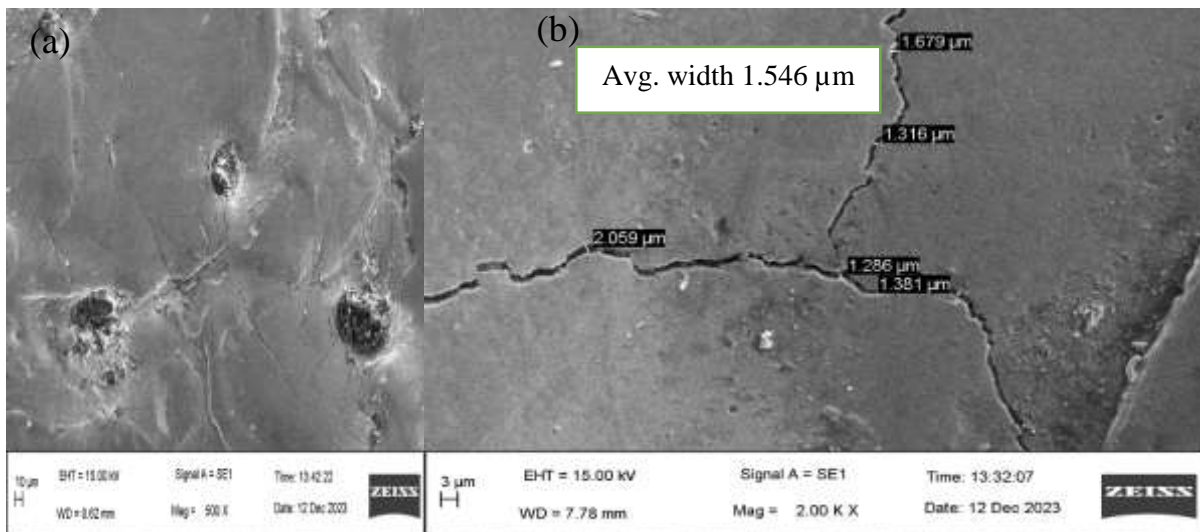


Fig. 7.2. SEM micrograph of Inconel 718 surface machined by titanium mixed EDM with powder concentration 5 g/l at the magnification of (a) 500× (b) 2000×.

In 2000× magnification, the width of the cracks has been measured using scale engraved by SEM machine itself. The average crack width for concentration of powder at 2 g/l, 5 g/l and 8 g/l are 1.463 μm, 1.546 μm and 2.497 μm respectively.

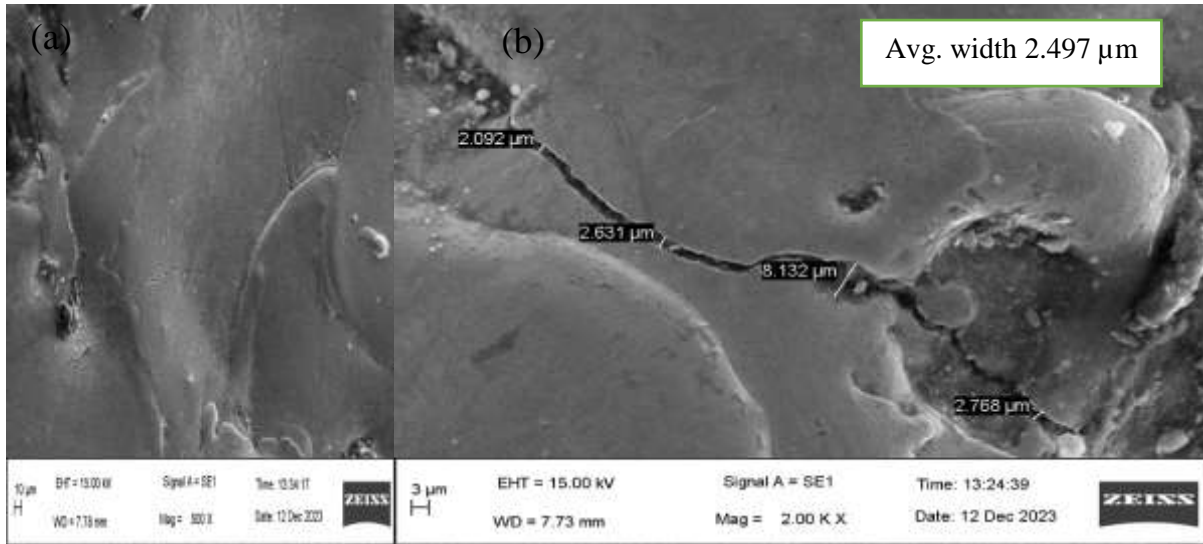


Fig. 7.3. SEM micrography of Inconel 718 surface machined by titanium mixed EDM with powder concentration 8 g/l at the magnification of (a) 500× (b) 2000×.

It is evident that the average width of the cracks increases when powder concentration increases. When the powder concentration increases, it induces extra thermal energy compared to the lower concentration of the powder. Due to which, the temperature of the machined surface increases and the amount of thermal contraction thus increases. Along with that, the localized sparks are generated at every point of the surface which enhances the number of localized contraction region and increases the crack width by contracting the crack edges from both the sides.

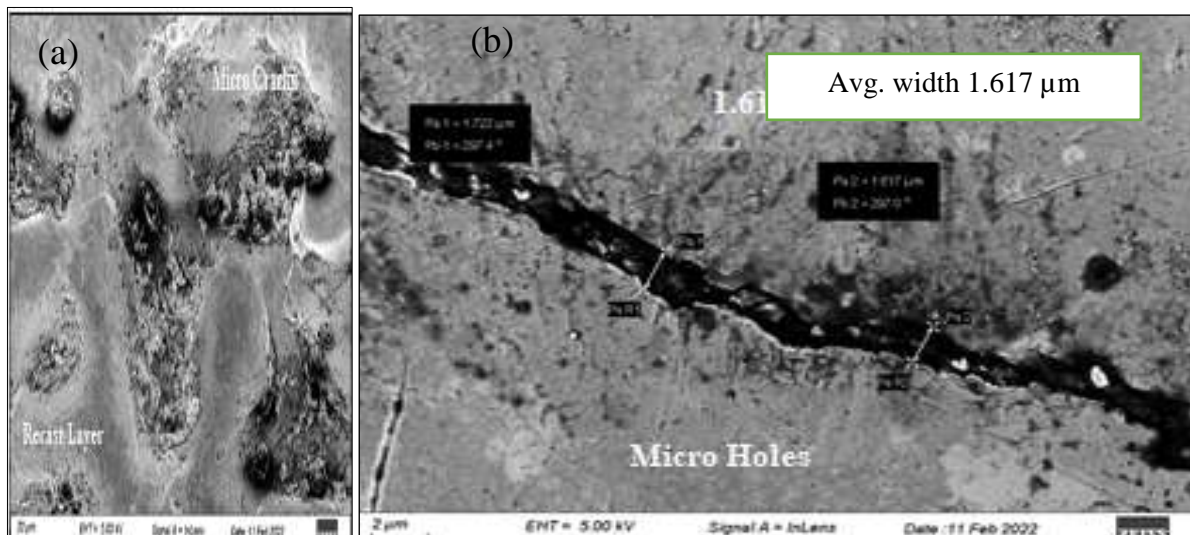
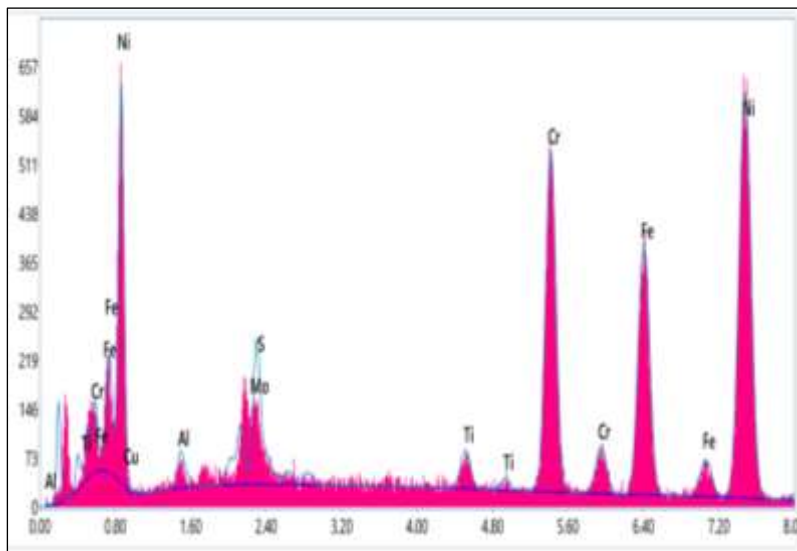


Fig. 7.4. SEM micrography of optimized Inconel 718 surface machined by titanium mixed EDM at the magnification of (a) 500× (b) 2000×.

In Fig. 7.4 (a) – (b), the SEM image of optimized surface of Inconel 718 has been represented. Fig. 7.4 (a) shows the recast layer and microcrack layers at low magnification. It has been observed that the distribution of the recast layer is proper and optimized compared to the SEM images of other concentrations of the powder. Fig. 7.4 (b) shows the average width of the microcracks of the optimized surface. The average width is found to be 1.617 μm , and it lies between the average width found for 5 g/l and 8 g/l.

7.2.2. Elemental analysis of Inconel 718 using EDX

The optimized surface has been investigated by elemental analysis with energy dispersive X-Ray analysis denoted as EDX (model name: Element, Maker's name: AMETEK) to find out elemental concentration by weight and atomic percentage. In Fig. 7.5, the peaks corresponding to the particles have been drawn which are present on the Inconel 718 surface machined by titanium mixed EDM with 8 g/l of concentration. Now, the weight and atomic percentage of each element have been shown in the table situated beside the figure. It is observed from the analysis that a small amount of copper and an increase of titanium have appeared on the surface. The presence of a very small amount of copper with 1.2% by weight indicates the material eroded from the electrode has been migrated towards the workpiece and included on the surface.



Element	Wt. %	Atomic %
Ni	49.8	48.6
Cr	19.4	21.4
Fe	20.1	20.6
Ti	2.7	2.9
Cu	1.2	1.1
Mo	2.5	4.5

Fig. 7.5. EDX analysis of Inconel 718 surface machined by titanium mixed EDM with powder concentration 8 g/l.

During the electric discharge, the work surface becomes extremely hot, which is why the melted material has been spread over the surface. The eroded electrode and powder particles

adhere to the surface at that high temperature. Further, that layer gets solidified along with the included particles during the cooling time.

7.2.3. Study of surface morphology of Titanium grade 2 using scanning electron microscopy

Further, the surface morphologies of Titanium Grade 2 sample have also been studied which are machined by same titanium powder with similar variation of concentrations. Fig. 7.6 (a) with Fig. 7.6 (b) represent SEM micrograph of Titanium Grade 2 surface machined when titanium concentration is 2 g/l at 500 \times and 2000 \times magnification respectively. Fig. 7.7 (a) with Fig. 7.7 (b) represent SEM micrograph of Titanium Grade 2 surface machined when titanium concentration is 5 g/l at 500 \times and 2000 \times magnification respectively. Finally, Fig. 7.8 (a) with Fig. 7.8 (b) represent SEM micrograph of Titanium Grade 2 surface machined when titanium concentration is 8 g/l at 500 \times and 2000 \times magnification respectively. The variations of the coarseness of redeposited layer deposited on the surface can be compared by Fig. 7.6 (a), Fig. 7.7 (a) with Fig. 7.8 (a). With increasing powder concentration, coarseness of surface decreases and the density of redeposited layer reduces. This phenomenon can directly be correlated with the decrease of surface roughness with increase of powder concentration. The primary reason for this phenomenon is the uniformity and enhanced density of the electrical spark applied on the surface with the increase of concentration. The uniform and dense spark removes the material from every points of the surface which reduces the chance of abrupt deposition of the redeposited layer. Hence the surface becomes uniform and less coarse.

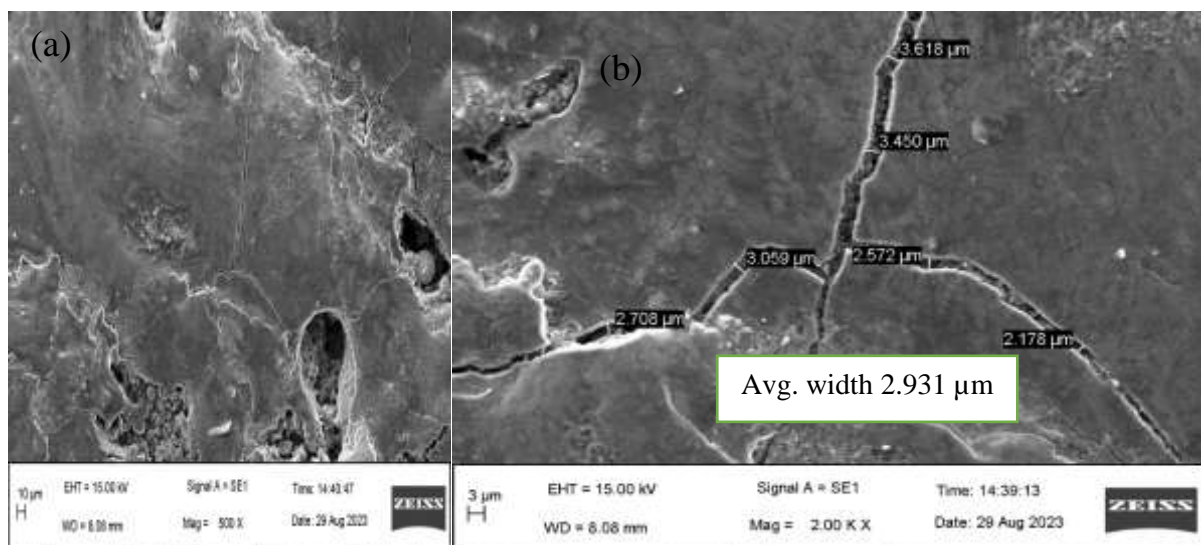


Fig. 7.6. SEM micrograph of Titanium Grade 2 surface machined by titanium mixed EDM with powder concentration 2 g/l at the magnification of (a) 500 \times (b) 2000 \times .

In 2000 \times magnification of SEM micrographies, the width of the cracks have been measured using SEM scale. It is evident that the average width of the cracks have been increased when powder concentration increases.

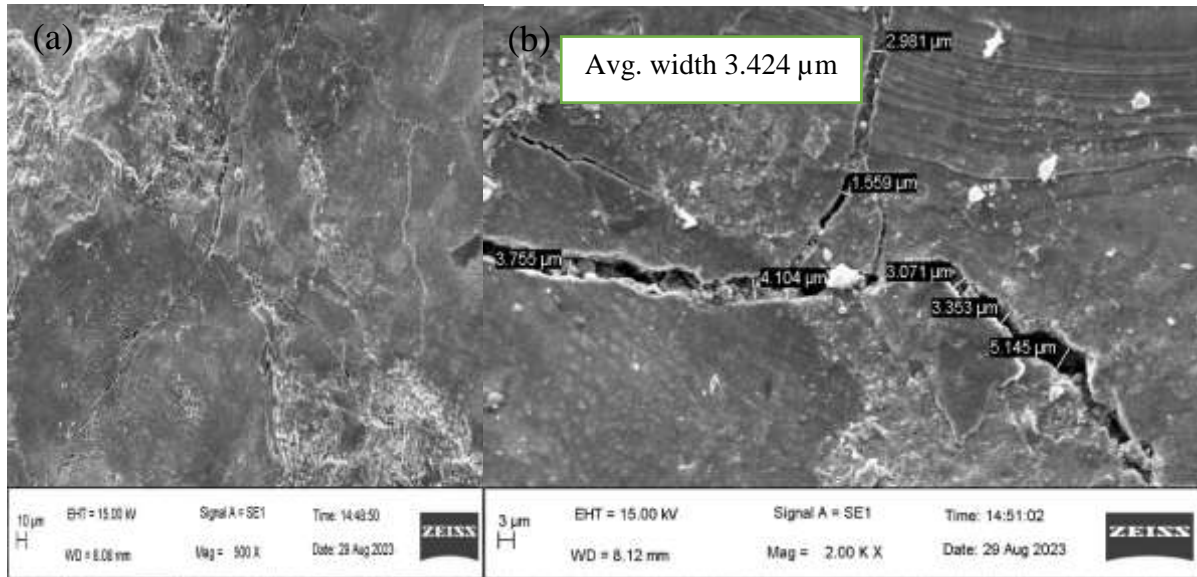


Fig. 7.7. SEM micrography of Titanium Grade 2 surface machined by titanium mixed EDM with powder concentration 5 g/l at the magnification of (a) 500 \times (b) 2000 \times .

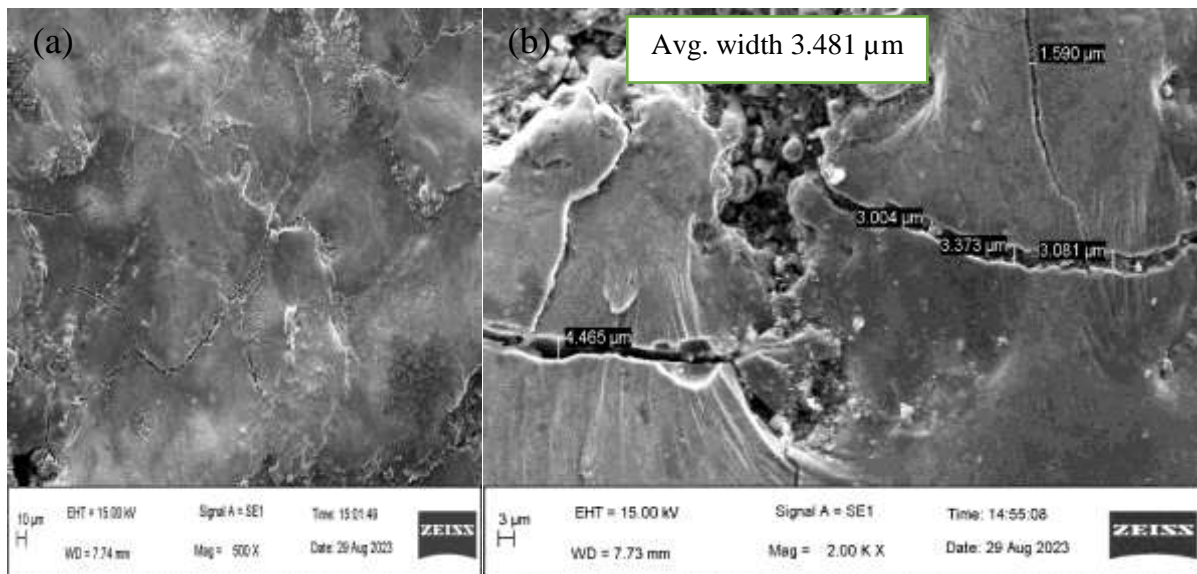


Fig. 7.8. SEM micrography of Titanium Grade 2 surface machined by titanium mixed EDM with powder concentration 8 g/l at the magnification of (a) 500 \times (b) 2000 \times .

The average crack width for 2 g/l, 5 g/l and 8 g/l of concentration of particles are 2.921 μm , 3.424 μm and 3.481 μm respectively. Like Inconel 718 surfaces, the effect of titanium powder is almost same in Titanium grade 2 surface. The increase of powder concentration induces the extra energy which enhances the surface contraction force during the thermal heating and

cooling cycle. Along with that, the extreme contraction from both the edges of the crack due to local sparks increases the crack width generated during the machining.

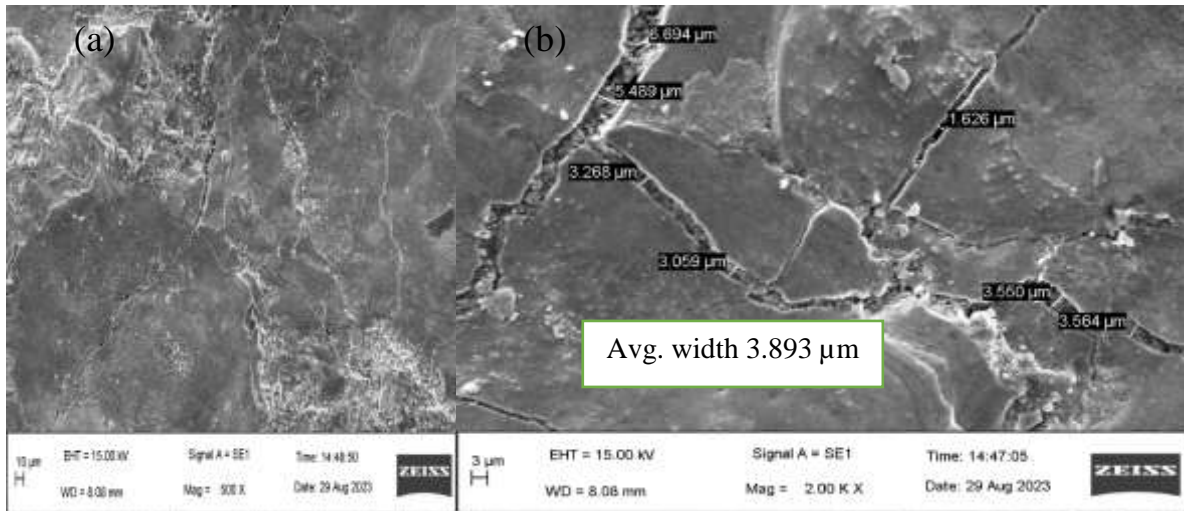


Fig. 7.9. SEM micrography of optimized Titanium Grade 2 surface machined by titanium mixed EDM at the magnification of (a) 500× (b) 2000×.

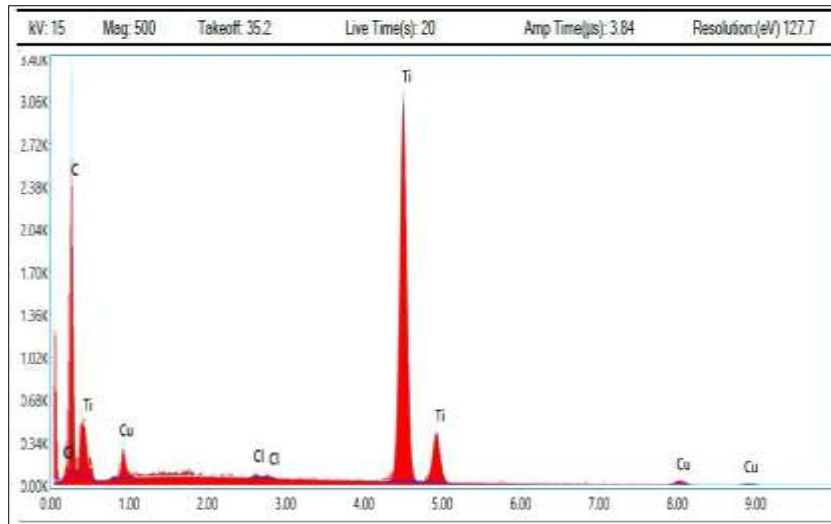
In Fig. 7.9 (a) – (b), the SEM image of optimized surface of Titanium grade 2 has been represented. Fig. 7.9 (a) shows the recast layer at low magnification. It has been observed that the distribution of recast layer is proper and optimized compared to the SEM images of other concentration of the titanium. Fig. 7.9 (b) shows the average width of the microcracks of the optimized surface. The average width is found 3.893 μm which has been found maximum among all the three samples machined by the different powder concentration.

However, interestingly, the average width of the cracks for Titanium Grade 2 machined surface is much lower than the average width of the titanium machined surface. This has happened because the difference of hardness of both the surfaces. Inconel 718 has less hardness compared to the Titanium grade 2 surface. The hard surfaces when passes through the thermal cycle, the contraction forces applied on the surface becomes high which increases the crack width. The rapid contraction of the harder surface accelerates the rate of rupture of the surface which enhances the average crack width compared to the soft Inconel 718 surface.

7.2.4. Elemental analysis of Titanium grade 2 using EDX

Fig. 7.10 represents the peaks corresponding to the particles situated over Titanium grade 2 surface during titanium mixed EDM for 8 g/l of concentration. It is observed from the analysis that a little amount of copper and an increase of titanium has appeared on the surface. The

presence of a very small amount of copper with 4.0 % by weight indicates the material eroded from the electrode has been migrated towards the workpiece and included to the surface.



Element	Wt. %	Atomic %
Ti	69.3	38.9
C	26.4	59.2
Cu	4	1.7

Fig. 7.10. EDX analysis of Titanium Grade 2 surface machined by titanium mixed EDM with powder concentration 8 g/l.

During the electric discharge, the work surface becomes extremely hot, the surface experience a deposition of melted material. The eroded electrode and powder particles adhere to the surface at that high temperature. Further, that layer gets solidified along with the included particles during the cooling time.

7.3. Characterization of Inconel 625 and Titanium grade 2 surface machined with graphite mixed EDM

The graphite mixed EDM of Inconel 625 and Titanium grade 2 surfaces have been analyzed by the study of atomic force microscopy (AFM) analysis, scanning electrode microscopy (SEM) and X-Ray diffraction analysis (XRD). The three dimensional micro surface roughness, recast layer deposition with crack thickness measurement and identification of atomic phase with transformation have been analyzed by AFM, SEM and XRD study respectively.

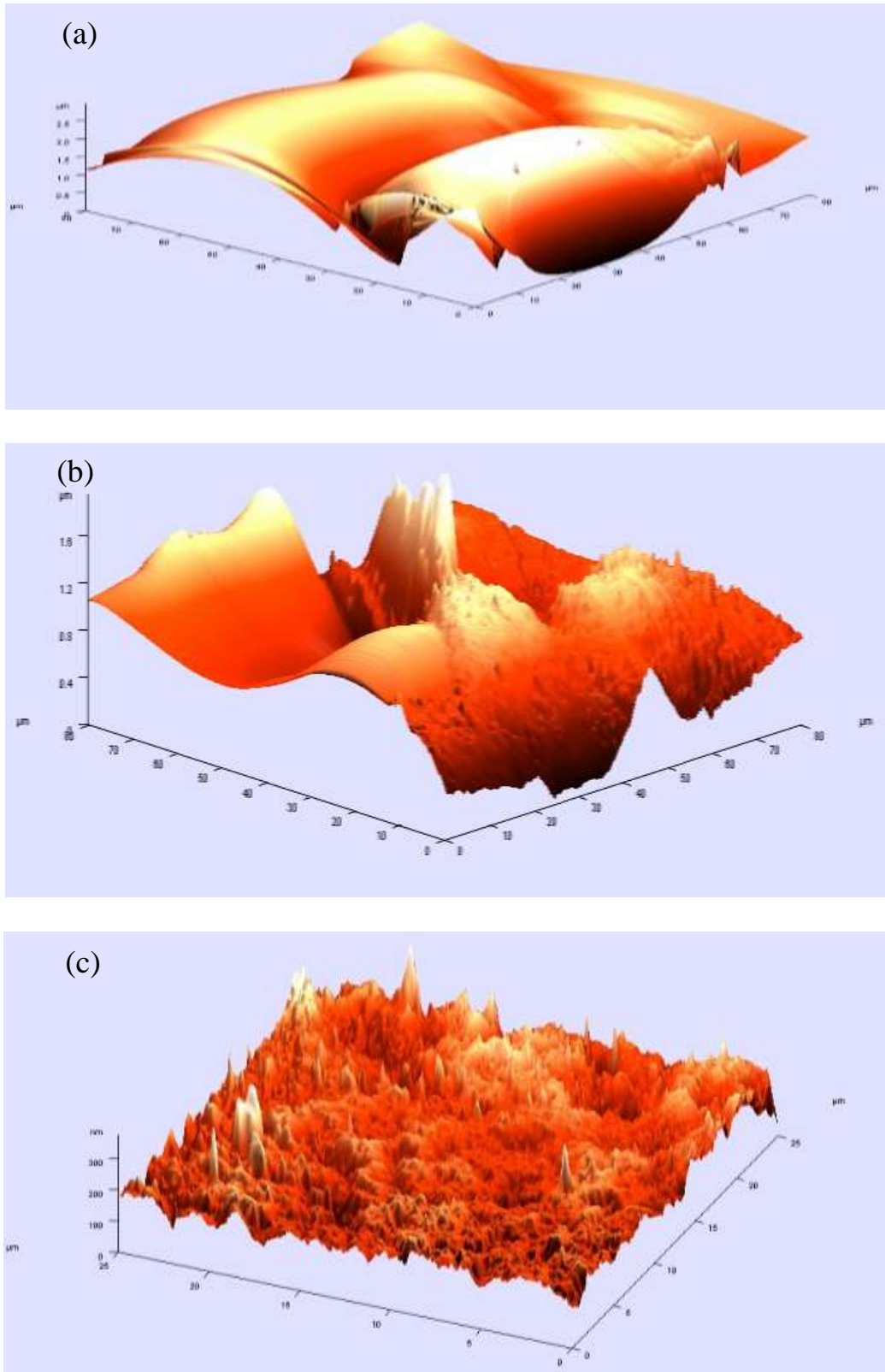


Fig. 7.11. AFM analysis of Inconel 625 sample machined by graphite mixed EDM at current of (a) 4 A (b) 8 A and (c) 12 A

7.3.1. AFM study of Inconel 625 surface

Atomic force microscopy (AFM) is used to capture the three dimensional surface morphology of the machined surface using interatomic van der Waal force. In this measurement, a very sensitive cantilever beam attached with a silicon tip of 10 nm is moved on the surface by making direct contact. The precise deflection of the beam is measured and sensed by an electronic sensor and the three dimensional image of the surface is generated. From the AFM images, the vertical projections are measured in nanoscale and the surface roughness can be calculated from the data. In the current study, the machine surfaces of Inconel 625 were analyzed by the scanning of a small area under AFM probe and the surface roughness has been calculated from the morphological data after the machining of graphite mixed EDM. A comparative study has been made to analyze the changes in surface roughness with the increase of current. Therefore, three samples machined with the current level of 4 A, 8 A and 12 A have been studied under the atomic force microscopy. Fig. 7.11 (a)-(c) represents the 3D roughness of the samples. The roughness calculated from measured data for the sample machined by current levels 4 A, 8 A and 12 A are 4.96 μm , 8.78 μm and 10.94 μm respectively. The deviations of the SR value measured by AFM to that from surface profilometer are 7.30%, 3.64% and 6.21%. The deviation for all the measurements are around 10%. Nevertheless the result indicates the measurements taken by AFM and surface profilometer are accepted for macro range.

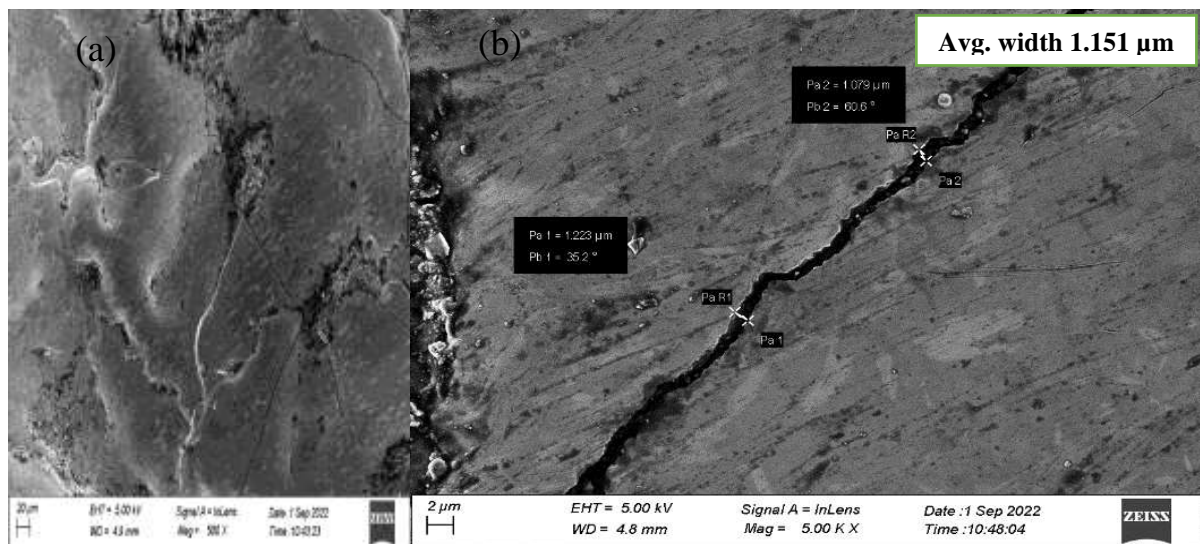


Fig. 7.12. SEM micrography of Inconel 625 surface machined by graphite mixed EDM with powder concentration 2 g/l at the magnification of (a) 500 \times (b) 5000 \times .

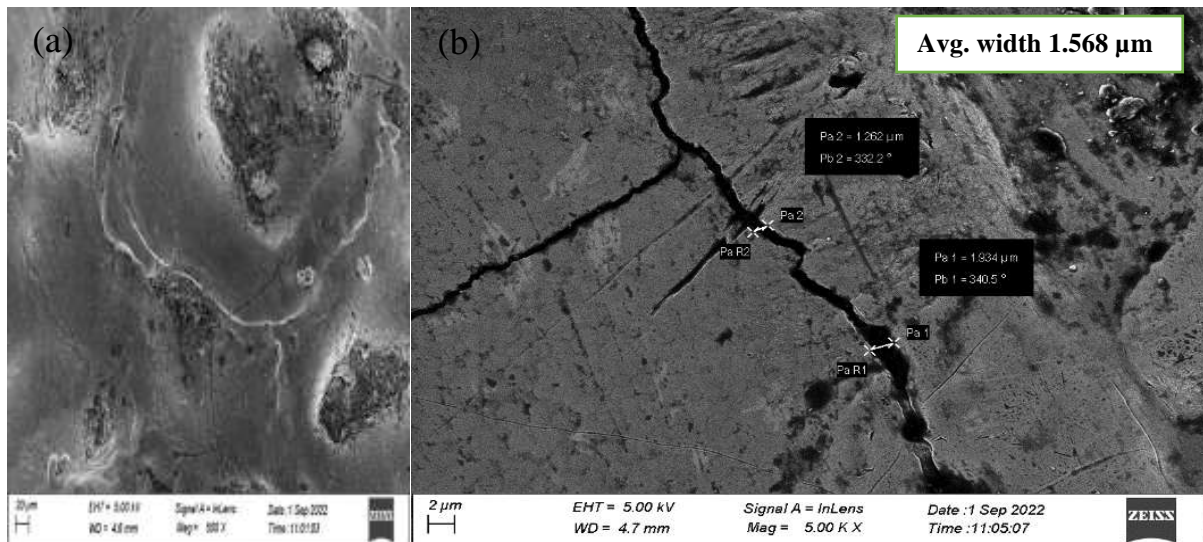


Fig. 7.13. SEM micrography of Inconel 625 surface machined by graphite mixed EDM with powder concentration 5 g/l at the magnification of (a) 500× (b) 5000×.

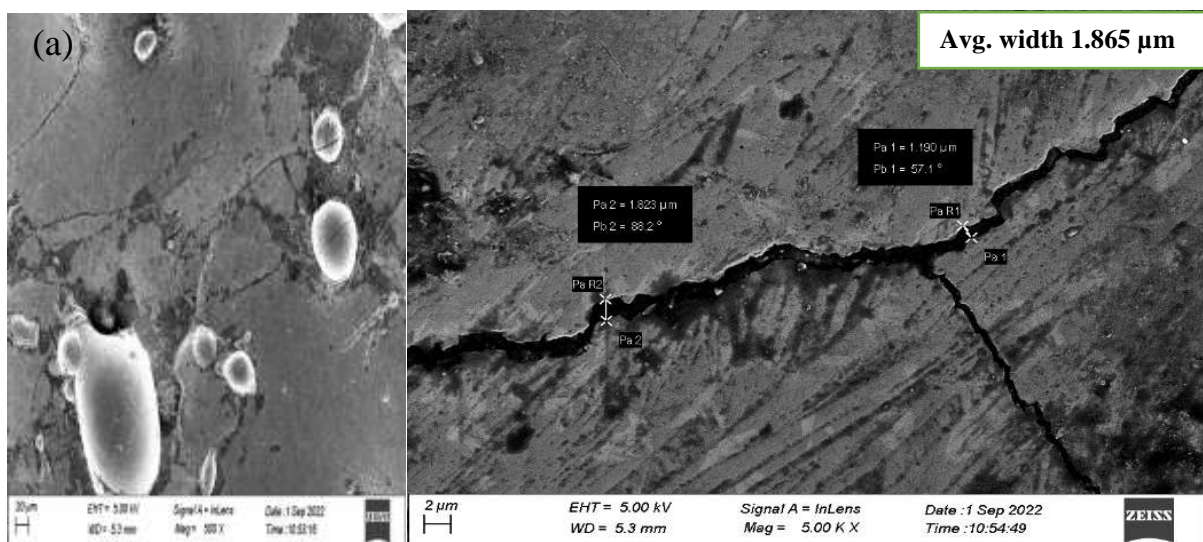


Fig. 7.14. SEM micrography of Inconel 625 surface machined by graphite mixed EDM with powder concentration 8 g/l at the magnification of (a) 500× (b) 5000×.

7.3.2. Study of surface morphology of Inconel 625 using scanning electron microscopy

In this section, study of the machined surface morphology has been discussed in qualitative and quantitative approach. Field effect scanning electrode microscope and scanning electrode microscope were used to capture the micrographs of the surface. The overall surface integrity and depositions were analyzed in 500× magnification and the detail crack width measurement was performed in 5000× magnification.

Fig. 7.12 (a), Fig. 7.13 (a) with Fig. 7.14 (a) represent small magnification surface micrographs for the Inconel 625 samples machined by a graphite concentration of 2 g/l, 5 g/l and 8 g/l respectively. As per qualitative investigations are concerned, it is clearly observed that the surface consists of irregular and complex shaped recast layers, deposition of powder particles in the form of globules and microcracks. After melting, an adhesive force acts between the detached molten material and the hot and newly generated surface. This adhesive force cannot be absolutely overtaken by the flushing force of dielectric flow and as a result the recast layers deposit on the surface itself. As the powder concentration increases, high energy discharges are applied by the electrode and powder particles. It helps to deposit the material at a faster rate than the discharge made by the low value of concentration. Hence the recast layer deposition decreases with the increase of powder concentration.

Fig. 7.12 (b), Fig. 7.13 (b) with Fig. 7.14 (b) represent the magnified view of the surface, focusing on the microcracks on it. The cracks are generated due to the thermal stress formed when sudden contraction takes place during the cooling period. The surface experiences a thermal stress due to the hard redeposited layers present over it. Due to this, the cracks are normally found at the periphery of the recast layer.

The quantitative analysis was done on each surface by measuring the crack width at two arbitrary points of the crack and showing the average of the measurements on the figures. The average crack width is found to be 1.151 μm , 1.568 μm and 1.865 μm for graphite concentrations of 2 g/l, 5 g/l and 8 g/l respectively. As discussed earlier, high thermal energy is generated when current increases and the thermal stress developed on the surface increases. This causes severe contraction on the surface. As a result, with the amplification of current, the width of the microcracks becomes wider. Controlling of current at an optimum level and increasing the graphite concentration can reduce the width of the microcracks.

7.3.3 Analysis of XRD pattern of Inconel 625 surface

Fig. 7. 15 represents the X-ray diffraction (XRD) study of different crystallographic planes present in the Inconel 625 machined surface. The super alloy consists mainly of two phases. Such as γ austenitic phase consists of the solid solution of iron and chromium in a nickel matrix (Ni-Fe-Cr) and γ'' intermetallic precipitating phase consists Ni_3Nb phase. In the Fig. 7. 15 (a), different XRD patterns have been plotted against 2θ angle ranging from 0° to 80° for the samples machined by three levels of current. The peaks correspond to the lattice plane of (111),

(200) and (220) are identified for all the three samples and it consists both the matrix and intermetallic phases of the alloys.

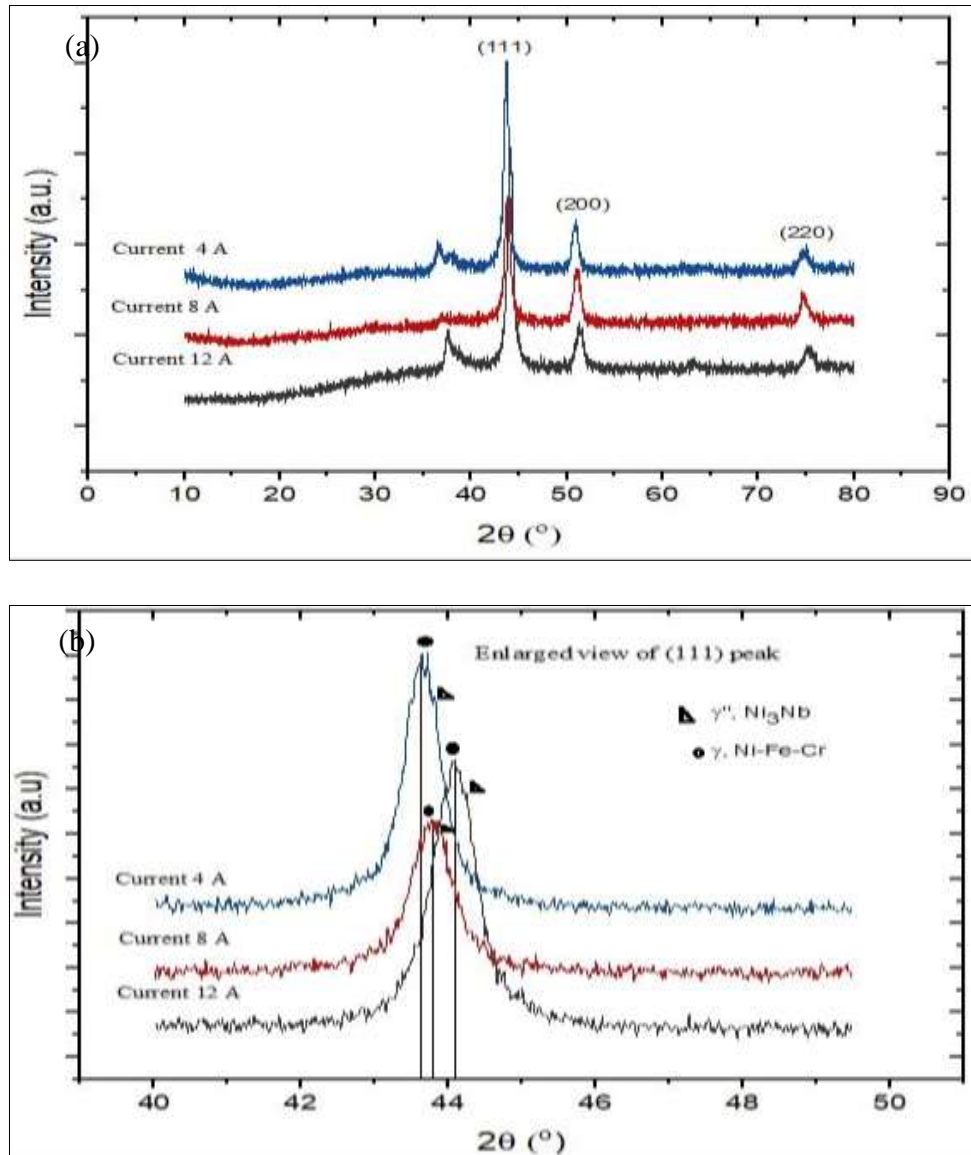


Fig. 7.15. XRD patterns of Inconel 625 surface machined by graphite mixed EDM at the current of 4 A, 8 A, 12 A with (a) complete view of all the planes (b) enlarged view of (111) plane.

From the Fig. 7.15 (a), it is observed that the peaks are placed at their proper position which determines there is no severe deformation takes place in the crystallographic planes during the machining. But a little right shift is observed in all the peaks at 44° angles which indicates a little deformation occurs in crystal structures. The right shift of the peak implies the angle of diffraction for the particular lattice plane has been increased. According to Bragg's law,

increase of angle reduces distance of the lattice planes. This can be explained as the formation of lattice distortion caused by increased internal

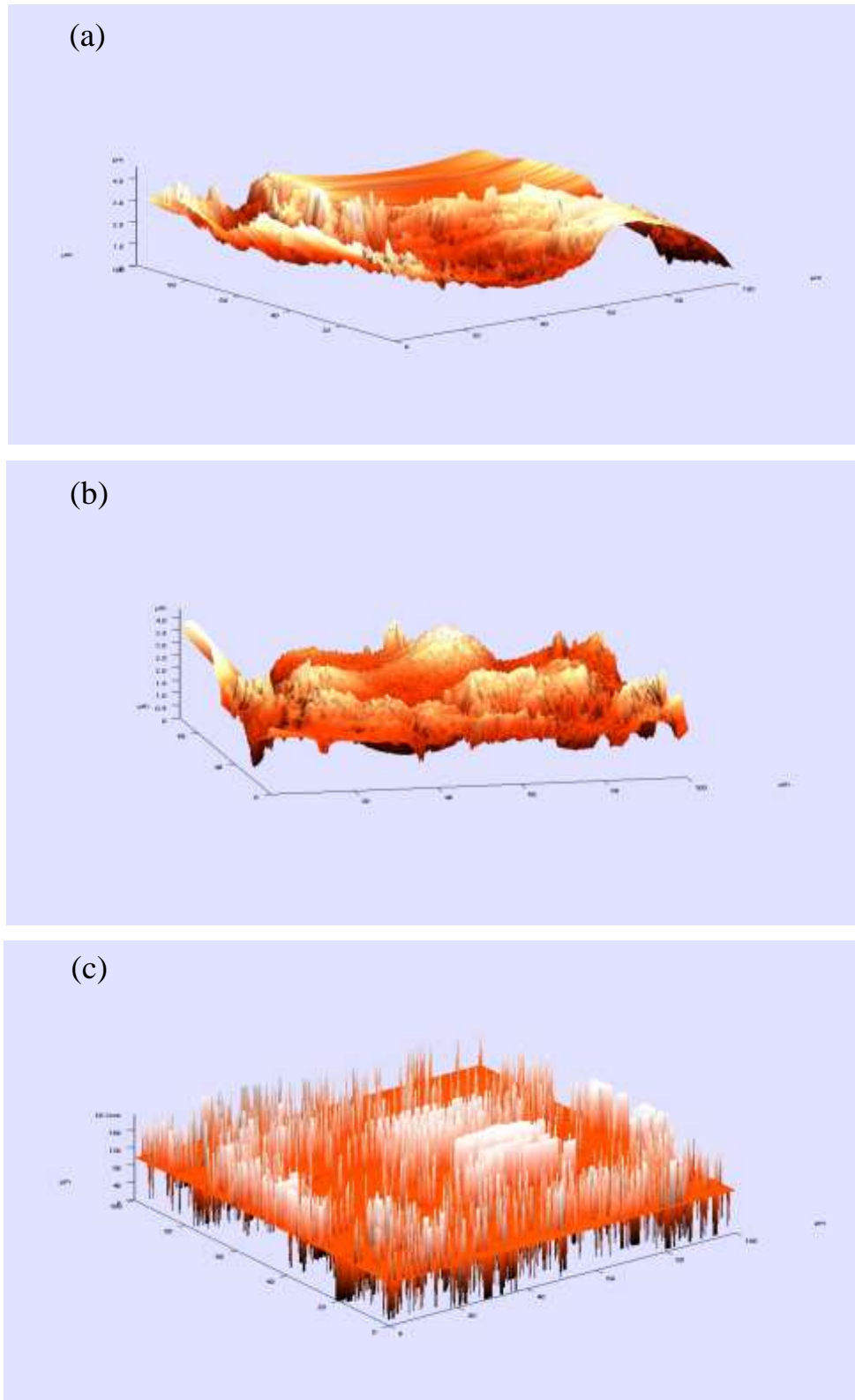


Fig. 7.16. AFM analysis of Titanium Grade 2 sample machined by graphite mixed EDM at current of (a) 4 A (b) 8 A and (c) 12 A.

energy of the crystal structure. During the machining, when current amplifies, a Strong electric field appeared in the spark. This increases the temperature of machined surface which is responsible for the vibration of the atoms at higher frequency and a longer period of time. During this time, atoms having a large atomic radius like niobium, molybdenum get dissociated from the crystal structure and small atoms like chromium and iron occupy the void portion. In this way, the lattice distance reduces due to the shifting of atoms and a slight transformation from γ'' or Ni_3Nb double austenitic phase to γ or Ni-Fe-Cr single austenite phase has happened when the temperature increases during the machining. According to Bragg's law, the decrement of lattice distance increases the fraction value equal to the $\sin \theta$. Hence, the θ value increases and causes the right shift of XRD peaks.

7.3.4. AFM study of Titanium Grade 2 surface

In the current study, the Titanium Grade 2 machine surface was analyzed by scanning of a small area under AFM probe and the surface roughness was calculated from the morphological data after the machining with graphite mixed EDM. A comparative study has been made to analyze the changes in surface roughness with the increase of current. Therefore, three samples machined with the current level of 4 A, 8 A and 12 A have been analyzed under the atomic force microscopy. Fig. 7.16 (a)-(c) represents the 3D surface generated on the samples. The surface roughness calculated from measured data for the sample machined by current levels 4 A, 8 A and 12 A are $6.48 \mu\text{m}$, $9.14 \mu\text{m}$ and $12.23 \mu\text{m}$, respectively. The deviations of the SR value measured by AFM from that of surface profilometer are 15.30%, 9.64% and 10.21%. The deviation for all the measurements are around or less than 15%. However, the result indicates the measurements taken by AFM and surface profilometer are accepted for macro range. The result of AFM study supports the readings taken by surface profilometer. The depth of the crater increases when enhanced current provides strong energy on the surface. Along with that, local sparks produce more number of craters within a particular range of area. The conjugate effect of these two phenomenon have been reflected in the study of AFM. Though the deviation of the result from surface profilometer is little higher but the variation of the surface roughness have been observed similar to profilometer.

7.3.5. Study of surface morphology of Titanium Grade 2 using scanning electron microscopy

In this study, the overall surface integrity and depositions were analyzed in $500\times$ magnification and the detail crack width measurement was performed in $5000\times$ magnification.

The Fig. 7.17 (a), Fig. 7.18 (a) with Fig. 7.19 (a) represent the small magnification surface micrographs for the Titanium Grade 2 samples machined by a graphite concentration of 2 g/l, 5 g/l and 8 g/l respectively. As per qualitative investigations are concerned, it is clearly observed the surface consists irregular and complex shaped recast layers, deposition of powder particles in the form of globules and microcracks. After melting, an adhesive force acts between the detached molten material and the hot and newly generated surface. This adhesive force cannot be absolutely overtaken by the flushing force of dielectric flow and as a result the recast layers deposit on the surface itself. As the powder concentration increases, high energy discharges are applied by electrode and powder particles. It helps to deposit the material at faster rate than the discharge made by low value of concentration. However, more concentration of particles reduce the redeposited layer dispersion.

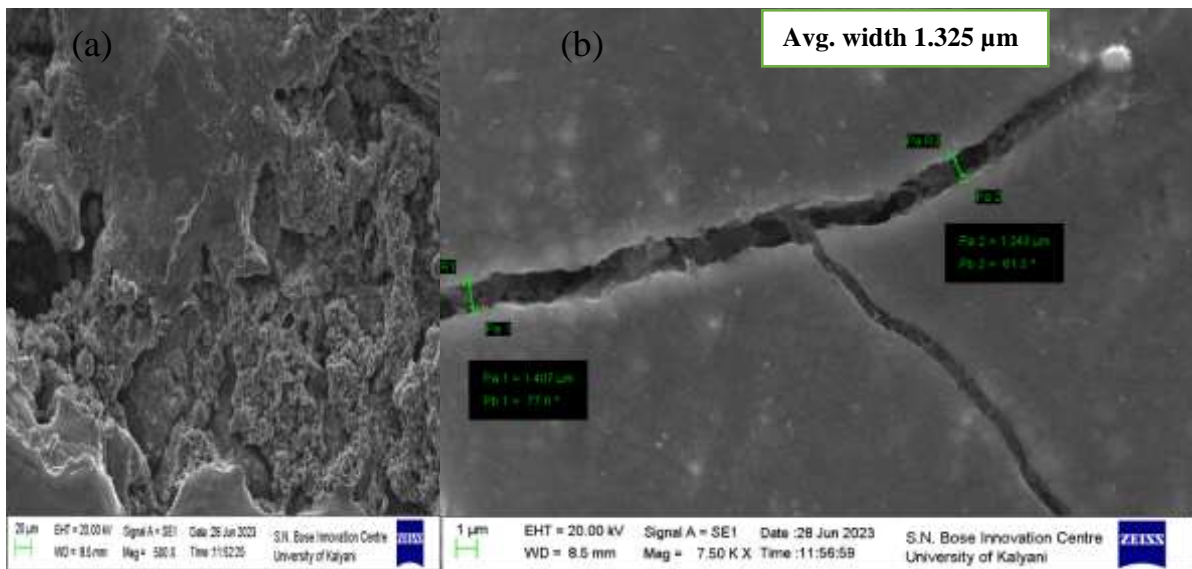


Fig. 7.17. SEM micrography of Titanium Grade 2 surface machined by graphite mixed EDM with powder concentration 2 g/l at the magnification of (a) 500× (b) 7500×.

The Fig. 7.17 (b), Fig. 7.18 (b) with Fig. 7.19 (b) represent the magnified view of the surface focusing the microcracks on it. The cracks are generated due to the thermal stress formed when sudden contraction takes place during the cooling period. The thermal stresses have been generated due to periodic heating and cooling and with a large gap between the temperatures of these two phenomenon. Due to which, the cracks are normally found at the periphery of the recast layer. The quantitative analysis was done on each surface by measuring the crack width at two arbitrary points of the crack and shown the average of the measurement on the figures. The average crack width are found 1.325 μm, 2.679 μm and 3.468 μm for graphite concentration of 2 g/l, 5 g/l and 8 g/l respectively. As discussed earlier, high thermal energy

generates when current increases and the thermal stress developed on the surface increases. This causes severe contraction on the surface. The high current flowing during the machining enhance the width of the microcracks. Controlling current at optimum level and increasing the graphite concentration can reduce the width of the microcracks.

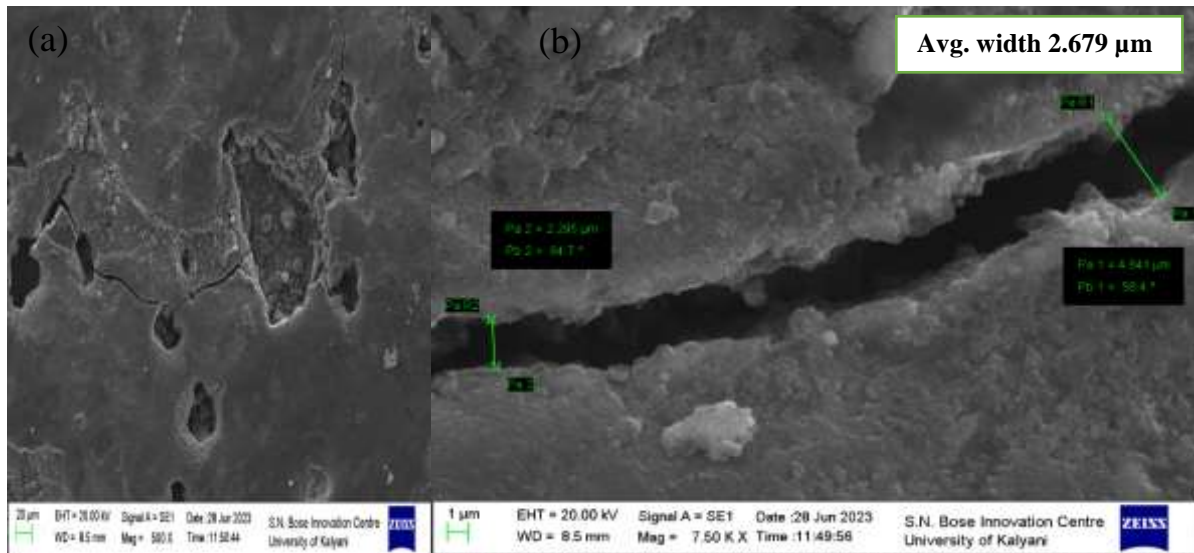


Fig. 7.18. SEM micrography of Titanium Grade 2 surface machined by graphite mixed EDM with powder concentration 5 g/l at the magnification of (a) 500× (b) 7500×.

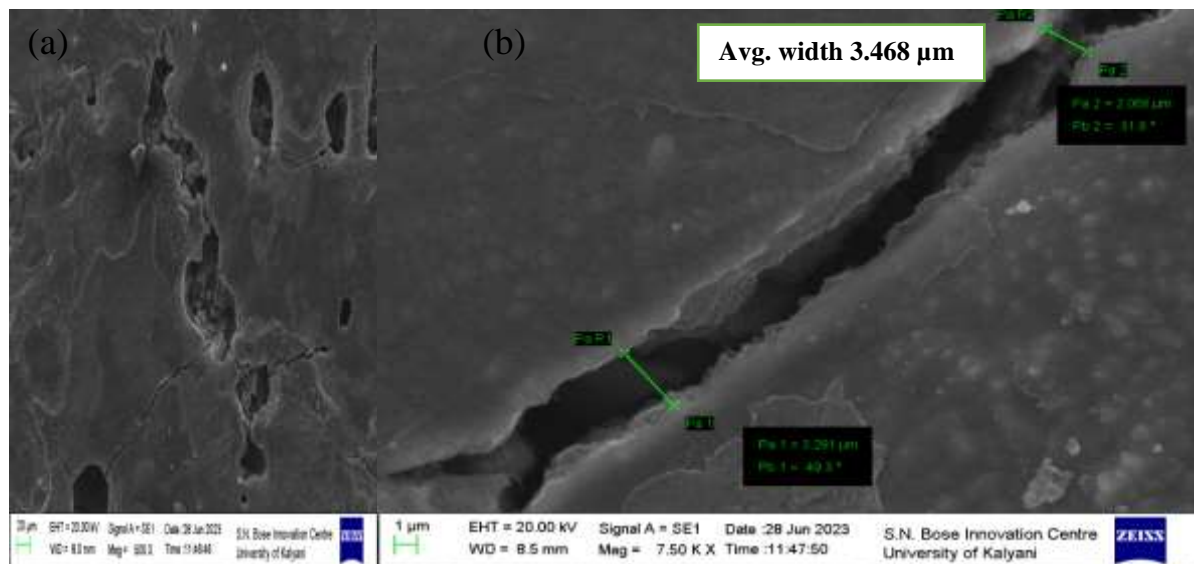


Fig. 7.19. SEM micrography of Titanium Grade 2 surface machined by graphite mixed EDM with powder concentration 8 g/l at the magnification of (a) 500× (b) 7500×.

However, it can be stated that the average width of the cracks for Inconel 625 machined surface is much lower than the average width of the titanium machined surface. This has happened because the hardness of the Titanium grade 2 is much higher than Inconel 625 due to which

the effect of thermal cycle impacted more on the Titanium surface and increases the average width of the crack compared to Inconel 625.

7.3.6 Analysis of XRD pattern of Titanium Grade 2 surface

The X-Ray diffraction patterns of Titanium Grade 2 machined surface machined under different current levels have been presented in Fig. 7.20. The analysis has been performed on three surface duly machined by graphite mixed EDM under three levels of current. In this graph, the data were plotted for 10^0 to 100^0 diffraction angles and all three data sets to study the changes of any shift in the peak. Firstly, it is visible that there exist four major peaks present in the graph. The corresponding planes for each peak are (100), (002), (101) and (102). Compared to several literature, it can be stated that the peak corresponding to plane (100) has the phase of TiO and TiC whereas the peak (002) refers only TiC. The peak (101) and (100) also refers to TiC. The presence of TiC on the surface can be explained by the chemical reaction takes place during the high temperature material removal process. Firstly, the direct reaction of graphite particles and molten titanium present in the dielectric fluid during the machining.

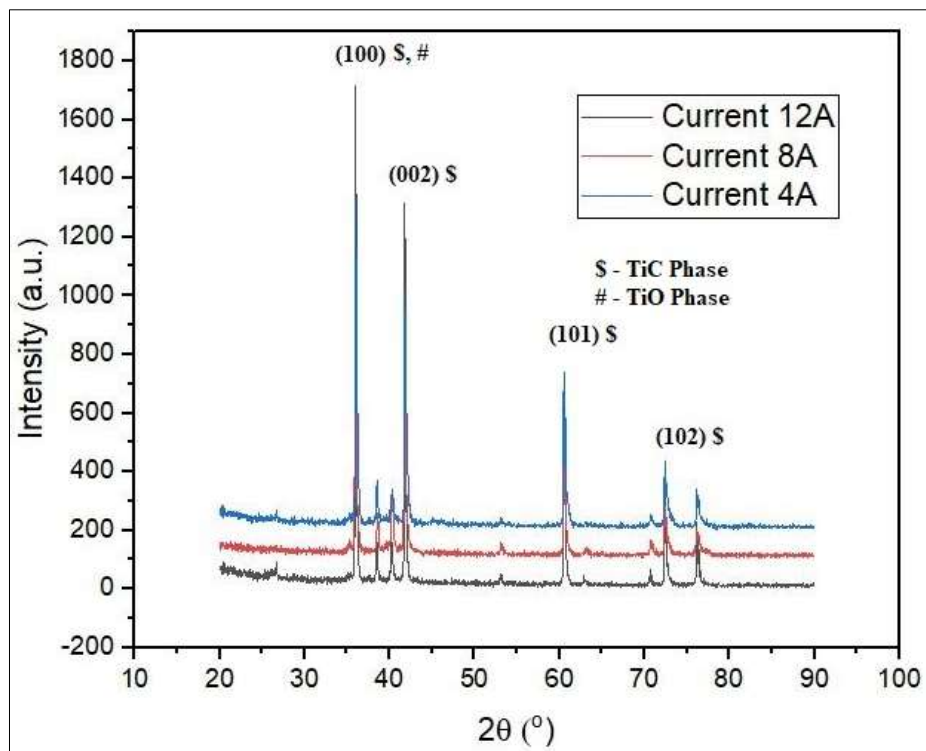


Fig. 7.20. XRD patterns of Titanium Grade 2 surface machined by graphite mixed EDM at the current of 4 A, 8 A, 12 A.

Secondly, the dielectric fluid itself is a carbon reach compound which gets dissociated at the high temperature and reacted with molten titanium. These causes extremely hard and brittle

structure of TiC shown in black in the figure. The dissolved oxygen present in the dielectric fluid reacted with titanium to form TiO phase. Along with that, TiO can be present as the impurity in the sample previously. The TiO phase formed due to the reaction with the rutile titanium phase present in the sample. The white layer of TiO film is very sticky and extremely hard which even has not been removed during the several machining operations. In SEM images, the white depositions are a TiO layer confirmed by XRD analysis. From Fig. 7.20, it is also evident that the hard TiC peaks are generated in all three samples. From the detailed analysis, it can be observed that there is no significant shift of the peaks for three different levels of current. Hence it can be concluded that there is no significant transformation happened in TiC or TiO phases with the changes of current level. The high energy thermal erosion may be sufficient to remove pure titanium metal but not so sufficient to break the strong interatomic bonding of TiC and TiO. However, unlike Inconel 625, the phase retention of Titanium Grade 2 during the graphite mixed EDM is much more stable because the interatomic structure of Ni_3Nb phase is much weaker than the TiC phase in respect to the portion of energy transferred through the machining. Hence metallurgical stability is quite better in case of Titanium Grade 2 compared to the Inconel 625 during the machining of graphite mixed EDM.

Chapter 8

Conclusion

In the present work, firstly, titanium mixed EDM has been applied to Inconel 718 and Titanium Grade 2 machining. The study has been performed on the material removal rate (MRR) and surface roughness. Secondly, graphite mixed EDM has been performed on Inconel 625 and Titanium Grade 2 materials. In this study, MRR, tool wear rate (TWR) and surface roughness have been analysed after the experiments. The conclusions of the present work are written below.

- The Inconel 718 samples have been successfully machined by varying five parameters. The RSM optimization process has been applied and it is found that the optimized values of surface roughness and MRR are $3.71\text{ }\mu\text{m}$ and $16.623\text{ mm}^3/\text{min}$, respectively. The deviations of the confirmatory test values from the optimized values are 1.89% and 2.18% respectively. Further, applying same optimization process on Titanium grade 2 result, the optimized values of surface roughness and MRR are found as $7.17\text{ }\mu\text{m}$ and $1.493\text{ mm}^3/\text{min}$ respectively. Here, the deviations of the confirmatory test results for surface roughness and MRR are 2.45% and 2.01% respectively. The fuzzy predicted model for Inconel 718 depicts that the errors between predicted and actual results are 3.36% and 4.73% for the surface roughness and MRR model respectively.
- From the above analysis, it can be found that the predicted optimized values of MRR and surface roughness are very much closer to the experimental value. The small deviations in the optimized result indicate that this model of optimization can be easily accepted for industrial application without further experimentation and optimization.
- The ANOVA results of the Inconel 718 machining process state that the common significant parameters for MRR and surface roughness are the powder concentration, current, voltage and pulse time. Also, for Titanium grade 2, the common significant parameters are current and powder concentration for both MRR and surface roughness and gap voltage and pulse on time are the other significant parameters for MRR and surface roughness respectively.
- A comparative analysis has been performed between Inconel 718 results and Titanium grade 2 result where responses of both materials have been compared with respect to common significant input parameters. It has been found that the values of MRR for Inconel 718 machining are much higher than Titanium grade 2 machining and, contradictorily, the values of surface roughness of Inconel 718 are much lower than those of Titanium grade 2.

- The SEM analysis of both Inconel 718 and Titanium Grade 2 surfaces represent that the distributions of recast layer become finer and the average width of the microcracks increases with the increase of powder concentrations. The EDX analysis of both the materials Inconel 718 and Titanium Grade 2 shows that the amounts of copper inclusion on the machined surface are 1.2% and 4% respectively.
- In the second study, machining of Inconel 625 and Titanium grade 2 has been performed completely by graphite mixed EDM with five different set of input parameters. From the RSM optimization processes, the optimized value of MRR, TWR and surface roughness of Inconel 625 machining are found as 26.136 mm³/min, 0.0800 mm³/min and 5.81 μm. The deviations the optimized result from the confirmatory test results are 1.03%, 2.51% and 4.03%, respectively. For the machining of Titanium grade 2, the optimized values of MRR, TWR and surface roughness are 1.409 mm³/min, 0.0922 mm³/min and 4.54 μm, respectively. The deviations of the optimized result from the confirmatory test result are 0.81%, 3.47% and 3.08% respectively. The neural network for the analysis of Inconel 625 has been constructed using 20 hidden layers. It has been found that the R value of overall performance is 0.94509.
- From these results, it can be concluded that the optimized predicted results for both materials are very much closer to the experimental result. However, these results can be well accepted in industry without performing any further experiments.
- The ANOVA results of Inconel 625 processing indicate that the common significant parameters for MRR and TWR are pulse current, powder concentration and mesh size. Similarly, the ANOVA results of Titanium Grade 2 reveal that current, powder concentration and pulse time are the common significant parameters for both the surface roughness and MRR.
- In this study, a comparative analysis has been performed between Inconel 625 result and Titanium grade 2 result machined by graphite mixed EDM. The results conclude that the value of MRR is much higher in the case of Titanium grade 2 machining compared to Inconel 625. However, the values of TWR and surface roughness are found closer to each other for both materials.
- The SEM analysis of Inconel 625 and Titanium grade 2 represents that the distributions of the recast layer become finer and the average width of microcracks increases with the increase of the powder concentration. The AFM studies for both Inconel 625 and Titanium

grade 2 confirm that the difference between surface roughness measured by AFM and profilometer is very small.

- The XRD analysis performed on the Inconel 625 surface confirms that there is a transformation of the secondary austenitic phase of nickel to the primary phase when the current increases from 4 A to 12 A. However, for titanium grade 2 samples, the XRD analysis for three different levels of current indicates that TiO and TiC phases have been generated when titanium reacted with dissolved oxygen and carbon present in the dielectric fluid.

Future scope of the work

Powder mixed electric discharge machining has not been commercialized for many EDM manufacturing industry yet. The mixing of powder is very difficult to separate and it is the prime reason for not being commercialized. Research may be performed to develop the setup by which the powder can easily be separated after the end of its use. Along with that, new arrangements may be done in which the powder mixing becomes homogeneous with the dielectric fluid.

Very few studies have been found where the study of microhardness has been performed after the machining of materials. In future, a detailed study of microhardness during the PMEDM can be performed and the influence of powders on microhardness can be studied.

In future, the effects of mesh size, mesh distribution and other significant parameters can be analysed for the changes in microcracks. The mesh size provides the surface area of the particle which determines the amount of charges induced and accumulated. The width of the microcrack is highly sensitive to thermal energy coming from the electrode. Hence, it will be pertinent research if the effects of mesh size have been studied.

Apart from graphite and titanium particles, the effects of other powder particles like silicon, silver, chromium, nickel and many more can be analysed on different responses.

Except for Inconel 718 and Titanium Grade 2, other nickel-based super alloys and hard materials like Be-Cu alloy, Monel and many more can be used to study the effect of these powders. In the present time, composite materials and their processing are one of the relevant topics of research. The effect of powder mixed EDM can be analysed on composite materials.

The characteristics of the thermal effect of EDM and PMEDM have not been studied extensively. Finite element-based thermal analysis can be performed to study the effects of powder concentration.

References

- [1] A. Y. Joshi, A. Y. Joshi. A systematic review on powder mixed electrical discharge machining. *Heliyon*, Vol. 5, 2019, 1-12.
- [2] R. Choudhary, G. Singh, Effects of process parameters on the performance of electrical discharge machining of AISI M42 High Speed Tool Steel Alloy. *Materials Today: Proceedings*, Vol. 5, 2018, 6313–6320.
- [3] J. P. Davim. *Nontraditional machining processes*. London: springer- Verlag, 2013.
- [4] R. Choudhary, H. Garg, M. Prasad, D. Kumar. Effect of Cryogenic Treatment of Tool Electrode on the Machining Performance and Surface Finish during Electrical Discharge Machining of Hastelloy C-4. *Materials Today: Proceedings*. Vol. 4, 2017, 1158–1166.
- [5] M. R. Shabgard, M. A. Badamchizadeh, G. Ranjbary, K. Amini. Fuzzy approach to select machining parameters in electrical discharge machining (EDM) and ultrasonic-assisted EDM processes. *Journal of Manufacturing System*. Vol. 32, 2013, 32-38.
- [6] A. P. Dwivedi, S. K. Choudhury. Improvement in the Surface Integrity of AISI D3 Tool Steel Using Rotary Tool Electric Discharge Machining Process. *Procedia Technology*, Vol. 23, 2016, 280–287.
- [7] G. Talla, D. K. Sahoo, S. Gangopadhyay, C. K. Biswas. Modeling and multi-objective optimization of powder mixed electric discharge machining process of aluminum/alumina metal matrix composite. *Engineering Science and Technology; an International Journal*. Vol. 18, 2015, 369–73.
- [8] D. R. Unune, C. K. Nirala, H. S. Mali. ANN-NSGA-II dual approach for modeling and optimization in abrasive mixed electro discharge diamond grinding of Monel K-500. *Engineering Science and Technology; an International Journal*. Vol. 21, 2018, 322-329.
- [9] S. Tripathy, D. K. Tripathy. Multi-attribute Optimization of Machining Process Parameters in Powder Mixed Electro-Discharge Machining Using TOPSIS and Grey Relational Analysis. *Engineering Science and Technology, an International Journal*. Vol. 19, 2016, 62–70.

- [10] A. Bhattacharya, A. Batish, G. Singh, V. K. Singla. Optimal Parameter Settings for Rough and Finish Machining of Die Steels in Powder-mixed EDM. *The International Journal of Advanced Manufacturing Technology*, Vol. 61, 2012, 537–548.
- [11] H. K. Kansal, S. Singh, P. Kumar. Effect of Silicon Powder Mixed EDM on Machining Rate of AISI D2 Die Steel. *Journal of Manufacturing Processes*, Vol. 9, 2007, 13–22.
- [12] M. P. Jahan, M. Rahman, Y. S. Wong. Study on the Nano-powder-mixed Sinking and Milling Micro-EDM of WC-Co. *The International Journal of Advanced Manufacturing Technology*, Vol. 53, 2011, 167–180.
- [13] S. T. Alam, A. N. Amin, M. I. Hossain, M. Huq, S. H. Tamim. Performance evaluation of graphite and titanium oxide powder mixed dielectric for electric discharge machining of Ti–6Al–4V. *SN Applied Sciences*. Vol. 3, 2021, 1-12.
- [14] C. Prakash, H. K. Kansal, B. S. Pabla, S. Puri. Experimental investigations in powder mixed electric discharge machining of Ti–35Nb–7Ta–5Zr β -titanium alloy. *Materials and Manufacturing Processes*. Vol. 32, 2017, 274-85.
- [15] S. F. Ou, C. Y. Wang. Effects of bioceramic particles in dielectric of powder-mixed electrical discharge machining on machining and surface characteristics of titanium alloys. *Journal of materials processing technology*. Vol. 245, 2017, 70-79.
- [16] S. K. Sahu, T. Jadam, S. Datta, G. Nandi. Effect of using SiC powder-added dielectric media during electro-discharge machining of Inconel 718 superalloys. *Journal of the Brazilian Society of Mechanical Sciences and Engineering*. Vol. 40, 2018, 1-9.
- [17] S. Patel, D. Thesiya, A. Rajurkar. Aluminium powder mixed rotary electric discharge machining (PMEDM) on Inconel 718. *Australian Journal of Mechanical Engineering*. Vol. 16, 2018, 21-30.
- [18] B. S. Khadar, R. M. Jagannadha, K. Murahari. Multi-objective optimization of process parameters for powder mixed electrical discharge machining of Inconel X-750 alloy using Taguchi-TOPSIS approach. *Strojnícky Casopis-Journal of Mechanical Engineering*. Vol. 71, 2021, 1-8.
- [19] S. Ahmad, M. A. Lajis, R. H. Haq, A. M. Arifin, M. N. Rahman, H. F. Haw, H. Abdullah. Surface roughness and surface topography of Inconel 718 in powder mixed dielectric

- electrical discharge machining (PMEDM). *International Journal of Integrated Engineering*. Vol. 10, 2018, 181-186.
- [20] S. Majumdar, N. K. Bhoi, H. Singh, Graphene nano-powder mixed electric discharge machining of Inconel 625 alloy: optimization of process parameters for material removal rate. *International Journal on Interactive Design Manufacturing*. Vol. 17, 2023, 2341-2347.
- [21] G. Talla, S. Gangopadhyay, C. K. Biswas, Effect of powder-suspended dielectric on the EDM characteristics of Inconel 625. *Journal of Materials Engineering and Performance*. Vol. 25, 2016, 704-717.
- [22] W. S. Zhao, G. Q. Meng, Z. L. Wang. The application of research on powder mixed EDM in rough machining. *Journal of Materials Processing Technology*, Vol. 129, 2002, 30-33.
- [23] H. Marashi, D. M. Jafarlou, A. A. Sarhan, M. Hamdi. State of the art in powder mixed dielectric for EDM applications. *Precision Engineering*, Vol. 46, 2016, 11-33.
- [24] M. S. Han, B. K. Min, S. J. Lee. Improvement of surface integrity of electro-chemical discharge machining process using powder-mixed electrolyte. *Journal of Materials Processing Technology*, Vol. 191, 2007, 224-227.
- [25] S. P. Dwivedi, R. Sahu. Effects of SiC particles parameters on the corrosion protection of Aluminum-based Metal Matrix Composites using Response Surface Methodology". *Jordan Journal of Mechanical & Industrial Engineering*. Vol. 12, 2018, 313-321.
- [26] M. Rahimi, H. Fazlollahtabar. Optimization of a closed loop green supply chain using Particle Swarm and Genetic Algorithms. *Jordan Journal of Mechanical & Industrial Engineering*, Vol. 12, 2018, 77-91.
- [27] R. Das, M. K. Pradhan, C. Das. Prediction of surface roughness in Electrical Discharge Machining of SKD 11 TOOL steel using Recurrent Elman Networks. *Jordan Journal of Mechanical & Industrial Engineering*. Vol. 7, 2013, 67-71.
- [28] D. Sharma, A. Bhowmick, A. Goyal. Enhancing EDM performance characteristics of Inconel 625 superalloy using response surface methodology and ANFIS integrated

- approach. *CIRP Journal of Manufacturing Science and Technology*. Vol. 37, 2022, 155-173.
- [29] S. Jarin, T. Saleh, M. Rana, A. G. Muthalif, M. Y. Ali. An experimental investigation on the effect of nanopowder for micro-wire electro discharge machining of gold coated silicon. *Procedia engineering*, Vol. 184, 2017, 171-177.
- [30] V. S. Jatti, S. Bagane. Thermo-electric modelling, simulation and experimental validation of powder mixed electric discharge machining (PMEDM) of BeCu alloys. *Alexandria Engineering Journal*, Vol. 57, 2018, 643-653.
- [31] Y. S. Kim, C. N. Chu. The effects of graphite powder on tool wear in micro electrical discharge machining. *Procedia CIRP*, Vol. 68, 2018, 553-558.
- [32] A. P. Tiwary, B. B. Pradhan, B. Bhattacharyya. Influence of various metal powder mixed dielectric on micro-EDM characteristics of Ti-6Al-4V. *Materials and Manufacturing Processes*. Vol. 34, 2019, 1103-1119.
- [33] G. Rajkumar, M. Saravanan, A. B. H. Bejathin, S. Sharma, S. P. Dwivedi, R. Kumar, S. Singh. Parametric optimization of powder-mixed EDM of AA2014/Si3N4/Mg/cenosphere hybrid composites using fuzzy logic. Analysis of mechanical, machining, microstructural, and morphological characterizations, *Journal of Composites Science*, Vol. 7, 2023, 380-405.
- [34] J. Singh, R. K. Sharma. Implementation of Taguchi method with hybrid decision making tools for prediction of surface characteristics for powder-mixed EDM of WC. *Perspectives in Science*. Vol. 8, 2016, 455-458.
- [35] M. G. Rathi, D. V. Mane. Study on effect of powder mixed dielectric in EDM of Inconel 718. *International Journal of Scientific and Research Publications*, Vol. 4, 2014, 1-7.
- [36] N. Singh, P. S. Bharti. Multi-Objective parametric optimization during micro-EDM drilling of Ti-6Al-4 V using teaching learning Based optimization algorithm. *Materials Today: Proceedings*, Vol. 62, 2022, 262-269.
- [37] S. Chakraborty, S. Mitra, D. Bose. Evaluation of response characteristics using sensitivity analysis and TLBO technique of powder mixed wire EDM of Ti6Al4V alloy. *CIRP Journal of Manufacturing Science and Technology*, Vol. 47, 2023, 260-272.

- [38] S. Dinesh, V. Vijayan, S. Thanikaikarasan, P. J. Sebastian. Productivity and Quality enhancement in Powder Mixed Electrical Discharge Machining for OHNS die steel by utilization of ANN and RSM modelling. *Journal of New Materials for Electrochemical System*, Vol. 22, 2019, 33-43.
- [39] S. Kumar, A. Batish, R. Singh, T. P. Singh. A hybrid Taguchi-artificial neural network approach to predict surface roughness during electric discharge machining of titanium alloys. *Journal of Mechanical Science and Technology*, Vol. 28, 2014, 2831-2844.
- [40] S. Mohanty, A. Mishra, B. K. Nanda, B. C. Routara. Multi-objective parametric optimization of nano powder mixed electrical discharge machining of AlSiCp using response surface methodology and particle swarm optimization. *Alexandria Engineering Journal*, Vol. 57, 2018, 609-619.
- [41] S. Padhee, N. Nayak, S. K. Panda, P. R. Dhal, S. S. Mahapatra. Multi-objective parametric optimization of powder mixed electro-discharge machining using response surface methodology and non-dominated sorting genetic algorithm. *Sadhana*. Vol. 37, 2012, 223-240.
- [42] S. Ramesh, M. P. Jenarthanan. Optimizing the powder mixed EDM process of nickel based super alloy. *Proceedings of the Institution of Mechanical Engineers, Part E: Journal of Process Mechanical Engineering*, Vol. 235, 2021, 1092-1103.
- [43] N. Faisal, K. Kumar. Optimization of machine process parameters in EDM for EN 31 using evolutionary optimization techniques. *Technologies*, Vol. 54, 2018, 1-16.
- [44] H. P. Nguyen, V. D. Pham, N. V. Ngo. Application of TOPSIS to Taguchi method for multi-characteristic optimization of electrical discharge machining with titanium powder mixed into dielectric fluid. *The International Journal of Advanced Manufacturing Technology*, Vol. 98, 2018, 1179-1198.
- [45] B. Elumalai, S. Gowri, P. Hariharan, K. V. Pillai. Experimental Investigations on μ ED Milling of Inconel 718 with Nano SiC Abrasive Mixed Dielectric. *Materials Research*, Vol. 25, 2021, 1-9.
- [46] G. Shanmugasundar, M. Vanitha, R. Čep, V. Kumar, K. Kalita, M. Ramachandran. A comparative study of linear, random forest and AdaBoost regressions for modeling non-traditional machining. *Processes*, Vol. 9, 2021, 1-14.

- [47] A. R. Kaigude, N. K. Khedkar, V. S. Jatti, S. Salunkhe, R. Cep, E. A. Nasr. Surface roughness prediction of AISI D2 tool steel during powder mixed EDM using supervised machine learning. *Scientific Reports*, Vol. 14(1), 2024, 1-12.
- [48] P. Peças, E. Henriques. Electrical discharge machining using simple and powder-mixed dielectric: The effect of the electrode area in the surface roughness and topography. *Journal of Material Processing Technology*. Vol. 200, 2008, 250–258.
- [49] P. J. Liew, J. Yan, T. Kuriyagawa. Carbon nanofiber assisted micro electro discharge machining of reaction-bonded silicon carbide. *Journal of Material Processing Technology*. Vol. 213, 2013, 1076–1087.
- [50] P. M. Abhilash, D. Chakradhar. Failure detection and control for wire EDM process using multiple sensors. *CIRP Journal of Manufacturing Science and Technolgy*. Vol. 33, 2021, 315–326.
- [51] K. Furutani, A. Saneto, H. Takezawa, N. Mohri, H. Miyake. Accretion of titanium carbide by electrical discharge machining with powder suspended in working fluid. *Precision Engineering*, Vol. 25, 2001, 138-144.
- [52] S. Mohal, H. Kumar. Study on the multiwalled carbon nano tube mixed EDM of Al-SiCp metal matrix composite. *Materials Today: Proceedings*, Vol. 4, 2017, 3987-3993.
- [53] M. Kolli, A. Kumar. Effect of Dielectric Fluid with Surfactant and Graphite Powder on Electrical Discharge Machining of Titanium Alloy using Taguchi Method. *Engineering Science and Technology, an International Journal*. Vol. 18, 2015, 524–535.
- [54] X. Bai, Q. Zhang, J. Zhang, D. Kong, T. Yang. Machining efficiency of powder mixed near dry electrical discharge machining based on different material combinations of tool electrode and workpiece electrode. *Journal of Manufacturing Processes*, Vol. 15, 2013, 474-482.
- [55] Y. S. Wong, L. C. Lim, I. Rahuman, W. M. Tee. Near-mirror-finish phenomenon in EDM using powder-mixed dielectric. *Journal of Materials Processing Technology*, Vol. 79, 1998, 30-40.
- [56] Z. J. Xie, Y. J. Mai, W. Q. Lian, S. L. He, X. H. Jie. Titanium carbide coating with enhanced tribological properties obtained by EDC using partially sintered titanium

- electrodes and graphite powder mixed dielectric. *Surface and Coatings Technology*, Vol. 300, 2016, 50-57.
- [57] B. Singh, J. Kumar, S. Kumar. Influences of process parameters on MRR improvement in simple and powder-mixed EDM of AA6061/10% SiC composite. *Materials and Manufacturing Processes*, Vol. 30, 2015, 303-312.
- [58] P. Malhotra, N. K. Singh, R. K. Tyagi, B. S. Sikarwar. Comparative study of rotary-EDM, gas assisted-EDM, and gas assisted powder mixed-EDM of the hybrid metal matrix composite. *Advances in Materials and Processing Technologies*, Vol. 7, 2021, 27-41.
- [59] V. Kumar, A. Kumar, S. Kumar, N. K. Singh. Comparative study of powder mixed EDM and conventional EDM using response surface methodology. *Materials Today: Proceedings*, Vol. 5, 2018, 18089-18094.
- [60] S. Prabhu, B. K. Vinayagam, AFM surface investigation of Inconel 825 with multi wall carbon nano tube in electrical discharge machining process using Taguchi analysis. *Archives of civil and mechanical engineering*, Vol. 11, 2011, 149-170.
- [61] Y. H. Guu, M. T. Hou. Effect of machining parameters on surface textures in EDM of Fe-Mn-Al alloy. *Materials Science and Engineering: A*, Vol. 466, 2007, 61-67.
- [62] N. Beri, S. Maheshwari, C. Sharma, A. Kumar. Surface quality modification using powder metallurgy processed CuW electrode during electric discharge machining of Inconel 718. *Procedia Materials Science*, Vol. 5, 2014, 2629-2634.
- [63] T. Yih-Fong, C. Fu-Chen. Investigation into some surface characteristics of electrical discharge machined SKD-11 using powder-suspension dielectric oil. *Journal of Material Processing Technology*. Vol. 170, 2005, 385–391.
- [64] C. Veiga, J. P. Davim, A. J. R. Loureiro. Review on machinability of titanium alloys: The process perspective. *Reviews on Advanced Materials Science*. Vol. 34, 2013, 148–64.
- [65] A. Hosseini, H. A. Kishawy. *Cutting Tool Materials and Tool Wear*. 2014. 31–56 p.
- [66] N. Khanna, J. P. Davim. Design-of-experiments application in machining titanium alloys for aerospace structural components. *Measurement*. Vol. 6, 2014, 280-290.

- [67] D. R. Sahu, A. Mandal. Critical analysis of surface integrity parameters and dimensional accuracy in powder-mixed EDM. *Materials and Manufacturing Processes*. Vol. 35, 2020, 430-441.
- [68] C. H. Lauro, S. L. M. Ribeiro Filho, L. C. Brandão, J. P. Davim. Analysis of behaviour biocompatible titanium alloy (Ti-6Al-7Nb) in the micro-cutting. *Journal of the International Measurement Confederation*, Vol. 93, 2016, 529–540.
- [69] A. Malik, N. Sanghvi. Optimization of laser-assisted jet electrochemical machining parameters by grey relational analysis and fuzzy logic. *World Journal of Engineering*, Vol. 19, 2021. 1-8.
- [70] T. Le, Surrogate neural network model for prediction of load-bearing capacity of CFSS members considering loading eccentricity. *Applied Sciences*, Vol. 10, 2020, 1-22.
- [71] Y. Javid. Multi-response optimization in laser cladding process of WC powder on Inconel 718. *CIRP Journal of Manufacturing Science and Technology*, Vol. 31, 2020, 406–417.
- [72] C. Y. Poon, B. Bhushan. Comparison of surface roughness measurements by stylus profiler, AFM and non-contact optical profiler. *Wear*, Vol. 190, 1995, 76-88.

Parametric Study and Optimization of Inconel 625 Processing by ANN and Desirability Function Approach During Graphite Mixed EDM

Sovan Bhowmick^a, Binod Barai^a, Debismita Naik^b, Subhasish Sarkar^{a,*}, Nisantika Biswas^c,
Swapan Kumar Maity^d, Gautam Majumdar^a

^a Mechanical Engineering Department, Jadavpur University, Kolkata, West Bengal 700032, India.

^b Department of Physical Sciences, Indian Institute of Science Education and Research, Kolkata, West Bengal 741246, India.

^c Department of Mechanical Engineering, Academy of Technology, Hooghly, West Bengal 712502, India.

^d Professor, Maulana Abul Kalam Azad University of Technology, West Bengal, Haringhata, West Bengal 741249

Received 12 Jun 2023

Accepted 15 Sep 2023

Abstract

In the present research, electric discharge machining (EDM) was performed on Inconel 625, a nickel-based superalloy by mixing graphite micro powder in dielectric fluid during machining. A Box-Behnken type RSM design was constructed for the experimental work varying five input parameters viz. current, pulse on time, duty cycle, powder concentration and mesh size of the powder to study their effects on material removal rate (MRR), tool wear rate (TWR) and surface roughness (SR). Further, back propagation type artificial neural network (ANN) was developed, trained and tested with the experimental data. Multi response desirability function was applied to the RSM model to maximize MRR, optimize TWR at a stipulated target value and minimize SR. The analysis of the experimental result indicates that current and powder concentration have the extreme influence on all the three responses. The obtained ANN model provides a mean error of prediction as 5.95%, 7.30% and 6.40% for MRR, TWR and SR respectively. The overall R value of the model is found as 0.945 which indicates that the ANN model is adequate to predict the responses for other combination of input parameters. From the desirability function analysis, the optimized value of MRR, TWR and SR are found as 26.135 mm³/min, 0.0800 mm³/min and 5.81 µm at current = 8.6 A, pulse on time = 35 µs, duty cycle = 0.5, powder concentration = 8 g/l and mesh size at 35 µm. The study of surface characterization of the Inconel 625 samples have been performed using AFM, SEM and XRD analysis. The AFM and SEM study revealed that the surface irregularities and the width of microcracks increase continuously with the increase of current.

© 2023 Jordan Journal of Mechanical and Industrial Engineering. All rights reserved

Keywords: EDM, MRR, surface roughness, TWR, ANN, SEM, XRD.

1. Introduction

In recent days, the demand for non-ferrous superalloys is increasing rapidly because of their light weight and magnificent mechanical properties. Inconel is a nickel-based ferrous alloy which is used in different engineering sectors such as aerospace, gas turbine manufacturing, nuclear power plant and automotive [1]. The high tensile strength, hardness, fatigue life and nearly zero corrosion rate made this alloy so demanding in these manufacturing industries. Inconel is also used in high-temperature applications since it retains almost all the mechanical properties at the elevated temperature [2]. With the increase of demand, the processing of materials needs to be more efficient for enhancing productivity [3]. Since the conventional way of Inconel processing is pretty poor, many non-conventional machining processes are used to cut the material. Electric discharge machining (EDM) is one of the convenient way that is highly used for Inconel processing [4].

EDM is a non-conventional machining process where material is removed by applying a series of high-energy electrical sparks at the gap of the electrode and the work surface. The high-energy spark generates temperature beyond the melting point of the material. The high temperature melts and removes the materials by forming a small crater on the surface [5]. In this process, no mechanical contact is established between the tool and the workpiece which makes it advantageous to machine any difficult to cut materials [6, 7]. However, the rate of material removal is very low and the surface unevenness is very high compared to conventional machining processes [8]. Several researches are performed to overcome the challenges like addition of different technologies, parametric optimization and many more. Powder mixed electric discharge machining (PMEDM) is a new technology which is proven efficient to improve the machining quality and material removal rate. In this process, tiny little electrically conductive particles are mixed with dielectric fluid used in EDM and applied before the machining. During the process, the particles arrange themselves in the form of chains at the spark gap. When the voltage is applied between the

* Corresponding author e-mail: subha.jumechanical@yahoo.com.



Full-length article

Parametric optimization and prediction of MRR and surface roughness of titanium mixed EDM for Inconel 718 using RSM and fuzzy logic

Sovan Bhowmick^a, Rupam Mondal^a, Subhasish Sarkar^{a,*}, Nisantika Biswas^b, Jhumpa De^b, Gautam Majumdar^a^a Mechanical Engineering Department, Jadavpur University, Kolkata, West Bengal 700032, India^b Department of Mechanical Engineering, Academy of Technology, West Bengal 712502, India

ARTICLE INFO

Available online xxxx

Keywords:

Powder mixed electric discharge machining
Inconel 718
RSM
Fuzzy logic
Desirability function
SEM
EDX

ABSTRACT

Powder mixed electric discharge machining (PMEDM) was developed to improve the machining rate and surface quality of conventional EDM. In this study, PMEDM was performed on Inconel 718 by adding titanium particles to the dielectric fluid. The input parameters selected for the experiment were powder concentration, pulse current, gap voltage, pulse on time and pulse off time and the effects of the input parameters were investigated on the material removal rate (MRR) and the surface roughness of the sample. Response surface methodology (RSM) was used to construct the design of experiment. Analysis of variance (ANOVA) was carried out to find out the significant input parameters for each response. Further, Mamdani based fuzzy logic was developed using the experimental data and used to predict the responses in optimized condition. The multi-objective optimization was performed using the RSM desirability function approach to maximize the MRR and minimize the surface roughness. From ANOVA, it is observed that powder concentration, pulse current, gap voltage and pulse on time are the significant input parameters for MRR and surface roughness. The fuzzy result is compared with the experimental data and found the accuracy of prediction is 89.21 % for MRR and 91.23 % for surface roughness. The optimized setting of input parameters is obtained as powder concentration = 8 g/l, pulse current = 9.5 A, gap voltage = 60 V, pulse on time = 150 μ s and pulse off time = 20 μ s and the corresponding optimum value of MRR and surface roughness are 16.623 mm³/min and 3.71 μ m respectively. The SEM result indicates that the width of the surface crack is found more in the optimized sample compared to the sample having the least surface roughness. From the EDX analysis, it is found that a very small amount of copper and titanium particles were included on the surface during the machining.

© 2022 CIRP.

Introduction

The increasing demands for newly developed materials to meet the challenging situation and highly inferior environment have given the birth of superalloys, high strength alloys, high temperature resistant materials etc. As a nickel based superalloy, Inconel with different grades can be used to meet the challenges as it possesses extremely good mechanical properties like high hardness and toughness, low corrosion rate and high fatigue strength [1]. Inconel 718 is extensively used in nuclear power plants, aerospace sector, defence sector, gas turbine manufacturing plant and other

manufacturing sectors. Due to its poor machinability Inconel is normally machined by nontraditional machining such as EDM, ECM etc.

Electric discharge machining (EDM) is a nontraditional machining process that produces an electrical spark that impinges on the workpiece and generates a high temperature due to which the material from the work surface removes by melting and vaporization [2]. The difficulties in EDM can be found as it provides a low material removal rate, high surface roughness and high tool wear rate. The process is found uneconomical where the superior quality of the surface is highly recommended to maintain mechanical properties like fatigue strength and corrosion resistance [3]. Several developments have been employed to overcome the difficulties in which hybridization of EDM process using rotary tool electrode, ultrasonic vibration-assisted electrode, cryogenic treatment on machined surfaces and mixing of electrically conductive micro and nanopowders

* Corresponding author.

E-mail address: subha.jumechanical@yahoo.com (S. Sarkar).



Contents lists available at ScienceDirect

Materials Today: Proceedings

journal homepage: www.elsevier.com/locate/matpr

A comparative study relating machining properties and surface characteristics of Inconel 625 during powder mixed electric discharge machining

Sovan Bhowmick^{a,*}, Subhasish Sarkar^a, Nisantika Biswas^b, Gautam Majumdar^a

^aJadavpur University, Kolkata, West Bengal 700032, India

^bAcademy of Technology, Hoogly, West Bengal 712502, India

ARTICLE INFO

Article history:
Available online xxxx

Keywords:
EDM
MRR
Surface roughness
Tool wear rate

ABSTRACT

In the current study, the machinability during the machining with powder mixed electric discharge machining was studied on Inconel 625 sample along with their surface characteristics. During the machining, separately three powders viz. titanium, graphite and silicon carbide were mixed in EDM oil dielectric fluid with a concentration of 4 g/l. The other electric parameters were kept constant. The comparative study was made to study the changes in MRR, surface roughness and tool wear rate. The analysis clearly indicates that, by the addition of titanium, graphite and silicon carbide in the order, the MRR decreases, surface roughness increases and tool wear rate increases. The SEM results of the machined sample indicate that the surface unevenness is increasing with changing of powders. The EDX result of the surface correlated the amount of copper transferred to the surface and the tool wear rate. Like the SEM result, EDX result also indicated the enhancement of the tool wear during the machining of above-said order of the powders.

Copyright © 2023 Elsevier Ltd. All rights reserved.

Selection and peer-review under responsibility of the International Conference on Advancements in Manufacturing Engineering – 2022.

1. Introduction

Powder mixed electric discharge machining is a modified and efficient conversion of normal EDM process where electrically conductive powder of micron or nano level mesh size is mixed homogeneously with the dielectric fluid before machining. The effectiveness of the modification is significantly good as the addition of powder improves several machining characteristics and material properties such as MRR, surface roughness, tool wear rate, microhardness, grain structure and white layer thickness. The effect of silicon carbide powder with kerosene oil was performed for copper and graphite electrode in an experimental study [1] and it is found that the graphite electrode with SiC powder gives 7.30 % better result than copper electrode. Another study presented by Kansal et al. [2] shows that the optimized MRR and surface roughness can be achieved when the silicon powder mixed kerosene dielectric was used at 4 g/l concentration along with other electrical parameters and their optimized values.

Apart from silicon based powder, Addition of graphite microparticles with kerosene electrode reduces the surface roughness at minimum level as 38 nm with 0.2 g/l concentration [3]. In a study made by Marashi et al. [4], it is observed that surface roughness had improved with the application of titanium powder by 69 % and 35 % at 6 A and 12 A peak currents. Dwivedi and Choudhury had studied the surface characterization of EDM surface of AISI D3 tool steel using scanning electrode micrography and found the inclusion of recast layer, surface crack and powder inclusion and recast layer thickness [5]. In another study [6], the surface crack of molybdenum and steel surface had been witnessed after the machining of die-sinking EDM at a specific setting of parameters. The EDX analysis of the machined sample was performed in a study [7] of graphite mixed PMEDM titanium sample and found the concentration of titanium and vanadium near the surface crack zone. Ekmecki and Ersoz [8] had studied the effect of SiC powder mixed EDM on surface topology of IF steel and concluded that the suspended particles present in the dielectric prevent the penetration of crack by producing small and uniform discharge. In another study, carbon nanotube based dielectric was used and it was found that at 4 g/l concentration, the MRR increases from

* Corresponding author.

E-mail address: svnhowmick1@gmail.com (S. Bhowmick).

A Brief Review of Experimental Investigations and Analytical Development of Powder Mixed Electric Discharge Machining (PMEDM)

Sovan Bhowmick^{1,a*}, Gautam Majumdar^{2,b} and Asish Bandyopadhyay^{3,c}

¹⁻³Mechanical Engineering Department, Jadavpur University, Kolkata – 700032, India

^asvnbhowmick1@gmail.com, ^bgmajumdarju@gmail.com, ^casishjumech@gmail.com

*Corresponding Author

Keywords: powder mixed electric discharge machining, metallurgical characteristics, nano particles, material removal rate, surface roughness, tool wear rate, white layer thickness, thermal characteristics

Abstract. Powder mixed electric discharge machining (PMEDM) is a newly developed technology in which EDM is performed by mixing electrically conductive micro or nano particles with dielectric fluid. The electrically conductive tiny particles when come at the gap of electrode and work piece, they will begin to create spark by the induction of electrode voltage which enhances the material removal and surface finish of the machined surface. In this paper a brief review has been done on different aspects of powder mixed electric discharge machining. It is observed that the researches are done in three main directions. Firstly, experimental studies are done to show the effect of several input process parameters on responses mainly material removal rate (MRR), surface roughness and tool wear rate. Secondly, the metallurgical characteristics of the machined surface are analyzed to measure the white layer thickness and amount of powder material inclusion onto the surface. The third one is the investigation of thermal characteristics of the tool and work pieces during the machining process. In these three sections of researches, the results of the investigation have been discussed in this review.

1. Introduction

In the present days, development of new materials are continuously going on to fulfill the needs of different industries like automobile, petrochemical, aerospace and many more by their suitable properties and efficient functioning in harsh environment. But in most of the cases the materials are difficult to process by conventional manufacturing process. The utmost objective of modern manufacturing science and technology is to process those materials with a proper rate of production and quality of manufacturing. Under non conventional machining process, electric discharge machining (EDM) is extremely useful to machine hard, non machinable and thermally conductive materials like Inconel, tool and die steel, composite materials and other super alloys. In this process, material is removed by a controlled electro erosive action produced by electric discharge or spark. The spark is established between the electrode and workpiece separated by a fine and precise gap nearly 10-125 μm known as spark gap. Due to the spark electrical erosion takes place which causes melting and vapourization of the tiny amount of material from the work piece. The tool electrode and the workpiece surface are submerged into the dielectric fluid to provide insulating environment for generating and transferring the spark towards workpiece. But in EDM, the rate of material removal is very less and also the quality of finish of the machined surface is poor compare to conventional machining processes.

Synthesis and Characterization of Titanium and Graphite Powder Mixed Electric Discharge Machining on Inconel 718

Sovan Bhowmick^{a,1}, Arindam Paul^b, Nisantika Biswas^c, Jhumpa De^c, Subhasish Sarkar^a and Gautam Majumdar^a

^a*Mechanical Engineering Department, Jadavpur University, India.*

^b*Department of Metallurgical and Material Engineering, Jadavpur University, India.*

^c*Department of Mechanical Engineering, Academy of Technology, India.*

Abstract. Electric discharge machining is extensively used to process difficult to cut materials such as superalloys, composite materials etc. The quality of machining can be improved by adding particles into the dielectric fluid which is commonly known as powder mixed electric discharge machining (PMEDM). In the present study, titanium and graphite powder are added to dielectric fluid and the effects of the powders have been analysed on material removal rate, surface roughness, microhardness and surface morphology analysis. Six experiments have been conducted considering each powder with three different levels of pulse current 4A, 8A and 12A. The analysis of the result indicates MRR, surface roughness and microhardness significantly increase with the increase of pulse current. Titanium mixed EDM improves the MRR and microhardness but reduces the surface quality. The SEM investigations elucidate that the samples machined with Titanium powder mixed with EDM have fewer surface defects, cracks, microholes and layer deposition compared to the sample machined with Graphite powder.

Keywords. Powder mixed electric discharge machining, MRR, surface roughness, microhardness, SEM.

1. Introduction



Electric discharge machining is a non-traditional machining process commonly used for machining or cutting conductive materials having poor machinability like superalloys, high strength alloys, composite materials etc. A die-sinking EDM is used in the tool and die manufacturing industry. The mechanism of the material removal is thermal corrosion that occurs on the surface of the workpiece. The difficulties faced during the machining are poor surface finish, low production rate, and poor surface integrity [1]. Several researches were done to enhance the surface quality and production rate out of which the most significant improvement is witnessed when the conductive metallic powder is added to the dielectric fluid during the machining process. In a study, The effect of graphite nanopowder on deionized water was investigated on Inconel 825 alloy and found a considerable improvement in MRR, surface quality and tool wear rate [2].

¹ Corresponding Author, Mechanical Engineering Department, Jadavpur University, Kolkata-700032 India, Email: svnbhowmick1@gmail.com